Postnatal development of articular cartilage

Mark van Turnhout

Thesis committee

Thesis supervisor
Prof. dr. ir. J.L. van Leeuwen
Professor of Experimental Zoology
Wageningen University

Thesis co-supervisor
Dr. ir. S. Kranenbarg
Assistant Professor
Experimental Zoology Group
Wageningen University

Other members
Prof. dr. J.S. Jurvelin, Kuopio University, Finland
Prof. dr. E. van der Linden, Wageningen University
Prof. dr. H. Weinans, Erasmus Medical Centre, Rotterdam
Dr. ir. C.W.J. Oomens, Eindhoven University of Technology

This research was conducted under the auspices of the Graduate School of Animal Sciences.

Postnatal development of articular cartilage

Mark van Turnhout

Thesis
submitted in fulfilment of the requirements for the degree of doctor
at Wageningen University
by the authority of the Rector Magnificus
Prof. dr. M.J. Kropff,
in the presence of the
Thesis Committee appointed by the Academic Board
to be defended in public
on Friday 12 November 2010
at 1:30 p.m. in the Aula.

Mark van Turnhout (2010). Postnatal development of articular cartilage.
Thesis, Wageningen University, Wageningen, the Netherlands

ISBN: 978-90-8585-783-9

Contents

Cartilage is one of the most important characteristics of vertebrates.

Ohtani et al. [258]

1 Introduction

1.1 Articular cartilage

Articular cartilage (AC) is the thin layer of soft tissue that lines the articulating ends of bones in the synovial joints [133, 152, 184], such as the ankle, hip, knee, shoulder and finger joints (figure 1.1) in mammals, birds and reptiles. In mammals, the tissue consists

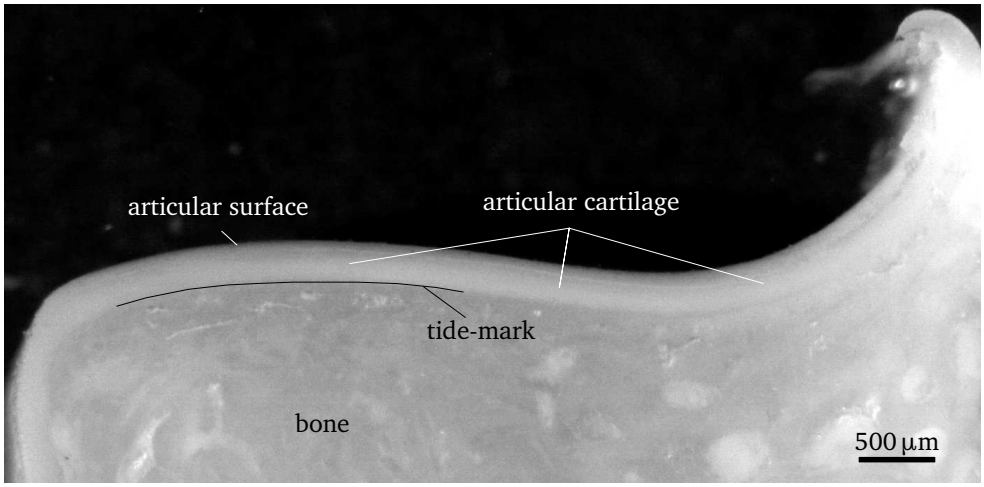

Figure 1.1: Photograph of the thin layer of articular cartilage and the supporting bone in an ovine cannon bone. A part of the tide-mark is marked with a thin black line.

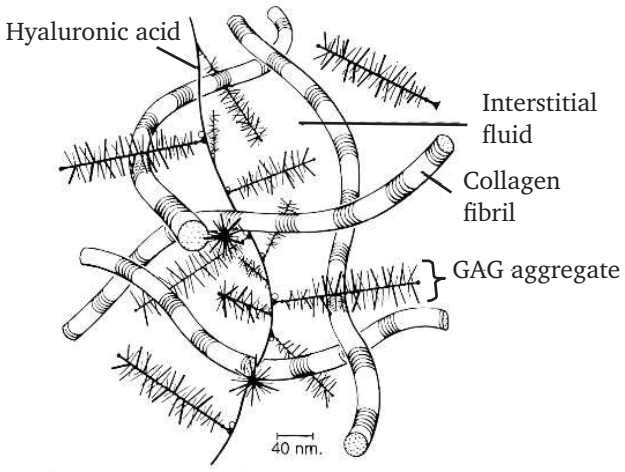

Figure 1.2: Components of AC. The ECM consists of collagen fibrils and proteoglycans. The proteoglycans consist of the hyaluronic acid with the branches of GAG aggregates. The ECM is saturated with the interstitial fluid. Adapted from [250, figure 8].

of a number of cells (chondrocytes, approximately 2 %–5 % of the total volume [120, 121, 315]) that are embedded in a porous extracellular matrix (ECM) that is saturated with fluid. The interface with the bone, the so-called tide-mark or chondro-osseous junction, is an impermeable discrete band of mineralized cartilage [226, 227, 232]. Adult AC is not penetrated by blood vessels and depends on diffusion and convection from the synovial fluid for the supply and removal of metabolic products [232, 242]. The function of AC in adult life is to distribute and transmit mechanical joint loads to the bone, and to provide a low friction environment for joint movement.

The interstitial fluid that saturates the porous ECM is the main component (approximately 80 % on a wet weight basis, figure 1.2) of AC [185, 221, 294]. The solid ECM accounts for approximately 20 % on a wet weight basis. The ECM consists mainly of collagen fibres (approximately 80 % on a dry weight basis, [52, 105, 106]) embedded in a proteoglycan (PG) matrix (approximately 20 % on dry weight basis). Each collagen fibril consists of a left-handed triple α-helix composed of three α-chains that are characterised by a Gly-X-Y amino acid sequence. X is frequently proline and Y is frequently hydroxyproline. The collagen in postnatal AC is mostly collagen type II ($\geq$ 85 %), which consists of three identical so-called α1(II)-chains and is a fibrillar collagen, i.e. collagen type II is capable of aggregating individual fribrils into a single fibre [87, 107, 108, 244, 313].

PGs are proteins substituted with at least one glycosaminoglycan (GAG, figure 1.3) chain [41, 240]. Aggrecan is the most abundant GAG in AC and consists of repetitive chains of chondroitin sulphate (CS, figures 1.3a- 1.3b) and keratan sulphate (KS, figure 1.3c) [98, 296, 335]. CS takes two forms in AC depending on the location of the sulphate group: chondroitin-6-sulphate (figure 1.3a) and chondroitin-4-sulphate (figure 1.3b) in a ratio of 9:1 in adult AC [29, 98]. Hyaluronic acid (HA, figure 1.3d) is the link protein

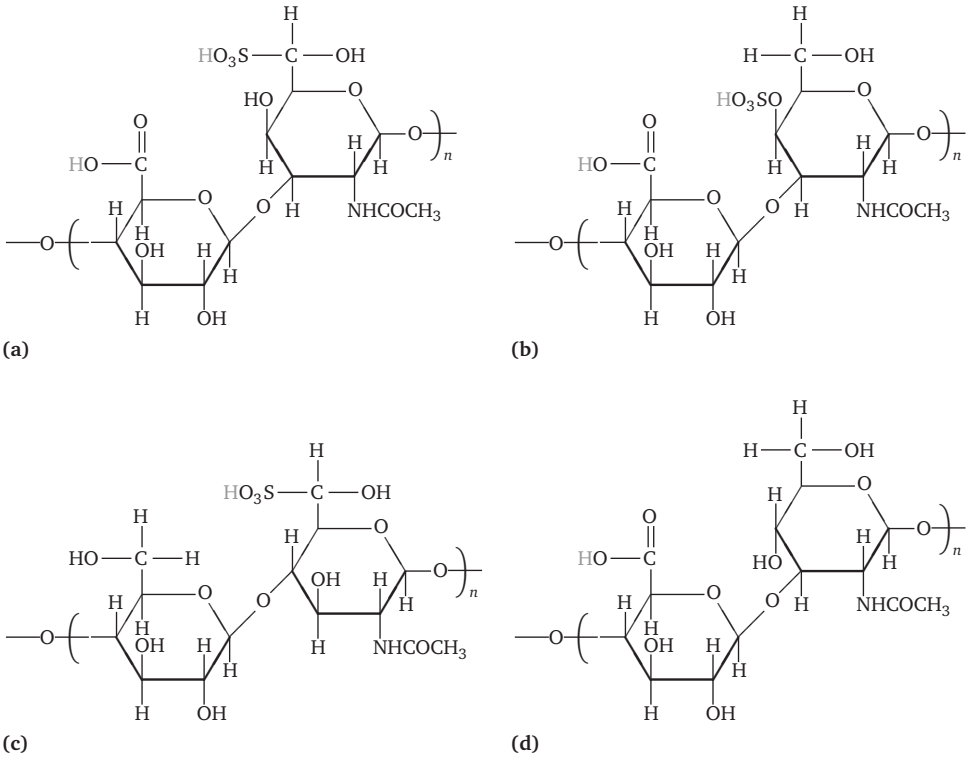

Figure 1.3: The GAGs in AC. With **(a-b)** chondroitin sulphate: $C_{14}H_{22}NO_{15}S$, **(a)** chondroitin-6-sulphate; and **(b)** chondroitin-4-sulphate; **(c)** keratan sulphate: $C_{14}H_{24}NO_{14}S$; and **(d)** hyaloronic acid: $C_{14}H_{22}NO_{11}$. The carboxyl groups (COOH) and the sulphate groups (SO_3H) may shed a proton (gray) and become negatively charged. Adapted from [240].

that binds the GAGs in AC [73, 98, 137, 142]. HA is named after the Greek word for glass 'hyalos (ὕαλος)' and is responsible for ACs 'glassy' (or 'velvet' [152]) look and its alternative name 'hyaline cartilage', e.g. [32, 185, 319]. The carboxyl groups (COOH) and the sulphate groups (SO_3H) in the GAGs are negatively charged (figure 1.3) and this is relevant for AC mechanics.

1.2 Articular cartilage mechanics

The global mechanical response of AC to external (joint) loads is an interaction of various mechanisms (figure 1.4). The chondrocytes play a negligible role for global cartilage mechanics due the small volume that they occupy in combination with their low stiffness compared with the ECM [22, 89, 197, 297]. Each extracellular component (fluid,

PG matrix, collagen) however, contributes to the mechanical behaviour of AC in multiple ways. The porous ECM and the interstitial fluid interact to form a biphasic material [40, 239, 251, 321, 322] with fluid transport described by Darcy's law[1] for flow through a porous medium [44, 249]. The non-collageneous part of the ECM behaves as a viscoelastic (i.e. strain-dependent) and incompressible material [351, 357].

The fixed negative charges in the ECM interact with the fluid to form a Donnan osmosis equilibrium[2] [16, 95, 117]. The fixed (negative) charge density (FCD) in the ECM is higher than the mobile charge density in the surrounding fluid, and thus leads to osmotic pressures that cause swelling of the tissue [206, 335, 350]. Another effect of the negative charges in the ECM is the chemical expansion stress [100, 157, 206, 354]: negative charges that are close together, repel one another. The magnitude of this effect is also affected by the mobile charge density because the mobile charges shield the fixed charges in the ECM [206, 354].

The collagen fibres in AC reinforce the ECM, in a one dimensional way. Because of their slender structure, collagen fibres only transmit mechanical loads in tension [14, 35, 180, 354]. The 1-D mechanical behaviour is viscoelastic (i.e. strain and strain rate dependent, [180, 301, 351]). Collagen fibres also bind fluid and the charges in the bound fluid do not contribute to the mobile charge density [230, 234, 357]. Thus, the collagen fibres indirectly affect osmosis and chemical expansion, because they are both affected by changes in the mobile charge density.

Two interesting macroscopic effects arise from the local interactions of the mechanisms described in the previous paragraphs: the different mechanical behaviour in transients (creep or relaxation) and equilibrium, and the tension-compression non-linearity. During deformation, the external load is first supported by the (incompressible) fluid fraction, and next gradually transmitted to the solid matrix as the fluid is expelled. As a result, huge forces are necessary for instantaneous deformation of AC, or alternatively: large peak forces do not result in large deformations of AC. The fluid phase does not support external loads at equilibrium, when fluid transport has ceased and all loads are transmitted to the solid ECM (figure 1.5).

[1] Darcy's law describes the relationship between the fluid flux through a porous medium, the resistance against this flux (permeability), and the pressure difference that drives the fluid flux. In its general form, Darcy's law is given by $q = -k\,\nabla p$, with q the Darcy flux (i.e. the fluid velocity in $\mathrm{m\,s^{-1}}$), k the hydraulic permeability in $\mathrm{mm^4\,N^{-1}\,s^{-1}}$ and ∇p the pressure gradient in Pa ($\mathrm{N\,m^2}$). In 1-D, this simplifies to $Q = -k\frac{A}{l}\Delta p$, with Q the fluid volume flux in $\mathrm{m^3\,s^{-1}}$, k the hydraulic permeability in $\mathrm{mm^4\,N^{-1}\,s^{-1}}$, A the cross section through which flow occurs in $\mathrm{m^2}$, l the length for the pressure difference in m, and Δp the pressure difference in Pa.

[2] The osmotic pressure gradient in equilibrium for Donnan osmosis is given by

$$\Delta\pi = RT\left(\phi_{\mathrm{int}}\sqrt{{c_F}^2 + 4\frac{\left(\gamma^{\pm}_{\mathrm{ext}}\right)^2}{\left(\gamma^{\pm}_{\mathrm{int}}\right)^2}{c_{\mathrm{ext}}}^2} - 2\phi_{\mathrm{ext}}c_{\mathrm{ext}}\right)$$

With R the universal gas constant, T the absolute temperature, $\phi_{\mathrm{int,ext}}$ [-] the osmotic coefficient for the internal and external ion concentrations, c_F the fixed charge density in $\mathrm{Meq\,ml^{-1}}$, $\gamma^{\pm}_{\mathrm{int,ext}}$ [-] the activity coefficients for the internal and external ion concentrations, and c_{ext} the external ion concentration in $\mathrm{Meq\,ml^{-1}}$. The coefficients $\phi_{\mathrm{int,ext}}$ and $\gamma^{\pm}_{\mathrm{int,ext}}$ are a function of c_F in cartilage [156], and c_F should be expressed with respect to the extra-fibrillar fluid fraction [230, 234, 357].

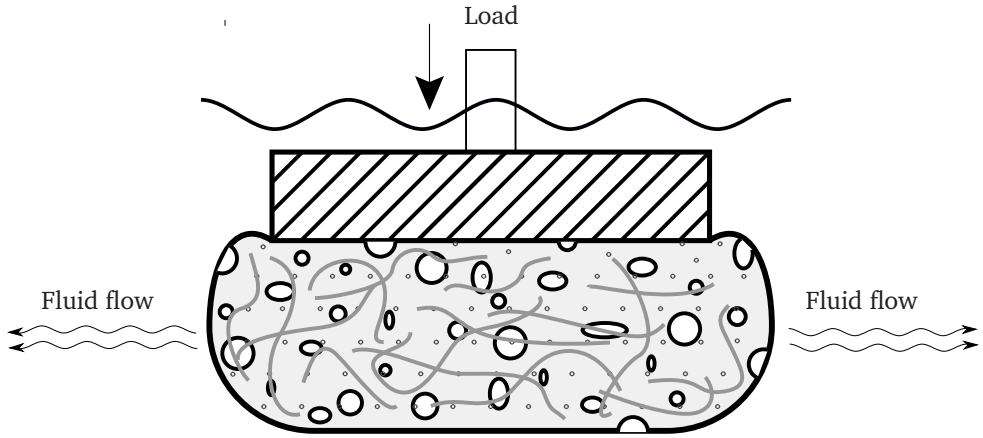

Figure 1.4: Cartoon of articular cartilage mechanics. Articular cartilage behaves as a porous matrix saturated with fluid, much like a sponge (light grey) submerged in water. Fluid flows out of the sponge when a compressive load is applied, and fluid flows into the sponge when the load is released. The collagen fibrils reinforce the matrix (sponge), much like shoe laces embedded in the sponge (dark grey curves). The negative charges in the matrix create an osmosis effect, as if we had dispersed salt (dark dots) in the sponge.

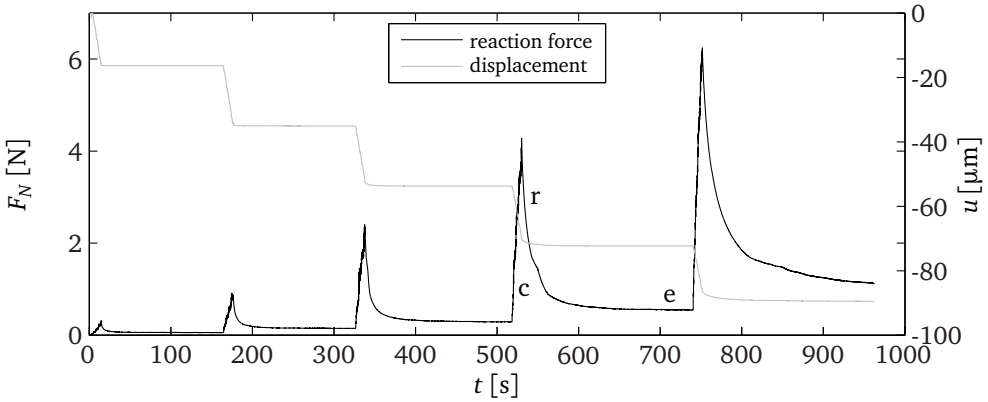

Figure 1.5: Example of macroscopic mechanical behaviour of ovine articular cartilage in indentation (relaxation) as a function of time t. A 1.5 mm diameter indenter is placed at the articular surface and then displaced with u according to the grey curve (right axis). The corresponding reaction force on the indenter F_N is shown as the black curve (left axis). During compression (c), instantaneous load is supported by the incompressible fluid phase, which results in high peak forces that are necessary to achieve the prescribed indenter displacement. During the relaxation phase (r), loads are gradually transferred to the solid matrix and reaction forces decrease at constant indentation. Given enough time, the tissue will reach an equilibrium (e) where the internal and external pressures are in equilibrium with the solid matrix.

The tension-compression non-linearity arises from the interaction of the collagen fibre network with the swelling pressures. The collagen network in unloaded AC counterbalances the internal osmotic pressures in the tissue [26, 30, 231, 233, 235, 248], and the PG matrix and collagen fibres are subjected to tension. Under compressive loading, the amount of tension in ECM is decreased until the external normal stress counterbalances local osmotic pressure. The ECM is subjected to compression with an external load that exceeds the local osmotic pressure. As a result, AC stiffness decreases in compression as the internal tension is first released (strain-softening), and then increases with further compression as the entire tissue becomes subjected to compression (strain-hardening).

Macroscopic deformation of the tissue in turn affects the local mechanical mechanisms. Volume changes of the porous ECM e.g. affect the local composition, and therefore the local contributions and interactions of the mechanical mechanisms. Volume changes also affect the pore size and this is relevant for the transient behaviour of AC [125, 206, 249], e.g. because it affects the resistance against fluid transport (the permeability in Darcy's law, [206, 356]).

1.3 Depth-dependent inhomogeneity and anisotropy of articular cartilage

Adult AC is an inhomogeneous and anisotropic tissue. In particular, differences in AC are observed over the depth of the tissue. Based on its macro-structure, AC is traditionally divided into three layers or zones (figure 1.6): from the articular surface to the tide-mark there is first a thin superficial layer, next a thicker transitional layer, and finally the thickest deep layer [37, 250, 364]. Between these layers there are marked differences, visible with a (polarised) light microscope, in cell volume and morphology [257] and collagen fibril orientation and in anisotropy [37].

Chondrocytes are most abundant in the superficial layer where they appear flattened with their long axis parallel to the articular surface. The transitional layer is characterised by less densely packed and near spherical chondrocytes. Chondrocyte cell count is lowest in the deep layer, but individual cell volume is larger compared with the superficial layer and transitional layer. The chondrocytes in the deep layer are clustered in chondrons, small groups of chondrocytes that share their pericellular matrix. Both the chondrons themselves and the distribution of the chondrons show a column-wise arrangement [120, 150, 162, 208, 226, 255, 310, 367].

The collagen network in the superficial layer is highly anisotropic with collagen fibrils predominantly oriented parallel with the articular surface. The transitional layer shows a low level of anisotropy and collagen fibril orientations appear to be randomly distributed. The collagen network in the deep layer is again highly anisotropic, but with collagen fibrils predominantly oriented perpendicular to the tide-mark. This pattern of collagen fibril organisation is often represented with an arcade-like model known as the 'gothic arc model of Benninghoff' or 'Benninghoff structure'. Collagen content and collagen fibril diameter both increase from articular surface to tide-mark [13, 83, 150, 210, 245, 282, 318, 333].

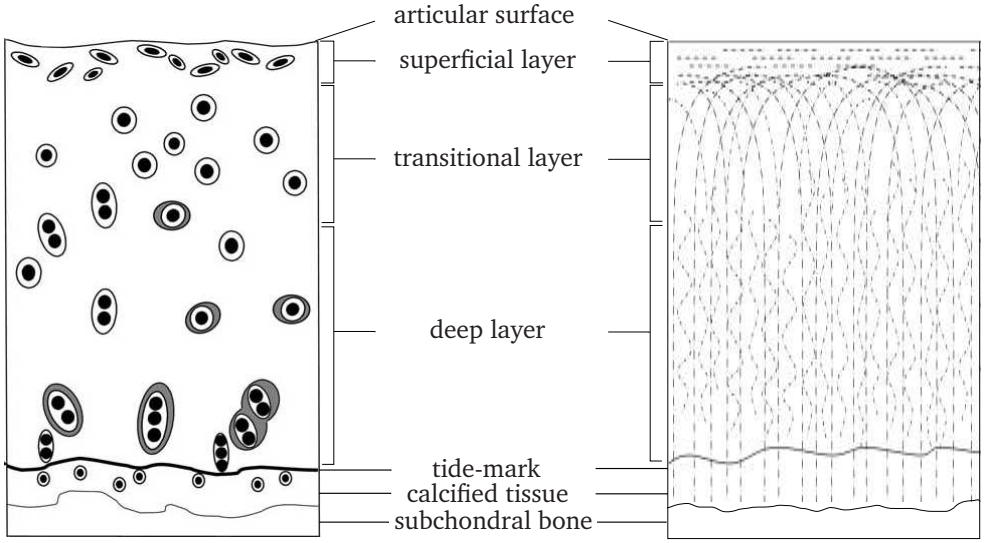

Figure 1.6: Sketch illustrating the layers/zones of articular cartilage: superficial, transitional and deep. The tide-mark is represented by the line that separates the articular cartilage from the calcified tissue and subchondral bone. The illustrations show examples of the depth-dependent cell morphology (left, adapted from [226, figure 1]), and collagen fibril structure (right, adapted from [333, figure 1]). Note that the chondrocytes (left) are not to scale.

The other components (fluid and PGs) also show a depth-dependent distribution. Fluid content (volume/total volume) decreases with distance from the articular surface [38, 221, 294]. PG content increases with distance from the articular surface and PG composition changes over the depth: between surface and bottom, the average PG molecule increases in size, the relative amount of keratan sulphate increases, and the fraction of chondroitin-4-sulphate to chondroitin-6-sulphate decreases [32, 98, 115, 177, 191, 370]. The FCD depends on the relative amounts of the various GAG's and is highest in the deep layer [138, 236, 341].

As a result of these changes in composition and structure, the mechanical behaviour of adult AC also varies over the tissue depth. AC stiffness in compression [74, 78, 103, 204, 293, 343, 372], tension [76] and shear [59, 60], and Poisson ratio [74, 80, 343] all increase with increasing distance from the articular surface. These depth-dependent mechanical properties are thought to be an important functional adaptation for the two main mechanical functions of AC, i.e. load distribution [110, 193, 293] and the establishment of a low friction environment [15, 110, 203, 293]. AC composition and structure may also vary over a joint surface, which is a further functional adaptation to local (mechanical) demands [19, 25, 50, 52, 57, 123, 159, 167, 289, 314].

Because of the depth-dependent mechanical properties of AC, chondrocytes at different depths experience different mechanical environments [75, 130, 198, 343, 359]. The mechanical environment is an essential factor for the functioning of the chondro-

cytes in development and maintenance of the (depth-dependent) tissue composition and structure [23, 70, 113, 126, 151, 222, 279, 306, 315, 317, 320, 337, 359] and experiments have shown that adult chondrocyte properties such as volume, shape and structure [21, 162, 208, 226, 360, 367], metabolism [144, 205, 311], ECM production [7, 20, 21, 90, 360], mechanical properties [89, 90], and response to mechanical stimuli [219, 280], vary over the tissue depth.

1.4 Postnatal changes in articular cartilage

During early development AC functions as a surface growth plate for the underlying bone [9, 139, 154]. Because the skeleton and joints are still developing after birth, AC has to accommodate both developmental and load bearing demands in early postnatal life. This transition in function from growth plate to mechanical support correlates with remarkable changes in the tissue.

The most obvious change is the decrease in thickness of the AC layer [57, 112, 154, 168, 282]. During skeletal growth, AC is absorbed in the deep layer due to the progression of endochondral ossification. AC growth occurs appositionally, i.e. from the articular surface [139, 154]. Postnatal AC becomes thinner because the endochondral ossification is faster than the appositional growth [33, 154]. There is further a decrease in chondrocyte density [139, 162], an increase in collagen density [50, 84, 167, 282, 348] and collagen fibril diameter [84, 107], and a decrease in fluid density [50]. GAG composition also changes: the ratio of chondrondroitin-6-sulphate over chondrondroitin-4-sulphate increases [98, 274] and the keratan sulphate amount increases [8, 346]. Finally, the change from articular cartilage to calcified tissue is not marked by a sharp tide-mark in perinatal animals, but is gradual and may cover a reasonable depth of the tissue.

Most of the depth-dependent characteristics described in the previous section are much less evident or absent at birth. Neonatal AC is generally considered to be a homogeneous tissue [50, 57, 168, 282]. Chondrocyte volume and shape for instance, appear homogeneous in neonatal AC [154, 162, 193, 242, 282], as well as the predominant collagen fibril orientation that is parallel to the articular surface over the entire tissue depth in neonatal AC [6, 168, 282]. The chondrocyte density gradient in neonatal AC, however, is more pronounced in perinatal than in adult AC [139, 154, 162].

1.5 Postnatal development of depth-dependent mechanical properties in articular cartilage

Neonatal AC has a much smaller gradient in mechanical properties over the depth of the tissue, than adult AC [193, 343, 349]. An important function of the depth-dependent postnatal changes in AC is to obtain the functional adult depth-dependent mechanical properties in the tissue. At present, our knowledge on the postnatal development of the depth-dependent mechanical properties is limited. Particularly, the relationships between composition, structure and mechanical behaviour in early postnatal life have

received little attention [69, 167, 193, 349], while these relationships have been extensively investigated for adult AC, e.g. [17, 18, 26, 30, 79, 79, 173, 183, 199, 204, 231, 233, 235, 298, 299, 356, 357, 371].

One of the reasons for our limited knowledge, is a lack of data. The number of experimental studies into the depth-dependent mechanical behaviour of pre-mature AC is small, and these studies [193, 343, 349] measure only a few sample points between birth an maturity. Detailed studies into the postnatal depth-dependent development of AC composition and structure, are also far from abundant. The postnatal development of the collagen network e.g., has only recently started to get some attention [168, 282]. Yet, collagen is the main component of the extracellular matrix and the adult collagen fibril structure has an important role for the depth-dependent properties of AC [17, 170, 218, 298, 354, 355].

This thesis aims to contribute to our knowledge on the postnatal development of the depth-dependent composition, structure and mechanical properties in mammalian articular cartilage. The work combines animal experiments with numerical simulations, and focusses on the role of the collagen network, the most abundant component of the (adult) ECM.

1.6 Outline of this thesis

Collagen structure in AC can be characterised by three parameters: the predominant collagen fibril orientation, collagen density and collagen network anisotropy. Because collagen fibrils are birefringent, polarised light microscopy is the most popular technique ('the gold standard of histology' [4, 363]) to investigate properties of the collagen network in AC. In **chapter 2** we therefore investigate how birefringent structures in general, and collagen structure in AC in particular, affect the parameters that are measured by quantitative polarised light microscopy. In this chapter we quantify the contributions of the three collagen network parameters (orientation, density and anisotropy) to the measured predominant fibril orientation and the measured total tissue birefringence (retardance). We show that collagen network anisotropy can be quantified when the retardance from polarised light microscopy is corrected for collagen densities.

In **chapter 3**, we investigate differences in predominant collagen orientation for equine articular cartilage in stillborn and adult animals with scanning electron microscopy and polarised light microscopy. We confirm and quantify the remark by Archer et al. [6] that the collagen fibrils in perinatal animals lie predominantly parallel to the articular surface, and we confirm and quantify the Benninghoff structure in the mature animals. We further observe a 'transitional' layer in the stillborn animals that is not correlated to changes in predominant collagen fibril orientation as in the adult Benninghoff structure.

Research into postnatal development of equine AC is hindered by limited resources of well defined material. We therefore turn to sheep as model animal in **chapter 4**. In this chapter, we study the collagen structure in 48 sheep divided over ten sample points between birth and maturity (72 weeks of age) with quantitative polarised light microscopy. We confirm the findings in chapter 3 and further map the temporal and spatial patterns of predominant collagen orientation in early postnatal life. The observation of

the transitional layer in the stillborn animals in chapter 3, is reproduced in the perinatal sheep in this study.

The results from chapter 4 are used in **chapter 5** to simulate how postnatal collagen fibril reorientation affects the depth-dependent mechanical properties of articular cartilage with a composition-based finite element model. This chapter describes the mechanical interactions in AC that occur due to postnatal collagen fibril reorientation. It shows that collagen fibril reorientation aids in the establishment of depth-dependent mechanical properties in AC. We observe that depth-dependent changes in collagen fibril strains due to postnatal collagen fibril reorientation correlate with depth-dependent changes in collagen density as reported in literature [282].

In **chapter 6**, we assess collagen density in the same sheep as in chapter 4 with Fourier transform infrared microspectroscopy. We confirm the afore mentioned depth-dependent changes in collagen density from literature [282], and further map the temporal and spatial patterns of collagen density in early postnatal AC. We observe that collagen density shows a valley at the location of the transitional layer for the perinatal animals, and that this valley disappears during early postnatal development.

To investigate interactions in postnatal collagen network development, we implement the results of chapters 2, 4 and 6 in the finite element model in **chapter 7**. We show the different contributions of the three collagen network parameters to the establishment of depth-dependent mechanical properties in AC. Based on the results, we suggest different functional roles for each of the three collagen network parameters: reorientation for depth-dependent mechanical properties, increase in density to limit collagen fibril strains, and anisotropy to limit gradients in the mechanical state for the upper half of the AC tissue.

Finally, in **chapter 8** we provide a synthesis of the results in this thesis. We discuss postnatal collagen network development in relation to the results in this thesis, and in relation to future challenges in postnatal AC development research.

Pi goes on and on and on,
And e *is just as cursed.*
I wonder where do they begin
When their digits are reversed?

Martin Gardner [119]

2

Modelling optical behaviour of birefringent biological tissues for evaluation of quantitative polarised light microscopy

Mark C. van Turnhout[1], Sander Kranenbarg[1] & Johan L. van Leeuwen[1]. *Journal of Biomedical Optics*, **14**(5):054018, September/October 2009. doi: 10.1117/1.3241986

[1]Wageningen University, Experimental Zoology Group, PO Box 338, 6700 AH, Wageningen, The Netherlands.

Abstract

Quantitative polarised light microscopy (qPLM) is a popular tool for the investigation of birefringent architectures in biological tissues. Collagen, the most abundant protein in mammals, is such a birefringent material. Interpretation of results of qPLM in terms of collagen network architecture and anisotropy is challenging, because different collagen networks may yield equal qPLM results.

We created a model and used the linear optical behaviour of collagen to construct a Jones or Mueller matrix for a histological cartilage section in an optical qPLM train. Histological sections of tendon were used to validate the basic assumption of the model. Results show that information about collagen densities is needed for the interpretation of qPLM results in terms of collagen anisotropy. A parameter that is independent of the optical system and that measures collagen fibre anisotropy is introduced, and its physical interpretation is discussed.

With our results, we can quantify which part of different qPLM results is due to differences in collagen densities, and which part is due to changes in the collagen network. Because collagen fibre orientation and anisotropy are important for tissue function, these results can improve the biological and medical relevance of qPLM results.

2.1 Introduction

Collagen is the most abundant protein in mammals [116]. The architecture of the collagen fibre network in various tissues is determined by functional demands on the tissue. Helical collagen architectures are for instance found in cylindrical flexible hydrostats such as the notochord [3, 195], the epidermis of cylindrical animals [85, 272] and the *annulus fibrosus* of intervertebral discs [161, 368]. Helically arranged collagen fibres in chameleon tongues are subject to large deformations and serve to store energy [127, 212]. In contrast, hydrostats that require resistance against bending show an orthogonal collagen architecture [178, 179].

The mechanical environment also plays an important role for the collagen architecture in e.g. cardiovascular structures [24, 124], the intestine [109] and articular cartilage [150, 171, 192]. Functional demands can also be optical. The cornea and sclera both need strength to resist the inner pressure of the eye. Yet we find different collagen architectures in these tissues, because the cornea needs to be transparent and the sclera needs to be totally opaque [46, 241].

Polarised light microscopy (PLM) is a popular technique to evaluate collagen architectures in a variety of biological tissues due to the collagen's (intrinsic) birefringent properties, see e.g. [109, 124, 155, 163, 166, 202, 323, 363]. PLM has further proven itself to be useful for the investigation of e.g. retinal nerve fibre layers [194], the *zona pellucida* [269, 295], meiotic spindles [223] and microtubules [324, 325]. In relation to articular cartilage (AC), PLM has been called 'the gold standard of histology' [4, 363].

In a pioneering PLM study on AC, Benninghoff [37] looked at AC that was positioned between two crossed polarisers. In this setup, anisotropic birefringent architectures appear bright when positioned at $\pm 45^\circ$ with the axis of the polarisers and go extinct when the sample is rotated to $\pm 0^\circ$. Isotropic birefringent architectures and nonbirefringent architectures appear dark when positioned between two crossed polarisers, irrespective of the rotation angle.

With the articular surface of the histological section at $\pm 45^\circ$ with the axis of the polarisers, the superficial zone and deep zone of the AC appear bright and go extinct when the sample is rotated. These zones are separated by a dark transitional zone, which shows little variation in light intensity when the sample is rotated. In these and some additional observations, Benninghoff found an arcade-like architecture with fibres arranged perpendicularly to the tide-mark in the deep zone, fibres that bend away in the transitional zone forming a more or less random architecture, and fibres aligned parallel with the surface in a thin zone at the articular surface. Benninghoff already noted that the arcade architecture serves as a model for the predominant fibre orientation only, a point that has particularly been stressed by scanning electron microscope (SEM) studies, e.g. [83, 328]. But where Benninghoff had to rely on qualitative measurements, advances in PLM now allow a quantitative analysis of PLM (qPLM) results [148, 237, 283, 288].

Birefringence is an intrinsic optical material property of collagen fibres. With qPLM, two parameters that are related to the birefringent architecture can be determined. We will use *retardance* to indicate measured extrinsic optical retardations [4, 148, 262]. This property is sometimes also called optical path difference [13, 187, 265], birefringence intensity [5, 192] or rotation independent birefringence [286]. From retardances

measured with different states of polarised light, we can calculate the *azimuth*. This is the measured predominant orientation of the birefringent structures in the plane of imaging.

Långsjö et al. [211] write that 'further investigations on the role of quantitative PLM in collagen fibre network studies are clearly warranted', and Oldenbourg [261] remarks that: 'The art and science of relating measured retardance and azimuth to structural information [on the molecular level] of the specimen is only in its infancy.' Rieppo et al. [283] remark that retardance alone cannot fully characterise the collagen architecture because it is influenced by both collagen density and the structural anisotropy of the fibre architecture.

To the best of our knowledge, a mathematical model that predicts qPLM results for given collagen structures has not been reported in the literature. Such a model is useful to investigate the merits and limitations of qPLM measurements for certain applications. Because collagen behaves as a linear retarder [61, 149, 163, 194, 196, 202, 228, 324], we can construct the optical effect of a given sample with the same mathematical framework that describes the effect of an optical train.

In the present paper we will use the linear optical behaviour of collagen to construct a Jones or Mueller matrix for a histological cartilage section in an optical qPLM train. We show how the intrinsic optical properties of a birefringent fibre network influence qPLM results, and show how knowledge of fibre densities can help to interpret these results. We will use AC as our example tissue for the interpretation of qPLM results, and tendon to validate the basic assumption of the model.

2.2 Methods

We simulated the effect of the LC-PolScope system for quantitative PLM [259, 261] for given collagen architectures. We used Jones calculus [165] to numerically simulate the intensity of the light on the camera as a result of the optical train and the sample therein, see section 'Simulation of optical train'. This was done with different polarisation states of the incident light on the sample, which resulted in different (simulated) light intensities. Next, we analysed these intensities as implemented in the LC-PolScope system [300] to evaluate the effects of different collagen architectures.

The angles we used to define the collagen architectures will be denoted by φ and the birefringence of a single fibre with unit density is δ. Simulated or measured retardance will be Δ and simulated or measured predominant fibre orientation will be ϕ.

We considered light that passes a sample of unit thickness with fibres of unit length and equal intrinsic birefringence. We were interested in the height-dependent collagen architecture from tide-mark to articular surface, or $0 \leq h \leq 1$ with h the normalised dimensionless cartilage height. The procedures described below were implemented in Matlab (version 7.6 R2008a, The MathWorks, Inc., 1984-2005) and Octave (version 3.0.1, www.octave.org, 2009).

2.2.1 Simulation of optical train and sample

We can simulate the optical train either with Jones calculus, or Mueller matrices and Stokes vectors. Solutions of the two methods are equal in the case of fully polarised light [86, 140]. We present the Jones calculus in this section and collect the corresponding Mueller matrices in the appendix. For each optical element in an optical train, Jones [165] defines two matrices. The orientation of the element is described by a rotation matrix R that depends on orientation angle θ as:

$$R(\theta) = \begin{bmatrix} \cos\theta & -\sin\theta \\ \sin\theta & \cos\theta \end{bmatrix} \tag{2.1}$$

The orientation-independent effect is described by a diagonal matrix N:

$$N = \begin{bmatrix} N_x & 0 \\ 0 & N_y \end{bmatrix} \tag{2.2}$$

Matrices N for an ideal polariser N_P and an ideal retarder N_R with retardance ε are given by

$$N_P = \begin{bmatrix} 1 & 0 \\ 0 & 0 \end{bmatrix}, \quad N_R(\varepsilon) = \begin{bmatrix} e^{-i\frac{\varepsilon}{2}} & 0 \\ 0 & e^{i\frac{\varepsilon}{2}} \end{bmatrix} \tag{2.3}$$

The total effect of the element can then be written as

$$M(\theta, \varepsilon) = R(\theta)N(\varepsilon)R(-\theta) \tag{2.4}$$

In the polarisation microscope we investigate, light passes a linear polariser P, a quarter wave plate Q, the sample S, two liquid crystals or variable retardance plates L_b and L_a and finally a linear analyser A, see figure 2.1. With J_0 the vector of the (unpolarised) incident light, the description of the light that reaches the camera J is given by

$$J = A \cdot L_a \cdot L_b \cdot S \cdot Q \cdot P \cdot J_0 \tag{2.5}$$

with the characteristics (rotation, retardation) as gathered in table 2.1. Note that the liquid crystals L_a and L_b apply a retardance of α and β respectively, values that are set by the analysis software.

The sample is composed of N_f collagen fibres that are modelled as ideal linear retarders. To find the matrix S for the sample we therefore calculate for N_f fibre directions

$$S = \prod_{n=1}^{N_f} R(\varphi(n)) \begin{bmatrix} e^{-i\frac{\eta(n)\delta}{2}} & 0 \\ 0 & e^{i\frac{\eta(n)\delta}{2}} \end{bmatrix} R(-\varphi(n)) \tag{2.6}$$

with $\varphi(n)$ the angle, $\eta(n)$ the (relative) collagen density in the n^{th} direction, and δ the birefringence of a single fibre with unit density.

In our simulations and analysis, we use the five-frame algorithm as described by Shribak and Oldenbourg [300]. Thus, we simulate five intensities with five settings

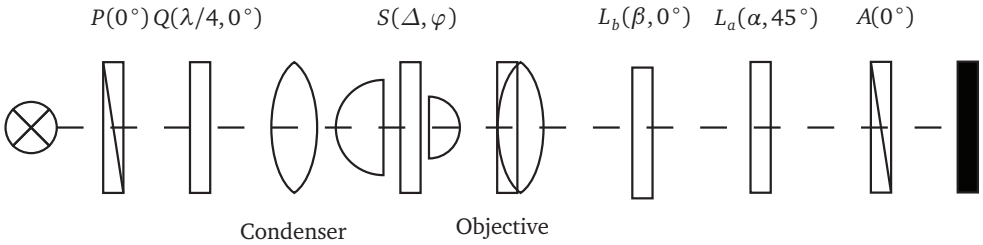

Figure 2.1: Optical train of the polarisation microscope, adapted from Shribak and Oldenbourg [300, figure 1b]. Light passes a linear polariser P, a quarter wave plate Q, the sample S, two liquid crystals or variable retardance plates L_b and L_a and finally a linear analyser A.

Table 2.1: Characteristics of the standard elements in the optical train.

element	type	variables
P	polariser	$\theta = 0$
Q	retarder	$\theta = 0$, $\varepsilon = \frac{\pi}{2}$
L_b	retarder	$\theta = 0$, $\varepsilon = \beta$
L_a	retarder	$\theta = \frac{\pi}{4}$, $\varepsilon = \alpha$
A	polariser	$\theta = 0$

for the liquid crystals (α and β). The analytical solution for the intensity in a pixel in this (ideal) system is:

$$I = \frac{I_0}{4}\left[1 + \cos\alpha \sin\Delta \sin 2\phi - \sin\alpha \left(\sin\beta \sin\Delta \cos 2\phi - \cos\beta \cos\Delta\right)\right] \tag{2.7}$$

With I_0 the intensity of the incident unpolarised light, ϕ the effective azimuth and Δ the effective retardance of the sample. With the five intensities we can eliminate the unknowns and find analytical expressions for ϕ and Δ as a function of the intensities [300, equation 20].

2.2.2 Collagen fibre network

We used two collagen networks for the simulations: a Benninghoff network and a gothic network. The networks were assumed uniform over the width (and thickness) of the sample, so we could use 1-D patterns for our examples. The first collagen fibre network was inspired by the Benninghoff model and modelled with an arcade. At the tide-mark, fibres are aligned perpendicularly to the tide-mark, and at the articular surface fibres are aligned parallel with the surface. We described this Benninghoff network with two

height-dependent angles φ:

$$\varphi_{1,2} = 90^\circ \pm \operatorname{atan}\left(\frac{h}{a\sqrt{1-h^2}}\right) \tag{2.8}$$

with $a = 1.2$. For the second collagen fibre network we also let fibres start perpendicular to the tide-mark, and use a linear angle definition for $\varphi_{1,2}$:

$$\varphi_{1,2} = 90^\circ \pm bh \tag{2.9}$$

with $b = 58.44^\circ$. Fibre orientations for these 2-D networks are shown in figure 2.2.

For 3-D networks, we need to project the collagen fibre onto the plane of imaging. A fibre that is defined in the plane of imaging with angle φ and density ρ and rotated out of this plane around an axis in the direction of the height of the sample will have projected angles

$$\varphi_p = \operatorname{atan}\left(\frac{\tan\varphi}{\cos\gamma}\right) \tag{2.10}$$

and projected density

$$\rho_p = \rho\sqrt{\cos^2\varphi\sin^2\gamma + \sin^2\varphi} \tag{2.11}$$

with γ the angle of rotation. This illustrated in figure 2.3.

We used two Benninghoff arcades to model 3-D networks for the simulations. In the simulations, we first used one Benninghoff arcade in the plane of imaging (as in the 2-D simulations) and a second Benninghoff arcade that is rotated out of the plane of imaging over three angles: 0°, 45°, and 90° . Second, we used a fixed network with two Benninghoff arcades with an angle of 45° between them, and rotated the plane of imaging over three angles: 0°, 45°, and 90°. When the plane of imaging is at 0°, one arcade is rotated over 22.5° and one arcade is rotated over -22.5° compared with the plane of imaging.

The Benninghoff network represents predominant fibre orientations only. Therefore, we introduced a second fibre network to model a random (macroscopically isotropic) fibre network. This is a 'zero retardance background' network that by definition does not influence the analysed azimuth values. Such a zero retardance network can be modelled with only two fibres in the plane of imaging that are perpendicular to each other. In our analysis we chose to define two angles for this network: 45° and 135°. A profile for the height-dependent distribution of collagen density in AC was taken from Venn and Maroudas [341] and scaled to have a maximum of unity. This profile is described by:

$$\rho_t(h) = 1.37h^2 - 1.49h + 1 \tag{2.12}$$

and is shown in figure 2.4.

Collagen density (equation 2.12) is divided over two networks, and within the networks over individual fibres. With V the fraction of the total projected collagen density

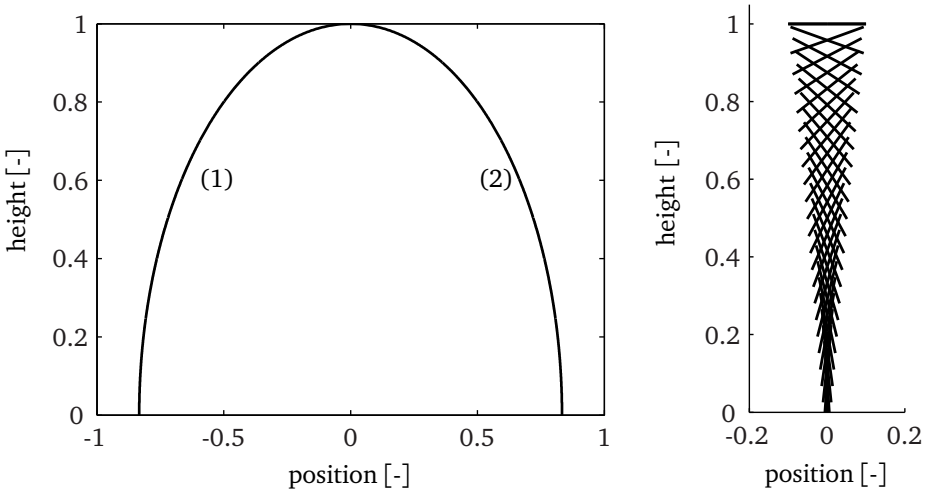

(a)

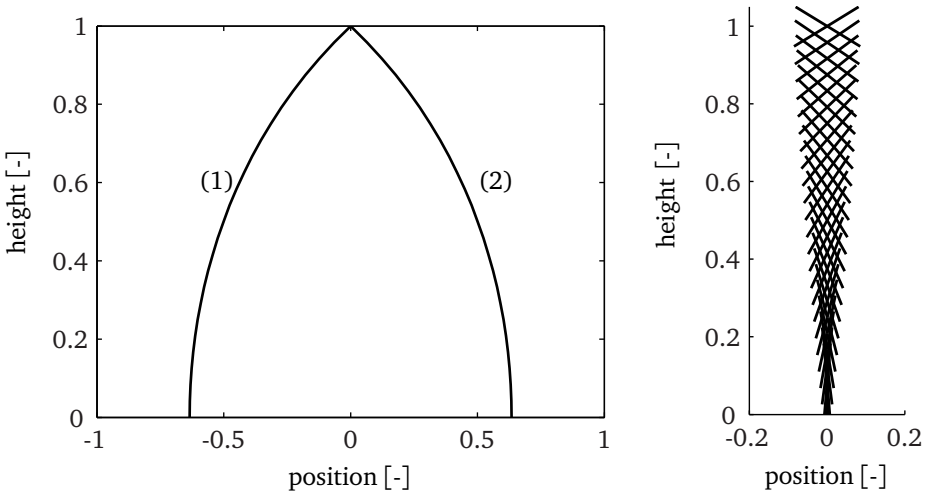

(b)

Figure 2.2: Collagen networks used in the simulations. Left: arcades described by two fibres (1,2) as a function of normalised height. Right: orientations for the two fibres in a series of points over the normalised height. With **(a)** Benninghoff network.; and **(b)** Gothic network.

ρ_p that is represented by the Benninghoff network, we can write for individual fibres:

$$\eta_1(h) = \frac{\rho_p(h)}{n_{f_1}} V(h) \tag{2.13}$$

$$\eta_2(h) = \frac{\rho_p(h)}{n_{f_2}} (1 - V(h)) \tag{2.14}$$

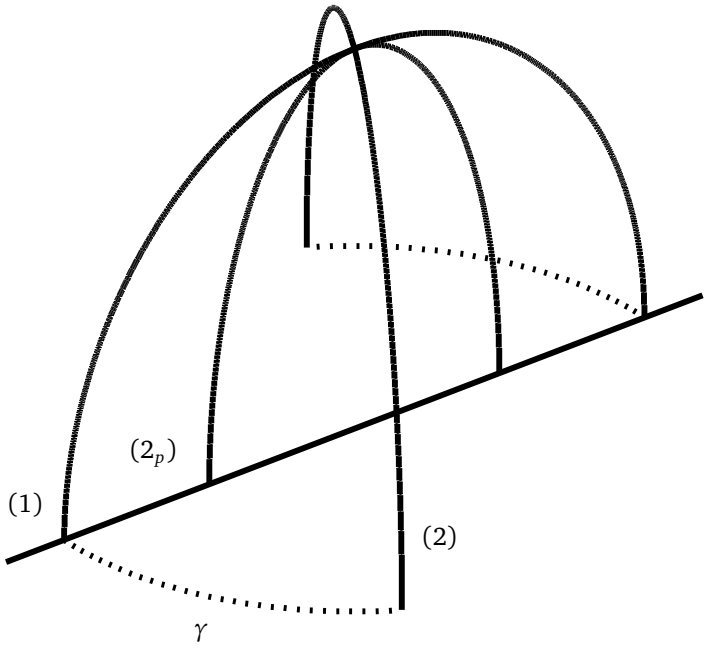

Figure 2.3: For 3-D networks, we project fibres onto the plane of imaging. The arcade that is defined in the plane of imaging (1) is rotated over angle γ out of the plane of imaging to give arcade (2). To analyse this arcade, we project it onto the plane of imaging, arcade (2_p).

Where η_1 represents relative collagen density for n_{f_1} individual orientations in the Benninghoff network, and η_2 represents relative collagen density for n_{f_2} individual orientations in the zero retardance network.

2.2.3 Experimental validation

To validate the basic assumption in the modelling of the sample, we performed experiments with sheep tendon. We tested in 2-D whether we could predict retardance and azimuth results for a known simple network that we constructed with tendon. This experiment tests the linear optical behaviour of collagen fibres.

Sheep tendon (superficial sesamoidean ligament and deep flexor tendon) was isolated and cut to a length of 5 cm. Isolated tendon was stretched on a small board with screws at 0.5 cm of the tendon endings. The board with stretched tendon was fixated at 4 °C in formalin (4 % in PBS overnight followed by 1 % in PBS overnight), washed four times in PBS and infiltrated with sucrose (20 % in PBS) overnight, and snap frozen in *n*-pentane. Frozen tendon was removed from the board and stored at -20 °C. Transverse sections

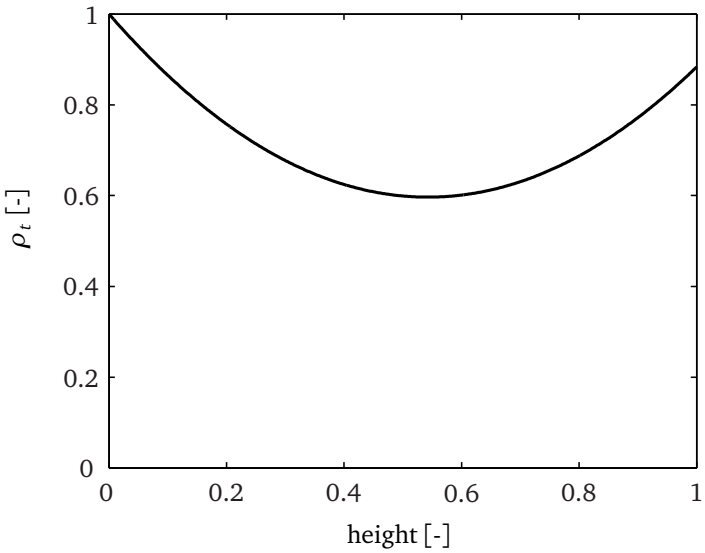

Figure 2.4: Profile for collagen density as function of dimensionless height. Adapted from Venn and Maroudas [341] and scaled to have a maximum of one.

(thickness 6 μm) were cut on a cryostat, put on a microscopy glass with a cover glass and mounted with aquamount.

Mounted tendon sections were analysed with the LC-PolScope system for qPLM [259, 261]. Images were obtained with a Zeiss Axiovert 200M microscope at a 20x/1x magnification, equipped with a Q-imaging monochrome HR Retiga EX 1350 camera. Recorded intensity images had a resolution of $0.62 \times 0.62\,\mu m^2$/pixel and were stored in 8 bit TIFF format. We used the five-frame setting with background correction as described by Shribak and Oldenbourg [300] with a swing of 0.1 [-]. The recorded images were analysed for predominant collagen fibril orientation and tissue retardance with custom written scripts implemented in Matlab (version 7.6 R2008a, The MathWorks, Inc., 1984-2005).

Two glasses with tendon were placed on top of each other and three image stacks were recorded: one with the lower tendon in focus, one with the upper tendon in focus, and one with focus between the two tendons. Images were analysed for average retardance and azimuth in a $50 \times 50\,\text{pixel}^2$ box in three positions: one for each tendon where there is no overlap with the other tendon, and one where the tendons overlap. We used the mathematical model with one point and two fibres to model the retardance Δ and azimuth ϕ for the position where the tendons overlap. Each tendon was represented by a collagen fibre with unit density, and birefringence δ and azimuth φ as measured in the nonoverlapping position. Predictions of the model were compared with the measured results at the position of overlap.

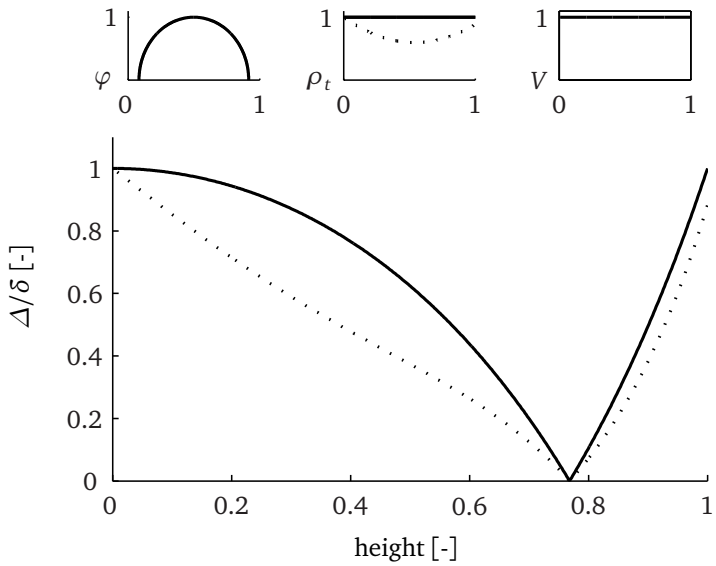

Figure 2.5: Retardance patterns (main panel) for two simulations with the Benninghoff network (top left panel), with collagen density (top middle panel) set to unity (solid) or adapted from Venn and Maroudas [341] (dashed) and V (top right panel) set to unity. Horizontal axes in the panels represent cartilage height as in the main panel.

2.3 Results

2.3.1 2-D retardance

Figure 2.5 displays the results for two analyses with the Benninghoff network only ($V = 1$) and two collagen density profiles. Retardance is zero for both analyses at the point where the two fibres that form the arcade are perpendicular to each other. This happens at $h = \sqrt{a^2/(1+a^2)}$ in our example, i.e. with $a = 1.2$ at $h = 0.77$. With collagen density set to unity, we find the maximum possible retardance $\Delta/\delta = 1$ at the points where the two fibres that form the arcade are parallel to each other: in our example at $h = 0$ and $h = 1$. With both collagen density and V set to unity, the retardance pattern represents the effects of collagen orientation only. With the nonconstant collagen density profile, we find that maximum possible retardance Δ/δ no longer equals 1, but that $\Delta/\delta \leq \rho_t$ because $\Delta_{\rho=\rho_t} = \rho_t \Delta_{\rho=1}$. Retardance in this pattern therefore represents effects of both collagen orientation and collagen density. Note that total collagen density is divided over two fibres and that therefore each fibre has a relative density of $\rho_t/2$.

The effect of parameter V is illustrated in figure 2.6. This shows the retardance pattern for the gothic network with collagen density and V set to unity, and a retardance pattern for the Benninghoff network with collagen density set to unity and V a function of height. We note two things: first, that the effect of V on the retardance pattern is equal to that of ρ_t: $\Delta_{V=V(h)} = V(h)\Delta_{V=1}$; and second, that different collagen networks can result in

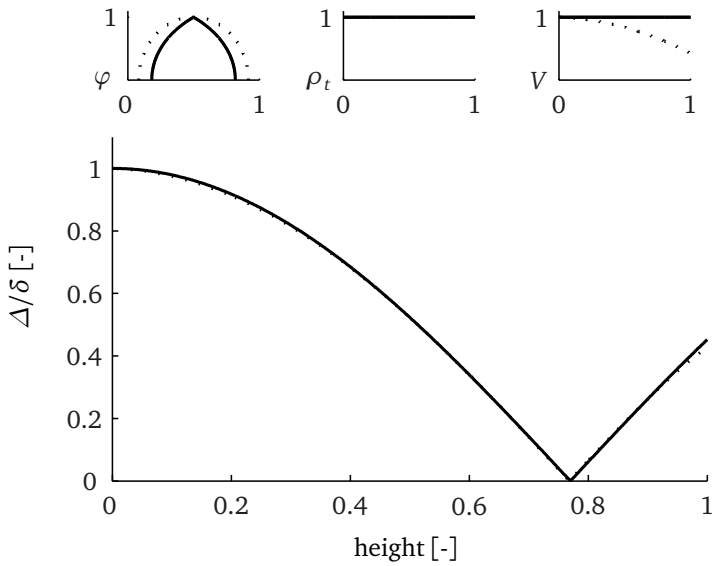

Figure 2.6: Two collagen networks with equal retardance results. Solid: gothic network (top left panel) with collagen density (top middle panel) and V (top right panel) set to unity. Dashed: Benninghoff network (top left panel) with collagen density (top middle panel) set to unity and values for V (top right panel) that result in the retardance pattern we observed for the gothic network (solid). Horizontal axes in the panels represent cartilage height as in the main panel.

equal retardance patterns.

2.3.2 2-D azimuth

Figure 2.7 shows the azimuth results for the 2-D simulations. Because of our choices for the definitions of the two networks, these results are the same for all 2-D simulations. The figure further shows that analysed azimuth does not change when total collagen density is adopted, or when more or less collagen is associated with the zero retardance background network (decreasing V).

2.3.3 3-D simulations

Figure 2.8 shows the results for simulations with one Benninghoff arcade in the plane of imaging (as in the 2-D simulations) and one arcade rotated out of the plane of imaging over three angles: 0°, 45°, and 90°. With both arcades in the plane of imaging, the results are equal to those from the 2-D simulations with collagen density and V set to unity (see figures 2.5 and 2.7). When an arcade is rotated out of the plane of imaging, we see that the point where the (projected) network behaves as isotropic, i.e. where retardance is zero and where analysed azimuth changes from 90° to 180°, shifts toward

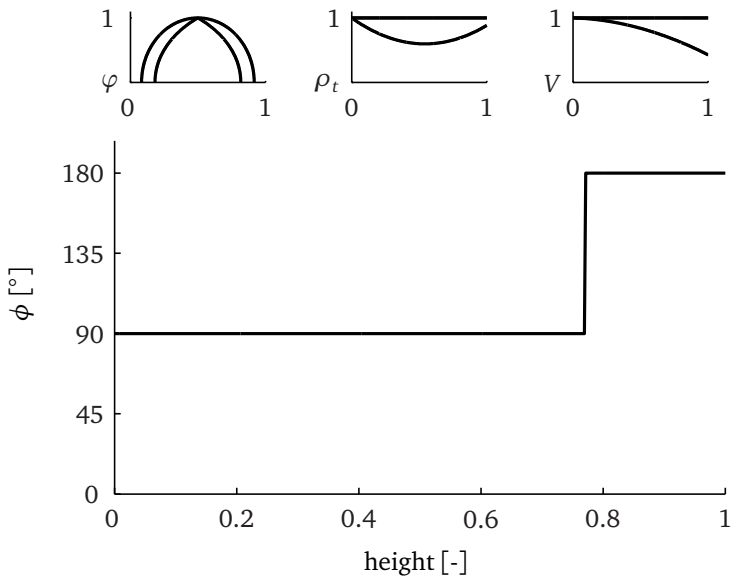

Figure 2.7: Azimuth results for the 2-D simulations. Azimuth (main panel) is 90° for $h < 0.77$ and 180° elsewhere for each combination of Benninghoff or gothic network (top left panel) with constant or height-dependent collagen density (top middle panel) and with constant or height-dependent V (top right panel). Horizontal axes in the panels represent cartilage height as in the main panel.

$h = 1$. Retardance near $h = 1$ becomes smaller as the second fibre is rotated more out of the plane of imaging. Note that total collagen density is now divided over four fibres and that therefore each fibre has a relative density of $\rho_t/4$.

In figure 2.9 we look at a single 3-D network with three different orientations of the plane of imaging: 0°, 45°, and 90°. When this network is viewed from the top, there is a predominant direction and the plane of imaging at 0° is in the direction of this predominant direction. When the plane of imaging is rotated away from the predominant direction (0°), we see that the point where the (projected) network behaves as isotropic, i.e. where retardance is zero and where analysed azimuth changes from 90° to 180°, shifts toward $h = 1$. Retardance near $h = 1$ becomes smaller as the plane of imaging is rotated further compared with the predominant direction (0°).

2.3.4 Experimental validation

For the experiments, results of three images with different focus were compared for each combination of two tendon sections. We checked whether the exact location of the 50x50 pixel^2 box or the size of the box influenced the results. There were no notable differences between choices of focus, boxes that were moved over the tendons or size of the box. We decided to present the data from the image that has the focus between the

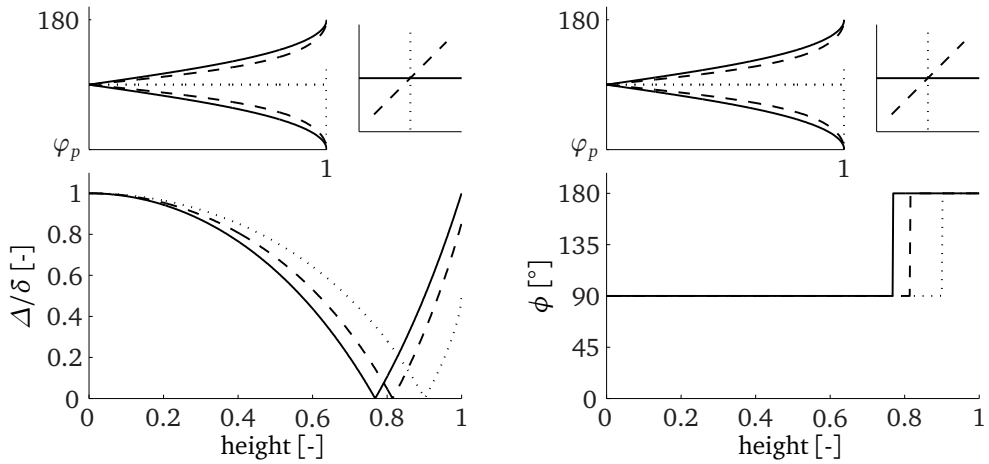

Figure 2.8: Results for three 3-D networks with two Benninghoff arcades. Left: retardance; right: azimuth. One arcade (solid) is in the plane of imaging, the second arcade is rotated out the plane of imaging over 0° (solid), 45° (dashed), and 90° (dotted). Top left panels: projected fibril angles for the rotated fibres ($0 \leq h \leq 1$, $0° \leq \varphi_p \leq 180°$). Top right panels: top view of the networks where the solid line represents one arcade in the plane of imaging.

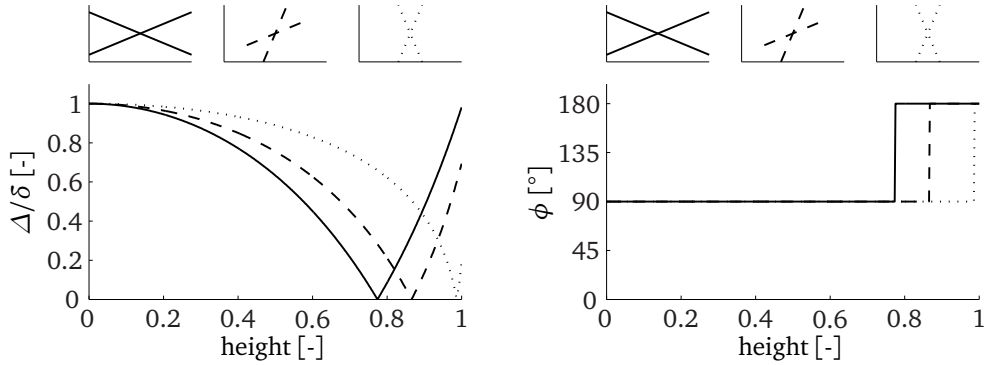

Figure 2.9: Results for a 3-D network with two Benninghoff arcades. Left: retardance; right: azimuth. Top panels show a top view of the two arcades in the networks, where the plane of imaging is represented by the horizontal.

two sections.

Figure 2.10 shows a representative image with focus between two tendon sections and the boxes that were used for the analysis. Results for four combinations with two sections are collected in table 2.2. The predictions for the azimuth of the combinations of tendons are excellent. The predictions for the retardance of the combinations of tendons differ approximately 10 % from the measurements.

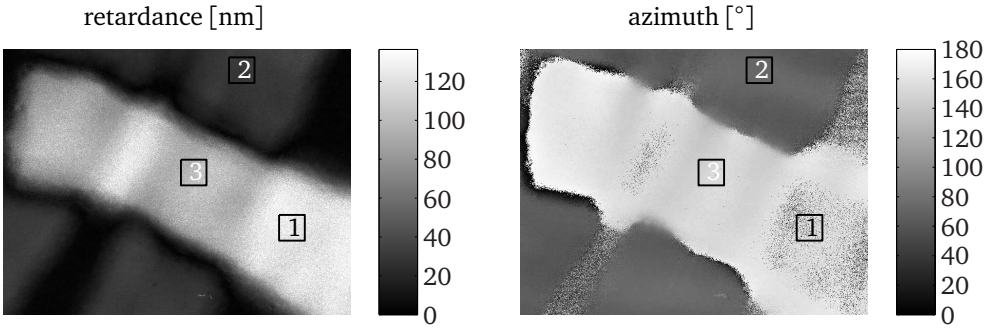

Figure 2.10: Example of qPLM results with two tendons on top of each other. Average retardance (left) and azimuth (right) for the squares labeled 1 and 2 (single tendon only) were used to predict the average results in the square labeled 3. Predicted results were compared with the measurement in square 3. Boxes measure $50 \times 50\,\text{pixel}^2 = 31 \times 31\,\mu\text{m}^2$.

Table 2.2: Results for the tendon experiments. Four combinations of two tendons each were analysed with qPLM. Results for single tendons (columns 2 and 3) were used to predict the experimental outcome of the combination of the two tendons. The experimental outcome is in column 4, the model prediction is given in column 5. Results for azimuth are on top in the table, results for retardance are at the bottom in the table.

	tendon 1	tendon 2	tendon 1&2	prediction
azimuth [°]				
combination 1	156	73	152	153
combination 2	161	86	158	157
combination 3	81	1.2	77	73
combination 4	178	118	122	124
retardance [nm]				
combination 1	124	30	100	95
combination 2	129	23	99	110
combination 3	122	54	83	72
combination 4	54	118	103	95

2.4 Discussion

It is well known that collagen fibre anisotropy and collagen density influence qPLM results, e.g. [5, 13, 192, 211, 363]. In the 2-D simulations in the theoretical part of this paper, we wrote collagen orientation as the sum of two networks: one representing the predominant orientations, and one representing an isotropic network that does not influence the azimuth results and has a retardance of zero. Total collagen density ρ_t was divided over these two networks: $\rho_t V$ for the predominant orientations, and $\rho_t(1-V)$ for the isotropic network. Results are determined only by collagen in the predominant network, with relative density $\rho_t V$. This explains why the effect of decreasing total collagen density ρ_t with a certain factor equals the effect of decreasing the (relative) amount of collagen in the predominant network V. Interpretation between ρ_t and V differs however. Total collagen density ρ_t is a parameter with physical meaning that can be measured outside qPLM. V is the fraction of total collagen that contributes to qPLM results: when collagen is present but fully incorporated in an isotropic network, we use physical values for ρ_t with $V = 0$ and arrive at the correct results.

The 2-D simulations further stress that different collagen networks can give equal qPLM results. Reconstruction of the collagen network from qPLM results is therefore not possible. Without information about collagen densities, the best we can do is to interpret azimuth results as a predominant orientation $\phi(h)$ and the retardance $\Delta(h)$ as a measure for the amount of collagen associated with this predominant angle. When collagen densities are known, we can do better. The retardance $\Delta(h)$ associated with a certain angle divided by the total amount of collagen $\rho_t(h)$ can be interpreted as a measure of network anisotropy: $\Delta/\rho_t = V$. When $V = 1$, we measure maximum possible retardance for the given amount of collagen which means that anisotropy is maximum and all fibres are oriented parallel. For $V = 0$ (when $\Delta = 0$), there is no collagen associated with the measured predominant direction, which means that we are looking at isotropic fibre orientations.

We illustrate this with results on cartilage retardance and collagen densities presented by Rieppo et al. for immature pigs (4 months old) and mature pigs (21 months old) [282, figure 6]. Collagen content increases from the immature sections to the mature sections. If the organisation of the collagen network in the mature section is equal to that of the collagen network in the immature section, retardance will scale directly with collagen content. If a collagen network is added that is more anisotropic than the immature network, retardance will increase more. If a collagen network is added that is less anisotropic than the immature network, retardance will increase less. At the articular surface, collagen content increases 40 % from 0.13 [-] for the immature pigs to 0.22 [-] for the mature pigs and retardance increases 20 % from $0.38{\cdot}10^{-3}$ [-] for the immature pigs to $0.48{\cdot}10^{-3}$ [-] for the mature pigs. Thus, the mature network is less anisotropic than the immature network. In terms of the model, the fraction of collagen that is associated with the predominant orientation, V, is smaller. At a distance of 800 µm from the articular surface collagen content increases with 45 % from 0.2 [-] for the immature pigs to 0.37 [-] for the mature pigs and retardance increases 70 % from $0.6{\cdot}10^{-3}$ [-] for the immature pigs to $2{\cdot}10^{-3}$ [-] for the mature pigs. Thus, the mature network is more anisotropic than the immature network. In terms of the model, the

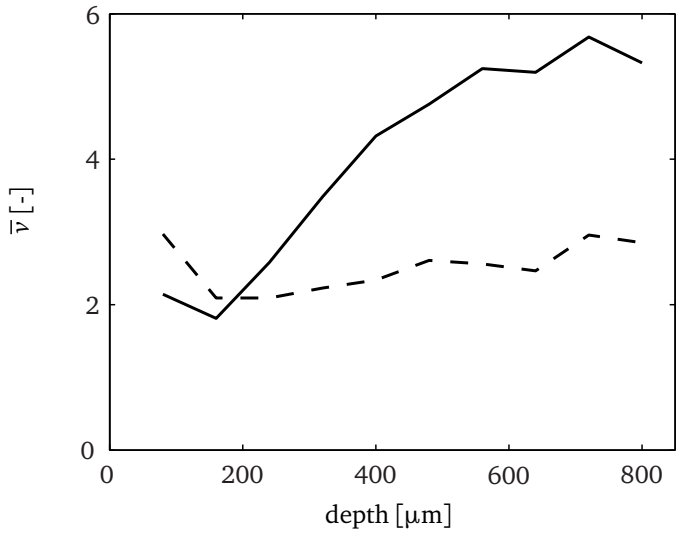

Figure 2.11: Measure for the fraction collagen associated with predominant orientation as a function of distance from the articular surface. Calculated from results presented by Rieppo et al. [282, figure 6]. Solid: results for a 21 months old pig; dashed: results for a 4 months old pig.

fraction of collagen that is associated with the predominant orientation, V, is larger.

Figure 2.11 shows $\overline{\nu} = 1000 \cdot (\text{retardance})/(\text{collagen content})$ for the data of Rieppo et al. [282] as a function of distance from the articular surface. This $\overline{\nu}$ differs from V by a scaling factor: $\overline{\nu} = \kappa V$. In the theoretical part of the study, we knew the birefringence per amount of collagen: $\delta = \pi/180$ per collagen fibre with unit density. We already scaled the retardance patterns with δ in the section 2.3. The factor κ represents the practical version of δ: birefringence per gram of fully anisotropic collagen, for instance. Because such information is not yet available, we cannot directly interpret $\overline{\nu}$ as a fraction of the collagen. We can however, compare values of $\overline{\nu}$ and say that at the articular surface, the fraction of collagen associated with the predominant orientation decreases with 40 % from $\overline{\nu} = 3$ for the immature pigs to $\overline{\nu} = 2.1$ for the mature pigs. At a distance of 800 μm from the articular surface, the fraction of collagen associated with the predominant orientation increases with 46 % from $\overline{\nu} = 2.9$ for the immature pigs to $\overline{\nu} = 5.3$ for the mature pigs. An increase of collagen network anisotropy near the tide-mark from immature to mature cartilage, is in line with SEM results on equine AC [328].

In another study, Rieppo et al. proposed three parameters as a measure for fibre parallelism [283]. Their microscope uses crossed polarisers between which the sample is rotated. The minimum light intensity that is observed when the sample is rotated is used for each of the three parallelism parameters. We cannot measure this minimum light intensity with our microscope, and therefore cannot use the methods proposed by Rieppo

et al. to present information on fibre parallelism. Calculation of $\overline{\nu}$ is independent of the microscope used, but does need information about collagen densities.

3-D simulations illustrate that qPLM information remains in principle 2D: only collagen in the plane of imaging contributes to the results. A collagen network that is not invariant to the plane of cutting, will give different results depending on the orientation of the cutting plane. This was experimentally shown by Király et al. [187]. Superficial split line patterns indicate the predominant orientation of collagen fibres in the most superficial cartilage layer across the articular surface. Király et al. found that sections cut perpendicular to these split lines showed decreased retardance in the superficial zone compared with sections cut parallel to the superficial split lines. This is illustrated in figure 2.9 with the dotted lines (perpendicular) and solid lines (parallel). Also, rotation of the section away from the parallel orientation shifts the position where the collagen network is isotropic in the plane of imaging toward the articular surface.

It is well known that measured retardance is a function of both collagen anisotropy and collagen density, e.g. [5, 13, 192, 211, 363]. Retardance measurements can explicitly be used to indicate the amount of birefringent material, e.g. [148, 260, 324]. The linear relationship between density of birefringent material and tissue retardance has been described for a variety of tissues [149, 163, 194, 196, 202, 228, 324] and the results presented by Bueno and Jaronski [61] suggest that collagen is indeed a linear retarder. Also, the linear relationship between collagen density and measured retardance is implicitly assumed when observed retardances are scaled with sample thickness [148, 211, 254, 262] and experimentally observed in the linear relationship between retardance and sample thickness [187, 269]. Our experiments with tendon confirm this: both retardance and azimuth of combinations of different amounts of birefringent material forming different simple networks can be predicted by the model using linear optical behaviour for collagen.

When Rieppo et al. [283] report that within a histological section of AC, collagen density and retardance need not be linearly related with each other, this is due to the influence of fibre anisotropy that varies over the section. This is e.g. illustrated in figures 2.5 and 2.6 where collagen density is constant but retardance varies due to collagen network variations. When the thickness of a histological section is increased, measured retardance will increase linearly with thickness only when it is safe to assume that collagen architecture and density are uniform over the thickness of the section [36, 187, 269].

Within a sample, relevant differences in collagen density can exist. In our example, adopted from the literature [341], the minimum collagen density is approximately 60 % of the maximum. Such profiles can explain why several authors report an increase in retardance toward the tide-mark where collagen density is highest [13]. If we want to evaluate the difference in retardance in terms of collagen network anisotropy, this difference in density should be taken into account. Also, comparison of absolute retardances in terms of collagen anisotropy between samples (particularly of different origin: age, species, joint, pathology, etc.) may prove seriously impaired by a lack of knowledge on the collagen density profiles. The example with the data from Rieppo et al. [282] shows that we need collagen densities to evaluate what part of the changed retardance between the immature and mature pigs is due to the increase in collagen density, and what part is due to collagen network remodelling.

Whether collagen density profiles need to be taken into account, depends on the application for the qPLM analysis and the desired interpretation of the results. Traditional zone estimation based on retardance [150, 171, 192, 289, 366], does not need to suffer from collagen density effects, as long as collagen density is relatively constant in the upper half of the tissue and sections are cut parallel to the superficial split lines. This is the case with the density profile shown in this work. Also, we would have to assume a very unrealistic pattern to explain the lack of retardance in the transitional zone by collagen density alone.

In this paper we have chosen to concentrate on the relation between collagen orientation, anisotropy and density and qPLM results. Other components of AC tissue have therefore been neglected, although the proteoglycan molecules are known to contribute to the measured retardance [187], for instance through the mechanism of form birefringence [13, 36, 305]. We have furthermore assumed that all collagen fibres share the same birefringence δ. This is a crude, but for now necessary, modelling step. For instance, collagen fibre diameter influences its birefringence [150, 363] and is reported to be depth dependent [13, 210, 318]. But little or no quantitative information about the possible influence on measured retardance is known, and we therefore decided to keep these simulations simple.

These effects, e.g. form birefringence and depth-dependent birefringence, can be incorporated in equation 2.6 as more information becomes available. Furthermore, the relationship between collagen architecture, anisotropy and density and retardance and azimuth we present here is directly applicable to all forms of qPLM [237, 283, 286, 288].

2.5 Conclusions

With the simulations we attempt a quantification of the actual architecture of the birefringent material, e.g. collagen in AC. We confirm that the problem is undetermined when one looks for a unique collagen architecture that describes certain qPLM results. Because we can only measure the projection of 3-D orientations onto the plane of imaging, qPLM results and their interpretation will always be limited to the 2-D plane of imaging.

Knowledge of collagen densities can greatly facilitate the interpretation of qPLM results in terms of collagen orientation and anisotropy. Correction of retardances for collagen densities will provide a better structural interpretation of qPLM results. By writing the collagen network as the sum of an anisotropic network with a single predominant orientation and an isotropic network, we have arrived at a parameter $\overline{\nu} = \kappa V$ that has physical meaning and can be seen as a measure for collagen anisotropy. Retardance is a measure for the absolute amount of collagen that can be associated with the predominant orientation; $V = \Delta/\rho$ measures the fraction of collagen that can be associated with the predominant orientation; and $1 - V$ measures the fraction of collagen that can be associated with an isotropic network.

Research into the relationship between collagen architecture and tissue function on the basis of qPLM results alone, is still subject to arbitrary choices of the representation of the 'true' collagen fibre network. Further advances can be modelled with this framework

when we learn more about single fibre birefringence and its relation to collagen fibre diameter.

Acknowledgements

We kindly thank prof. Rudolf Oldenbourg at the Marine Biological Laboratory, Woods Hole, Massachussets, USA, for making his code and algorithm for analysis of raw PLM results available to us. At our own group, we thank Marcel Jaklofsky and Henk Schipper for the experimental qPLM results on tendon.

2.A Jones and Mueller matrices

The Jones matrix J and Mueller matrix M of an ideal polariser at an azimuth θ are [86]:

$$J = \begin{bmatrix} \cos^2\theta & \sin\theta\cos\theta \\ \sin\theta\cos\theta & \sin^2\theta \end{bmatrix} \tag{2.15}$$

$$M = \frac{1}{2}\begin{bmatrix} 1 & \cos 2\theta & \sin 2\theta & 0 \\ \cos 2\theta & \cos^2 2\theta & \sin 2\theta\cos 2\theta & 0 \\ \sin 2\theta & \sin 2\theta\cos 2\theta & \sin^2 2\theta & 0 \\ 0 & 0 & 0 & 0 \end{bmatrix} \tag{2.16}$$

The Jones matrix J and Mueller matrix M for an ideal retarder with phase shift ε at an azimuth θ are [86]:

$$J = \begin{bmatrix} \cos\frac{\varepsilon}{2} + \mathrm{i}\sin\frac{\varepsilon}{2}\cos 2\theta & \mathrm{i}\sin\frac{\varepsilon}{2}\sin 2\theta \\ \mathrm{i}\sin\frac{\varepsilon}{2}\sin 2\theta & \cos\frac{\varepsilon}{2} - \mathrm{i}\sin\frac{\varepsilon}{2}\cos 2\theta \end{bmatrix} \tag{2.17}$$

$$M = \begin{bmatrix} 1 & 0 & 0 & 0 \\ 0 & \cos^2 2\theta + \cos\varepsilon\sin^2 2\theta & (1-\cos\varepsilon)\sin 2\theta\cos 2\theta & \sin\varepsilon\sin 2\theta \\ 0 & (1-\cos\varepsilon)\sin 2\theta\cos 2\theta & \sin^2 2\theta + \cos\varepsilon\cos^2 2\theta & -\sin\varepsilon\cos 2\theta \\ 0 & -\sin\varepsilon\sin 2\theta & \sin\varepsilon\cos 2\theta & \cos\varepsilon \end{bmatrix} \tag{2.18}$$

The Mueller matrix for the sample can be obtained from the Jones matrix by calculation of [302]:

$$M = A(J \otimes J^c)A^{-1}, \quad A = \begin{bmatrix} 1 & 0 & 0 & 1 \\ 1 & 0 & 0 & -1 \\ 0 & 1 & 1 & 0 \\ 0 & \mathrm{i} & -\mathrm{i} & 0 \end{bmatrix} \tag{2.19}$$

with J^c the complex conjugate of the Jones matrix J. The Mueller matrix can also be calculated directly (in line with equation 2.6) for N_f fibres as

$$M = \prod_{n=1}^{N_f} M_{R(\varphi(n),\eta(n)\delta)} \tag{2.20}$$

with $M_{R(\varphi(n),\eta(n)\delta)}$ the ideal retarder (equation 2.18) at azimuth $\varphi(n)$ and with birefringence $\eta(n)\delta$.

Who does not know that a horse falling from a height of three or four cubits will break his bones, while a dog falling from the same height or a cat from a height of eight or ten cubits will suffer no injury?

Galileo Galilei [118]

3

Quantitative description of collagen structure in the articular cartilage of the young and adult equine distal metacarpus

Mark C. van Turnhout[1], Monique B. Haazelager[1], Merel A.L. Gijsen[1], Henk Schipper[1], Sander Kranenbarg[1] & Johan L. van Leeuwen[1]. *Animal Biology*, **58**(4):353–370, December 2008. doi: 10.1163/157075608X383674

[1]Wageningen University, Experimental Zoology Group, PO Box 338, 6700 AH, Wageningen, The Netherlands.

Abstract

The orientation and organisation of collagen fibrils play an important role in the mechanical functioning of the articular cartilage (AC) that covers the surfaces in the diarthrodial joints. In the adult animal, typically an arcade-like 'Benninghoff structure' is found. Because the remodelling capacity of the collagen network in the adult animal is limited, this Benninghoff structure needs to develop before the animal reaches maturity, and it needs to develop correctly.

The aim of this study is to use quantitative polarised light microscopy (qPLM) and scanning electron microscopy (SEM) techniques to investigate if this Benninghoff structure is already present in the young animal, and to quantitatively investigate possible differences in collagen structure in the equine distal metacarpus of the young and adult animal.

In total, 21 forelimbs of 13 horses are used. In animals of age 10 months and older, we find an arcade-like Benninghoff structure for the collagen fibril network in both the qPLM and SEM study. The qPLM study shows that the collagen's predominant orientation is parallel to the articular surface throughout the entire cartilage depth in two animals directly after birth. These findings are supported by SEM results on a foal.

We conclude that structural remodelling of the collagen network in AC occurs in the first months after birth. Because animals start with collagen parallel to the articular surface and need to remodel this structure to a Benninghoff architecture, and because collagen structure is an important parameter for AC mechanics and mechanobiology, these results suggest implications for AC epigenetics.

3.1 Introduction

Articular cartilage (AC) is the thin layer of tissue that covers the surfaces of bones in diarthrodial joints. Its function is to provide a low friction environment for joint movement and to transmit loads. To fulfil this function, AC needs a certain composition and structure which it develops during early life [50, 51, 143, 154]. At maturity, AC composition may to some degree still be adapted to fit changing functional demands [50, 289], but the remodelling capacity of the collagen network in the mature animal is limited [49, 159, 252, 289]. In fact, most differences we observe in the collagen network in AC at this point are associated with wear, trauma and pathologies.

The orientation and organisation of the collagen fibrils play an important role in the mechanical function of AC [39, 136, 150, 171, 192, 285]. The classical model of AC collagen architecture is that of Benninghoff [37]. From the articular surface to the bone, this model describes first a thin superficial zone with collagen fibrils arranged parallel to the articular surface, next a thicker transitional zone where the collagen fibrils seem to lack a predominant orientation, and finally the thickest deep zone where the collagen fibrils are oriented in the radial direction more or less perpendicular to the subchondral bone.

This model has been confirmed in a variety of species and anatomical sites [150, 175], but notably in specimens past the juvenile age. The collagen network in the young developing animal is known to be subject to compositional remodelling. For instance, Bland and Ashhurst [42, 43] looked at the temporal distribution of different collagen types in fetal and young rabbit AC. They were unable to show type II collagen, the major collagen component in adult AC (over 90 %), in rabbit AC before 3 weeks post natal in the menisci and before 6 weeks post natal in the tibial plateau. Brama et al. [50] showed an increase in collagen content in the equine metacarpophalangeal joint up to an age of 5 months, and no changes afterwards. Structural remodelling too, has been shown in e.g. mouse [150] and rabbit AC [154]. The focus in these studies is on the differentiation in superficial/transitional/deep zones and to the best of our knowledge a quantitative description and comparison of collagen structure in developing and full-grown AC has not yet been reported.

Quantitative polarised light microscopy (qPLM) is a popular technique to evaluate collagen structure in AC [237, 286, 288, 333] and is sometimes called 'the gold standard of histology' [4, 363]. What is measured with qPLM are properties of birefringent structures, c.q. collagen fibrils. Two parameters are measured: retardance and azimuth of the birefringent structure. The retardance is a combined measure for structural anisotropy and collagen amount [13, 36, 187]: low retardance indicates either a low amount of collagen, or a low degree of structural anisotropy, or both. In the transitional zone, where according to the Benninghoff model the fibril architecture shows low structural anisotropy compared with the other zones, we therefore expect the retardance to show a minimum. This fact is often used to determine zone thickness with PLM [150, 159, 188, 192, 213, 289, 365, 366]. The second parameter is the azimuth, which is the predominant orientation of the birefringent structures [171, 286, 288].

Scanning electron microscopy (SEM) has the advantage over qPLM that it is able to visualise individual fibrils. It is particularly SEM studies that have stressed that the azi-

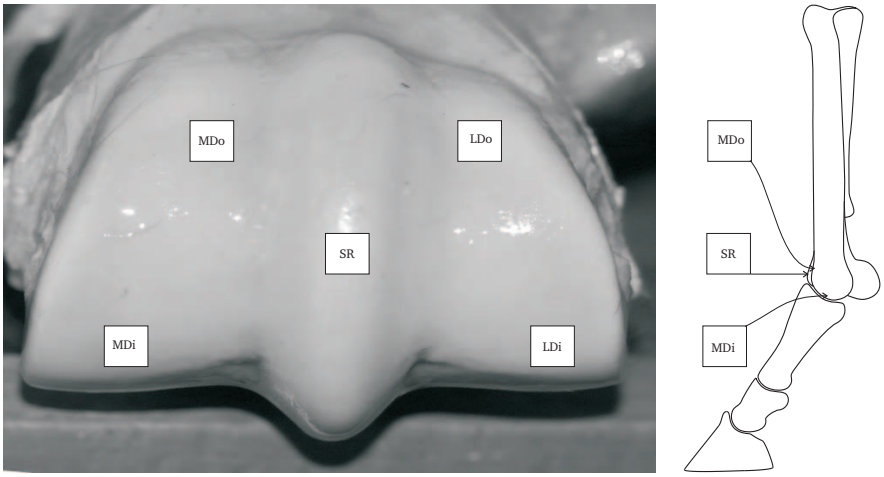

Figure 3.1: The distal metacarpus (right limb) and the five sample sites used in this study: mediodorsal (MDo), laterodorsal (LDo), sagittal ridge (SR), mediodistal (MDi) and laterodistal (LDi).

muth that we find with qPLM is a predominant orientation only and not the orientation of every single fibril [82, 83, 150, 309]. The objective of this study is to use qPLM and SEM techniques to quantitatively investigate differences in collagen structure in the equine distal metacarpus of the young and adult animal.

3.2 Methods

3.2.1 Scanning Electron Microscopy (SEM)

Nine forelimbs of five horses were collected from a local abattoir (VOF Paardenslachterij, Nijkerk, The Netherlands), and processed on the day of slaughter. The approximate age in years of 4 horses was obtained from the owner. The age of the fifth horse (a foal) is only known to be below one year. See table 3.1 for details.

Skin and subcutaneous tissue were removed and the metacarpophalangeal joint was carefully opened. Full depth cartilage plugs were taken from the distal metacarpus using a hollow drill and a chisel at the medial and lateral distal parts of the joint (MDi and LDi, see figure 3.1).

The cartilage plugs were then fixed (25 % glutaraldehyde in 0.2 M sodium cacodylate buffer) for 4 days, washed and infiltrated with sucrose (25 % on PBS) overnight, snap frozen in liquid nitrogen and stored at -80 °C until further processing. Frozen samples were split in two with a scalpel and hammer, placed in water and dehydrated with a series of alcohol solutions (70 %, 80 %, 90 % and 96 % for 15 min each, 100 % once for 5 min and twice for 10 min) and finally dried with a critical point dryer using CO_2 (CPD 020, Balzers, Liechtenstein) to avoid surface tension and surface damage. These samples

were glued on a sample holder with conductive carbon cement (Leit- C, Neubauer Chemicalien, Germany) and stored overnight for the glue to dry. The surface of the sample was sputter coated with 8 nm platinum in a dedicated preparation chamber (Oxford Instruments CT 1500 HF, Eynsham, England) for a better reflection of electrons.

SEM imaging was performed with a field emission scanning electron microscope (JEOL 6300 F, Tokyo, Japan) in vacuum at room temperature using a focussed electron beam of 3.5 kV with a work distance of 16 mm. Digital images were recorded at a scan rate of 100 seconds/full frame (Orion, 6 E.L.I. sprl., Belgium) and stored in 8 bit TIFF format.

We first collected an overview of the full depth cartilage layer at a magnification of 70x. Next, approximately ten to twenty high magnification images (10.000x) were collected at different heights in the cartilage layer for analysis with a Fast Fourier Transformation (FFT). The resulting 2-D power spectrum showed an ellipse like bright spot centred at the image with its long axis in the direction of the predominant fibril orientation. When we scanned the intensity on a line with a certain azimuth starting in the centre, we therefore found the highest values when the azimuth of the line corresponds with the ellipse's long axis [186, 271]. Figure 3.2a shows an example of a SEM image in the 2 year old animal with a magnification of 10.000x. These images measure 2528 pixels by 2030 pixels and were cropped to a circle positioned in the centre with a radius of 927 pixels to minimise FFT artifacts. The cropped image was subjected to 2-D FFT and this resulted in a power spectrum, see figure 3.2b. Note that FFT introduced a 90 ° phase shift in the power spectrum. We corrected for this phase shift in this example. From the spectrum we could detect the predominant orientation from the shape of the ellipse in the centre. This is illustrated in figure 3.2c, a thresholded binary image of the power spectrum that shows the core of the ellipse.

The analysis was implemented in Matlab (version 7.2R14, The MathWorks, Inc., 1984-2005). Results were interpolated to 20 equidistant points and will be presented as a function of dimensionless height, i.e. from the tide-mark, $h = 0$, to the articular surface, $h = 1$. We expressed the azimuth with respect to the articular surface, i.e. 0 ° and 180 ° are parallel to the articular surface; 90 ° is perpendicular to the articular surface. Because of the small sample size, we treated all measurements independently for the presentation of height dependent results.

3.2.2 Quantitative polarised light microscopy (qPLM)

Eight forelimbs of six horses with known age were collected from the Faculty of Veterinary Medicine of the University of Utrecht (The Netherlands) and an additional four forelimbs from two adult horses were collected from a local abattoir (VOF Paardenslachterij, Nijkerk, The Netherlands), see table 3.1 for details. Forelimbs provided by Utrecht University were obtained frozen and were thawed at 5 °C overnight before processing. Limbs collected from the abattoir were fresh and processed on the day of slaughter.

Skin and subcutaneous tissue were removed and the metacarpophalangeal joint was carefully opened. Split line patterns were created on the articular surface of the distal metacarpus with a sharp round needle charged with Indian ink. The needle was inserted perpendicular to the articular surface at 2 mm intervals and excess ink was removed by

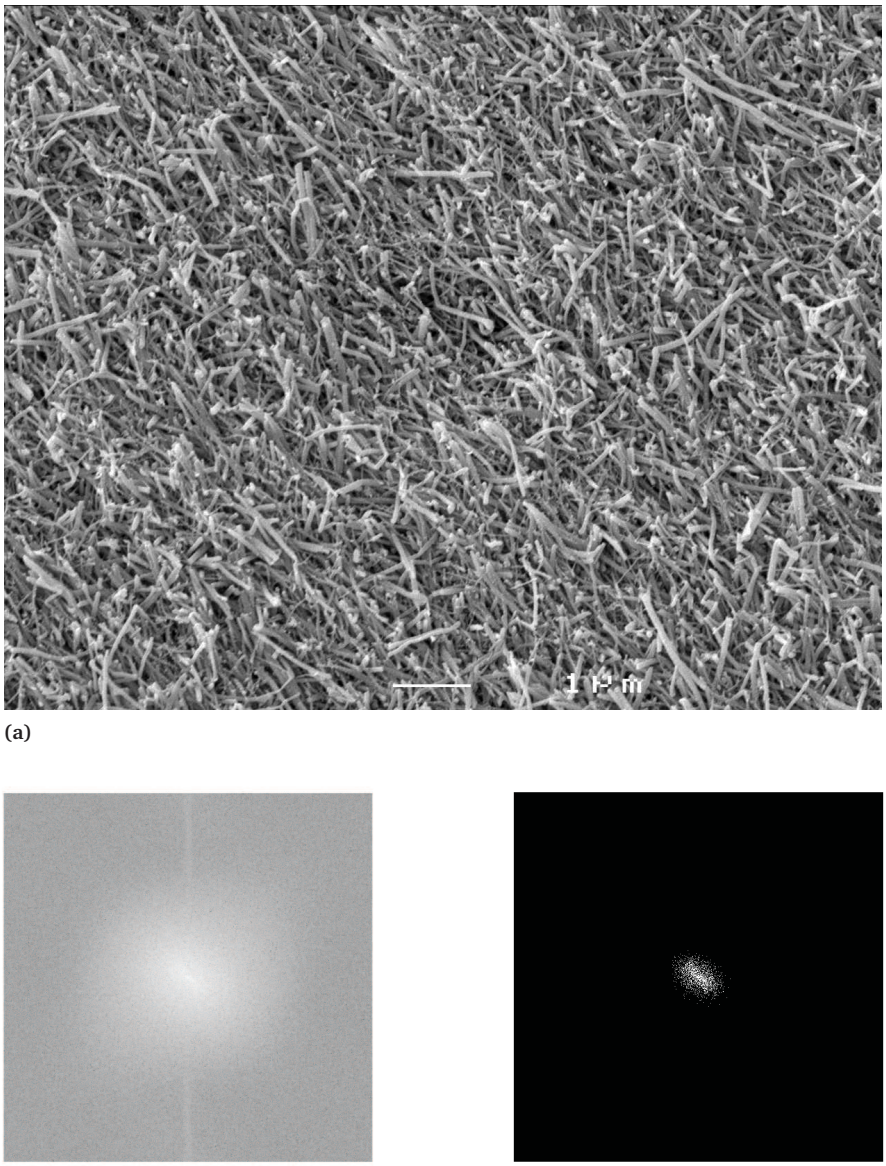

(a)

(b) **(c)**

Figure 3.2: Example illustrating predominant fibril orientation detection through 2-D Fast Fourier Transform (FFT) analysis. **(a)** Original SEM image at a magnification of 10.000x. **(b)** The power spectrum after 2-D FFT and correction for the phase shift introduced by the FFT. The predominant orientation corresponds to the long axis of the ellipse in the centre. **(c)** A binary version of the power spectrum, illustrating the core of the ellipse.

Table 3.1: The age and the origin of the limbs used in this study. The animals labelled 0 months of age, were stillborn. Horses labeled 'sem' were used for the scanning electron microscope study, horses labeled 'plm' were used for the polarised microscopy study.

Horse	age	left	right	origin	breed
sem1	1 year	x	x	abattoir	Frysian
sem2	1 year	x	x	abattoir	Dutch warmblood
sem3	1.5 years	x		abattoir	Dutch warmblood
sem4	2 years	x	x	abattoir	Dutch warmblood
sem5	$<$ 1 year	x	x	abattoir	Dutch warmblood
plm1	0 months	x	x	Utrecht	Shetland
plm2	0 months	x		Utrecht	unknown
plm3	4.5 months	x		Utrecht	unknown
plm4	10 months	x	x	Utrecht	unknown
plm5	12 months		x	Utrecht	unknown
plm6	120 months		x	Utrecht	unknown
plm7	adult	x	x	abattoir	unknown
plm8	adult	x	x	abattoir	unknown

rinsing. The resulting split line pattern was recorded with a Nikon D-100 digital camera with a Micro-Nikon 55 mm objective.

Samples were taken from the sagittal ridge (SR), the distal part of the medial side (MDi) and lateral side (LDi) and dorsal parts of the medial side (MDo) and lateral side (LDo), see figure 3.1. A dentist drill was used to introduce rectangular carvings and from these full depth cartilage plugs (i.e. including a piece of the subchondral bone) were extracted using a chisel. These samples were fixed with formalin, decalcified with EDTA (10 % EDTA, pH 7.4) for two weeks, washed and infiltrated with sucrose (25 % sucrose on PBS) overnight, snap frozen in liquid nitrogen and stored at -80 °C until further processing, and finally cut parallel to the superficial split lines to 5 μm thick histological slices with a cryostat (Reichert 2800N).

Two macroscopically normal histological samples for each sample site were mounted with water and analysed with the LC-PolScope system for qPLM [259, 261]. Images were obtained with a Zeiss Axiovert 200M microscope at a 5x/1.6 magnification, equipped with a Q-imaging monochrome HR Retiga EX 1350 camera. Recorded intensity images had a resolution of 1.59 μm^2/pixel and were stored in 8 bit TIFF format. We used the five frame setting with background correction as described by Shribak and Oldenbourg [300] with a swing of 0.03 [-]. The recorded images were analysed for predominant collagen fibril orientation and tissue retardance with custom written scripts implemented in Matlab (version 7.2R14, The MathWorks, Inc., 1984-2005).

A representative section with a width of 170 pixels that reaches from the tide-mark to the articular surface was extracted from the images. The results were averaged over

this width and are presented as a function of dimensionless height after interpolation to 400 equidistant points. The azimuth was expressed with respect to the articular surface. Average retardance was obtained by taking the arithmetic mean of the 170 pixels and used to determine the position of the birefringence minimum in the transitional zone. To obtain an average orientation over these 170 pixels with predominant fibril azimuth, the arithmetic means did not suffice [174, 334]. We therefore introduced a retardance weighted average azimuth ($\overline{\varphi}$) that is obtained by maximising the function

$$I(\overline{\varphi}) = \sum_{k=1}^{K} \Delta(k) \left| \begin{bmatrix} \cos\overline{\varphi} & \sin\overline{\varphi} \end{bmatrix} \cdot \begin{bmatrix} \cos\varphi(k) \\ \sin\varphi(k) \end{bmatrix} \right| \tag{3.1}$$

for $\overline{\varphi}$.

The summation over the absolute values of the inner dot product found the line with smallest difference in angles compared with all lines K described by the azimuth values φ. The retardance $\Delta(k)$ is a measure for the amount of collagen that is associated with azimuth $\varphi(k)$. Through multiplication of the inner dot product with the retardance, we assigned a lower importance to azimuth values with a lower retardance, which may indicate that 1) there is fewer collagen in this pixel; or that 2) the predominant orientation belongs to a collagen structure with a low level of anisotropy; or 3) a combination of these two. Maximisation of equation (3.1) was done with Matlab's built in function 'fminbnd' on a interval of $0 < \overline{\varphi} \leq \pi$. Final curves for each site were averages from two separate qPLM slices taken from each sample.

3.3 Results

3.3.1 SEM study

In the older animals, SEM images show that the collagen fibrils exhibit structural anisotropy in varying degrees depending on the height in the cartilage. Structural anisotropy is most clearly visible at the articular surface and at the tide-mark. In the foal however, the cartilage appears more chaotic throughout the entire cartilage layer. Figure 3.3 shows an example of the collagen structure close to the tide-mark in the foal and in the adult animals. The difference in structural anisotropy is also apparent from the power spectra: the adult animal shows a more pronounced ellipse than the young animal. When the spectrum resembled a circle more than an ellipse as in this example for the foal, we rotated the image and repeated the analysis. The observed predominant orientation then rotated with the image, confirming that we found an objective measure for orientation.

The height dependent orientation patterns we find in the foal differ from those found in the other animals, again particularly in the deep zone. Figure 3.4 shows these patterns for the foal and for the older animals. In the foal, the orientation of the fibrils appears to vary around 0° (or 180°) throughout the entire cartilage depth (figure 3.4a). Visual inspection of the SEM images shows that the orientation we find in the foal belongs to a near isotropic structure for $h < 0.8$, see for instance figure 3.3a. Near the articular surface, SEM images in the foal show an anisotropic structure as in the older animals.

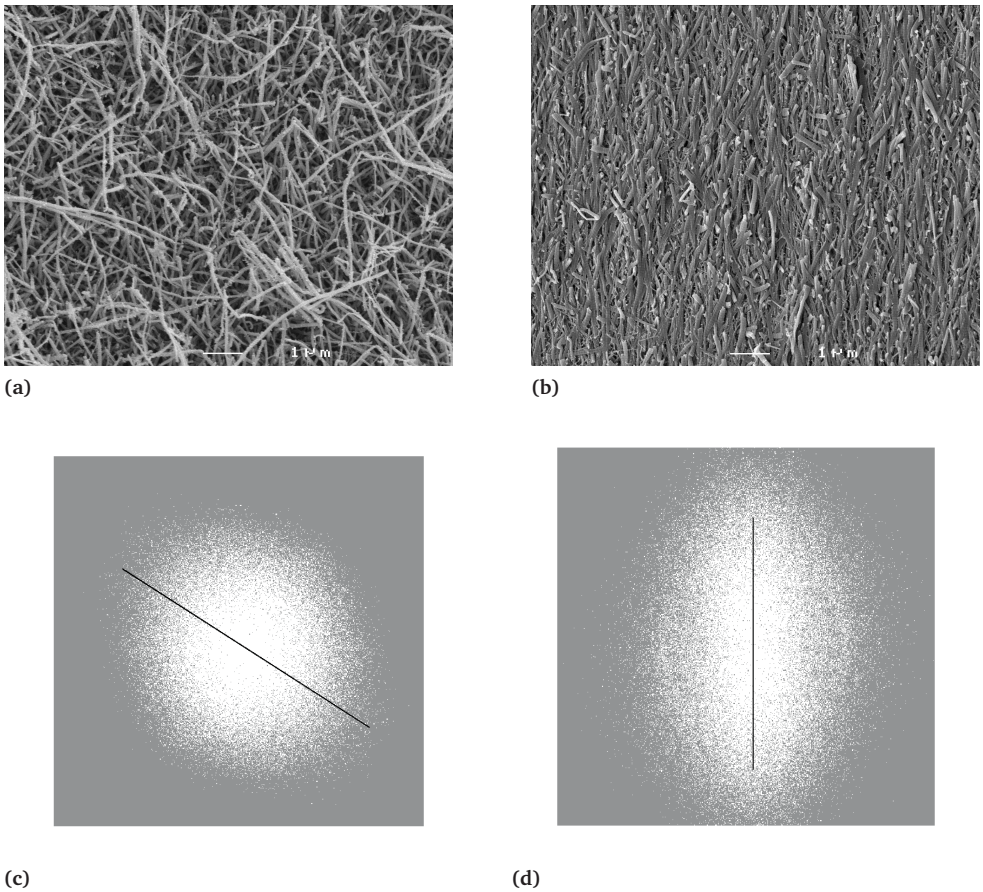

(a) **(b)**

(c) **(d)**

Figure 3.3: Example of SEM results close to the tide-mark in the young and adult animal. Top (panel a and b) SEM images at a magnification of 10.000x; bottom (panel c and d) binary representation of the centre of the power spectrum (white on a gray background) with detected predominant orientation (black line); left (panel a and c) results for the foal; right (panel b and d) results for an adult horse.

In the other animals, an arcade-like Benninghoff structure appears (figure 3.4b): collagen is aligned perpendicularly to the subchondral bone in the deep zone (approximately 80 % of the tissue height), then curves away to form an arcade, and is finally aligned with the articular surface.

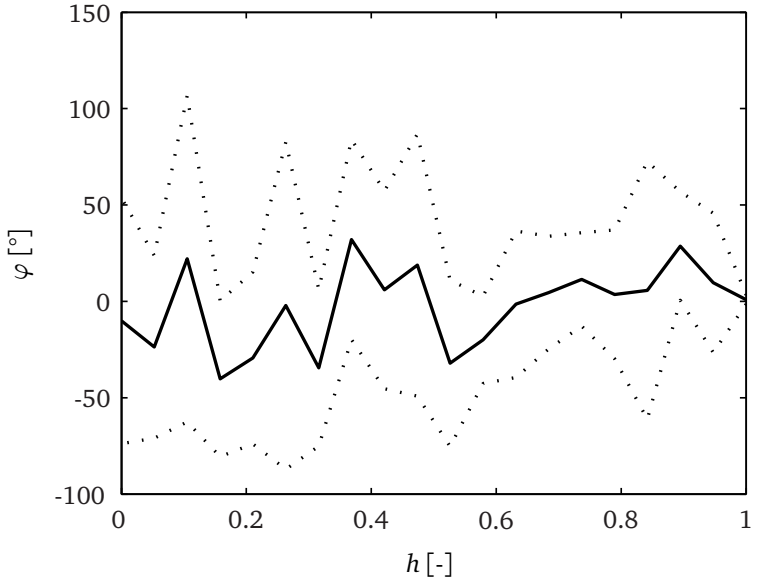

(a)

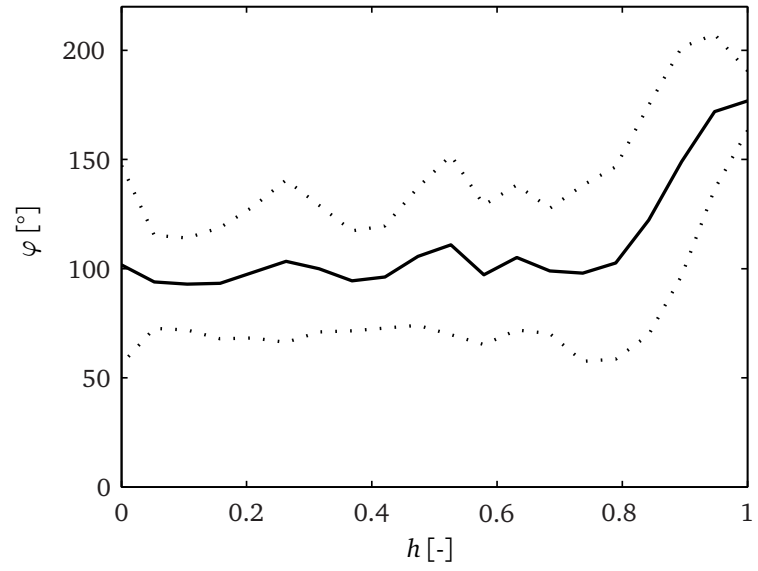

(b)

Figure 3.4: Average predominant fibril orientation ± standard deviation from the SEM study as a function of dimensionless height. With **(a)** results for three samples from the foal ($n = 3$); and **(b)** results for all samples in the animals 1 year and older ($n = 14$).

3.3.2 qPLM study

Figure 3.5 shows the azimuth results for the 5 anatomical sites for three animals of ages 0 months, 4.5 months and 10 years. We can see that these three animals show different patterns from each other; and that within the stillborn (0 months) and adult animal there seems to be little variation with anatomical site. The animal of age 4.5 months does show some variation between the anatomical sites.

When we collect all orientation pattern results, again two distinct collagen orientation profiles are found in the qPLM study (figure 3.6). We cannot find differences between left or right limbs or between the anatomical sites and therefore pool the data as independent measurements (due to the sample size, as in the SEM study). The first pattern belongs to the stillborn animals and is shown in figure 3.6a. Here, we find that the predominant fibril orientation is aligned with the articular surface over the complete cartilage height in these animals. The second pattern is found in the animals of age 10 months and older and is shown in figure 3.6b. These animals show an arcade-like Benninghoff structure with fibrils perpendicular to the subchondral bone in the deep zone that bend in the transitional zone until they are aligned parallel with the articular surface. The patterns we observe in the animal of age 4.5 months show a mixture of these two primary patterns (shown in figure 3.5).

Figures 3.6a and 3.6b show the average retardance patterns that correspond to these orientation patterns. Retardance appears to be larger in the older than in the stillborn animals. This apparent rise in retardance is accompanied by an increase in variation that is just as high. The minimum in the retardance pattern that is associated with the transitional zone, can be found in all samples and the height of this minimum d_m is collected in table 3.2.

Finally, we present the overall cartilage thickness as a function of age in table 3.3.

Table 3.2: Dimensionless height of the retardance minimum in the transitional zone d_m per animal, site and left/right limb and the mean $\overline{d_m}$ per age (in months). The star for the horses of age 0 indicates that this is the mean for both horses of age 0 taken together, not for the individual animals.

		LDo		LDi		MDo		MDi		SR		$\overline{d_m}$
horse	age	l	r	l	r	l	r	l	r	l	r	
plm1	0	0.97	0.93	0.95	0.93	0.96	0.96	0.95	0.95	0.95	0.96	0.93*
plm2	0	0.93		0.86		0.89		0.87		0.90		0.93*
plm3	4.5	0.87		0.87		0.77		0.78		0.93		0.84
plm4	10	0.87	0.87	0.85	0.91	0.83	0.84	0.83	0.84	0.91	0.86	0.86
plm5	12		0.81		0.87		0.81		0.94		0.95	0.88
plm6	120		0.93		0.90		0.83		0.84		0.88	0.88
plm7	adult	0.89	0.90	0.88	0.89	0.81	0.81	0.86	0.88	0.83	0.80	0.85
plm8	adult	0.90	0.92	0.86	0.91	0.88	0.88	0.88	0.90	0.90	0.90	0.89

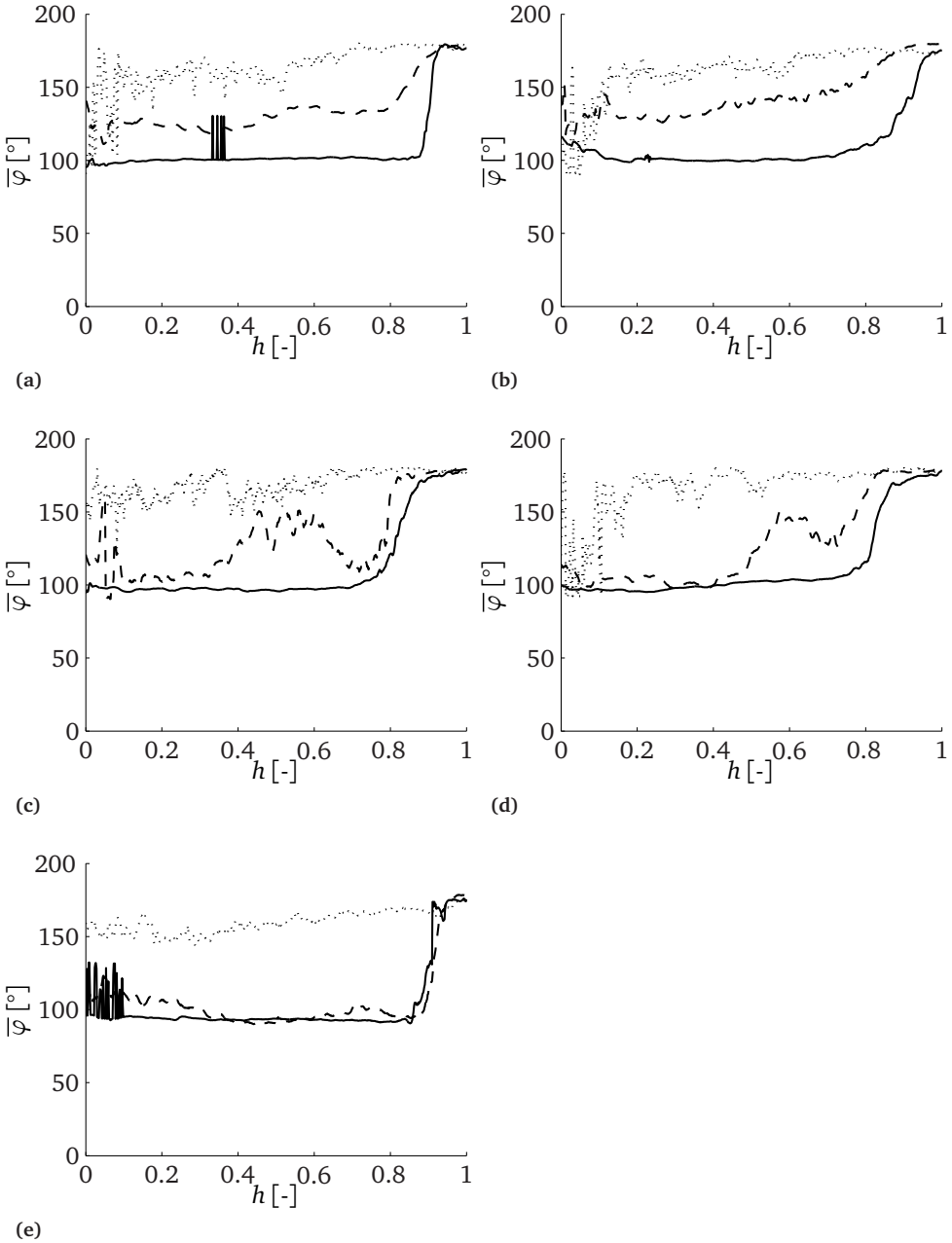

Figure 3.5: Predominant collagen fibril orientation in the stillborn animals (dotted), the animal of 4.5 months old (dashed) and the animal of 10 years old (solid) for the five different sample sites. **(a)** Mediodorsal; **(b)** Laterodorsal; **(c)** Mediodistal; **(d)** Laterodistal; and **(e)** Sagittal ridge.

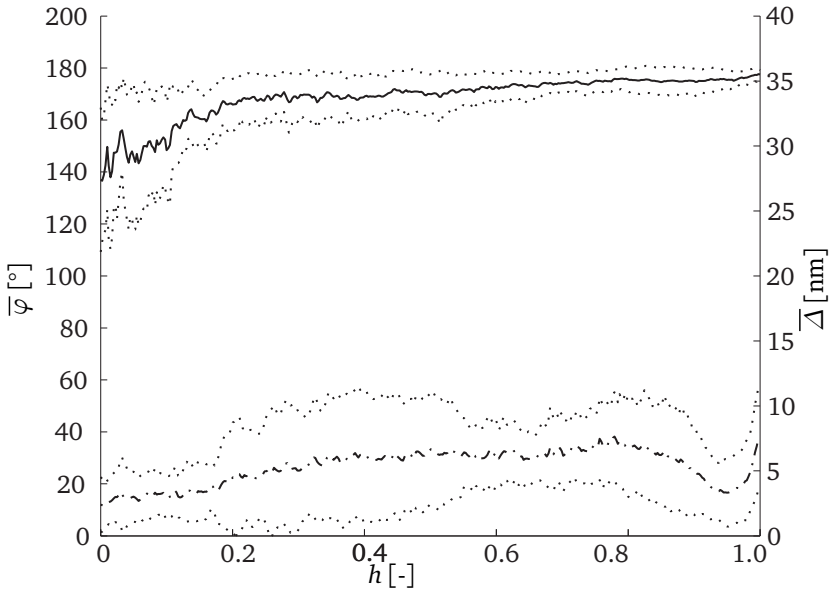

(a)

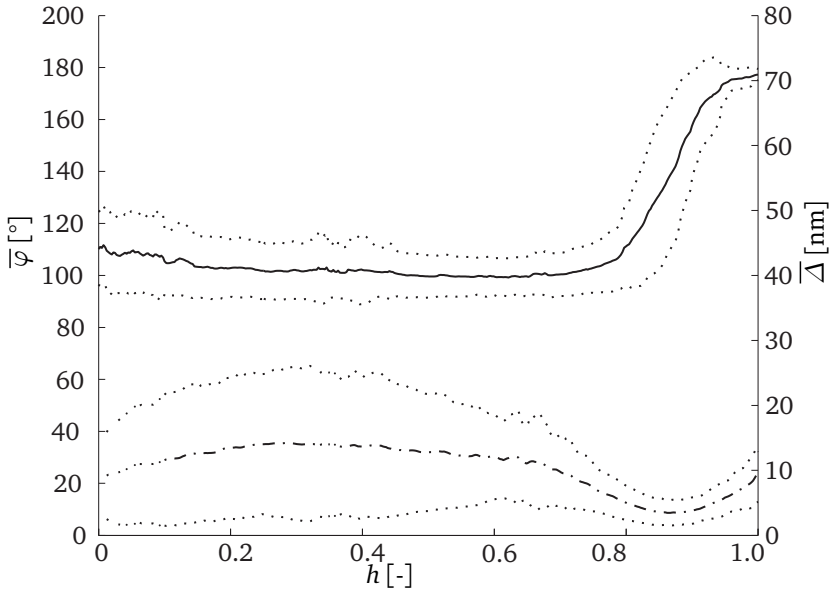

(b)

Figure 3.6: Average predominant fibril orientation ± standard deviation (upper half of the graph, left axis) and corresponding average retardance ± standard deviation (bottom half of the graph, right axis) from the qPLM study as a function of dimensionless height for all sites. With **(a)** results for the stillborn animals ($n = 15$); and **(b)** results for all sites in the animals age 10 months and older ($n = 40$).

It shows significantly higher values for the stillborn animals than in the other animals. From age 4.5 months onwards, no significant differences in cartilage thickness are detected.

Table 3.3: Cartilage thickness as a function of age in the qPLM study. The last column collects the data for the two adult animals and the animal with age 120 months.

	0 months	4.5 months	10 months	12 months	> 12 months
d [mm]	2.10 ± 0.72	1.08 ± 0.23	0.93 ± 0.14	1.30 ± 0.68	1.06 ± 0.13
n	15	5	9	5	25

3.4 Discussion

In both parts of the study, we were able to confirm the Benninghoff model in our sample of animals of age 10 months and older. Strikingly, we find in the qPLM study that collagen is predominantly arranged parallel to the articular surface throughout the entire cartilage depth in the stillborn animal. At 4.5 months we seem to find intermediate results between this parallel structure and the adult Benninghoff structure. This marked result is confirmed in the SEM study were we observe such a parallel arrangement in the foal. Even if the exact age of this foal is not known and the variation we find is large, the results suggest that the Benninghoff structure is not found in this animal, whereas it is found in the SEM experiments with older animals. The SEM experiments further show that the predominant orientation in the young animals belongs to collagen fibrils with a nearly isotropic architecture.

Another interesting finding is that the minimum in retardance that is associated with the isotropic transitional zone is already present in the stillborn animals, while no zonal differentiation is apparent from the orientation patterns. This onset of a transitional zone without a change in collagen fibril orientation has also been reported by Hughes et al. [150] in 7 day old mouse AC. This indicates that some degree of structural differentiation over the cartilage height may already be present at birth. It also shows that the use of orientation patterns for determination of the different zones as recently proposed by Julkunen et al. [171] will not suffice in young animals.

Brama and coworkers performed biochemical studies on the developing AC in the same equine joint. They did not investigate depth dependent or structural parameters, but concentrated on compositional differences as a function of site, age and exercise. Looking at the data they present for collagen content, we find that they report a large increase in collagen content up to an age of 5 months [50] and little or no adaptation after this age [49, 53]. Furthermore, they report site related differences in a variety of parameters that do not exist at birth, but are fully developed at an age of 5 months [50, 51]. The current study concentrates on height dependent collagen structure and the results indicate that in line with the work by Brama and coworkers, structural changes

in the collagen fibre network also occur in the first 5 months after birth.

Brama et al. [50, 52] report compositional differences between the chosen sites from an age of 5 months onwards. It is very likely that the structural changeover in developing AC is a function of biomechanical loading, as is the compositional changeover. Therefore differences in collagen structure between sites that are subject to different loading patterns would not be unexpected. In this study however, the number of samples probably is too small to show this in terms of collagen structure. Because of the small sample size, it is conceivable that differences in loading patterns between animals may have confounded differences in loading patterns between the sites within an animal. We do find that cartilage thickness is significantly higher in the stillborn animals than in the older animals, which is in line with the results of Brommer et al. [57] and Firth and Greydanus [112]. However, we add that this is due to one of the two stillborn animals that had a very thick cartilage layer (> 2 mm). Cartilage thickness in the second stillborn animal is in line with that found in the other animals.

Caveats in this preliminary study are the small number of animals we were able to use; the temporal distribution of the sample points; and the limited knowledge on the ages and loading history of the animals. The difference in cartilage thickness between the two stillborn animals for instance may be explained by differences in the developmental stage of the fetuses, since we do not know the gestational age of these animals. Furthermore, we had to resign ourselves to the use of different breeds of horses, which is likely to have increased variations we find between animals, and we had no control over the ages of the animals that we could use. Still, we are confident that the results we report on collagen orientation in stillborn and adult horses will hold, since these follow unambiguously from both age categories even when little or no differences can be found in the other parameters.

As such, these findings suggest implications for AC epigenetics. AC remodels during growth and maturation from a homogenous tissue to a tissue with site specific composition [50, 52, 154] and mechanical properties [57]. It does so under the influence of mechanical loads [53, 143, 252] that vary over the joint surfaces [48, 145, 264]. The collagen fibre network plays an important role in the mechanical properties of AC in general [12, 192, 201, 351], and in the differentiation in cartilage mechanics over the tissue height: global cartilage loads will result in different strains over the cartilage height due to its depth dependent structure and composition [293, 356, 357]. In fact, the relationship between cartilage loads and depth dependent collagen structure is strong enough for Wilson et al. [355] to be able to predict depth and site dependent collagen structure as a function of global cartilage loads.

Given that the collagen fibre network in the newborn animal is nearly uniform over the cartilage height, the question now arises to what degree the depth dependent mechanical properties manifest in the newborn animal. Also, one might ask to what degree this is the result of the differences in collagen fibre network; to what degree such depth dependent mechanical properties in the newborn animal are necessary to develop the distinct depth dependent collagen structure at maturity; and what the role is of the other cartilage components in the development of cartilage mechanics and structure. We intent to address these questions in future work.

3.5 Conclusions

In the cartilage on the equine distal metacarpus, we find different collagen structures in young (2 stillborn animals) and older animals (9 animals older than 10 months). The transition between the two structures takes place in the first months after birth as we see a transitional structure in a 4.5 months old animal.

In the two stillborn animals that we analysed, the predominant collagen fibril orientation is parallel to the articular surface throughout the entire cartilage depth. The minimum in the retardance patterns suggest the onset of a transitional zone, but this zone is not yet apparent from fibril arrangement.

In the animals older than 10 months that we analysed, we find the classical Benninghoff structure with the three zones. In the deep zone, collagen fibrils are predominantly arranged perpendicular to the subchondral bone, in the superficial zone, they are aligned parallel to the articular surface. In the transitional zone, we find a low retardance which indicates a less anisotropic collagen structure, and that the azimuth patterns describe an arcade-like structure.

Acknowledgements

We thank prof. R. Oldenbourg for kindly making his code and algorithm for analysis of the raw PLM results available to us. We thank VOF Paardenslagerij, Nijkerk, The Netherlands and prof. dr. P.R. van Weeren and dr. H. Brommer at the Faculty of Veterinary Medicine of Utrecht University, The Netherlands, for the generous gift of the equine limbs.

From Wageningen University, we thank mr. A. van Aelst at the Wageningen electron microscopy Centre for the help with the SEM experiments and dr. N. de Ruijter at the Plant Cell Biology group for the help with the PLM experiments.

The use of an ovine model circumvents the ethical and financial problems associated with the use of bipedal animal models.

Armstrong, Read & Price [10]

4

Postnatal development of collagen structure in ovine articular cartilage

Mark C. van Turnhout[1], Henk Schipper[1], Bas Engel[2], Willem Buist[3], Sander Kranenbarg[1] & Johan L. van Leeuwen[1]. *BMC Developmental Biology*, **10**:62, June 2010.
doi: 10.1186/1471-213X-10-62

[1]Wageningen University, Experimental Zoology Group, PO Box 338, 6700 AH, Wageningen, The Netherlands.
[2]Wageningen University, Biometris, PO Box 100, 6700 AC Wageningen The Netherlands.
[3]Wageningen University & Research, Biometris, PO Box 100, 6700 AC Wageningen The Netherlands.

Abstract

Background: Articular cartilage (AC) is the layer of tissue that covers the articulating ends of the bones in diarthrodial joints. Across species, adult AC shows an arcade-like structure with collagen predominantly perpendicular to the subchondral bone near the bone, and collagen predominantly parallel to the articular surface near the articular surface. Recent studies into collagen fibre orientation in stillborn and juvenile animals showed that this structure is absent at birth. Since the collagen structure is an important factor for AC mechanics, the absence of the adult Benninghoff structure has implications for perinatal AC mechanobiology. The current objective is to quantify the dynamics of collagen network development in a model animal from birth to maturity. We further aim to show the presence or absence of zonal differentiation at birth, and to assess differences in collagen network development between different anatomical sites of a single joint surface. We use quantitative polarised light microscopy to investigate properties of the collagen network and we use the sheep (*Ovis aries*) as our model animal.

Results: Predominant collagen orientation is parallel to the articular surface throughout the tissue depth for perinatal cartilage. This remodels to the Benninghoff structure before the sheep reach sexual maturity. Remodelling of predominant collagen orientation starts at a depth just below the future transitional zone. Tissue retardance shows a minimum near the articular surface at all ages, which indicates the presence of zonal differentiation at all ages. The absolute position of this minimum does change between birth and maturity. Between different anatomical sites, we find differences in the dynamics of collagen remodelling, but no differences in adult collagen structure.

Conclusions: The collagen network in articular cartilage remodels between birth and sexual maturity from a network with predominant orientation parallel to the articular surface to a Benninghoff network. The retardance minimum near, but not at, the articular surface at all ages shows that a zonal differentiation is already present in the perinatal animals. In these animals, the zonal differentiation can not be correlated to the collagen network orientation. We find no difference in adult collagen structure in the nearly congruent metacarpophalangeal joint, but we do find differences in the dynamics of collagen network remodelling.

4.1 Background

The articulating ends of bones in the diarthrodial joints are covered with a thin layer of articular cartilage (AC). During early development AC functions as a surface growth plate for the underlying bone [9, 139, 154]. In adult life, AC functions as a load bearing surface that transmits loads and provides a low friction environment. Between birth and skeletal maturity, AC has to accommodate both developmental and load bearing demands.

AC has been shown to develop from a fairly homogeneous tissue to a tissue with site specific composition [50, 52, 154] and site specific mechanical properties [57]. It is accepted that this development is affected by mechanical loads [53, 143, 252] that vary over the joint surfaces [48, 145, 264]. It is reasonable to assume that mechanical loads also affect the development of the collagen network, and that the differences in mechanical properties in adult life partly reflect differences in collagen network.

It is well known that the composition of the collagen network in AC changes during postnatal development: e.g. collagen type I is replaced by collagen type II [42, 43, 247], and the amount of collagen increases [50, 282, 348]. Structural remodelling of the collagen network in terms of the three zones has also been described for postnatal development [150, 154]. However, the remodelling capacity of the collagen network in adult AC is limited [49, 159, 252, 289, 326, 340]. Therefore, differences in collagen structure in adult AC are most likely already present at birth, or developed during postnatal cartilage maturation.

In adults, collagen fibre orientation and organisation are important parameters for the mechanical functions of AC [99, 143, 150, 285]. The collagen network partly determines AC stiffness [198, 266, 299, 362] and Poisson ratio [192] and in transient loads it also influences interstitial fluid flow [110, 216, 224, 342]. Across species and anatomical sites, adult AC shows what is known as 'a Benninghoff structure' [37, 99, 150, 154, 282, 328, 369]. This structure is characterised by three layers in AC: from articular surface to tide-mark there is first a thin layer with collagen fibres mainly oriented parallel to the articular surface, second there is a thicker transitional zone where the collagen fibres appear to lack a predominant orientation, and third there is the deep zone where collagen fibres are mainly oriented perpendicular to the tide-mark.

Recently, (semi) quantitative studies into collagen fibre orientation in stillborn and juvenile animals versus adults have confirmed that the Benninghoff structure is absent at birth and that it is developed during early postnatal life [168, 282, 328]. Van Turnhout et al. [328] looked at equine AC in stillborn and mature animals. They found that collagen fibre orientation in the stillborn animals was predominantly parallel to the articular surface throughout the complete cartilage layer. In the adult animals, they confirmed the Benninghoff structure. They also noticed that some zonal differentiation was already present in the stillborn AC, although this was not reflected in the depth-dependent collagen orientation. Rieppo et al. [282] looked at juvenile and adult porcine AC. For the juvenile animals, they also found that a major part of the collagen fibrils was predominantly oriented parallel to the articular surface throughout the complete cartilage layer. In the adult animals, they confirmed the Benninghoff structure. Julkunen et al. [168] looked at rabbit AC from age 4 weeks to 18 months at six time points. Their results

confirm the findings by Van Turnhout et al. [328] and Rieppo et al. [282].

Since the collagen network is an important factor for AC mechanics, these 'remarkable structural alterations during development and growth' [167] in part explain the stiffening of the AC layer during development [167]. Investigations into how the collagen network affects cartilage mechanics during postnatal development and the mechanical implications of the absence of a Benninghoff structure, can be performed with fibril reinforced finite element models, e.g. [199, 215, 357], provided that we have (quantitative) data on the collagen network at the time points of interest. Knowledge on the dynamics of collagen network development is also important for the validation of collagen remodelling algorithms, e.g. [355]. And finite element modelling of the time line of collagen structure development in AC will provide insight into the mechanical environment that goes with this development. Finally, better insight into the mechanobiology of cartilage development will help to mimic this process *in vitro*, which is important in the field of cartilage tissue engineering.

Last year's studies [168, 282, 328] showed evidence of postnatal collagen network remodelling in AC, but they had their limitations in showing its dynamics. Van Turnhout et al. [328] used two sample points (stillborn and adult) and had a limited number of animals. Rieppo et al. [282] used three sample points (4 months, 11 months and 21 months) that did not include perinatal animals. The study by Julkunen et al. [168] does contain more and earlier sample points in a time resolved manner. However, perinatal animals were not included in this study and the number of early sample points is still too limited to convincingly show the dynamics of collagen structure remodelling. These authors did show differences in collagen structure development between different joint surfaces (femur and tibia).

The objective of the present research is therefore to quantify the development of the collagen network in a model animal from birth to maturity. We further aim to shed more light on the zonal differentiation at birth as noted by Van Turnhout et al. [328], and to assess differences in (the development of) the collagen network between different anatomical sites of a single joint surface. We will look at anatomical sites that are expected to have different loading histories. We use quantitative polarised light microscopy (qPLM), sometimes called 'the gold standard of histology' [4, 363], to investigate properties of the collagen network and we use the sheep (*Ovis aries*) as our model animal.

4.2 Methods

4.2.1 Animals

Animals were obtained from a local sheep farm. We obtained 50 female sheep for 9 sample points (five sheep for each sample point, and five spare sheep), at ages 2 weeks, 4 weeks, 8 weeks, 12 weeks, 20 weeks, 28 weeks, 36 weeks, 52 weeks and 72 weeks. An additional four stillborn lambs were used (labelled age = 0 weeks). Animals were kept at the farm with their mother until sacrifice or the age of 12 weeks. Animals that were 12 weeks old were collected at the farm and housed at the universities laboratory animal facility 'Ossekampen' until sacrifice.

Animals were kept together at pasture with ample space. They had ad lib access to water and food. The animals were born between 24th of February 2007 and 21st of March 2007. In September and October the disease blue tongue spread over the Netherlands and we had to house the animals temporarily inside a barn. Due to the disease, three infected animals had to be excluded from the experiment. All animals were closely monitored, and the other animals showed no clinical signs of blue tongue infection. A further three animals were excluded from the experiment due to accidents with a dog and a male sheep. Therefore, the total number of animals at the end of the experiment was 48, and the number of animals for the first sample point (0 weeks, stillborn) and the last sample point (72 weeks) was four. Animals were weighed prior to sacrifice.

4.2.2 Sample preparation

Animals for the sample points from 2 weeks to 12 weeks were collected at the farm and sacrificed with an overdose of T61. Animals for the remaining sample points were brought to an abattoir to be sacrificed. The animals' legs were collected immediately following sacrifice. For each animal we randomly selected either the two left legs or the two right legs for qPLM analysis. At each sample point, the ratio left:right was either 3:2, 2:3 or 2:2.

Skin and subcutaneous tissue were removed from the metacarpophalangeal joints (figure 4.1) and they were carefully opened. Split line patterns were created on the articular surface of the distal metacarpus with a sharp round needle charged with Indian ink for two of the five animals per sample point (additional figure 4.A.1). The needle was inserted perpendicular to the articular surface at 2 mm intervals and excess ink was removed by rinsing. The resulting split line patterns were recorded with a Nikon D-100 digital camera with a Micro-Nikon 55 mm objective and used to determine the cutting orientation for this sample point.

We used a dental saw to take the medial and lateral hemispheres from the distal end of each cannon bone. These hemispheres were fixed with formalin and decalcified with EDTA (10 % EDTA, pH 7.4) until the hemispheres could be cut with a razor blade. The hemispheres were then divided into a rostral, a distal and a caudal sample (figure 4.1). Of these, the distal site is expected to be subject to a more static load and the rostral and caudal sites are expected to be subject to a more intermittent load during locomotion [57]. These samples were washed and infiltrated with sucrose (25 % sucrose on PBS) overnight, snap frozen in liquid nitrogen and stored at $-80\,^{\circ}\mathrm{C}$ until further processing, and finally cut parallel to the superficial split lines (as observed in two of the five animals) to 7 µm thick histological slices with a cryostat (Reichert 2800N).

4.2.3 Quantitative polarised light microscopy

The birefringent material in cartilage are the fibrils in the collagen network and qPLM measures two parameters of birefringent structures: azimuth and retardance. The azimuth φdoes not measure individual fibril orientations, but is the predominant orientation of the collagen fibres in the network in the pixel. The retardance Δ is a measure of

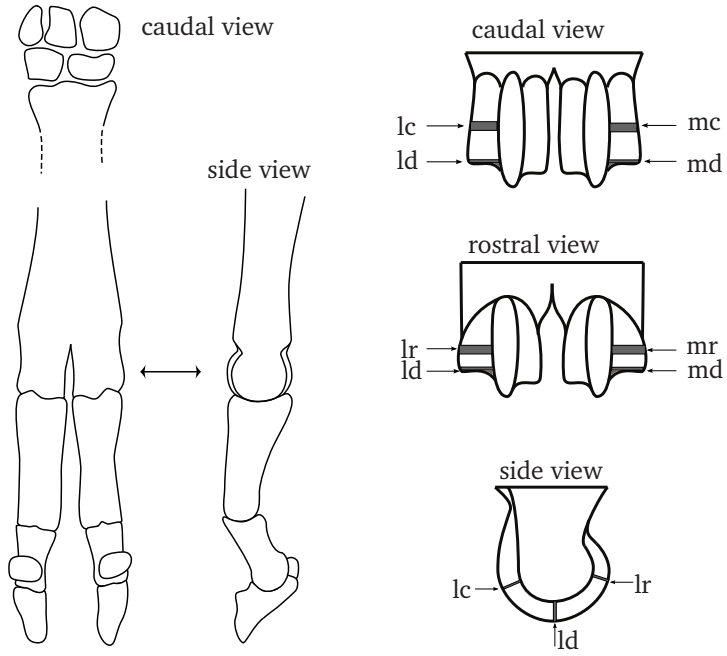

Figure 4.1: Sketch of sample sites. Left: sketch of the bones in the lower fore leg of a sheep. The double arrow shows the distal metacarpus that was used in this study. Note that the proximal sesamoids are not drawn. Right: sketch of anatomical sampling sites with l - lateral, m - medial, c - caudal, d - distal, and r - rostral.

the amount of birefringent material (e.g. collagen fibrils) that is associated with azimuth φ [329]: low retardance indicates one of three things: that 1) there is fewer collagen in this pixel; or that 2) the measured orientation belongs to a collagen network with a low level of anisotropy; or 3) a combination of these two.

Macroscopically normal histological samples were mounted with water and analysed with the LC-PolScope system for qPLM [259, 261]. Images were obtained with a Zeiss Axiovert 200M microscope at a 5x/1.6 magnification, equipped with a Q-imaging monochrome HR Retiga EX 1350 camera. Recorded intensity images had a resolution of $1.59\,\mu m^2$/pixel and were stored in 8 bit TIFF format. We used the five frame setting with background correction as described by [300]. The recorded images were analysed for predominant collagen fibril orientation and tissue retardance with custom written scripts implemented in Matlab (version 7.8.0 R2009a, The MathWorks, Inc., 1984-2005).

4.2.4 Data analysis

Azimuth and Retardance patterns

We extracted a rectangular region of interest (ROI) with a width of 101 pixels from the qPLM images. This ROI reaches from articular surface to the cartilage / bone inter-

face, i.e. up to the calcified tissue in young animals, and up to the tide-mark in older animals. The azimuth was expressed with respect to the articular surface (figure 4.2). Retardance patterns as a function of height were obtained for each sample by taking the

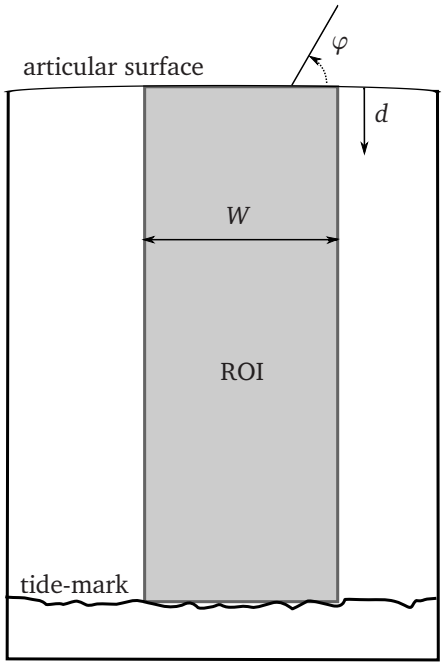

Figure 4.2: Example for data analysis. For each sample a region of interest (ROI) is extracted from the images. The width W of this region is 101 pixels, and it runs from $d = 1$ pixel at the articular surface to $d = D$ pixels at the cartilage / bone interface. The predominant orientation φ is expressed relative to the articular surface. For sample pattern calculations, we used the 101 pixels over the width of the ROI at each depth $d = 1, 2, 3, \ldots, D$.

arithmetic mean over the width of 101 pixels at each depth d. These patterns were used to determine the maximum retardance near the articular surface and the position of the retardance minimum in the transitional zone. To obtain an average azimuth at depth d from 101 values with predominant fibril azimuth, the arithmetic mean did not suffice [174, 334]. This is because the predominant orientation of two fibres with azimuth 1 ° and 179 ° is 0 ° (or 180 °), and not 90 °. We therefore introduced a retardance weighted average azimuth ($\overline{\varphi}$) that is at each depth d obtained by maximising the function I

$$I(\overline{\varphi}) = \sum_{w=1}^{W} \Delta(w) \left| \begin{bmatrix} \cos\overline{\varphi} & \sin\overline{\varphi} \end{bmatrix} \cdot \begin{bmatrix} \cos\varphi(w) \\ \sin\varphi(w) \end{bmatrix} \right| \tag{4.1}$$

for $W = 101$ pixels over the width of the ROI, and for $\overline{\varphi}$ on the interval $0 < \overline{\varphi} \leq \pi$ [328]. The summation over the absolute values of the inner dot product found the line with the

smallest difference in angles compared with all W lines described by the azimuth values $\varphi(w)$. The multiplication with the retardance $\Delta(w)$ assigned a smaller importance to the azimuth in pixels with low retardance, i.e. to pixels with less collagen associated with the predominant orientation $\varphi(w)$ [328].

For statistical analysis of the orientation patterns we calculated for each sample an orientation index $\overline{I}$. This index is defined as the average dot product of the sample azimuth pattern with a reference pattern with continuous azimuth $\theta = 180°$:

$$\overline{I} = \frac{1}{D}\sum_{d=1}^{D}\left|\left[\cos\left(\overline{\varphi}(d)\right) \quad \sin\left(\overline{\varphi}(d)\right)\right]\cdot\begin{bmatrix}\cos\theta\\ \sin\theta\end{bmatrix}\right| = \frac{1}{D}\sum_{d=1}^{D}\left|\cos\left(\overline{\varphi}(d)\right)\right| \tag{4.2}$$

with D the number of points (pixels) over the depth of the sample (figure 4.2).

Average azimuth patterns between samples

We used the sample patterns $\overline{\varphi}$ to calculate average azimuth patterns $\overline{\phi}$ between samples. Because of differences in cartilage thickness, the number of samples that we can analyse decreases once we are at a depth larger than D for the shortest dataset in the sample pool. Thus, we maximised equation (4.3) to analyse the azimuth patterns at each depth d over the available samples $S(d)$ at that depth d:

$$I(\overline{\phi}, d) = \sum_{s=1}^{S(d)}\left|\left[\cos\left(\overline{\phi}\right) \quad \sin\left(\overline{\phi}\right)\right]\cdot\begin{bmatrix}\cos\left(\overline{\varphi}(s)\right)\\ \sin\left(\overline{\varphi}(s)\right)\end{bmatrix}\right| \tag{4.3}$$

with s the sample number, $\overline{\phi}$ on the interval $0 < \overline{\phi} \leq \pi$ and d up to the mean cartilage thickness of the samples: $0 < d \leq \overline{D}$.

Statistical analysis

Data were analysed with generalized linear mixed models because some of the variables analysed are not normally distributed. Also, measurements on the same animal and position within an animal are dependent. This excludes conventional analyses such analysis of variance or regression that are intended for normally distributed and independent data. We therefore used the penalized quasi-likelihood methodology described by Schall [291], Breslow & Clayton [56] and Engel & Keen [102]. Calculations were performed with GenStat [268]. The models comprised random effects with associated components of variance, that allowed for dependence between observations of the same animals and the same anatomical sites. Thus, we used a nested structure within animal for hind leg / fore leg, lateral / medial and caudal / distal / rostral sites. In particular, this allowed for additional dependence within animals between duplicate observations on the same site. We are interested in the development of differences between the different anatomical sites with age. Therefore, fixed effects (systematic effects) comprised main effects and all second order interactions for factors age, hind leg / fore leg, lateral / medial site and caudal / distal / rostral site in the initial models.

Models were fitted separately to four response variables: cartilage thickness D, the orientation index $\bar{I}$, the maximum retardance value near the articular surface $\Delta_{\max}$, and the position of the retardance minimum near the articular surface $d|_{\Delta_{\min}}$. For the variables D, $\Delta_{\max}$ and $d|_{\Delta_{\min}}$, we used a log link and gamma variance function, with a multiplicative dispersion parameter. For the variable $\bar{I}$, we used a logit link $\left(\text{logit}\, p = \log p/(1-p)\right)$ and binomial variance function with an additional multiplicative dispersion parameter. Random effects on the link scale were assumed to follow normal distributions. Tests were based on an approximate F-test [181] applied to the adjusted dependent variate from the last iteration step of the iterative re-weighted restricted maximum likelihood algorithm [102] that we used. The link functions provide the relationship between the linear predictor and the mean of the distribution function and the chosen link and variance functions were needed to achieve satisfactory (normally distributed) residuals for the models. Non-significant ($p > 0.05$) higher order interactions were dropped from the initial models.

We used the following symbols in the models: μ: intercept; A_j, j=0, 2, 4, 8, 12, 20, 28, 36, 52, 72: age in weeks; $B_k, k = 1, 2$: fixed factor hind leg / fore leg; C_l, l=1, 2: fixed factor lateral site / medial site; D_m, m=1, 2, 3: fixed factor caudal site / distal site / rostral site; L_i: random factor individual lamb; and $(LB)_{ik}$, $(LBC)_{ikl}$ and $(LBCD)_{iklm}$ nested random factors within lamb. The final model that we fitted for each covariate, is presented in the results section. In the text, we quantify significant differences as mean ± standard error as predicted by the model. For the model with the logit link (for $\bar{I}$), we can only present the mean, and not the standard errors. In the figures, we use raw means and associated standard deviations, and not model predictions, to illustrate the results.

4.3 Results

Figure 4.3 shows an example of qPLM results at 0 weeks and 72 weeks. As expected, cartilage thickness decreases, retardance increases (figure 4.3a) and predominant collagen orientation changes (figure 4.3b) between these ages. Examples of qPLM results at all ten ages are provided in additional figure 4.A.2.

The total number of samples was 1122. For each tested variable, the differences associated with the factor age (A) are much larger than differences between the different anatomical sites. The following sections provide the average results per age and details on (significant) site-dependent differences.

4.3.1 Cartilage thickness

As expected, there is a main effect of cartilage thickness D with age (table 4.1: A_j, $p < 0.001$). D decreases in early life (figure 4.4a) such that at 28 weeks, D is at 34.6 % ± 2.10 % of its thickness at 0 weeks. No significant changes in D occur after 28 weeks (figure 4.4a): at 72 weeks D is at 37.6 % ± 2.07 % of its thickness at 0 weeks.

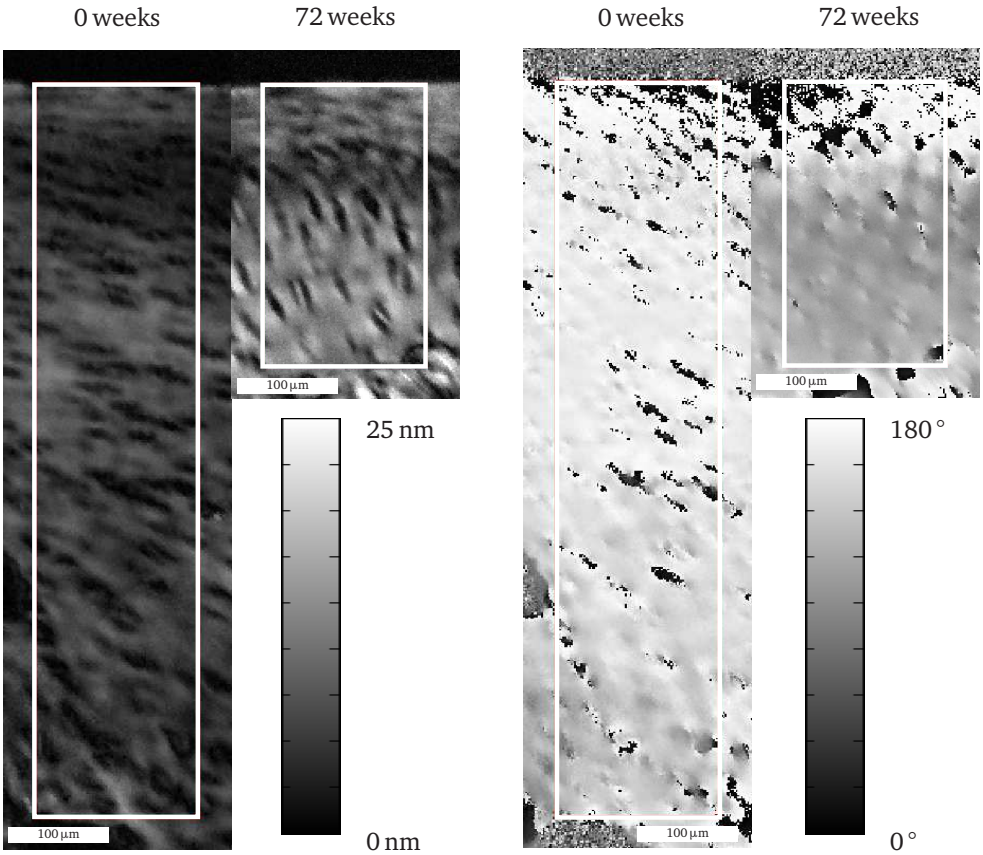

Figure 4.3: Example of qPLM results with regions of interest at 0 weeks and 72 weeks of age. The width of each region of interest is 101 pixels = 161 µm. The articular surface is at the top of the figures. With **(a)** retardance; and **(b)** azimuth.

Table 4.1: Results for the statistical model for cartilage depth d with log-link and gamma variance function. Letters for the fixed terms represent: A_j – age, B_k – fore / hind, C_l – lateral / medial and D_m – caudal / distal / rostral. Combinations represent interactions between these factors.

fixed term	A_j	B_k	C_l	D_m	$(AB)_{jk}$	$(AC)_{jl}$	$(AD)_{jm}$
p-value	< 0.001	< 0.001	0.053	< 0.001	0.021	< 0.001	< 0.001

The final model for the covariate cartilage thickness D with log-link and gamma variance function on the log scale is:

$$\mu+A_j+B_k+C_l+D_m+(AB)_{jk}+(AC)_{jl}+(AD)_{jm}+L_i+(LB)_{ik}+(LBC)_{ikl}+(LBCD)_{iklm} \quad (4.4)$$

The results are gathered in table 4.1 and figure 4.4.

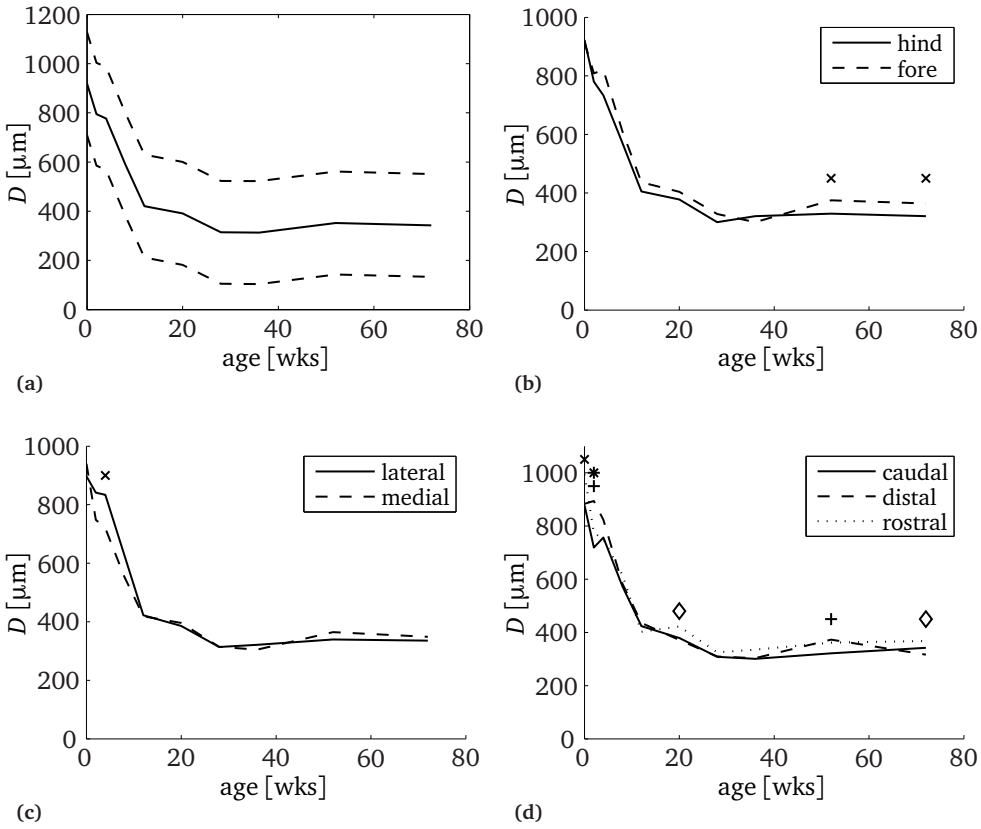

Figure 4.4: Cartilage thickness. **(a)** Mean cartilage thickness D (solid) ± standard deviation (dashed) for all samples at each age; **(b)** Mean cartilage thickness D as a function of age for hind legs (solid) and fore legs (dashed). The model predicts significant differences for: 'x' - fore leg > hind leg; **(c)** Mean cartilage thickness D as a function of age for lateral site (solid) and medial site (dashed). The model predicts significant differences for: 'x' - lateral site > medial site; **(d)** Mean cartilage thickness D as a function of age for the caudal site (solid), distal site (dashed) and rostral site (dotted). The model predicts significant differences for: 'x' - rostral site > caudal site, '+' - distal site > caudal site, '*' - distal site > rostral site, and '⋄' - rostral site > distal site.

For the factor hind leg / fore leg, there is a main effect (table 4.1: B_j, $p < 0.001$) and an interaction with age (table 4.1: $(AB)_{jk}$, $p = 0.021$). For the main effect, the model predicts that cartilage is 6.40 % ± 2.15 % thicker in the fore legs than in the hind legs. For the interaction with age, cartilage in the fore legs is thicker than the cartilage in the hind legs at all ages but 0 weeks and 36 weeks (hind legs thicker, figure 4.4b). The interaction with age results in significant differences at 52 weeks (fore legs 14.3 % ± 7.29 % thicker) and 72 weeks (fore legs 13.7 % ± 7.25 % thicker).

For the factor lateral site / medial site, there is no main effect (table 4.1: C_l, $p = 0.053$), but there is an interaction with age (table 4.1: $(AC)_{jl}$, $p < 0.001$). This interaction does not show a trend (figure 4.4c) and is only significant at age 4 weeks (lateral site 15.8 % ± 7.40 % thicker).

For the factor caudal site / distal site / rostral site, there is a main effect (table 4.1: D_m, $p < 0.001$) and an interaction with age (table 4.1: $(AD)_{jm}$, $p < 0.001$). For the main effect, the model predicts that cartilage is 4.50 % ± 2.12 % thicker at the distal site than at the caudal site, and cartilage is 7.36 % ± 2.18 % thicker at the rostral site than at the caudal site. The interaction with age does not show a trend (figure 4.4d), but there are significant differences at ages 0 weeks (rostral 14.1 % ± 7.31 % thicker than caudal), 2 weeks (distal 25.0 % ± 8.00 % thicker than caudal, and distal 14.6 % ± 7.33 % thicker than rostral), 20 weeks (rostral 14.3 % ± 7.32 % thicker than distal), 52 weeks (distal 16.3 % ± 7.45 % thicker than caudal) and 72 weeks (rostral 16.3 % ± 7.43 % thicker than distal).

In the following sections, we present overviews of azimuth (figure 4.5b) and retardance (figure 4.7b) as a function of age. For these figures, cartilage depth as a function of age is estimated from an exponential fit through the data for all samples. This fit is given by

$$D_f(t) = 618\left(0.52 + \mathrm{e}^{-0.11t}\right) \tag{4.5}$$

with D_f the cartilage depth in μm and t the age in weeks.

4.3.2 Collagen orientation

Predominant collagen orientation changes with age (figure 4.5a). Predominant collagen orientation is parallel to the articular surface for most of the cartilage depth for the youngest animals. As age increases, predominant collagen orientation in the deep cartilage changes, first at a depth where the future transitional zone will appear for animals of age 8 weeks and 12 weeks. At the age of 20 weeks, we first see a Benninghoff structure: predominant collagen orientation changes from parallel to the articular surface to a predominant orientation more towards the perpendicular with the subchondral bone in the deep cartilage. With increasing age, predominant collagen orientation in the deep cartilage aligns further towards the perpendicular to the cartilage / bone interface. The patterns in figure 4.5a appear to converge to an azimuth between 120 ° and 160 ° near the cartilage / bone interface. Thus for the youngest samples, azimuth decreases in the deep zone near the cartilage / bone interface, and in the older samples, azimuth increases in the deep zone near the cartilage / bone interface.

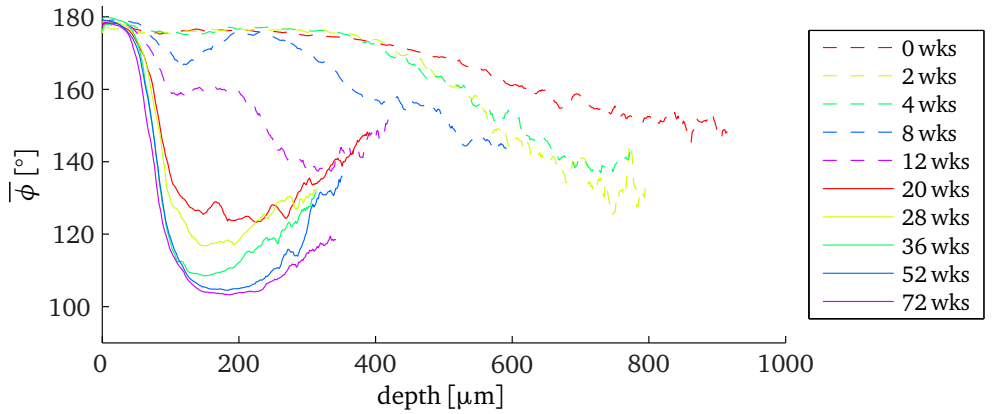

(a)

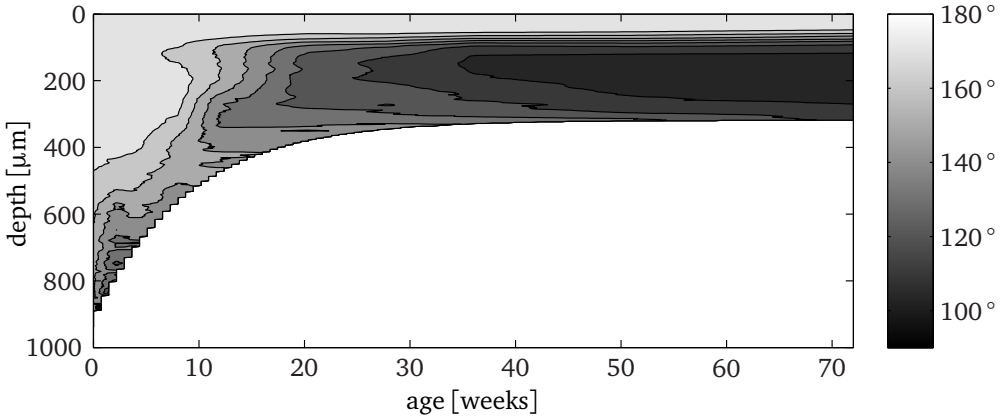

(b)

Figure 4.5: Predominant collagen orientation per age. With **(a)** Mean predominant collagen orientation $\overline{\phi}$ as a function of age and cartilage depth. Colours represent age in weeks; and **(b)** Overview of the results per age in a contour plot.

The final model for the covariate orientation index $\overline{I}$ with logit-link and binomial variance function on the logit scale is:

$$\mu + A_j + B_k + C_l + D_m + (AD)_{jm} + L_i + (LB)_{ik} + (LBC)_{ikl} + (LBCD)_{iklm} \qquad (4.6)$$

The results are gathered in table 4.2 and figure 4.6.

There is a main affect of age on the orientation index $\overline{I}$ (table 4.2: A_j, $p < 0.001$). As expected, $\overline{I}$ is close to 1 for the youngest animals and decreases with age (figure 4.6a), as less collagen fibres are predominantly oriented parallel to the articular surface. At 20 weeks, $\overline{I}$ is 0.21 lower than at 0 weeks. After 20 weeks, no significant differ-

Table 4.2: Results for the statistical model for orientation index $\overline{I}$ with logit-link and binomial variance function. Letters for the fixed terms represent: A_j – age, B_k – fore / hind, C_l – lateral / medial and D_m – caudal / distal / rostral. Combinations represent interactions between these factors.

fixed term	A_j	B_k	C_l	D_m	$(AD)_{jm}$
p-value	< 0.001	0.560	0.013	< 0.001	0.011

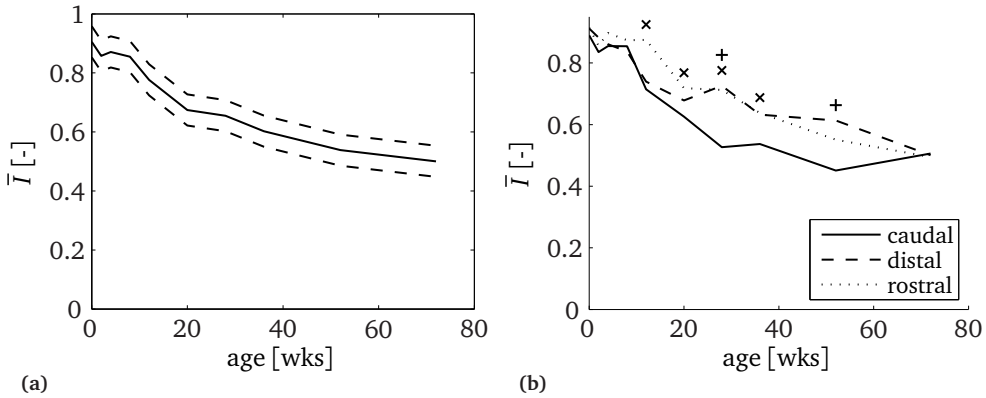

Figure 4.6: Orientation index. With **(a)** Mean orientation index $\overline{I}$ (solid) ± standard deviation (dashed) as a function of age; and **(b)** Mean orientation index $\overline{I}$ as a function of age for the caudal site (solid), distal site (dashed) and rostral site (dotted). The model predicts significant differences for: 'x' - rostral site > caudal site and '+' - distal site > caudal site.

ences between successive age groups occur, although $\overline{I}$ at 72 weeks (0.41 lower than at 0 weeks) does differ significantly from $\overline{I}$ at 36 weeks (0.31 lower than at 0 weeks).

There is a main effect for lateral sites versus medial sites (table 4.2: C_l, $p = 0.013$). The model shows that $\overline{I}$ is 0.22 higher at the lateral site. Inspection of the average orientation patterns for these sites per age (additional figure 4.A.3) indicates two differences: 1) the medial site appears to be further in the development of the Benninghoff structure at ages 4 weeks, 12 weeks and 52 weeks; and 2) the depth where the predominant collagen fibre orientation is halfway in the transition from superficial zone to deep zone, is smaller for the medial site than for the lateral site at ages 28 weeks, 36 weeks and 52 weeks. Both effects result in a lower value of $\overline{I}$.

For the factor caudal site / distal site / rostral site, there is a main effect (table 4.2: D_m, $p < 0.001$) and an interaction with age (table 4.2: $(AD)_{jm}$, $p = 0.011$). For the main effect, the model predicts that $\overline{I}$ is 0.06 higher at the distal site than at the caudal

site, and $\bar{I}$ is 0.08 higher at the rostral site than at the caudal site. The interaction with age shows significant differences between 12 weeks and 52 weeks (figure 4.6b). $\bar{I}$ is higher at the rostral site than at the caudal site at 12 weeks (0.16), 20 weeks (0.09), 28 weeks (0.20) and 36 weeks (0.10). $\bar{I}$ is higher at the distal site than at the caudal site at 28 weeks (0.21) and 52 weeks (0.17).

Inspection of the average orientation patterns for these sites per age (additional figure 4.A.4) shows that the caudal site develops its Benninghoff structure earlier in life than the rostral and distal site: predominant collagen orientation at a depth of 100 µm at 28 weeks is 104° at the caudal site against 127° at the rostral site and 125° at the distal site. The average orientation patterns do not show a trend for differences between development for the rostral site and distal site. At 72 weeks of age, all site-dependent variation in collagen orientation has vanished(figure 4.6b).

Figure 4.5b finally, shows an overview of the dynamics of the azimuth results for all samples (sites) per age taken together (interpolated from figure 4.5a).

4.3.3 Retardance

The retardance values change during development, but the general retardance patterns appear indifferent to age (figure 4.7). For all ages from articular surface towards the bone, retardance first has a maximum near the articular surface, followed by a minimum at a depth of $\approx$ 50 µm that is in turn followed by another maximum deeper in the cartilage.

The final model for the maximum retardance near the articular surface $\Delta_{\max}$ with log-link and gamma variance function on the log scale is:

$$\mu + A_j + B_k + C_l + D_m + (AD)_{jm} + (BD)_{km} + L_i + (LB)_{ik} + (LBC)_{ikl} + (LBCD)_{iklm} \quad (4.7)$$

The results are gathered in table 4.3.

Table 4.3: Results for the statistical model for the maximum retardance near the articular surface $\Delta_{\max}$ with log-link and gamma variance function. Letters for the fixed terms represent: A_j – age, B_k – fore / hind, C_l – lateral / medial and D_m – caudal / distal / rostral. Combinations represent interactions between these factors.

fixed term	A_j	B_k	C_l	D_m	$(AD)_{jm}$	$(BD)_{km}$
p-value	< 0.001	0.172	0.396	0.179	0.034	0.005

There is a main effect of age with the maximum retardance near the articular surface $\Delta_{\max}$ (table 4.3: A_j, $p < 0.001$). $\Delta_{\max}$ increases with age until 36 weeks when it is 164 % ± 20.0 % higher than at 0 weeks (figure 4.8a). No significant changes occur after 36 weeks: at 72 weeks, $\Delta_{\max}$ is 154 % ± 19.3 % higher than at 0 weeks,

There are no other main effects, but there are two significant interactions with the factor caudal site / distal site / rostral site (table 4.3: $(AD)_{jm}$, $p = 0.034$ and $(BD)_{km}$,

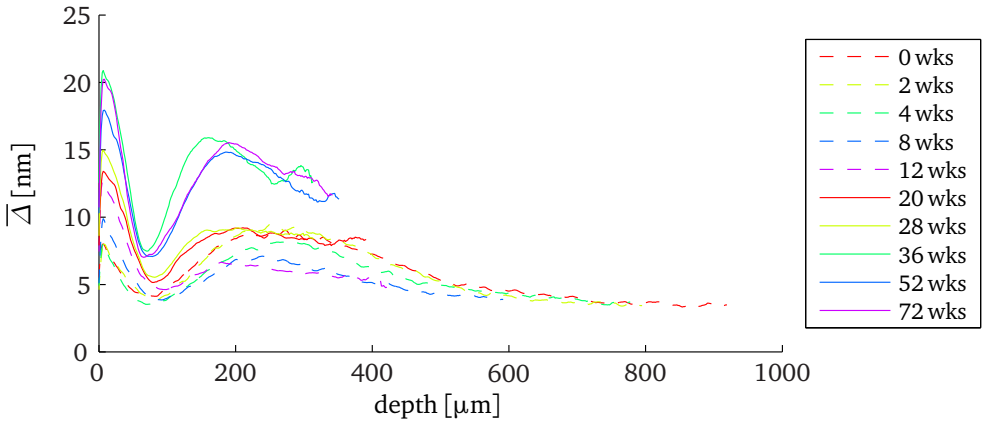

(a)

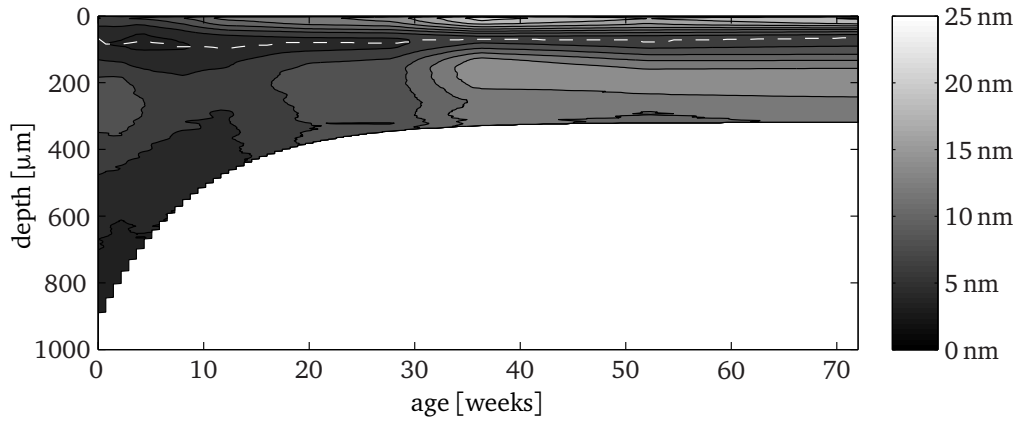

(b)

Figure 4.7: Retardance per age. With **(a)** Mean sample retardance as a function of cartilage depth. Colours represent age in weeks; and **(b)** overview of the results in a contour plot. The dashed white line marks the retardance minimum.

$p = 0.005$). The interaction with age $(AD)_{jm}$ shows significant differences at ages 0 weeks (distal 30.3 % ± 12.8 % higher than rostral), 2 weeks (caudal 25.0 % ± 12.2 % higher than rostral, and distal 41.3 % ± 13.8 % higher than rostral) and 20 weeks (rostral 28.4 % ± 12.6 % higher than distal), but no trend (figure 4.8b). The interaction of caudal site / distal site / rostral site with hind legs / fore legs $(BD)_{km}$ is due to the caudal site: $\Delta_{\max}$ is 18.7 % ± 4.92,% higher in the hind legs than in the fore legs for the caudal site. The model shows no differences between hind legs and fore legs for the rostral and distal site.

The final model for the position of the retardance minimum near the articular surface $d|\Delta_{\min}$ with log-link and gamma variance function on the log scale is the same as for

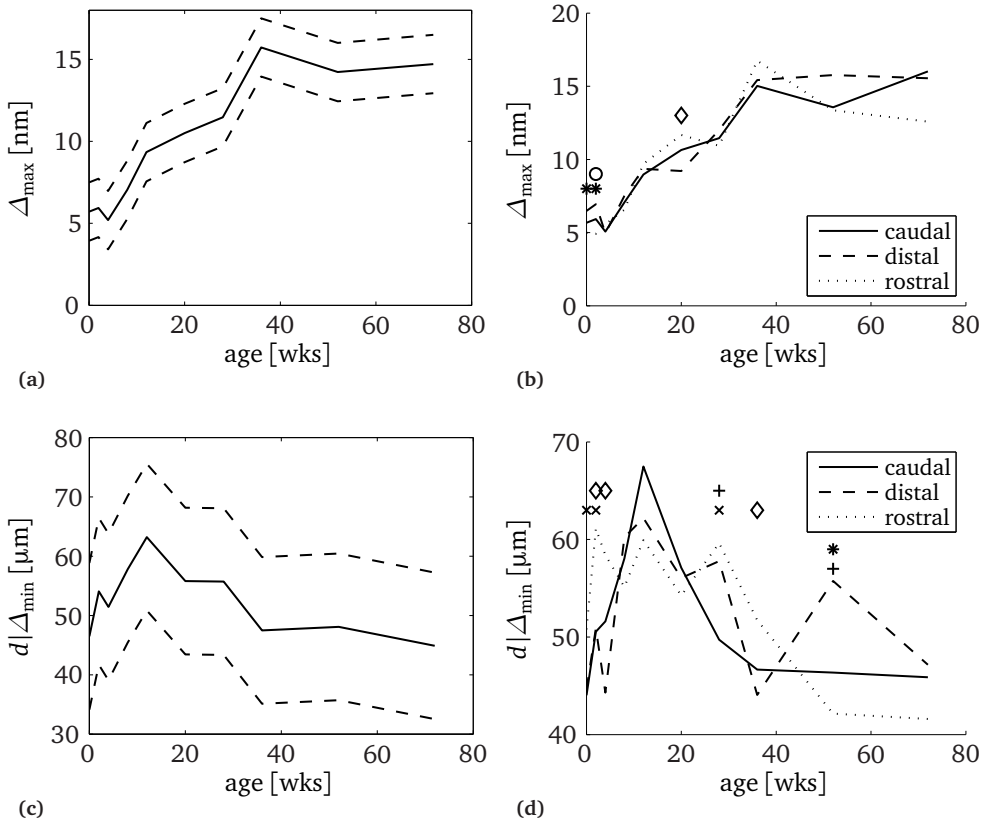

Figure 4.8: Retardance maximum and minimum. With **(a)** Mean of the maximum retardance near the articular surface Δ_{max} (solid) ± standard deviation (dashed) as a function of age; **(b)** Mean of the maximum retardance near the articular surface Δ_{max} as a function of age for the caudal site (solid), distal site (dashed) and rostral site (dotted). The model predicts significant differences for: '*' - distal site > rostral site, '◇' - rostral site > distal site, and 'o' - caudal site > rostral site; **(c)** Mean position of the retardance minimum near the articular surface $d|\Delta_{min}$ (solid) ± standard deviation (dashed) as a function of age; and **(d)** Mean position of the retardance minimum near the articular surface $d|\Delta_{min}$ as a function of age for the caudal site (solid), distal site (dashed) and rostral site (dotted). The model predicts significant differences for: 'x' - rostral site > caudal site, '+' - distal site > caudal site, '*' - distal site > rostral site, and '◇' - rostral site > distal site.

the orientation index (equation 4.6). There is a main effect of the factor age on $d|\Delta_{min}$ (table 4.4: A_j, $p = 0.003$). With increasing age, $d|\Delta_{min}$ first increases until 12 weeks and next deceases until 72 weeks of age (figure 4.8c). At the maximum at 12 weeks, $d|\Delta_{min}$

Table 4.4: Results for the statistical model for the position of the retardance minimum near the articular surface $d|\Delta_{\min}$ with log-link and gamma variance function. Letters for the fixed terms represent: A_j – age, B_k – fore / hind, C_l – lateral / medial and D_m – caudal / distal / rostral. Combinations represent interactions between these factors.

fixed term	A_j	B_k	C_l	D_m	$(AD)_{jm}$
p-value	0.003	0.733	0.002	0.536	< 0.001

is 35.4 % ± 7.63 % higher than at 0 weeks. At 36 weeks of age an older, the model shows no difference for $d|\Delta_{\min}$ with 0 weeks of age.

The interaction of caudal site / distal site / rostral site with age (table 4.4: $(AD)_{jm}$, $p < 0.001$) has significant differences at ages 0 weeks (rostral 17.2 % ± 8.59 % higher than caudal), 2 weeks (rostral 19.1 % ± 8.72 % higher than caudal, and rostral 21.7 % ± 8.91 % higher than distal), 4 weeks (rostral 28.4 % ± 9.40 % higher than distal), 28 weeks (rostral 17.4 % ± 8.59 % higher than caudal, and distal 16.4 % ± 8.53 % higher than caudal), 36 weeks (rostral 17.7 % ± 8.62 % higher than distal) and 52 weeks (distal 18.7 % ± 8.69 % higher than caudal, and distal 30.1 % ± 9.52 % higher than rostral), but these effect do not show a trend (figure 4.8d). There is also a significant main effect for lateral site / medial site (table 4.4: C_l, $p = 0.002$): $d|\Delta_{\min}$ is 7.14 % ± 2.31 % higher at the lateral site.

Figure 4.7b finally, shows an overview of the dynamics of the retardance results for all samples (sites) per age taken together (interpolated from figure 4.7). The position of the retardance minimum is marked with a dashed white line.

4.4 Discussion

The results on cartilage thickness are mostly in line with previous work. Brommer et al. [57] for instance, analysed site-dependent development of cartilage thickness in the equine proximal phalanx. As we did in our study, they found that cartilage thickness decreases during development, and they found no site-dependent differences in cartilage thickness in mature animals. In our study, cartilage at the caudal site is thinner than at the rostral and distal site and cartilage in the fore legs is thicker than in the hind legs, although the differences are small (< 8 %). Cartilage thickness has been shown to respond to mechanical loads during development [143, 189, 190, 256] and the results for the development of the collagen network suggest influences of different loading regimes at different anatomical sites. However, cartilage thickness in the mature animal is thought to relate to joint congruency, i.e. the similarity of the two articulating cartilage surfaces [55, 304]. This explains why we find only small site-dependent differences in cartilage thickness in the nearly congruent joint that we investigated. This leaves us with the difference in cartilage thickness between hind legs and fore legs. Contrary to the remark by Simon [303] that cartilage is in general thicker in the hind limbs, we find that

cartilage is thicker in the fore limbs, and that the difference increases slightly between birth and maturity.

As in previous studies on collagen structure in horses [328], pigs [282] and rabbits [168], we find that the perinatal predominant collagen fibre orientation is parallel to the articular surface throughout most of the cartilage depth and that this arrangement changes to an arcade-like Benninghoff structure as the cartilage matures. We also confirmed the presence of a retardance minimum in the perinatal animals as noted earlier by Van Turnhout et al. [328]. The collagen remodelling process appears finished at 36 weeks of age in our sheep in this joint (e.g. figures 4.5b and 4.7b): the differences in qPLM results are small after this age and three of the four measured parameters (D, $\Delta_{\max}$, and $d|\Delta_{\min}$) do not change significantly between 36 weeks and 72 weeks of age. Hunziker et al. [154] found no noteworthy changes after puberty in the structural organization of rabbit AC and 36 weeks is also approximately when the sheep are sexually mature: the first ovulation or puberty in the sheep occurs at $\approx$ 6 months of age or at a mass of 30 kg to 35 kg, and this transition lasts $\approx$ 5 weeks [114]. It is well before skeletal maturity, which occurs around 12 months of age [66, 147, 238]. Also, the slaughter mass results (additional figure 4.A.5) show that the animals still developed after the age of 36 weeks.

The fact that collagen orientation appears to vary in the deep zone (figure 4.5a) is related to our decision to average sample profiles up to the mean depth of the sample pool. There are samples that are shorter than this mean depth and the number of samples that we (can) use to average therefore decreases from the minimum depth in the sample pool to the mean depth. The benefit of this procedure is that it better captures the superficial and transitional zones: e.g., the observation that the absolute depth of the retardance minimum appears invariant to age is evident when analysed in this manner. The downside is that from the minimum depth to the mean depth in the sample pool, we have an increasing proportion of data that is very close to the cartilage / bone interface. The azimuth data in particular may deviate from the deep zone data at the cartilage / bone interface, where the collagen ensures the integration of these two tissues. Inspection of the individual orientation patterns has shown that the azimuth is in fact fairly constant in the deep zone (additional figure 4.A.6), and that the deviations towards the cartilage / bone interface in figure 4.5a are largely due to the increasing influence of cartilage / bone interfaces as described above.

We find site dependent differences in collagen network remodelling (additional files 3 and 4). Both $\overline{I}$ and $d|\Delta_{\min}$ are higher at the lateral site than at the medial site (table 4.2 and 4.4, C_l, $p = 0.013$ and $p = 0.002$). $\overline{I}$ is higher for less advanced Benninghoff structures and for Benninghoff structures with higher $d|\Delta_{\min}$. The results for $d|\Delta_{\min}$ suggest that its smaller value for the medial sites is correlated to the smaller values of $\overline{I}$. Thus, the transitional zone is at a larger depth at the lateral side, i.e. the superficial zone is thicker at the lateral side.

Also, the caudal site develops different from the distal and rostral sites: it develops its Benninghoff structure earlier in life (figure 4.6b, additional file 3) and maximum retardance is higher in the hind legs for the caudal site, but not for the distal and rostral site (table 4.3, $(BD)_{km}$, $p = 0.005$). These observations suggests a loading regime during development that is different for the caudal sites compared with the rostral and distal sites.

In the last sample point however, we find no site dependent differences in predominant collagen orientation patterns (additional file 3) or the orientation index $\overline{I}$ (figure 4.6b). Gründer [128] reports a faster structural development for sheep tibial AC compared with femural AC, Julkunen et al. [168] showed that collagen structure development and adult collagen structure both differ between femur and tibia in rabbits, and Brama et al. [54] showed changes in collagen structure in juvenile foals as a result of exercise training. However, Egger et al. [99] did not find differences in collagen structure in adult elephant knee cartilage and they propose that this is due to the congruency in the elephant knee. This hypothesis is supported by our data: in the examined nearly congruent joint that was subjected to physiological loads, we also find no differences in collagen orientation between sites on the same cartilage surface for the oldest (adult) animals.

Our data shows that the predominant collagen orientation first changes at a depth that marks the proximal boundary of the transitional zone in the mature animal (figure 4.5a). The resulting intermediate pattern for predominant collagen orientation that we find at 12 weeks, is similar to the intermediate pattern found in a 4.5 month year old horse [328], in 11 month old pigs [282], and in rabbits of 4 weeks to 6 weeks [168]. This intermediate pattern is present for all anatomical sites in the current study. This suggests that the depth-dependent pattern of collagen remodelling is similar across species, joints and anatomical sites, except for the timing (e.g. earlier development for the caudal site in this study, figure 4.6b and additional file 3). The difference in species (porcine versus ovine) and anatomical location (metacarpus versus knee) can explain why Rieppo et al. [282] found that collagen remodelling was not finished when their pigs reached sexual maturity.

The absence of a Benninghoff collagen structure at birth may have implications for postnatal morphogenesis. Results of simulations with finite element models [33, 72] and *in vitro* experimental results [306] show correlations between hydrostatic pressure and inhibition of ossification and between shear strains and promotion of ossification. An effect of the Benninghoff collagen structure is that it limits cartilage swelling, and it thereby effectively increases the hydrostatic (osmotic) pressure in the deep zone [18, 26, 235]. The development of the Benninghoff structure might thus serve to prevent ossification and maintain a functional cartilage layer in the adult animal. It would be interesting to see if cartilage ossification is promoted when the Benninghoff collagen structure cannot develop.

The retardance minimum near the articular surface is traditionally associated with the transitional zone, a layer with a weak anisotropic collagen arrangement, in adult animals [37, 150]. Our special interest in this retardance minimum appears to have been justified. Not only is it present at birth without evidence of differentiation in collagen orientation, which is confirmed by earlier work on equine [328] and porcine cartilage [282], it is also the only parameter that is similar in the youngest and oldest animals (figure 4.8c). During cartilage maturation, its thickness decreases to about one third of the perinatal thickness; collagen fibre orientation changes from a network predominantly parallel to the articular surface over the cartilage depth to a Benninghoff structure; and maximum retardance increases to about twice that of neonatal cartilage. Compared to these developmental changes, the depth of the retardance minimum ($\approx 50\,\mu m$) appears relatively indifferent to the remodelling process (figure 4.8c). Thus, a layer with

a weak anisotropic collagen arrangement, or less collagen, or both, is already formed before birth. This can for instance be a result of *in utero* movement and muscular loads on the joint [135, 263]. If so, then apparently the mechanical state in this layer does not change enough after birth to result in a much stronger anisotropic collagen fibre arrangement. If *in utero* joint loading is responsible for the emergence of this layer, we would predict its absence in animal models that e.g. lack skeletal muscle activity [122]. Finite element models may help to explain what is so special about this layer, and its location.

With this paper, we provide essential information for analysis of the role of the collagen fibre network during development, e.g. by fibril reinforced finite element models [199, 215, 357]. It is the first time that the dynamics of post natal remodelling of collagen fibre organisation have been time and space resolved from birth to maturity. Therefore, we were able to present the first solid observation of a retardance minimum in perinatal animals, more or less at a fixed distance ($\approx 50\,\mu m$) from the articular surface. This is an important step towards a better understanding of the mechanobiology of articular cartilage development. With additional information on collagen densities during development, we will be able to interpret the retardance minimum as a region with less collagen or a region with more anisotropic collagen and see how much this interpretation changes during development. With additional information on the development of glycosaminoglycan concentrations and fixed charge densities in the AC, it becomes possible to estimate the mechanical environment that drives the depth-dependent AC development in general, and depth-dependent collagen orientation remodelling in particular.

4.5 Conclusions

The collagen network in articular cartilage remodels between birth and sexual maturity from a network with predominant orientation parallel to the articular surface to a Benninghoff network. Changes in predominant collagen orientation occur first at a depth that marks the proximal boundary of the transitional zone in adult animals. This is the first solid observation of the dynamics of collagen structure remodelling, and provides important information for the further investigation of articular cartilage mechanobiology.

The fact that the retardance minimum near the articular surface is present at all ages shows that a zonal differentiation is already present in the perinatal animals. However, the zonal differentiation can not be correlated to changes in collagen network orientation in these animals. Furthermore, we were able to show that the depth of this retardance minimum is fairly constant during development. Without information on the development of collagen densities, we cannot tell if this retardance minimum is the result of a region with less collagen or a region with collagen with less anisotropic predominant orientations; and we cannot tell whether the relative contributions (less collagen and less anisotropic arrangement) change during development. We intent to address this in a future publication.

We observe differences in the dynamics of collagen remodelling between different

anatomical sites, but in the adult animals we see no difference in collagen structure (i.e. they are all similar Benninghoff structures) or cartilage thickness. We expect that this is due to the congruency of the joint that we investigated. Comparison of the data in the current paper with other data on collagen remodelling in literature, suggests that the general pattern of collagen remodelling (i.e. where the first changes in collagen orientation occur) is similar between joints and species.

Authors contributions

MvT carried out the design of the study and its coordination, the data processing, analysis and interpretation, and drafting the manuscript; and participated in acquisition of data and the statistical analysis. HS carried out the acquisition of data (histology and microscopy), and participated in data analysis and interpretation and drafting the manuscript. BE and WB carried out the statistical analysis and participated in the interpretation of data and drafting the manuscript. SK and JvL participated in the design of the study and its coordination, data analysis and interpretation and critical revisions of the manuscript. All authors read and approved the final manuscript.

Acknowledgements

We kindly thank Wim van de Laan for providing the sheep. From Wageningen University, we thank the people at De Haar / Ossekampen laboratory animal facility for taking care of the sheep; and Dr. Norbert de Ruijter at the Plant Cell Biology group for support with the qPLM equipment. In our own group we thank Adwin van den Brink for help with tissue processing; and Dr. Martin Lankheet for his critical review of the manuscript.

4.A Additional figures

2 weeks, left hind leg, lateral

72 weeks, left hind leg, medial

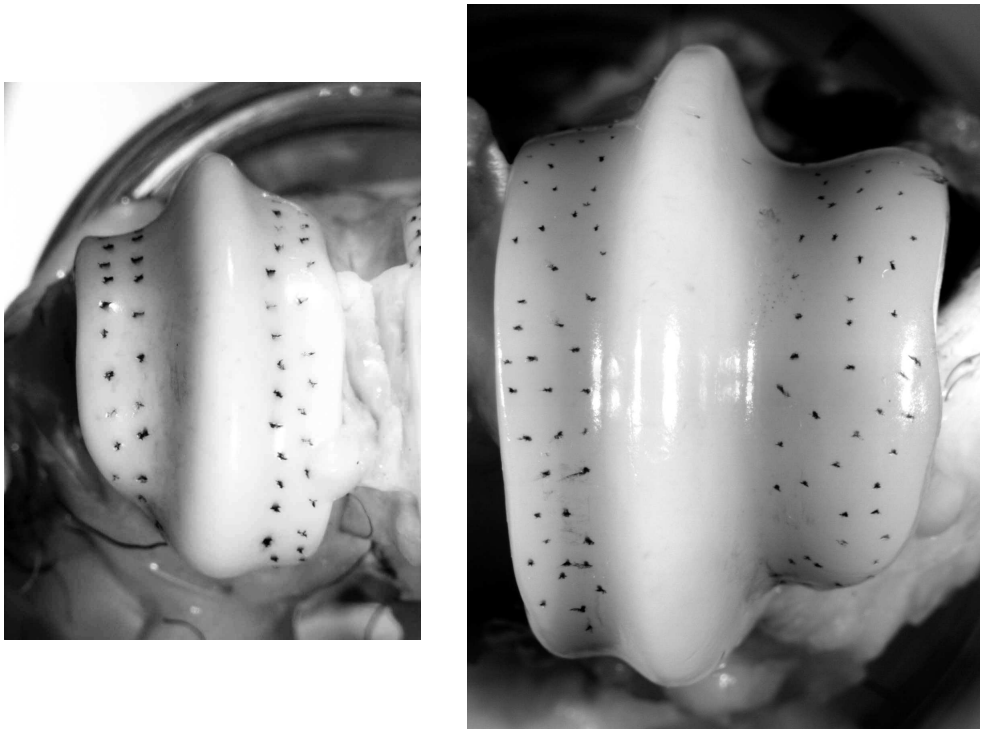

Figure 4.A.1: Illustration of split lines. Left: lateral side of a left hind leg in a 2 week old lamb. Right: medial side of a left hind leg in a 72 week old lamb.

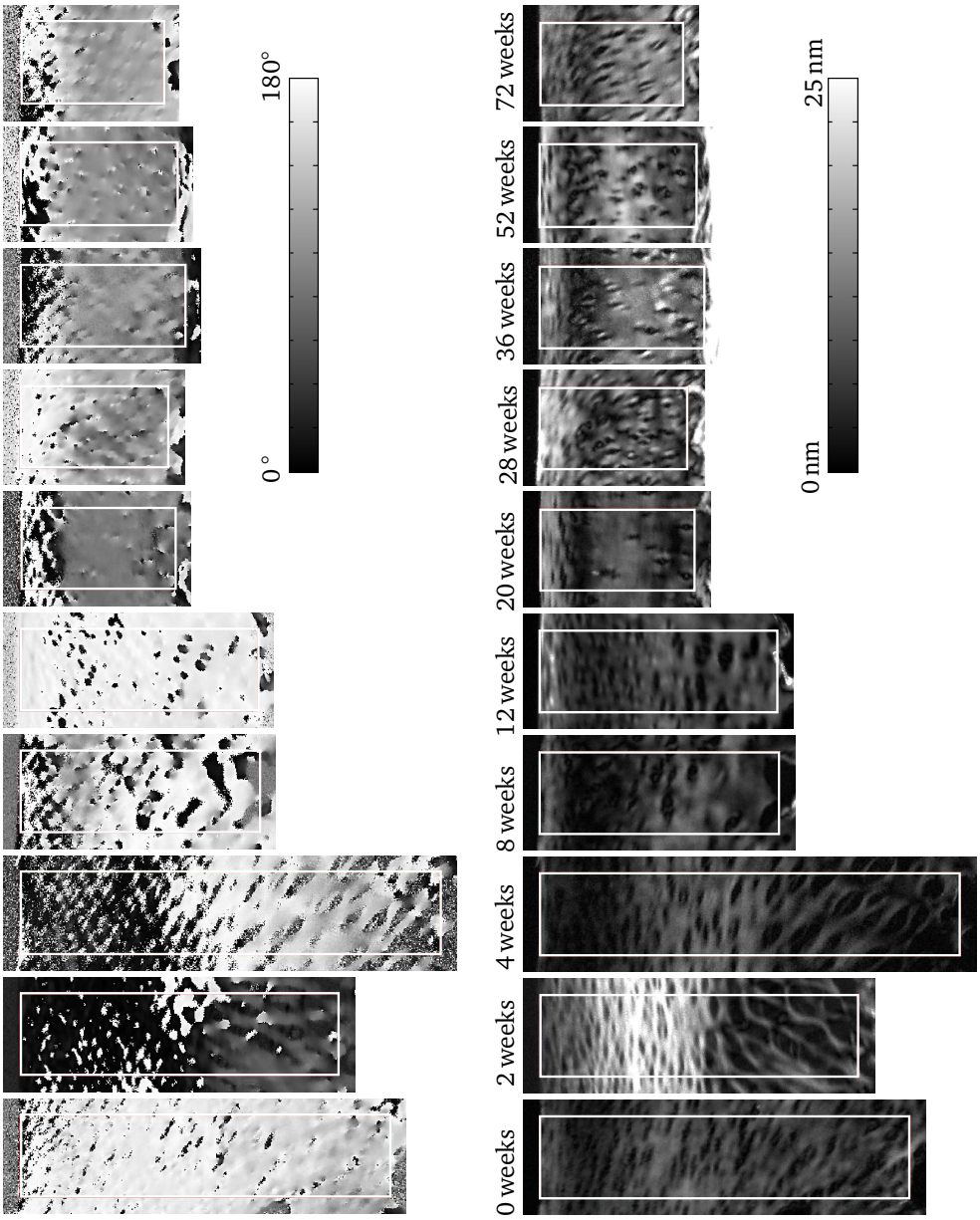

Figure 4.A.2: Examples of PLM images for all ten age points. Left: azimuth results. Right: retardance results.

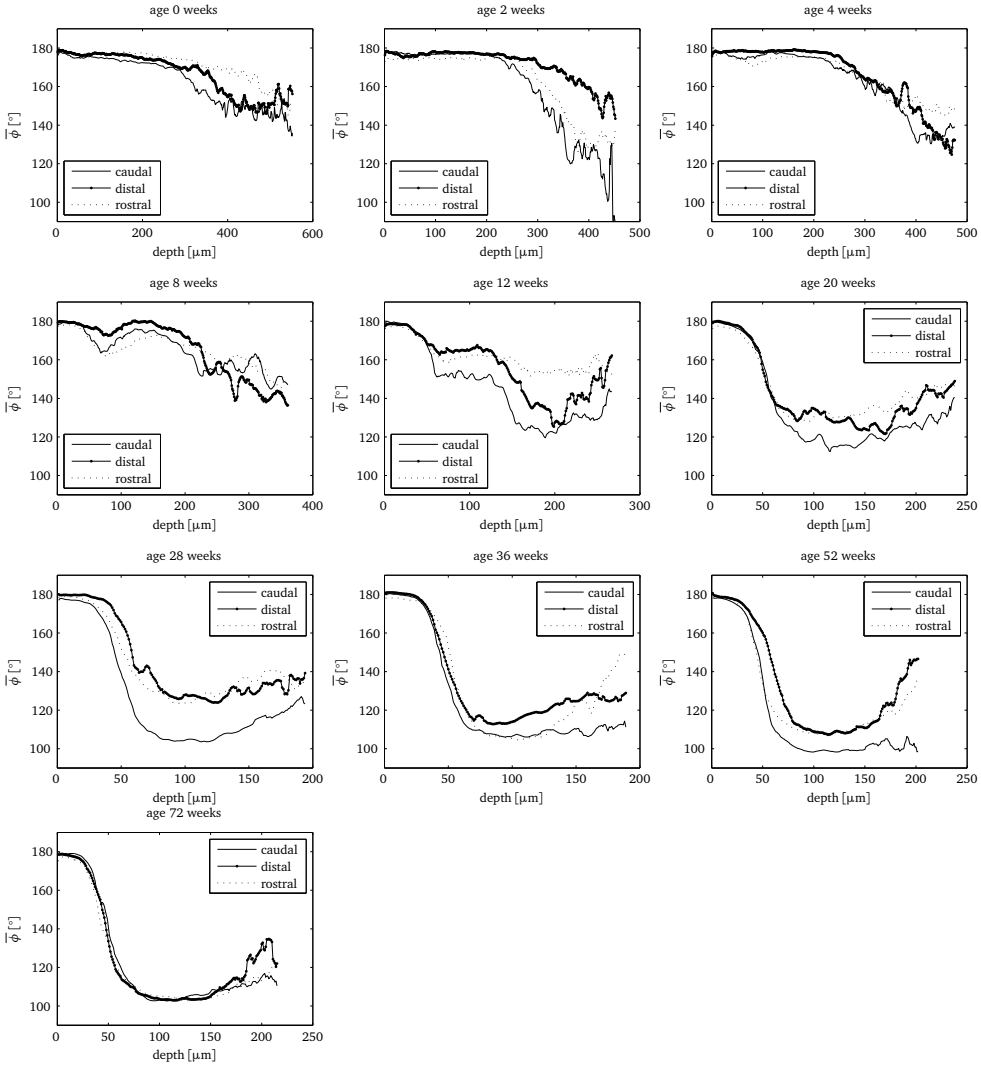

Figure 4.A.3: Orientation patterns for caudal / distal / rostral sites.Average orientation patterns for all ten ages divided in caudal, distal and rostral samples.

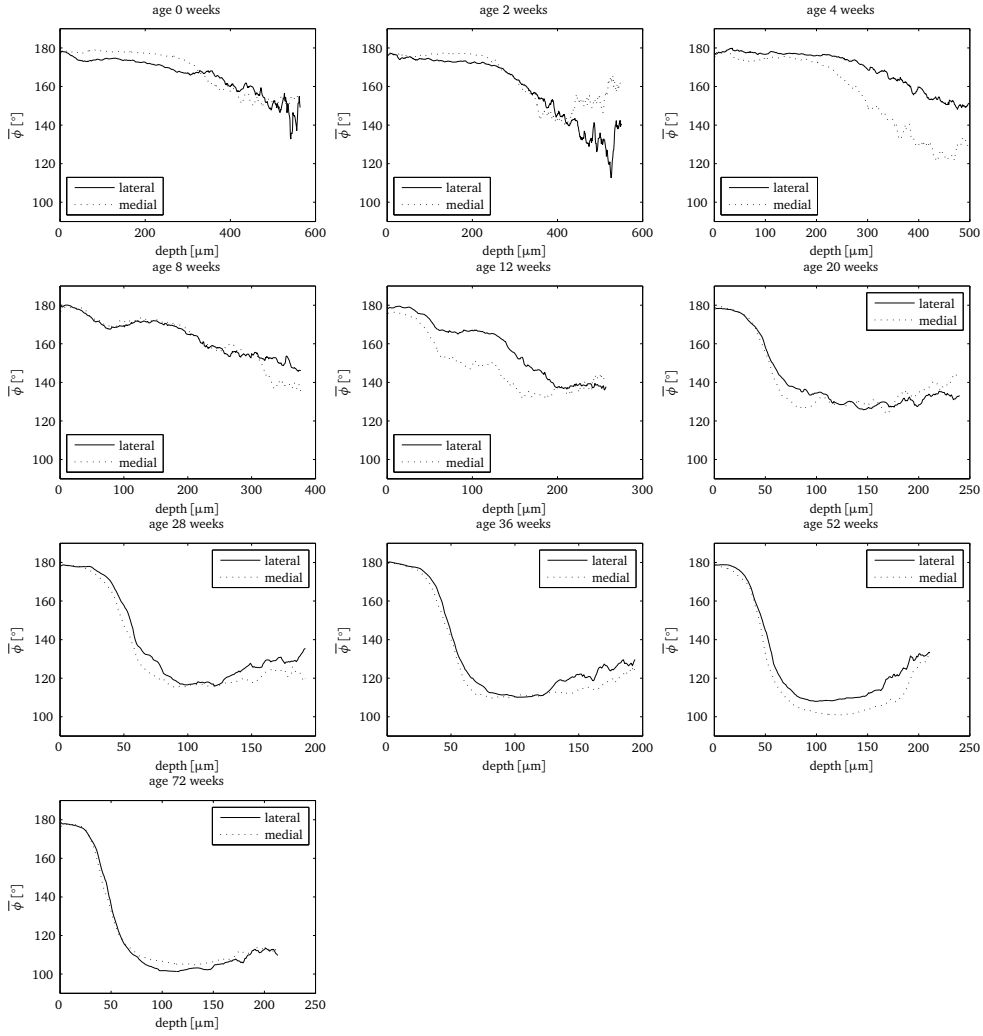

Figure 4.A.4: Orientation patterns for lateral / medial sites. Average orientation patterns for all ten ages divided in lateral and medial samples.

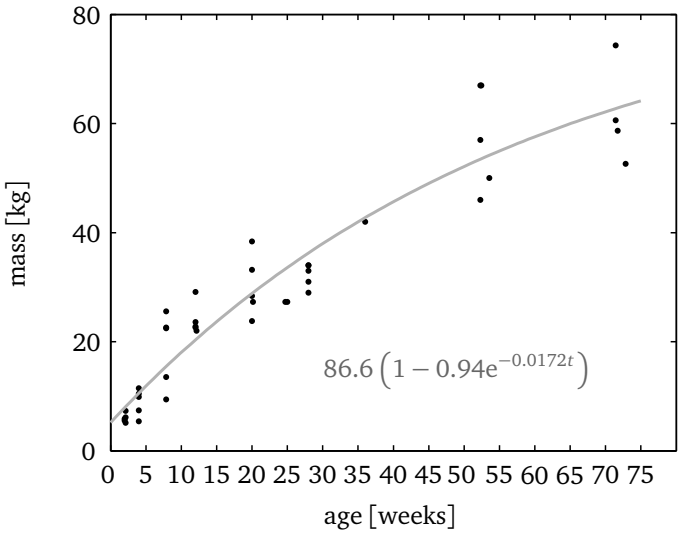

Figure 4.A.5: Slaughter mass together with the exponential fit. The mass at 36 weeks is an estimate from the butcher, because these animals were not weighed prior to sacrifice.

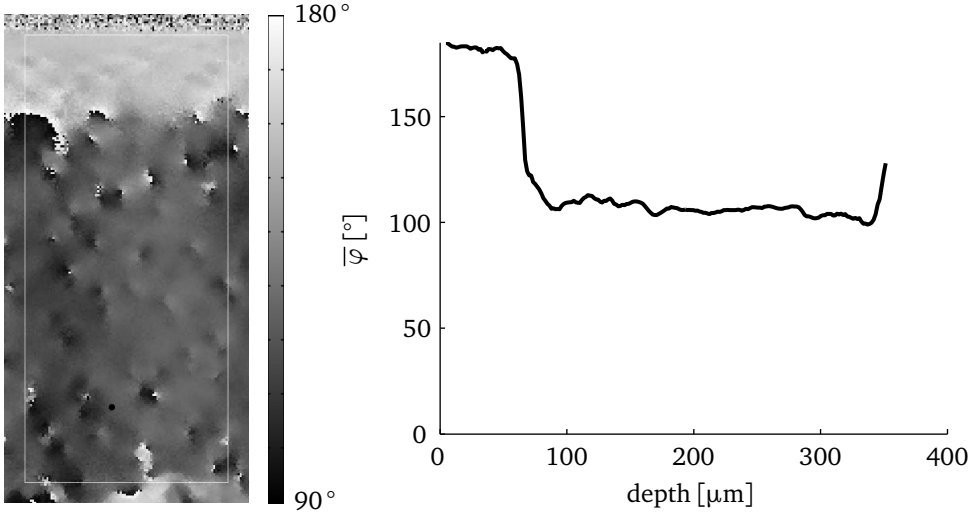

Figure 4.A.6: Constant azimuth in the deep zone. Illustration of the constant azimuth in the deep zone for a 72 week old animal. Left: azimuth PLM image with ROI. The articular surface is on top of the image. Right: corresponding orientation pattern. The azimuth is fairly constant in the deep zone up until the last 3 % of the total depth.

In the computer model, all the microfilaments were given certain quantitative properties with names that mean something to physicists: a 'viscous damping coefficient' and an 'elastic spring constant'. Never mind exactly what these mean: they are the kind of things physicists like to measure in a spring.

Richard Dawkins [93]

5

Contribution of postnatal collagen reorientation to depth-dependent mechanical properties of articular cartilage

Mark C. van Turnhout[1], Sander Kranenbarg[1] & Johan L. van Leeuwen[1]. *Biomechanics and Modeling in Mechanobiology*, online first, June 7th, 2010.
doi: 10.1007/s10237-010-0233-7

[1]Wageningen University, Experimental Zoology Group, PO Box 338, 6700 AH, Wageningen, The Netherlands.

Abstract

The collagen fibril network is an important factor for the depth-dependent mechanical behaviour of adult articular cartilage (AC). Recent studies show that collagen orientation is parallel to the articular surface throughout the tissue depth in perinatal animals, and that the collagen orientations transform to a depth-dependent arcade-like structure in adult animals.

Current understanding on the mechanobiology of postnatal AC development is incomplete. In the current paper, we investigate the contribution of collagen fibril orientation changes to the depth-dependent mechanical properties of AC. We use a composition-based finite element model to simulate in a 1-D confined compression geometry the effects of ten different collagen orientation patterns that were measured in developing sheep.

In initial postnatal life, AC is mostly subject to growth and we observe only small changes in depth-dependent mechanical behaviour. Functional adaptation of depth-dependent mechanical behaviour of AC takes place in the second half of life before puberty. Changes in fibril orientation alone increase cartilage stiffness during development through the modulation of swelling strains and osmotic pressures. Changes in stiffness are most pronounced for small stresses and for cartilage adjacent to the bone.

We hypothesize that postnatal changes in collagen fibril orientation induce mechanical effects that in turn promote these changes. We further hypothesize that a part of the depth-dependent postnatal increase in collagen content in literature, is initiated by the depth-dependent postnatal increase in fibril strain due to collagen fibril reorientation.

5.1 Introduction

Articular cartilage (AC) consists of a hypo-cellular porous extracellular matrix (≈ 20 % wet weight) that is saturated with fluid (≈ 80 % wet weight). The (solid) extracellular matrix is made of mostly collagen (≈ 80 % dry weight) and the negatively charged proteoglycan matrix (≈ 20 % dry weight), e.g. [248]. The relative fractions of these components and the predominant orientation of the collagen fibrils vary over the tissue depth. Experiments have shown that as a result, the mechanical behaviour of healthy adult articular cartilage is depth-dependent [60, 75, 78, 80, 103, 128, 130, 204, 293, 359, 372]. The equilibrium stiffness of AC increases with increasing distance from the articular surface and this is linked to increasing osmotic pressures with increasing distance from the surface, e.g. [193, 204, 343, 357, 359]. The collagen network is thought to be an important factor for the mechanical behaviour of AC in transient loads [173, 199, 204, 215, 298, 299], but also contributes to the equilibrium stiffness, e.g. [79, 200, 204]. The collagen network in unloaded healthy adult AC counterbalances the internal osmotic pressures in the tissue, and loss of collagen results in larger swelling strains and therefore smaller osmotic pressures [26, 30, 231, 233, 235, 248].

The depth-dependent collagen fibril arrangement in adult AC is commonly referred to as 'Benninghoff structure' [37, 150, 282, 369] and is characterised by three layers: from articular surface to tide-mark there is first a thin layer with collagen fibrils mainly oriented parallel to the articular surface, second there is a thicker transitional zone where the collagen fibrils appear to lack a predominant orientation, and third there is the deep zone where collagen fibrils are mainly oriented perpendicular to the tide-mark. Recent studies in mammals show that the Benninghoff structure is absent at birth and that the predominant orientation of collagen fibrils in perinatal AC is parallel to the articular surface throughout most of the tissue depth [167, 168, 282, 328, 331].

When we assume that the depth-dependent mechanical properties of adult AC partly reflect the effects of a depth-dependent adult collagen structure [167, 169, 197, 214, 217, 298], we can expect that the depth-dependent mechanical properties manifest less in the AC of perinatal animals that lack differentiation in collagen fibril orientation over the tissue depth. Since collagen loss affects free swelling behaviour of AC, we can expect that a close to 90 ° change in collagen orientation in the deep zone during development also affects free swelling behaviour in a similar way. AC stiffness increases during postnatal development [57, 167, 193, 349, 358], and the postnatal changes in collagen fibril orientation may contribute to this stiffening.

We cannot rely on experiments with AC from different developmental stages, e.g. [59, 193], if we want to estimate to what degree the postnatal changes in collagen fibril orientation contribute to the (depth-dependent) mechanical behaviour of AC. In such experiments, it will be very hard to separate the effects of changes in collagen orientation from the other developmental effects such as changes in proteoglycan content. With composition-based finite element models however, e.g. [17, 197, 217, 356], effects of different collagen fibril orientations can be investigated with all other parameters constant. The Fibril Reinforced Poro-Viscoelastic Swelling (FRPVS) model for AC is such a compositional based model that can model realistic collagen fibril orientations [171, 351, 352, 356]. Wilson et al. [357] used the FRPVS model to simulate the confined

compression experiments on adult bovine AC by [293]. They showed that the FRPVS model could capture the depth-dependent mechanical properties as measured by [293] based on AC composition and structure alone [357].

Our knowledge on the interaction between the mechanical driving mechanism for postnatal AC development and the changing mechanical state due to postnatal AC development is still limited. The postnatal reorientation of collagen fibrils has only recently been described quantitatively [168, 331] and the implications for AC mechanics have not been thoroughly investigated. Such investigations will contribute to our understanding of the mechanobiology of development, maintenance and degeneration of AC, and may be helpful when we try to mimic functional adaptation of AC *in vitro*, e.g. in the field of tissue engineering.

In the current paper we investigate how the mechanical environment changes in postnatal AC as a result of changes in predominant collagen fibril orientation. We implement recently published data by Van Turnhout et al. [331] on collagen fibril orientation in developing sheep from birth to maturity in the FRPVS model. We will use the same 1-D confined compression geometry as in [357] and investigate how the (depth-dependent) effective aggregate modulus, osmotic pressures and fibril strains change as a result of changes in predominant collagen fibril orientation.

5.2 Methods

For a detailed description of the modelling theory of the FRPVS model, we refer to existing literature, e.g. [170, 171, 351, 356, 357]. Briefly, this is a biphasic model with the solid phase divided into a viscoelastic fibrillar part that represents the collagen network and a viscoelastic non-fibrillar part that represents the remainder of the extracellular matrix. The model accounts for osmotic pressures due to the negative charges in the solid matrix and strain-dependent permeability and compressibility. Initial fluid fractions, fixed charge densities and collagen fractions and orientations are defined locally (per integration point), and the model accounts for the distinction between intra- and extrafibrillar fluid when it updates the local composition and mechanical state.

We created ten meshes for the ten developmental stages presented in [331]. Before the simulations, these meshes differed only in implemented collagen fibril orientations. We used the FRPVS model with depth-dependent composition and material parameters as described in [357]. Thus, with z the dimensionless depth, the initial fluid volume fraction for each mesh was $n_{\mathrm{f}} = 0.9 - 0.2z$. The initial collagen volume fraction for each mesh was $n_{\mathrm{coll}} = 1.4z^2 - 1.1z + 0.59$. The initial fixed charge density [Meq/ml] for each mesh was $c_{\mathrm{F}} = -0.1z^2 + 0.24z + 0.035$. Collagen density and matrix density were both 1.43 g/ml, for each mesh. Because we are only interested in the equilibrium response, collagen fibrils were modelled as elastic (as opposed to viscoelastic) and permeability was kept constant (as opposed to strain-dependent) [357].

We used the original data that was presented by Van Turnhout et al. [331, figure 3] to simulate the effect of collagen fibril orientation remodelling during development. The patterns for the mean predominant collagen orientation for the ten time points was scaled to equal (dimensionless) length and smoothed with a 5-point moving average. As

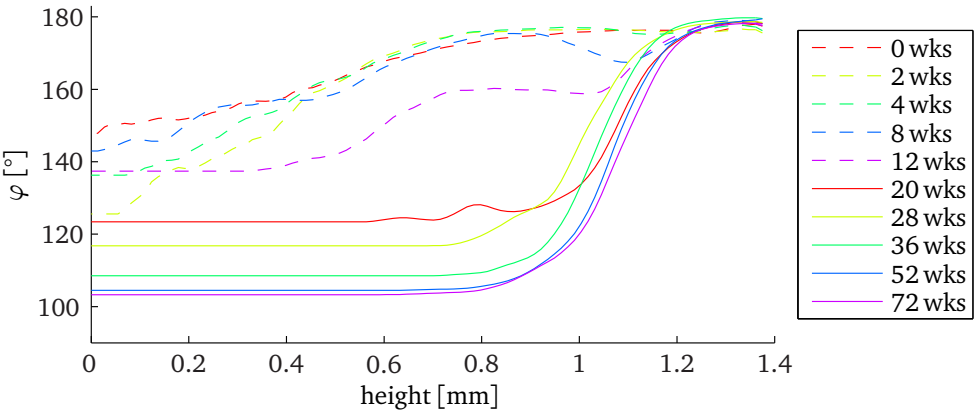

Figure 5.1: Fibril directions that were used in this study for the 10 different ages. Adopted from figure 4.5.

described by Van Turnhout et al. [331], the original patterns do not accurately reflect the fact that collagen orientation becomes constant in the deep zone. We therefore kept the deep zone orientation constant once a minimum was encountered. The resulting ten patterns that were used in this study for the ten different ages in [331] are collected in figure 5.1. In the simulations, these patterns were modelled with two fibrils in each integration point. One fibril followed the pattern, its companion followed the pattern mirrored in the vertical axis (or mirrored in 90 °in figure 5.1). In this manner, an arcade-like configuration was formed, suitable for 1-D analysis.

The finite element geometry was similar to that described by Wilson et al. [357, section 2.4]. The simulations comprised of a 1-dimensional model with a single column of 33 equally thick axisymmetric pore pressure elements (CAX4P), see figure 5.2. Because of the osmosis in the model, the mesh has to be allowed to equilibrate with its environment before the simulation can start at t_0. The initial mesh height was adapted for each mesh such that the height of each mesh after the initial equilibrium step was $h_0 = h_{\max}(t_0) = 1.375\,\text{mm}$. We prescribed zero pore pressure at the top of the model, i.e. fluid can move freely through this surface. All other surfaces were assumed to be impermeable. Displacements in the radial direction were suppressed. The model was axially compressed in a stepwise manner with 10^{-3} % strain/second in 1 % intervals, and allowed to reach equilibrium after each compressive step (relaxation).

We used the applied normal stress σ and mesh height $h_{\max}$ at equilibrium for computation of global strain ε_g and global effective aggregate modulus H_{Ag}:

$$\varepsilon_g = \frac{h_0 - h_{\max}}{h_0}, \qquad H_{Ag} = \frac{\partial \sigma}{\partial \varepsilon_g} \tag{5.1}$$

with h_0 the mesh height at the start of the simulation. We used the element thickness d at equilibrium for computation of local strain ε_l and local effective aggregate modulus

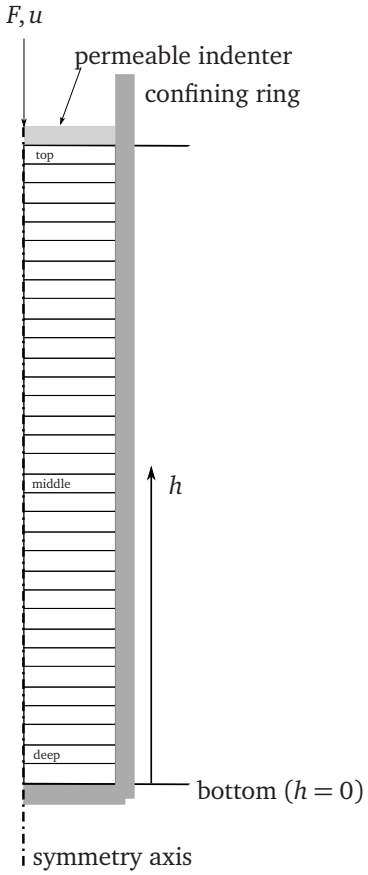

Figure 5.2: Mesh for the confined compression simulations. The mesh is divided into 33 elements and is supported by an impermeable bottom and confined by an impermeable ring. The displacement is applied to the permeable indenter at the articular surface. The layers labelled deep, middle and top are used to present the results.

$H_A(h)$ for each element:

$$\varepsilon_l = \frac{d(t_0) - d}{d(t_0)}, \qquad H_A(h) = \frac{\partial \sigma}{\partial \varepsilon_l} \tag{5.2}$$

with $d(t_0)$ the element thickness at the start of the simulation.

5.3 Results

5.3.1 Initial equilibrium

As expected, the changes in collagen fibril orientations change the mechanical state in the cartilage at t_0 (figure 5.3, table 5.1). The global swelling strain (calculated with equation 5.1) decreases with increasing age (table 5.1, ε_i). The changes in depth-dependent swelling strain (calculated with equation 5.2) correlate with changes in depth-dependent fibril orientation (figure 5.3a, table 5.1). Between ages, local swelling strains are similar where the fibril orientations are also similar (at the top of the mesh), and changes in local swelling strain are large where the changes in fibril orientations are also large (at the bottom of the mesh).

Depth-dependent changes in fibrils strains at t_0 also correlate with changes in fibril

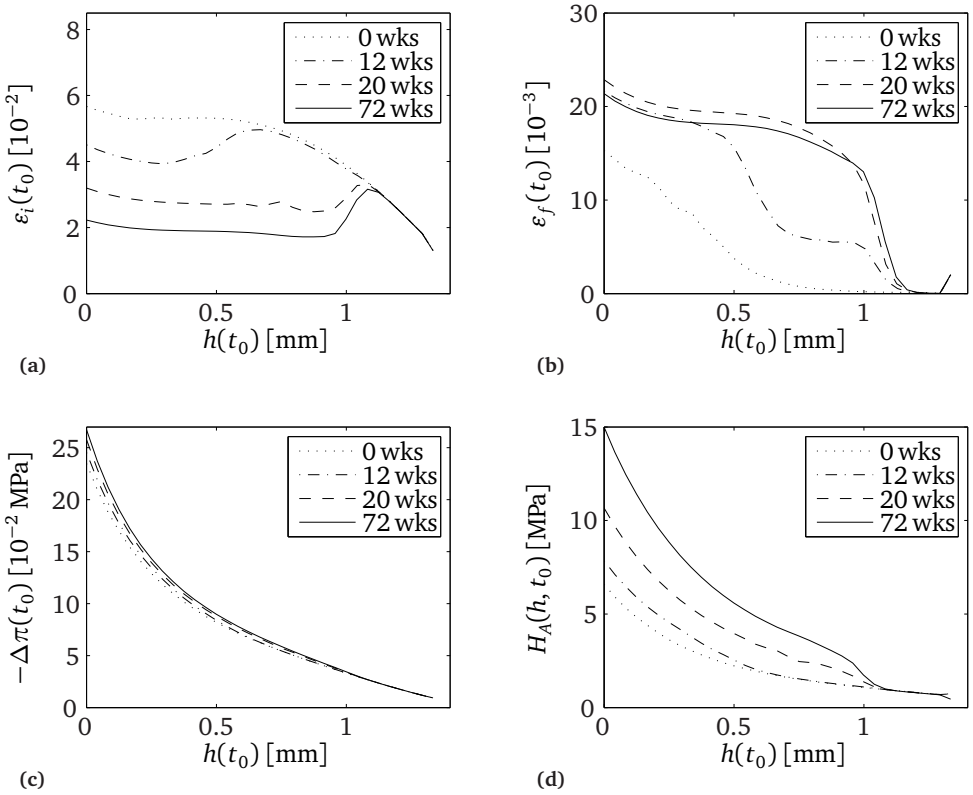

Figure 5.3: Mechanical state as a function of mesh height h at the start of the simulation (t_0) for four ages. With: **(a)** initial swelling strain ε_i; **(b)** fibril strain ε_f; **(c)** osmotic pressures $-\Delta\pi$; and **(d)** local effective aggregate modulus $H_A(h)$.

Table 5.1: Mechanical state for three layers (t - top, m - middle and d - deep) at the start of the simulation (t_0) for all ages. With: ε_i - initial swelling strain, including global swelling strain (g), ε_f - fibril strain, $-\Delta\pi$ - osmotic pressures, and $H_A(h)$ - local effective aggregate modulus.

	$\varepsilon_i(t_0)\,[10^{-2}]$				$\varepsilon_f(t_0)\,[10^{-3}]$			$-\Delta\pi(t_0)$ [kPa]			$H_A(h,t_0)$ [MPa]		
age	g	t	m	d	t	m	d	t	m	d	t	m	d
0 weeks	4.68	1.30	5.18	5.55	2.01	1.68	14.3	9.21	66.3	209	0.74	1.80	5.90
2 weeks	4.30	1.30	5.19	3.49	2.03	0.88	22.1	9.22	66.6	226	0.74	1.81	8.68
4 weeks	4.47	1.30	5.19	4.30	2.02	1.05	21.1	9.21	66.5	219	0.74	1.81	7.20
8 weeks	4.62	1.30	5.18	5.18	2.00	1.73	17.4	9.21	66.4	212	0.74	1.80	6.19
12 weeks	4.08	1.30	4.95	4.36	2.01	8.95	20.9	9.22	67.1	219	0.74	1.87	7.10
20 weeks	2.78	1.30	2.69	3.09	2.01	18.8	22.1	9.23	71.2	229	0.66	3.19	9.68
28 weeks	2.59	1.30	2.28	2.66	2.01	18.5	21.6	9.24	72.1	233	0.64	3.74	11.1
36 weeks	2.27	1.30	1.97	2.30	2.01	17.9	21.0	9.24	72.7	236	0.51	4.31	12.8
52 weeks	2.13	1.30	1.87	2.18	2.01	17.7	20.7	9.24	72.8	237	0.46	4.52	13.5
72 weeks	2.08	1.30	1.85	2.15	2.01	17.7	20.6	9.24	72.9	237	0.45	4.58	13.7

orientation (figure 5.3b, table 5.1, ε_f). Fibril strains are higher near the bottom of the mesh for all ages, and fibrils strain near the bottom of the mesh increase with increasing age. Between ages, fibrils strains are similar at the top of the mesh. However, contrary to the swelling strains (monotonic increase with age), fibril strains near the bottom of the mesh increase between 0 weeks and 20 weeks, and then show a small decrease to 72 weeks.

Osmotic pressures at t_0 increase from the top of the mesh to the bottom of the mesh for all ages (figure 5.3c, table 5.1, $-\Delta\pi$). Between ages, $-\Delta\pi$ is similar at the top of the mesh, and there is a gradual increase of $-\Delta\pi$ with depth and age towards the bottom of the mesh.

These changes in the mechanical state at t_0 (figures 5.3a-5.3c) affect the local effective aggregate modulus $H_A(h)$ at t_0 (figure 5.3d). As with the previous parameters $H_A(h)$ is similar between ages at the top of the mesh. Towards the bottom of the mesh, $H_A(h)$ increases with increasing age, and the increase is larger for greater depth (smaller height).

5.3.2 Confined compression equilibrium

The global strain/stress – stiffness relationships show the expected tension-compression nonlinearity (figure 5.4), i.e. first strain softening for small strains, and then strain hardening for larger strains (figure 5.4a). The transition between strain softening and strain hardening shifts towards larger global strain/stress between 0 weeks (minimum H_A at 0.05 %/40 kPa) and 72 weeks (minimum H_A at 0.08 %/67 kPa). H_A is larger for increasing age for all simulated global strains (figure 5.4a), and for global stresses up to $\approx$ 0.15 MPa (figure 5.4b). The increase in H_A between ages is largest for small

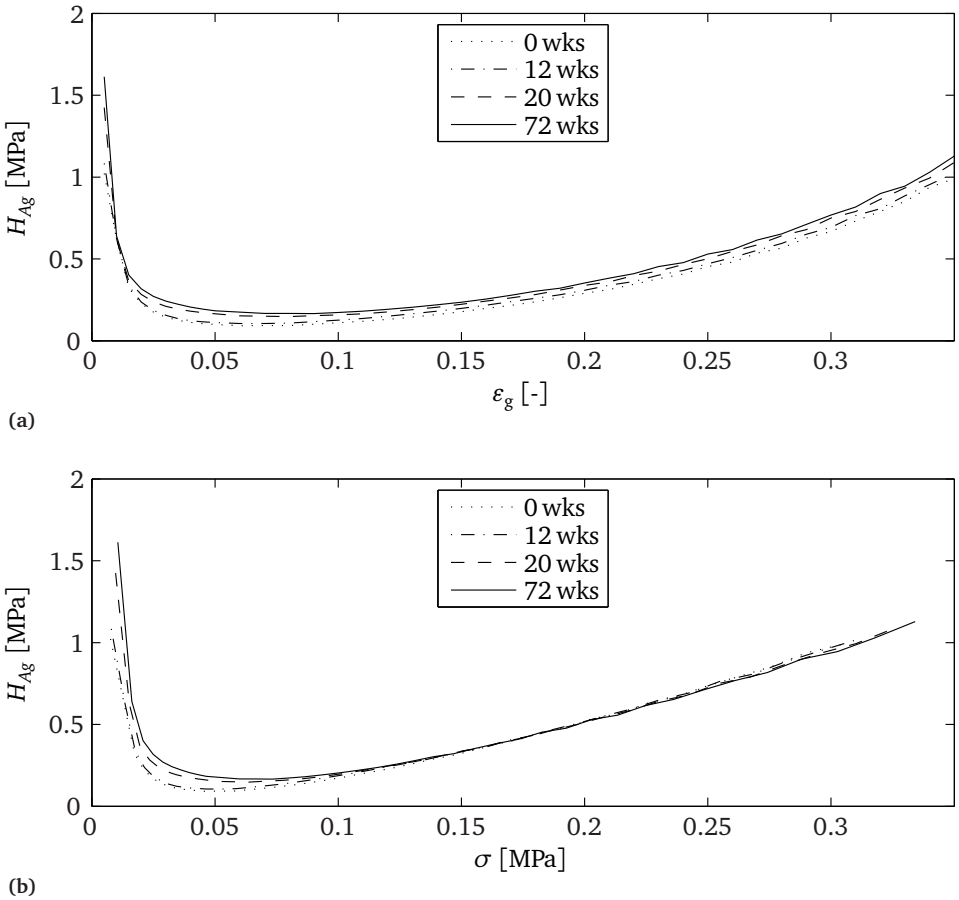

Figure 5.4: Global effective aggregate modulus H_{Ag} as a function of **(a)** global strain ε_g; and **(b)** global stress σ.

strains/stresses.

The local effective aggregate modulus $H_A(h)$ in compression is similar between ages for cartilage layers that are past their (local) tension-compression transition, i.e. that are loaded in compression (figures 5.5a, 5.5c and 5.5e, table 5.2). For the (deep) cartilage layers that are still loaded in tension, $H_A(h)$ decreases with increasing strain, and $H_A(h)$ remains larger for increasing ages. The local strains ε_l change between ages (figures 5.5b-5.5f). For a large range of global strains ($\varepsilon_g \leq 20\,\%$), local strains increase near the top of the mesh, and decrease near the bottom of the mesh for increasing ages (figures 5.5b-5.5d). Local strains become similar between ages for large global strains (figure 5.5f). The location of the tension-compression boundary is at a smaller height for increasing ages, although the differences are small (figures 5.5a- 5.5f).

The osmotic pressures increase over the entire cartilage depth during compression

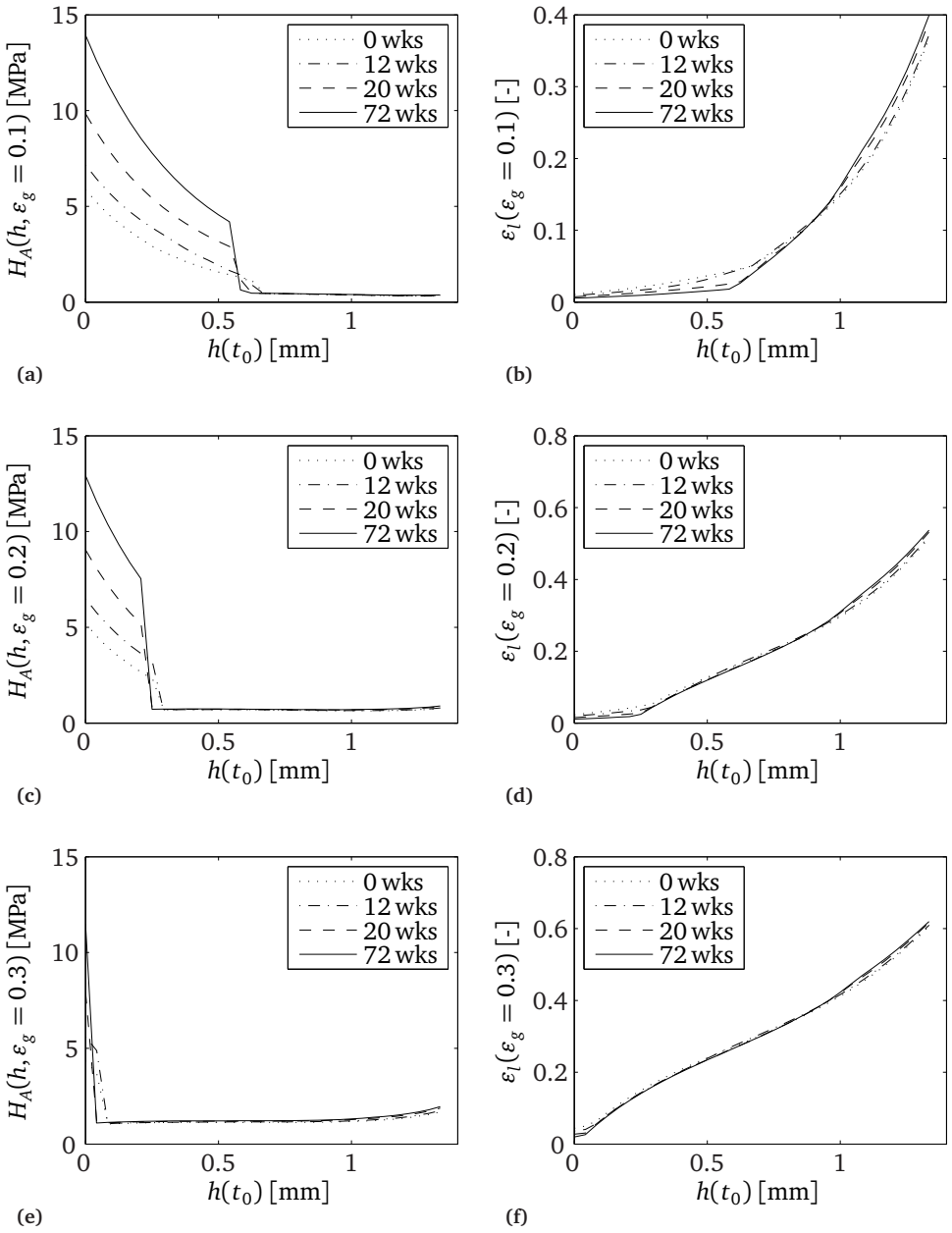

Figure 5.5: Mechanical state as a function of mesh height h at three levels of global strain ε_g for four ages. With: **(a, c** and **e)** - local effective aggregate modulus $H_A(h)$ at **(a)** $\varepsilon_g = 10\,\%$, **(c)** $\varepsilon_g = 20\,\%$, and **(e)** $\varepsilon_g = 30\,\%$; and **(b, d** and **f)** local strain ε_l at **(b)** $\varepsilon_g = 10\,\%$, **(d)** $\varepsilon_g = 20\,\%$, and **(f)** $\varepsilon_g = 30\,\%$.

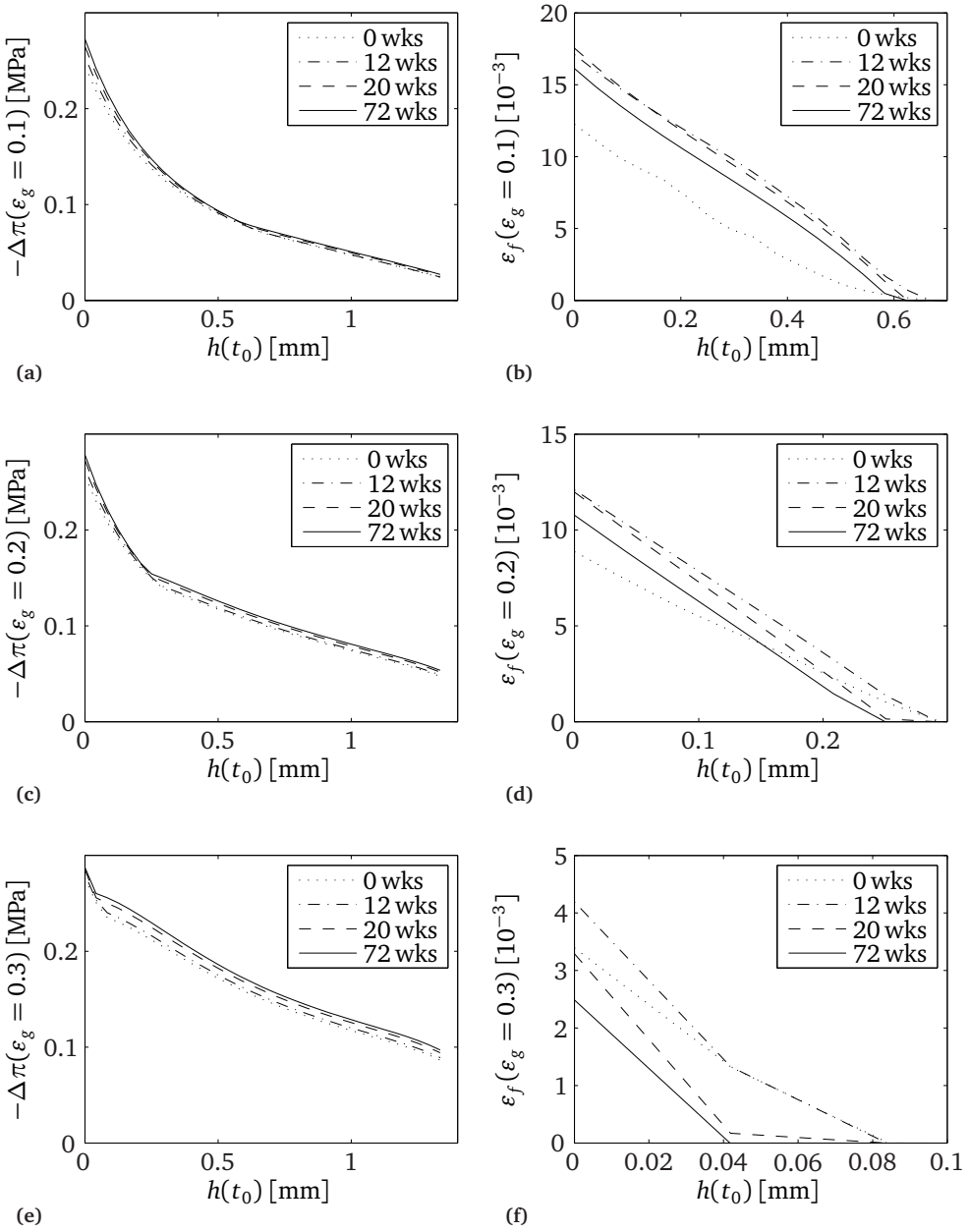

Figure 5.6: Mechanical state as a function of mesh height h at three levels of global strain ε_g for four ages (continued). With: **(a, c** and **e)** - osmotic pressures $-\Delta\pi$ at **(a)** $\varepsilon_g = 10\,\%$, **(c)** $\varepsilon_g = 20\,\%$, and **(f)** $\varepsilon_g = 30\,\%$; and **(b, d** and **f)** local fibril strain ε_f at **(b)** $\varepsilon_g = 10\,\%$, **(d)** $\varepsilon_g = 20\,\%$, and **(f)** $\varepsilon_g = 30\,\%$. Note the differences in scale for $h(t_0)$ in panels **(b, d** and **f)**.

Table 5.2: Local effective aggregate modulus $H_A(h)$ [MPa] for three layers (top, middle and deep) in the simulations at three levels of global strain (10 %, 20 % and 30 %) for all ages.

age [weeks]		0	2	4	8	12	20	28	36	52	72
$\varepsilon_g = 10\,\%$	top	0.31	0.32	0.32	0.31	0.32	0.35	0.36	0.36	0.37	0.37
	middle	1.07	1.01	1.04	1.06	0.88	0.46	0.46	0.47	0.47	0.47
	deep	5.20	7.97	6.53	5.51	6.43	8.86	10.2	11.8	12.4	12.6
$\varepsilon_g = 20\,\%$	top	0.76	0.77	0.77	0.76	0.79	0.85	0.86	0.88	0.89	0.89
	middle	0.69	0.69	0.69	0.69	0.70	0.71	0.72	0.72	0.73	0.73
	deep	4.53	7.25	5.87	4.86	5.76	8.06	9.35	10.8	11.4	11.6
$\varepsilon_g = 30\,\%$	top	1.68	1.72	1.71	1.69	1.75	1.88	1.90	1.93	1.95	1.95
	middle	1.13	1.15	1.14	1.13	1.16	1.19	1.20	1.21	1.21	1.22
	deep	3.69	6.27	5.00	4.03	4.88	1.22	1.09	1.10	1.10	1.10

(figures 5.6a-5.6e). At small global strains, osmotic pressures are similar between ages at the top of the model (figure 5.6a, table 5.1). For larger strains, osmotic pressures become higher for increasing ages over the entire cartilage depth (figure 5.6c-5.6e)

The fibril strains at the top of the model become zero during compression (figures 5.6b-5.6f). At 10 % global strain, fibril strains are zero in the upper half of the model (figure 5.6b), and the region with zero fibril strain increases with increasing global strain (figures 5.6d-5.6f). The pattern that we observed at t_0, an increase in fibril strain up to age 20 weeks and next a small decrease in fibril strain up to 72 weeks (figure 5.3b), is still present at 10 % global strain (figure 5.6b). For larger strains, changes occur. At 20 % global strain, the age for the maximum fibril strains is 12 weeks (figure 5.6d) and the difference between 0 weeks and 72 weeks is much smaller than at smaller strains (figures 5.3b and 5.6b). At very large strains, fibril strains are lower for the animals of 72 weeks than for the animals of 0 weeks (figure 5.6f).

We finally present the local strain-stiffness relationships for the three layers top, middle and deep for four ages (figure 5.7). The top layer is subjected to compression for local strains larger than 10 % and the ε_l-$H_A(h)$ relationship is similar for all ages (figure 5.7a). Changes occur for the ε_l-$H_A(h)$ relationships for different ages for layers at a larger depth (figures 5.7b-5.7c). Three observations should be noted: (1) $H_A(h)$ remains larger near the bottom of mesh for increasing ages, (2) the tension-compression transition shifts towards smaller local strains for deeper layers, and (3) these effects are larger for deeper layers.

5.4 Discussion

To evaluate the contribution of postnatal collagen orientation development, we performed ten simulations with the composition-based FRPVS model which differed only

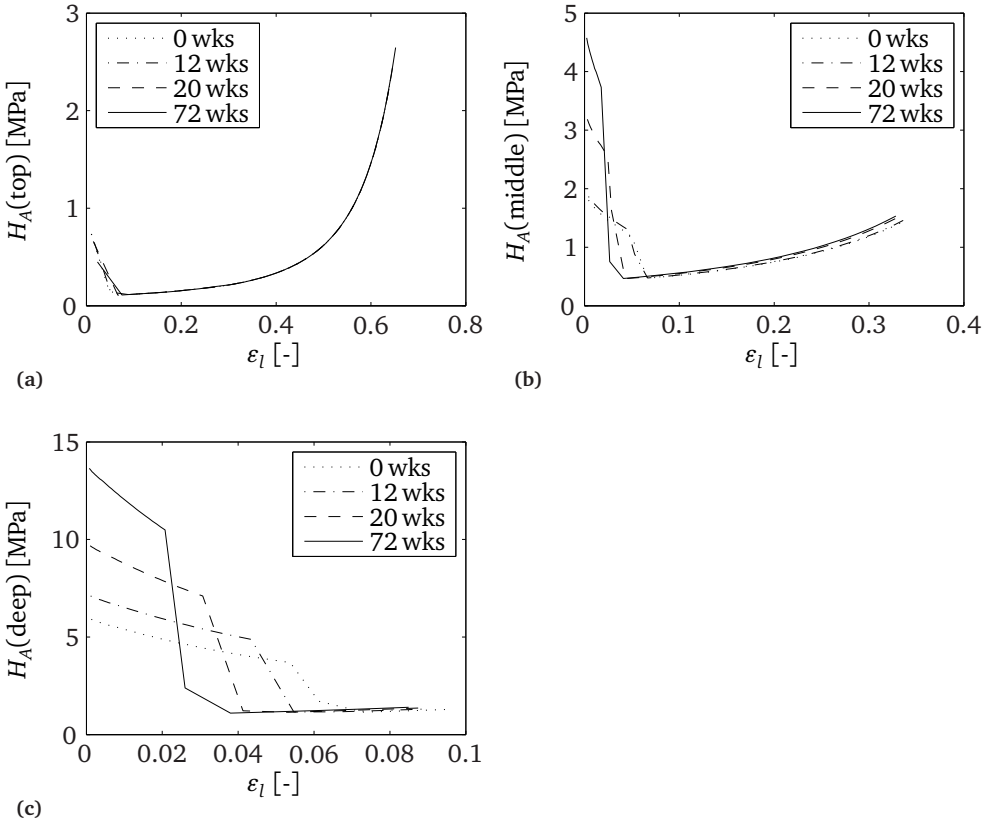

Figure 5.7: Local effective aggregate modulus $H_A(h)$ as a function of local strain ε_l for three layers in de model: **(a)** top, **(b)** middle, and **(c)** deep.

in predominant collagen fibril orientation. And we used measurements on collagen fibril orientation in developing sheep between birth (0 weeks) and maturity (72 weeks) [331] for the collagen orientations.

The differences in local swelling strain after the initial equilibrium step, ε_i, in these simulations are the result of the differences in collagen fibril orientation only, as all other parameters were constant. For $h > 1.12$ mm (the 'superficial layer'), collagen orientations are similar between the ten meshes (figure 5.1), and this is reflected in table 5.1 and figure 5.3: ε_i, $-\Delta\pi$, $H_A(h)$ and ε_f are similar for the top layer for all ten simulations. As expected, the changing fibril orientations for $h < 1.12$ have a direct effect on ε_i (figure 5.3a, table 5.1, ε_i), and they thereby indirectly influence the local osmotic pressures $-\Delta\pi$ (figure 5.3c, table 5.1). These osmotic pressures are known to be an important factor for the equilibrium stiffness of AC, e.g. [30, 79, 204, 248]. Our simulations show that equal osmotic pressures in the middle and deep zone for simulations for increasing

ages, result in increasing values for $H_A(h)(\varepsilon_g = 0)$ for increasing ages (figure 5.3, table 5.1). Thus, the direct effect of changing fibril orientations (smaller ε_i) and the indirect effect of changing fibril orientations (larger $-\Delta\pi$) interact to increase AC stiffness.

The changing fibril orientations affect $H_A(h)$ over the entire region of simulated strains and change the tension-compression behaviour (figure 5.7). Initially, the AC is subject to swelling and thus under tensile stress (figure 5.3a). With increasing global stress, we reduce the amount of swelling until the global stress equals the osmotic pressures. From that point on, a further increase in global stress subjects the AC to compression and compressive stress [357]. H_A decreases with the reduction in tension, and $H_A(h)$ increases with an increase in compression (figures 5.4 and 5.7), and the local strain for the tension-compression transition becomes smaller with increasing age (figure 5.7). Combined with an increase in $H_A(h)$ at zero strain for increasing age (figure 5.3d), this results in higher gradients for the tension behaviour of $H_A(h)$ as a function of ε_l for deeper layers (figure 5.7). Although the tension-compression transition shifts to lower ε_l for deeper layers with increasing age (figure 5.7), the transition is associated with higher osmotic pressures for deeper layers with increasing age, i.e. with larger global stresses. Thus, the deeper layers are in fact subject to tension, and therefore retain their high pre-compression $H_A(h)$, for an increasing range of global stresses for increasing ages.

The sheep that were used to obtain the experimental data on collagen orientations reached puberty around the age of 36 weeks [331]. Figure 5.1 shows that the remodelling of predominant collagen orientation is mostly done by that age, and that the largest difference in (deep zone) collagen orientation is that between 12 weeks and 20 weeks. In our simulations, we also find the largest effects between 12 weeks and 20 weeks. This is also the age span with the largest rate of change for ε_i, ε_f, $-\Delta\pi$ and $H_A(h)$ (not shown). Consequently, our simulations show that the changes in depth-dependent mechanical properties are nearly finished at 36 weeks of age (e.g. tables 5.1-5.2). Cartilage thickness decreases during postnatal development and Van Turnhout et al. [331] estimated a time constant of -0.017 weeks for the cartilage thickness in their data. This means that 73 % of the decrease in cartilage thickness occurs before 12 weeks of age, 89 % occurs before 20 weeks of age and cartilage thickness is almost stabilised at 36 weeks of age when 98 % of the decrease in cartilage thickness has occurred. The temporal patterns of collagen fibril reorientation and decrease in cartilage thickness suggest that the changes that we see in AC in the first half of postnatal life to puberty are more related to growth mechanisms (largest decrease in thickness), while the second half of postnatal life to puberty is used for the depth-dependent functional adaptation of AC (largest changes in collagen orientation and consequently mechanical properties). This is in line with the remark by Hunziker et al. [154] that cartilage may only then begin to assume a more mature anisotropic morphological structure as the shaping process of the joint approaches completion.

These simulations do not provide a full description of postnatal AC development. The influence of the collagen network on transient mechanical behaviour of AC [110, 111, 204] for instance, is also a factor for the mechanical state that drives postnatal AC development and as such deserves attention. The depth-dependent increase in collagen content is also a factor, as are (depth-dependent) changes in FCD and fluid fraction.

Also, the simulated geometry was limited to 1-D confined compression. Within these limitations, our simulations provide further insight into postnatal mechanobiology of AC. They show that analysis of experiments on depth-dependent mechanical properties of premature AC [193, 343, 349] should also take the changing fibril orientations into account. An increase in collagen content itself for instance, is associated with an increase in osmotic pressures through the modulation of intra- and extra-fibrillar fluid: collagen binds fluid that is therefore no longer available for osmosis, and this increases the effective FCD [230, 234, 357]. The increase in collagen content and its influence on osmotic pressure is cited by Williamson et al. [349] as an explanation for the increase of 180 % in confined compression modulus from foetal to adult bovine AC. Our results show that a part of this 180 % can be attributed to changes in collagen orientation between foetal and adult AC. These changes may also help to roughly predict temporal and spatial patterns of postnatal changes such as collagen content increase and FCD increase and possibly the development of e.g. functional interstitial fluid support [15, 203] or the depth-dependent phenotype of adult chondrocytes, e.g. [20, 21, 197, 361].

The simulations in this paper do not clarify why the predominant collagen orientation in the deep zone changes. Based on Wilson et al. [355] who showed that principal strains in the matrix are a good predictor for collagen fibril orientation in AC, we hypothesise that (vertical) swelling strains are responsible. The bottom layer of AC is subjected to vertical swelling strains for almost the entire regime of physiological strains in our simulations, contrary to the upper layers (figures 5.6b-5.6d). The current depth-dependent mechanical behaviour for the simulations for the young animals in this paper is mostly due to our choice for depth-dependent composition (i.e. equal to that of the adult). For our hypothesis to hold, depth-dependent mechanical behaviour needs to be present in the AC of perinatal animals. This is not unlikely, since Klein et al. [193] showed that both proteoglycan content and collagen content increased with depth for foetal and newborn bovine cartilage. Also, experimental results on the mechanics of foetal [193] and neonatal [59] AC show that depth-dependent mechanical behaviour is indeed present in perinatal AC.

Two mechanisms affect the initial swelling strain in our hypothesis during postnatal collagen reorientation. First, a portion of the load is transferred from the matrix to the collagen fibrils (figures 5.3a-5.3b), leading to lower swelling strains and higher strains in the collagen fibrils during development. Since we propose that swelling strains initiate deep zone collagen reorientation, this effect reduces the driving mechanism in our hypothesis. Second however, osmotic pressures increase (figure 5.3c) because the decreasing swelling strain reduces the free fluid available for osmosis [26, 30, 231, 233, 235, 248]. The rise in osmotic pressure in turn affects the matrix and fibril strains in compression: the initial swelling state (AC loaded in tension) is maintained for a larger range of compressive stresses (figures 5.6b-5.6d). Thus, although the swelling strains in our hypothesis become smaller during development, these swelling strains persist for a larger range of global stresses. And this persistence of swelling strains under physiological loads in turn reinforces the driving mechanism for the development of a Benninghoff structure under our hypotheses.

The increased strains during development in the fibrils in the deep zone also persist for larger global stresses. Rieppo et al. [282] found that collagen content increases during

development, and that it increases more in the deep zones of the AC than at the surface of the AC. Based on our simulations, we suggest that this differentiation in collagen content increase is partly initiated by the differentiation in fibril strain. However, if the increase of collagen content in the deep zone is related to the higher fibril strains, two mechanisms are expected to further affect osmotic pressures and fibril strains. First, osmotic pressures and therefore fibril strains will increase through the modulation of intra- and extra-fibrillar fluid content. Second, fibril strains will be less when more collagen is present for given osmotic pressures and orientations. Results of different simulations with the current geometry (results not shown) indicate that when we take both mechanisms into account, osmotic pressures increase and initial matrix and fibril strains (in the deep zone) are indeed a little lower when collagen is added (and everything else is kept equal). As in the previous paragraph, this state also persists for a larger range of compressive stresses due to the rise in osmotic pressures.

Acknowledgements

The authors are grateful to Dr. Wouter Wilson and Dr. René van Donkelaar at the Materials Technology group of the Faculty of Biomedical Engineering of Eindhoven University of Technology for the use of, and support with, the FRPVS model.

. . . I was just the engineer. I'm the music dolly – it's the music who do it.
Lee 'Scratch' Perry, cited in [176]

6

Postnatal development of depth-dependent collagen density in ovine articular cartilage

Mark C. van Turnhout[1], Henk Schipper[1], Barend van Lagen[2], Han Zuilhof[2], Sander Kranenbarg[1] & Johan L. van Leeuwen[1]. *BMC Developmental Biology*, **10**:108, October 2010. doi: 10.1186/1471-213X-10-108

[1]Wageningen University, Experimental Zoology Group, PO Box 338, 6700 AH, Wageningen, The Netherlands.
[2]Wageningen University, Laboratory for Organic Chemistry, PO Box 8026, 6700 EG, Wageningen, The Netherlands.

Abstract

Background: Articular cartilage (AC) is the layer of tissue that covers the articulating ends of the bones in diarthrodial joints. Adult AC is characterised by a depth-dependent composition and structure of the extracellular matrix that results in depth-dependent mechanical properties, important for the functions of adult AC. Collagen is the most abundant solid component and it affects the mechanical behaviour of AC. The current objective is to quantify the postnatal development of depth-dependent collagen density in sheep (*Ovis aries*) AC between birth and maturity. We use Fourier transform infra-red micro-spectroscopy to investigate collagen density in 48 sheep divided over ten sample points between birth (stillborn) and maturity (72 weeks). In each animal, we investigate six anatomical sites (caudal, distal and rostral locations at the medial and lateral side of the joint) in the distal metacarpus of a fore leg and a hind leg.

Results: Collagen density increases from birth to maturity up to our last sample point (72 weeks). Collagen density increases at the articular surface from $0.23\,\mathrm{g/ml} \pm 0.06\,\mathrm{g/ml}$ (mean $\pm$ s.d., $n = 48$) at 0 weeks to $0.51\,\mathrm{g/ml} \pm 0.10\,\mathrm{g/ml}$ ($n = 46$) at 72 weeks. Maximum collagen density in the deeper cartilage increases from $0.39\,\mathrm{g/ml} \pm 0.08\,\mathrm{g/ml}$ ($n = 48$) at 0 weeks to $0.91\,\mathrm{g/ml} \pm 0.13\,\mathrm{g/ml}$ ($n = 46$) at 72 weeks. Most collagen density profiles at 0 weeks (85 %) show a valley, indicating a minimum, in collagen density near the articular surface. At 72 weeks, only 17 % of the collagen density profiles show a valley in collagen density near the articular surface. The fraction of profiles with this valley stabilises at 36 weeks.

Conclusions: Collagen density in articular cartilage increases in postnatal life with depth-dependent variation, and does not stabilize up to 72 weeks, the last sample point in our study. We find strong evidence for a valley in collagen densities near the articular surface that is present in the youngest animals, but that has disappeared in the oldest animals. We discuss that the retardance valley (as seen with polarised light microscopy) in perinatal animals reflects a decrease in collagen density, as well as a decrease in collagen fibril anisotropy.

6.1 Background

Articular cartilage (AC) is the thin layer of soft tissue that covers the articulating ends of the bones in diarthrodial joints. Healthy adult AC is characterised by a depth-dependent composition [248, 294, 341] and structure [37, 83, 150, 364]. These characteristics result in depth-dependent mechanical properties [59, 77, 293, 357] that are important for the functions of adult AC, specifically load distribution and the establishment of a low friction environment [15, 77, 193].

AC consists of a number of cells (chondrocytes, $\approx$ 2 % to 5 % of the wet volume, [121]) embedded in a porous extracellular matrix (ECM) that is saturated with fluid ($\approx$ 80 % wet weight). The ECM consists of collagen and negatively charged proteoglycan molecules. Collagen is the most abundant ECM component ($\approx$ 75 % of dry weight, e.g. [248]). Both the predominant orientation in the collagen network and the amount of collagen in the network affect the mechanical behaviour, and thus the functioning, of AC [26, 30, 235, 330]. The collagen network remodels between birth and maturity: the adult depth-dependent structure is absent at birth [6, 168, 282, 328, 331], collagen type I is replaced by collagen type II [42, 43, 247], and collagen densities increase [50, 167, 348] with depth-dependent variation [282].

Our knowledge on the depth-dependent development of collagen densities is limited. Most studies that investigate postnatal collagen density measure total collagen content as opposed to depth-dependent collagen density profiles [50, 167, 348]. Rieppo et al. [282] measured depth-dependent collagen density profiles in porcine AC in three sample points (4 months, 11 months and 21 months) that did not include perinatal animals. Their results [282] are presented with a 80 μm resolution over the depth of the tissue.

The ECM is produced and maintained by chondrocytes that are affected by their local mechanical environment [336, 359]. During postnatal development, AC develops a functional depth-dependent composition and structure. Postnatal collagen density profiles are important for our understanding of postnatal AC development. To unravel the (depth-dependent) mechanobiology of the development of ECM structure and composition, we need better time- and space-resolved collagen density profiles. Information on collagen densities is also essential for the interpretation of optical retardation results from polarised microscopy studies (PLM) [329]. The cited studies into postnatal development of collagen orientation [6, 168, 282, 328, 331] all use PLM.

We aim to quantify depth-dependent collagen densities in AC between birth and maturity, and with better spatial resolution than previously reported over the depth of the tissue in a model animal. Recently, we measured postnatal collagen orientation remodelling in a group of 48 sheep (*Ovis aries*) divided in ten age groups between birth and maturity [331]. We use the same animals and anatomical sites for the current study. Second, we aim to assess differences in (the development of) collagen density between different anatomical sites of this single joint surface. In our previous PLM study [331] we found a retardance valley between $\approx$ 30 μm and $\approx$ 80 μm from the articular surface for all age categories. Since such a valley can be caused by a minimum in collagen densities, or by a decrease in collagen fibre anisotropy [329], we wish to examine whether a valley in collagen density is present at that location.

We use Fourier transform infrared microspectroscopy (FTIRμS) to measure collagen

density in AC. The infra-red absorption at a certain wavenumber $A(\overline{\nu})$ is proportional to the amount of absorbing material present in the light path according to the Bouguer-Lambert-Beer absorption law [34, 270]:

$$A(\overline{\nu}) = a(\overline{\nu})bc \tag{6.1}$$

with $a(\overline{\nu})$ the (constant) absorption coefficient at wavenumber $\overline{\nu}$, b the optical path length and c the concentration of the absorbing material. With a constant thickness (optical path length b) of histological sections, equation 6.1 relates absorption directly to concentrations: $A(\overline{\nu}) \sim c$. With FTIRμS an absorption spectrum in the infra-red regime is obtained using a polychromatic light source and Fourier transforms of interferograms, as opposed to measuring absorption at individual wavenumbers with monochromatic light sources.

6.2 Methods

6.2.1 Animals

The animal experiment was described previously [331]. Briefly, we obtained five female sheep for each of nine sample points from a local sheep farm. Sample points occurred at ages 2, 4, 8, 12, 20, 28, 36, 52 and 72 weeks. An additional four stillborn lambs were used (labelled age = 0 weeks). Animals were kept at the farm with their mother until sacrifice or the age of 12 weeks. Animals that were older than 12 weeks were collected at the farm and housed at the universities laboratory animal facility 'Ossekampen' until sacrifice. The total number of animals at the end of the experiment was 48. The number of animals for the first sample point (0 weeks, stillborn) and the last sample point (72 weeks) was four, and the number of animals for the other sample points was five. The experiment was approved by the Wageningen University Animal Experiments Committee.

6.2.2 Sample preparation

We used the same tissue blocks to obtain histological slices as those used in our earlier publication [331]. Summarising, the animals' legs were collected immediately following sacrifice and skin and subcutaneous tissue were removed from the metacarpophalangeal joints (figure 6.1). The joints were carefully opened and we used a dental saw to take the medial and lateral hemispheres from the distal end of each cannon bone. These hemispheres were fixed with formalin and decalcified with EDTA (10 % EDTA, pH 7.4) until the hemispheres could be cut with a razor blade. The hemispheres were then divided into a rostral, a distal and a caudal sample (figure 6.1). Of these, the distal site is expected to be subject to a more static load and the rostral and caudal sites are expected to be subject to a more intermittent load during locomotion [57]. These samples were washed and infiltrated with sucrose (25 % sucrose in PBS) overnight, snap frozen in liquid nitrogen and stored at −80 °C until further processing, and finally cut to 7 μm thick

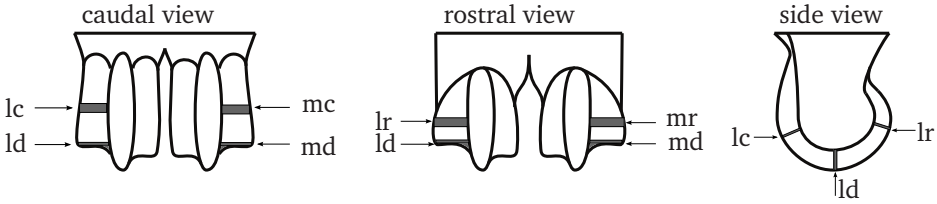

Figure 6.1: Sketch of the ovine distal metacarpus with the anatomical sampling sites with l - lateral, m - medial, c - caudal, d - distal, and r - rostral.

histological slices with a cryostat (Reichert 2800N). Histological slices were collected on Potassium Bromide (KBr) disks for FTIRμS analysis.

6.2.3 FTIRμS system

We used a rectangular field of view (FOV) of 160 μm by 40 μm that was aligned with the long side parallel to the articular surface (figure 6.2). The width of the FOV (160 μm) was chosen to correspond with the width of the FOV in our previous study [331]. The height of the FOV (40 μm) was chosen as a trade off between resolution over the depth of the cartilage, and the necessary assessment time: a FOV with an area of $\frac{1}{x}$ of a given FOV, needs x^2 more scans to achieve the same signal/noise resolution of the spectra. With this FOV, we scanned a linear profile, along a path perpendicular to the articular surface, with measurements at 20 μm intervals (figure 6.2c). For each point in each profile, we obtained a single spectrum over the interval $600\,\mathrm{cm}^{-1} \leq \overline{\nu} \leq 4000\,\mathrm{cm}^{-1}$ with the results of 32 scans and with a resolution of $4\,\mathrm{cm}^{-1}$. Two successive FOVs partly overlap to achieve a certain number of scans (> 10) over the depth of the tissue. As a result, we have an a priori smoothing effect for our profiles that uses actual measurements (as opposed to moving averages or linear interpolation). Measurements were performed with a BrukerTensor 27 IR spectrometer, connected to a Bruker Hyperion 2000 IR-microscope (Bruker Optics). This microscope has a liquid nitrogen-cooled MCT-detector – such a detector enables the detection of small amounts of material, ultimately down to monomolecular layers [292]. Both machines are controlled by Bruker's OPUS software. All spectra were baseline corrected with a so-called rubber baseline correction before further processing. This rubber baseline correction consists of finding a convex envelope of the spectrum and subtracting the convex part of the envelope lying below the spectrum from the spectrum [273].

We used an internal NaN_3 standard to minimise the effects of variations in the size of the FOV between histological slices [284]. We formed a reference disk of a KBr-NaN_3 mixture that was placed under the KBr disk that carried the histological slices. The spectrum of NaN_3 contains a sharp peak at $\overline{\nu} = 2036\,\mathrm{cm}^{-1}$ and a sharp peak at $\overline{\nu} = 640\,\mathrm{cm}^{-1}$ (figure 6.3a). We used the peak value of the sharp peak at $\overline{\nu} = 2036\,\mathrm{cm}^{-1}$ to normalise all spectra. A single reference disk was used for all measurements and the standard deviation of the peak value in this disk was 3 % for 30 measurements over the disk area.

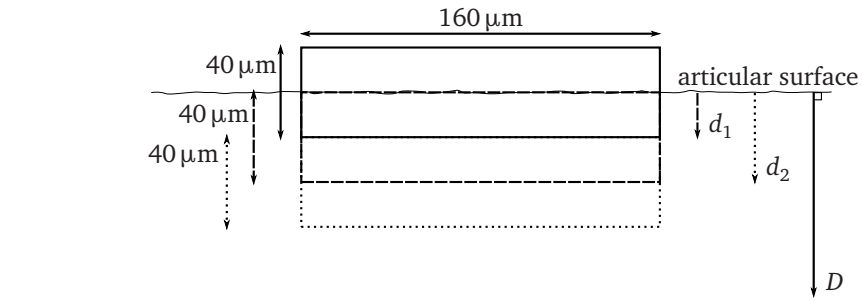

(a)

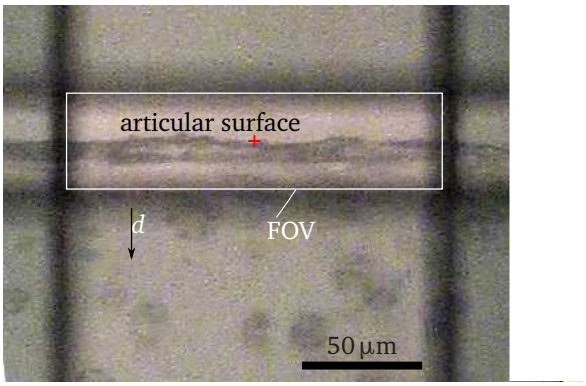

(b)

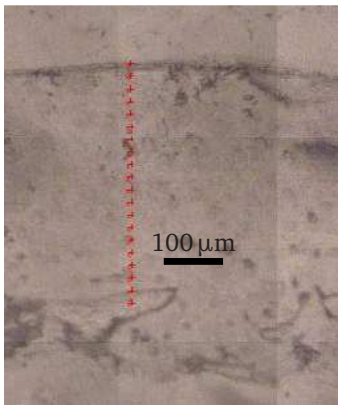

(c)

Figure 6.2: Example of FTIRµS analysis. **(a)** The rectangular FOV of $160 \times 40\,\mu m^2$ is aligned with the articular surface, and next a linear profile perpendicular to the articular surface with 20 µm intervals is scanned. The depth of the measurement is measured from the articular surface to the centre of the FOV. The first scan is at depth $d_0 = 0\,\mu m$ and only has AC for half of its FOV, the second scan is at $d_1 = 20\,\mu m$ and measures the first 40 µm of the superficial layer, the third scan is at $d_2 = 40\,\mu m$ and measures the FOV for $20\,\mu m \leq d \leq 60\,\mu m$, etc. We do not present the results for the first scan at d_0. **(b)** Example of FOV aligned with the articular surface at d_0. **(c)** Example of a line scan with 20 µm intervals perpendicular to the articular surface. Crosses show the centre of the (aligned) FOV.

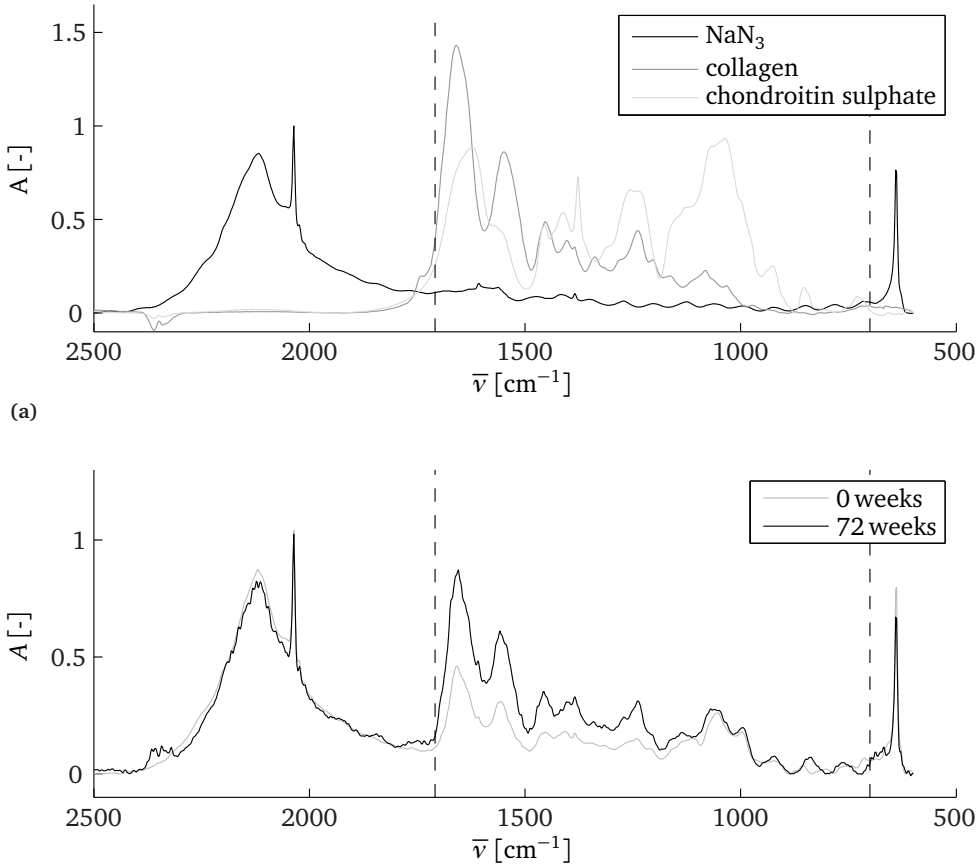

Figure 6.3: Example of FTIRμS absorption (A) spectra. The vertical lines define the parts of the spectra that were used for the quantitative analysis, i.e. $700\,\mathrm{cm}^{-1} \leq \overline{\nu} \leq 1710\,\mathrm{cm}^{-1}$. With **(a)** pure component spectra of the internal standard NaN_3 (black), collagen (1.35 g/ml, dark gray) and chondroitin sulphate (3.19 g/ml, light gray); and **(b)** sample spectra from a single FOV at $d = 100\,\mu\mathrm{m}$ for 0 weeks (gray) and 72 weeks (black).

6.2.4 FTIRμS calibration

Because the ECM consists mostly of collagen type II and glycosaminoglycans (GAGs), we used collagen (bovine tracheal collagen type II, Sigma-Aldrich) and chondroitin-sulphate (bovine tracheal chondroitin sulphate A, Sigma-Aldrich) as standards for pure component spectra. Chondroitin sulphate (or GAG) densities cannot be reliably obtained from FTIRμS spectra [287]. We therefore only quantify collagen densities and we checked whether changes in chondroitin sulphate densities affect our collagen density analysis. We used a least square fitting approach with the data for $700\,\mathrm{cm}^{-1} \leq \overline{\nu} \leq 1710\,\mathrm{cm}^{-1}$ for quantification of collagen content (figure 6.3b), i.e. we exclude the large NaN_3 peaks from the fitting procedure. With the pure component spectra we estimated constants $\hat{a}$ and $\hat{c}$ such that the least square difference between the left hand side and right hand side of equation 6.2 was minimised:

$$s_{\mathrm{sample}} - s_{\mathrm{NaN_3}} = \hat{a} s_{\mathrm{col}} + \hat{c} \qquad 700\,\mathrm{cm}^{-1} \leq \overline{\nu} \leq 1710\,\mathrm{cm}^{-1} \tag{6.2}$$

With s_{sample} the sample spectrum, $s_{\mathrm{NaN_3}}$ the spectrum of the internal reference, and s_{col} the spectrum of the collagen standard.

To relate the estimated $\hat{a}$ and $\hat{c}$ to actual collagen densities, we formed and measured a sequence of 36 KBr disks that contained known amounts of the collagen (6 amounts, $0.23\,\mathrm{g/ml} \leq \rho_{col} \leq 1.35\,\mathrm{g/ml}$) and chondroitin sulphate (6 amounts, $0.05\,\mathrm{g/ml} \leq \rho_{cs} \leq 0.32\,\mathrm{g/ml}$) standards. We estimated constants $\hat{a}$ and $\hat{c}$ with equation 6.2 for this sequence. We applied linear regression to find the constants b_1 and b_2 for the relation between the density of the collagen standard ρ_{col} and chondroitin sulphate standard ρ_{cs}, and the estimated constant $\hat{a}$:

$$\rho_{\mathrm{col}} = b_1 \hat{a} + b_2, \quad \rho_{\mathrm{cs}} = b_3 \hat{a} + b_4 \tag{6.3}$$

The linear relationship between ρ_{col} and the estimated $\hat{a}$ (equation 6.3) is described with equation 6.4:

$$\rho_{\mathrm{col}} = 1.45\hat{a} + 1.24 \cdot 10^{-2}, \qquad r^2 = 0.98 \tag{6.4}$$

In equation 6.4, zero is included in the 95 % confidence interval ($-2.92 \cdot 10^{-2} \leq b_2 \leq 5.41 \cdot 10^{-2}$) for the intercept $b_2 = 1.24 \cdot 10^{-2}$. The relationship between ρ_{cs} and the estimated $\hat{a}$ (equation 6.3) is described by equation 6.5:

$$\rho_{\mathrm{cs}} = 1.64 \cdot 10^{-2}\hat{a} + 1.79 \cdot 10^{-1}, \qquad r^2 = 2.2 \cdot 10^{-3} \tag{6.5}$$

In equation 6.5, zero is included in the 95 % confidence interval ($-1.06 \cdot 10^{-1} \leq b_1 \leq 1.39 \cdot 10^{-1}$) for the slope $b_3 = 1.64 \cdot 10^{-2}$ and the correlation between ρ_{cs} and $\hat{a}$ is near zero ($r^2 = 2.2 \cdot 10^{-3}$). Thus, the analysis of collagen densities is not affected by the amounts of GAG. Because of the near zero intercept for the linear relationship between ρ_{col} and $\hat{a}$ ($b_4 = 1.24 \cdot 10^{-2}$, equation 6.4), we quantified collagen densities with equation 6.6:

$$\rho_{\mathrm{col}} = 1.45\hat{a} \tag{6.6}$$

With $\hat{a}$ estimated with equation 6.2.

To obtain mean depth-dependent profiles between samples, we started at the articular surface (d_1 in figure 6.2a) and took the mean of the measurements at d_1 of the samples in the pool. We then moved one measurement point towards the calcified tissue and repeated this with d_2 in figure 6.2a, etc. Note that because of differences in cartilage thickness, the number of samples that we can analyse decreases once we are at a depth larger than D for the shortest dataset in the sample pool. We used the exponential fit for cartilage thickness that we found in our previous study [331, equation 2] to show age- and depth-dependent results:

$$D_f(t) = 618\left(0.52 + \mathrm{e}^{-0.11t}\right) \tag{6.7}$$

with D_f the cartilage thickness in μm and t the age in weeks.

6.2.5 Statistical analysis

Data were analysed with generalized linear mixed models because some of the variables analysed are not normally distributed. Also, measurements on the same animal and position within an animal are dependent. This excludes conventional analyses such as analysis of variance or regression that are intended for normally distributed and independent data. We therefore used the penalized quasi-likelihood methodology described by Schall [291], Breslow & Clayton [56] and Engel & Keen [102]. Calculations were performed with GenStat [268]. The models comprised random effects with associated components of variance, that allowed for dependence between observations of the same animals and the same anatomical sites. Thus, we used a nested structure within animal for hind leg/fore leg, lateral/medial and caudal/distal/rostral sites. In particular, this allowed for additional dependence within animals between duplicate observations on the same site. We are interested in the development of differences between the different anatomical sites with age. Therefore, fixed effects (systematic effects) comprised main effects and all second order interactions for factors age, hind leg/fore leg, lateral/medial site, and caudal/distal/rostral site in the initial models.

Models were fitted separately to three response variables: collagen density at the surface ρ_s, maximum collagen density ρ_{max}, and the presence of a collagen density valley near the articular surface v. For the variable ρ_{max} we used an identity link and normal distribution. For the variable ρ_{max}, we used a log link and gamma variance function, with a multiplicative dispersion parameter. For v we obtained the position of the minimum collagen density in the first 5 samples points over the depth. We then scored each collagen density profile with 0 (the minimum is found in the first sample point, i.e. does not results in a valley) or 1 (the minimum occurs after the first sample point and results in a valley). We tested these scores with a logit link $\left(\mathrm{logit}\, q = \log q/(1-q)\right)$ and binomial variance function. For each model, random effects on the link scale were assumed to follow normal distributions. Tests were based on an approximate F-test [181] applied to the adjusted dependent variate from the last iteration step of the iterative re-weighted restricted maximum likelihood algorithm [102] that we used. The link functions provide the relationship between the linear predictor and the mean of the distribution function

and the chosen link and variance functions were needed to achieve satisfactory (normally distributed) residuals for the models. Non-significant ($p > 0.05$) higher order fixed factor interactions were dropped from the initial models.

We used the following symbols in the models: μ: intercept; A_j, j=0, 2, 4, 8, 12, 20, 28, 36, 52, 72: age in weeks; $B_k, k = 1, 2$: fixed factor hind leg/fore leg; C_l, l=1, 2: fixed factor lateral site/medial site; D_m, m=1, 2, 3: fixed factor caudal site/distal site/rostral site; L_i: random factor individual animal; and $(LB)_{ik}$, $(LBC)_{ikl}$ and $(LBCD)_{iklm}$ nested random factors within animal. The final model that we fitted for each covariate, is presented in the results section. We aimed for analysis of two samples for each of six sites (figure 6.1), for each of two legs, for each of 48 animals, i.e. 1152 samples. Due to the loss of two fore legs and a few missing values, the total number of samples was 1132. In the text, we quantify significant differences as mean ± standard error as predicted by the model. In the figures and text, we use raw means and associated standard deviations, and not model predictions, to present the results.

6.3 Results

We show examples of sample spectra for 0 weeks and 72 weeks (figure 6.3b). Analysis of all spectra with equations 6.2 and 6.6 yields the averaged collagen densities per age group (figure 6.4) and the statistical results (figure 6.5).

The final model for the collagen density at the surface ρ_s is

$$y_{ijklm} = \mu + A_j + B_k + C_l + D_m + (AD)_{jm} + L_i + (LB)_{ik} + (LBC)_{ikl} + (LBCD)_{iklm} \quad (6.8)$$

with y_{ijklm} the predictor. There is a main effect for the factor age for ρ_s (table 6.1: A_j, $p < 0.001$). In general, ρ_s increases with age, up to the last sample point: from $0.23\,\mathrm{g/ml} \pm 0.06\,\mathrm{g/ml}$ (mean ± s.d., $n = 48$) at 0 weeks to $0.51\,\mathrm{g/ml} \pm 0.10\,\mathrm{g/ml}$ ($n = 46$) at 72 weeks (figure 6.5a). An exception is the measurement at 28 weeks that is lower than the value at 20 weeks and 36 weeks. The interaction of the fixed factor age with the fixed factor caudal site / distal site / rostral site (table 6.1: $(AD)_{jm}$, $p = 0.026$) shows significant effects at 4 weeks and 72 weeks, where ρ_s is lower for the rostral site than for the distal site and caudal sites (table 6.2).

Table 6.1: Results for the statistical model for the collagen density at the surface ρ_s with log-link and gamma variance function. Letters for the fixed terms represent: A_j – age, B_k – fore / hind, C_l – lateral / medial and D_m – caudal / distal / rostral. Combinations represent interactions between these fixed factors.

fixed term	A_j	B_k	C_l	D_m	$(AD)_{jm}$
p-value	< 0.001	0.207	0.212	0.966	0.026

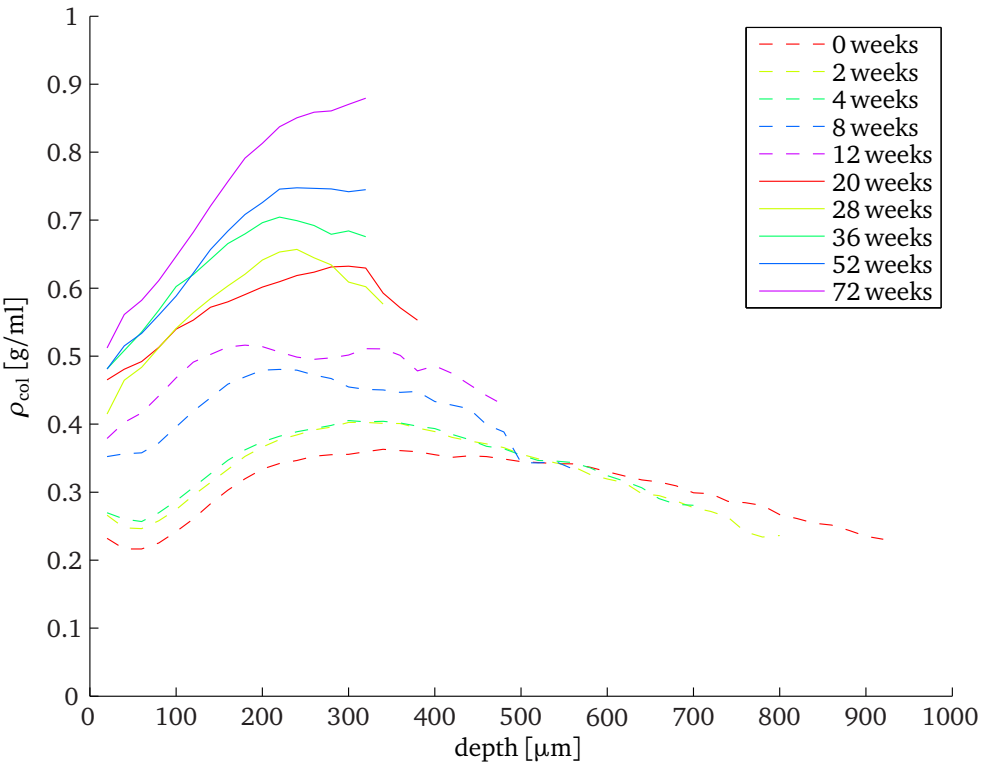

Figure 6.4: Mean collagen density as a function of cartilage depth for the ten ages.

Table 6.2: Mean collagen density at the surface ρ_s [g/ml] per age for caudal site, distal site and rostral site from the statistical model. The associated standard error is 0.0155 [g/ml]. Stars mark values that are significantly different from the value for the rostral site at that age.

age [weeks]	0	2	4	8	12	20	28	36	52	72
ρ_s [g/ml] caudal	0.22	0.27	0.26*	0.36	0.37	0.45	0.43	0.48	0.49	0.53*
ρ_s [g/ml] distal	0.25	0.27	0.26*	0.34	0.38	0.46	0.40	0.48	0.47	0.54*
ρ_s [g/ml] rostral	0.23	0.26	0.30	0.36	0.39	0.48	0.42	0.47	0.48	0.46

The final model for the maximum collagen density ρ_{max} has no fixed factor interactions and is

$$\eta = \mu + A_j + B_k + C_l + D_m + L_i + (LB)_{ik} + (LBC)_{ikl} + (LBCD)_{iklm} \tag{6.9}$$

where the conditional expectation of y_{ijklm} for given η is $\text{logit}^{-1}(\eta)$, the inverse of

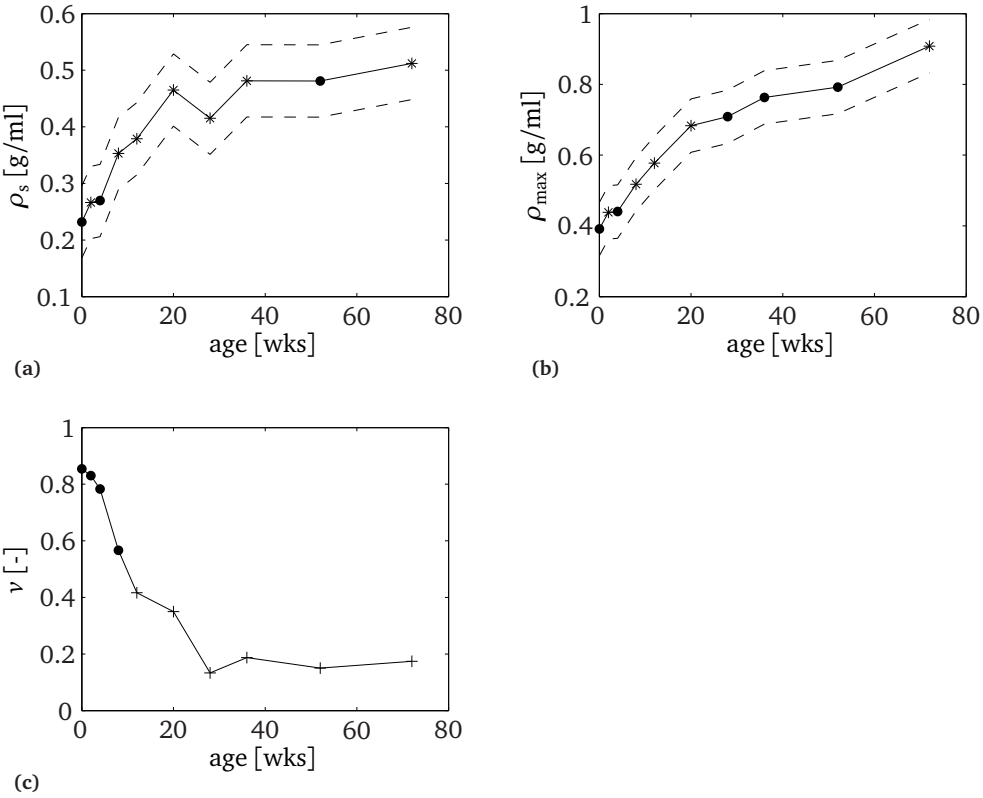

Figure 6.5: Statistical results for collagen density profiles. With **(a)** mean collagen density at the surface ρ_s (solid) ± standard deviation (dashed) as a function of age. Stars mark values that are significantly different from the value at the previous age; **(b)** mean maximum collagen density ρ_{max} (solid) ± standard deviation (dashed) as a function of age. Stars mark values that are significantly different from the value at the previous age; and **(c)** mean scores for the presence of the collagen density valley ν as a function of age. Crosses mark values that are significantly different from the value at 0 weeks.

the link function. There is a main effect for the factor age for ρ_{max} (table 6.3: A_j, $p < 0.001$). ρ_{max} increases monotonically with age, up to the last sample point: from 0.39 g/ml ± 0.08 g/ml (mean ± s.d., $n = 48$) at 0 weeks to 0.91 g/ml ± 0.13 g/ml ($n = 46$) at 72 weeks (figure 6.5b). There is a significant effect for the factor lateral site / medial site for ρ_{max} (table 6.3: C_l, $p = 0.006$): maximum collagen density is 2.72 %±1.00 % (mean ± s.e.) higher at the medial site than at the lateral site.

The final model for the presence of a collagen density valley ν has no fixed factor interactions and is therefore equal to equation 6.9. There is only a significant effect for

Table 6.3: Results for the statistical model for the maximum collagen density $\rho_{\max}$ with log-link and gamma variance function. Letters for the fixed terms represent: A_j – age, B_k – fore / hind, C_l – lateral / medial and D_m – caudal / distal / rostral.

fixed term	A_j	B_k	C_l	D_m
p-value	< 0.001	0.169	0.006	0.422

Table 6.4: Results for the statistical model for the presence of a collagen density valley v with logit-link and binomial variance function. Letters for the fixed terms represent: A_j – age, B_k – fore / hind, C_l – lateral / medial and D_m – caudal / distal / rostral.

fixed term	A_j	B_k	C_l	D_m
p-value	0.007	0.873	0.480	0.063

the factor age for v (table 6.4: A, $p = 0.007$): v decreases between birth and maturity (figure 6.5c). There are no significant differences between successive ages (figure 6.5c). However, a significant decrease in the score for v occurs between 0 weeks and 12 weeks. The score v at 72 weeks does differ significantly from v at 12 weeks. The mean score at 0 weeks is 0.85, i.e. at this age $\approx 85\,\%$ (41 out of 48) of the measurements shows a valley in the first 5 sample points over the depth (figure 6.5c). The mean score at 12 weeks is 0.41 (25 out of 60), and the mean score at 72 weeks is 0.17 (8 out of 46).

6.4 Discussion

As expected [50, 167, 282, 348], we find that collagen content increases with age between birth and maturity: both ρ_s (figure 6.5a) and $\rho_{\max}$ (figure 6.5b) show a positive correlation with age. Contrary to the cartilage thickness and collagen orientation parameters that we measured in the same animals [331], collagen density does not appear to stabilise between 36 weeks and 72 weeks. It thus appears that the potential for collagen remodelling is different between collagen orientation and collagen density. The potential for collagen reorientation appears to be correlated to changes in cartilage thickness [331], whereas collagen density in the current study still increases after cartilage thickness has stabilised in these animals (36 weeks, [331]). Both an increase in the number of collagen fibrils and an increase in collagen fibril thickness results in increased collagen densities. Neither polarised light microscopy, which we used in our previous study [331], nor FTIRμS in the current study is capable of measuring collagen fibril thickness. Additional measurements, e.g. with electron microscopy, will be necessary to elucidate to what degree collagen fibril thickness contributes to the observed collagen density.

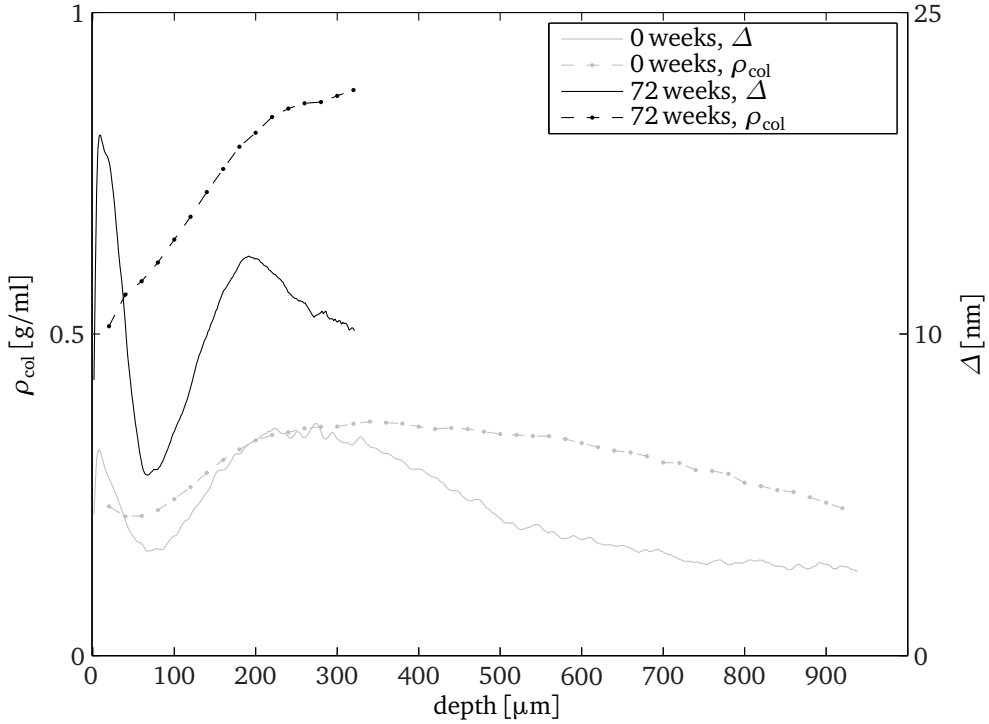

Figure 6.6: Mean collagen densities (ρ_{col}, dashed) for 0 weeks (gray) and 72 weeks (black) together with mean retardance results (Δ, solid) from our previous study [331]. The valley in collagen density can partly explain the retardation valley in the youngest animals, but not in the oldest animals.

In the current study, we investigated the possible presence of a valley in collagen density near the articular surface, prompted by the presence of a retardance valley at that location in our polarised light microscopy study on the same animals [331]. The data on porcine AC by Rieppo et al. also shows some evidence for a valley in collagen density near the articular surface for the youngest age group, but not for the older age groups [282, figure 2a]. Similarly, we find strong evidence for a valley in collagen density in the youngest animals that disappears with increasing age (table 6.4, figure 6.5c). This means that the retardance valley near the articular surface that is present in all age categories [331], must be interpreted differently for the youngest than for the oldest animals (figure 6.6). The retardance patterns measure primarily a combination of collagen densities and collagen fibril anisotropy [329, 331] and the collagen density results (figure 6.6) show that the retardance valley reflects a decrease in collagen fibril anisotropy, and not a decrease in collagen density, in the adult animals. A decrease in collagen fibril anisotropy is the traditional interpretation of decreased retardance near the articular surface [37, 150, 246, 366]. Our current results suggest that interpretation

of retardance valleys near the articular surface in immature AC is less straightforward: the retardance valley in perinatal animals also reflects a decrease in collagen density (figure 6.6).

Hunziker et al. [154] showed that AC grows appositionally. The superficial zone supplies the stem cells for AC growth. Daughter cells that are displaced horizontally, remain confined to the superficial zone and replenish the stem-cell pool and affect lateral growth. Daughter cells that move vertically downwards form a zone with a rapidly dividing and proliferating pool of cells for rapid clonal expansion. This zone affects longitudinal growth and is located at the transitional and upper deep layer of AC [154]. The location (distance from the articular surface) of the collagen density valley in our study appears to coincide with the zone of rapidly dividing daughter cells in the study by Hunziker et al. [154]. Hunziker et al. further showed that the proliferation activity of this pool of cells decreased with age and had ceased when AC thickness stabilised. The valley in collagen density that we observe in our study also gradually disappears with age, and also stabilises when cartilage thickness stabilises (36 weeks, figure 6.5c). These similarities in the spatial and temporal patterns of cell proliferation and the presence of a collagen density valley, suggest a relationship between the cell activity and collagen production in this zone. Dedicated investigations will be required to show whether or not such a relationship exists.

FTIRμS is a technique that has gained popularity for the investigation of the collagen network of AC in the last decade [47]. FTIRμS was first applied to biological tissues when it became possible to use a microscope in the light path [27]. The first applications of FTIRμS for AC were investigated at the start of the current century [68, 276]. Biochemical analysis of hydroxyproline content is an alternative and well-established technique to quantify collagen density in AC. However, this technique has a limited spatial resolution and is used to measure total collagen content as opposed to depth-dependent profiles, e.g. [50, 167, 348]. The main benefit of FTIRμS is the high spatial resolution that can be achieved [287]. With histological slices as in our study, FTIRμS is a relatively easy and fast technique to obtain depth-dependent collagen density profiles in AC. Apart from the overlapping spectra of the AC components (figure 6.3a), quantitative FTIRμS is challenging because small changes in peak shape and position may occur as a result of the local composition or structure of the proteins [287]. The baseline correction finally, lacks a theoretical or physical background and its implementation is to a certain degree arbitrary. In our experience, the choice of baseline correction hardly influences the quantitative results, as long as the same baseline correction is applied to all samples and calibration sequences.

We treated the samples with sucrose and this hinders analysis of GAG densities because the FTIRμS signal of sucrose interferes with the signal of the sugar groups in the GAGs. When we attempted GAG quantification on samples that were not treated with sucrose, we found similar to Rieppo et al. [287] that GAG densities can not be reliably obtained from FTIRμS spectra. This is probably because collagen is much more abundant in AC than the GAGs [248], and because the absorption for collagen is higher than for chondroitin sulphate for equal amounts of pure components (figure 6.3a).

Several approaches have been used for quantitative analysis of AC FTIRμS spectra, e.g. integrated peak areas [68], (partial) least square fits [92], Euclidean distance analysis

[276] and deconvolution approaches [287]. Analysis with integrated peak areas is the most straightforward, and with our calibration sequence we estimated an error of 5 % for collagen densities for a 4:1 ratio of collagen to chondroitin sulphate [248, 341]. However, since the development of the ratio of collagen to chondroitin sulphate is unknown, we selected a different approach to analyse our spectra because we could show that chondroitin sulphate density does not affect the parameter $\hat{a}$ ($r^2 = 2.2 \cdot 10^{-3}$, equation 6.5).

The spatial and temporal collagen density profiles in the current study are similar to those in a previous FTIRμS study into postnatal AC development by Rieppo et al. [282]. Rieppo et al. [282] looked at domestic pig AC from the femoral groove at 4 months, 11 months and 21 months of age. As in our study, they found that collagen density shows a maximum between the superficial and deep zone in the youngest age group, and that collagen density increases monotonically between the superficial and the deep zone for the oldest animals [282, figure 4a]. Also, the order of magnitude of collagen density in the adult animals in our study is in line with previous reports on total AC density, e.g. ≈ 1.4 g/ml for bovine [294] and human AC [30].

In our previous study on collagen orientation [331], we observed that the caudal site developed differently from the distal and rostral sites. We can not show such a difference in the current study. We do find significant but small (2.7 %) differences in $\rho_{\max}$ between lateral sites and medial sites (medial sites higher). In our previous study [331], we found an effect for the lateral sites and medial sites for the collagen orientation pattern (superficial zone thicker at lateral site). Whether or not these effects are related cannot be resolved from these studies. Dedicated finite element models can be an aid for a functional analysis of these effects, e.g. [330, 357]. In our previous study [331] we found that differences during development had disappeared in the last sample point (72 weeks). In that study, we explained the lack of differences in the mature animals by the near congruent joint that we investigated. Our current results support that explanation: we observe very little differences in collagen density over this near congruent joint surface. It thus appears that the expected different loading regimes for the different sites (more static at the distal site, intermittent at the caudal and rostral sites) have little influence in the joint and animal that we investigated.

Finite element models can also assist in a functional analysis of the depth-dependent collagen density development in postnatal life, e.g. [17, 167, 357]. We performed such a functional analysis [330] with our earlier data on collagen orientation remodelling [331]. In that functional analysis [330] we found a marked increase in AC stiffness near the bone, but not at the articular surface. Thus, the effect of postnatal collagen reorientation is the (further) development of depth-dependent mechanical properties in AC. These depth-dependent mechanical properties of AC are thought to be important for the adult functions of AC [110, 193, 203, 293]. In the current study, collagen density increases most in the deep cartilage. Because cartilage stiffness correlates positively with collagen density [26, 349] we hypothesise that this depth-dependent distribution of collagen density also contributes to the development of a depth-dependent gradient in mechanical properties of AC in postnatal life.

With this paper, we complement our earlier data on postnatal collagen reorientation in the same animals [331]. The combination of the two data sets provides better tools

for functional analysis of the role of the collagen fibre network during development, e.g. by composition based finite element models [17, 330, 357]. Also, the combination of retardance results and collagen density results (figure 6.6) enabled us to further illustrate the peculiar nature of the transitional zone in the perinatal animals [328, 331]. We thus contribute to a better understanding of the mechanobiology of articular cartilage development. With additional information on the development of GAG concentrations and fixed charge densities in the AC, it becomes possible to estimate the mechanical environment that drives the depth-dependent AC development in general, and depth-dependent collagen remodelling in particular.

6.5 Conclusions

Collagen densities in articular cartilage increase in postnatal life with depth-dependent variation: the increase in collagen density at the articular surface is smaller than the increase in maximum collagen density in the deep cartilage. Collagen density does not stabilise by 72 weeks, the last sample point in this study. Because cartilage stiffness correlates positively with collagen density [26, 349], we predict that the depth-dependent pattern of collagen density remodelling contributes to the functional depth-dependent gradient in the mechanical properties of AC.

We find strong evidence for a valley in collagen densities near the articular surface ($d < 100\,\mu$m) that is present in the youngest animals, but that has disappeared in the oldest animals. A valley in retardance near the articular surface is traditionally interpreted as the result of a decrease in collagen anisotropy. Our current results show that the retardance valley in perinatal animals also reflects a decrease in collagen density.

Authors contributions

MvT carried out the design of the study and its coordination, the data acquisition (FTIRμS-measurements), processing, (statistical) analysis and interpretation, and drafting the manuscript. HS carried out the acquisition of data (sample preparation & histology), and participated in data analysis and interpretation and drafting the manuscript. BvL assisted with the data acquisition and participated in the interpretation of data and critical revisions of the manuscript. HZ participated in the interpretation of data and critical revisions of the manuscript. SK and JvL participated in the design of the study and its coordination, data analysis and interpretation and critical revisions of the manuscript. All authors read and approved the final manuscript.

Acknowledgements

We kindly thank Wim van de Laan for providing the sheep. From Wageningen University, we thank the people at De Haar / Ossekampen laboratory animal facility for taking care of the sheep, and we thank Dr. Bas Engel from the Biometris group for his support with the statistics.

I can't be as confident about computer science as I can about biology. Biology easily has 500 years of exciting problems to work on. It's at that level.

Donald Knuth, Computer Literacy Bookshops Interview (1993)

7

Modelling postnatal collagen structure development in articular cartilage: interactions of orientation, density and structure

Mark C. van Turnhout[1], Sander Kranenbarg[1] & Johan L. van Leeuwen[1]. Submitted.

[1]Wageningen University, Experimental Zoology Group, PO Box 338, 6700 AH, Wageningen, The Netherlands.

Abstract

The collagen fibril network is an important factor for the depth-dependent mechanical behaviour of adult articular cartilage (AC). Recent studies have quantified how predominant collagen fibril orientation, collagen densities and collagen network anisotropy change in postnatal life. These studies showed that the collagen network in postnatal AC is subject to extensive remodelling.

Our understanding on the development of functional depth-dependent mechanical properties in postnatal AC is incomplete. In the current paper, we investigate the interactions of postnatal collagen fibril reorientation, collagen density increases and collagen network anisotropy changes. We use a composition-based finite element model to simulate in a 1-D confined compression geometry the effects of the different collagen parameters that were measured in developing sheep.

Both increases in collagen density and collagen reorientation contribute to the depth-dependent mechanical behaviour of AC. There is an interaction and the combined effect is larger than the sum of the separate effects. We find further evidence for the hypotheses that collagen density increases correlate with increased fibril strains due to collagen fibril reorientation.

Our results suggest that the transitional layer in adult animals serves to smooth gradients in the mechanical state of the tissue. However, the current paper is unable to elucidate a similar mechanical role for the transitional layer in the AC of the perinatal animals.

7.1 Introduction

Articular cartilage (AC) consists of a hypo-cellular porous extracellular matrix (≈ 20 % wet weight) that is saturated with fluid (≈ 80 % wet weight). The (solid) extracellular matrix is made of mostly collagen (≈ 80 % dry weight) and negatively charged proteoglycan molecules (≈ 20 % dry weight), e.g. [248]. The functions of AC in adult life are to support and distribute mechanical loads and to provide a low friction environment for joint movement. The mechanical behaviour of AC has an important role for these (mechanical) functions [151, 193, 216, 220, 249, 293].

The collagen network is the main component of the extracellular matrix and experiments show a large influence of this network on AC mechanics [26, 30, 31, 183, 231, 233, 235]. Over the past decade, a growing number of computational investigations with fibril-reinforced finite element models appeared that stressed the role of the adult collagen network in AC mechanics, e.g. [17, 170, 218, 298, 330, 354, 355]. The collagen fibrils in AC provide a 1-D reinforcement of the extracellular matrix. Because of their slender structure, collagen fibres only transmit mechanical loads in tension [14, 35, 180, 354]. The collagen network in unloaded healthy adult AC counterbalances the internal osmotic pressures in the tissue, and loss of collagen results in larger swelling strains [26, 30, 231, 233, 235, 248] and therefore smaller osmotic pressures and tissue stiffness [154, 162, 193, 242]. The fact that collagen fibrils bind fluid also affects osmotic pressures and tissue stiffness [230, 234, 357].

In early postnatal life, AC functions as a growth plate for joint development [9, 139, 154], and the composition and structure that are needed for a functional tissue in adult life still need to develop. The collagen network in particular, is subject to extensive remodelling in postnatal life: collagen amounts [50, 84, 167, 282, 332, 348] and collagen fibril diameter [84, 107] increase; the predominant collagen fibril orientation changes from a transversely isotropic structure with fibrils parallel to the articular surface in neonatal AC to a depth-dependent arcade-like structure in adult life [6, 168, 282, 331]; and collagen network anisotropy is reported to increase, with depth-dependent variation [158, 168, 282].

Our knowledge on the mechanobiology of AC development in postnatal life and AC maintenance in adult life is still limited. The process of postnatal AC development is important, because AC in adult life has lost most of its remodelling capacity [94, 182, 220]. In particular, the adult collagen network has estimated turnover times of ≈ 400 years and its remodelling capacity is very limited [25, 31, 49, 106, 159]. Better understanding of the mechanobiology of postnatal AC development will also benefit our knowledge on adult AC maintenance and is relevant when we want to use AC postnatal development as a model for functional cartilage tissue engineering, e.g. [193, 281, 347].

To our knowledge, investigations into the functional role of collagen network remodelling in postnatal AC development are currently limited to a single study [330]. That study uses the composition-based Fibril Reinforced Poro-Viscoelastic Swelling (FRPVS) model for AC [351, 352, 356, 357] and focusses on the contribution of collagen fibril reorientation. In the current study, we also take the postnatal development of collagen density and collagen network anisotropy into account in order to expand our current knowledge on the functional role of postnatal collagen network remodelling. As input

for the model, we use the original data on sheep at ten developmental stages from birth to maturity presented by Van Turnhout et al. [331, 332].

7.2 Methods

For a detailed description of the modelling theory of the FRPVS model, we refer to existing literature, e.g. [170, 171, 351, 356, 357]. Summarising, this is a biphasic model with the solid phase divided into a viscoelastic fibrillar part that represents the collagen network and a viscoelastic non-fibrillar part that represents the remainder of the extracellular matrix (the PG molecules). The model accounts for osmotic pressures due to the negative charges of the PG molecules and strain-dependent permeability and Poisson ratio. Initial fluid fractions, fixed charge densities and collagen fractions and orientations are defined locally (per integration point), and the model accounts for the distinction between intra- and extra-fibrillar fluid for the calculation of osmotic pressures when it updates the local composition and mechanical state.

The methodology is similar to that in our publication on the effects of postnatal collagen reorientation [330]. Thus, we simulate sequences of ten meshes for the ten developmental stages presented by Van Turnhout et al. [330–332]. We use the FRPVS model with material parameters as described in [357]. For each mesh, we use the same initial fluid volume fraction ($n_\mathrm{f} = 0.9 - 0.2z$ with z the dimensionless depth), initial fixed charge density ($c_\mathrm{F} = -0.1z^2 + 0.24z + 0.035$ in [Meq/ml]), and matrix density (1.43 g/ml), as in our previous study [330]. We only consider the equilibrium response and collagen fibrils are therefore modelled as elastic and permeability is kept constant [357].

We use the original data by Van Turnhout et al. [331, 332] to simulate the effects of the postnatal development of predominant collagen orientation, collagen densities, and collagen network anisotropy in AC (figures 7.1 and 7.2). First, we investigate the interaction of predominant collagen orientation and collagen densities. The patterns for the predominant collagen orientation (figure 7.1a, the primary network) are adopted from [331, figure 3], similar to our approach in [330]. The collagen density patterns (figure 7.1b) are adopted from [332, figure 2]. Collagen network anisotropy is constant in these simulations.

The FRPVS model divides the collagen network in two portions: a primary network that simulates a predominant collagen orientation network, and a secondary network that simulates an 'isotropic' network with random collagen fibril orientations [351, 356, 357]. This division in two networks with this distribution of collagen densities was used by Van Turnhout et al. [329] to model the optical effects of collagen fibril networks in polarised light microscopy. They showed that retardance patterns from polarised light microscopy divided by collagen densities provided a semi-quantitative description $\overline{\nu}$ of collagen network anisotropy. In the second part of the study, we adopt the formulation by Van Turnhout et al. [329] for use with the FRPVS model to simulate postnatal development of collagen network anisotropy. The mean retardance patterns per age that are needed for the calculation of the anisotropy parameter $\overline{\nu}$ are adopted from [331, figure 5]. Similar to the orientation patterns [330, 331], retardance in the deep zone is

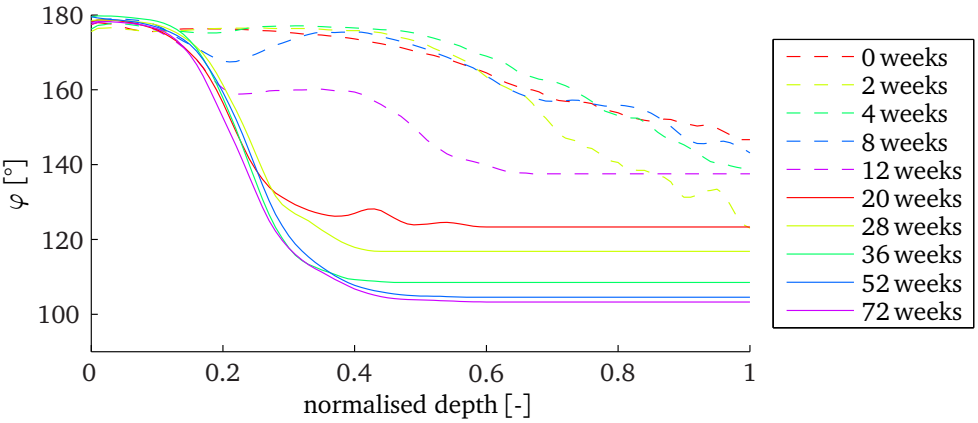

(a)

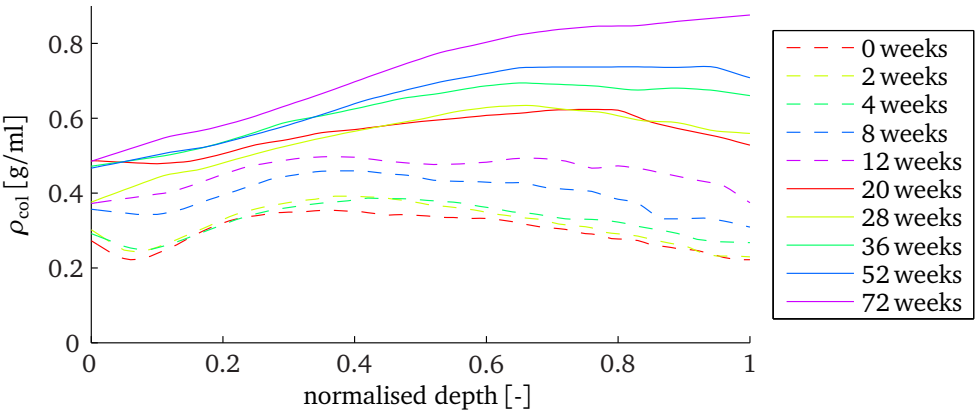

(b)

Figure 7.1: Depth-dependent parameters for the 10 different ages that are used for model input in the study as a function of normalised depth: from 0 – the articular surface to 1 – the tide-mark. With **(a)** Predominant collagen fibril orientation φ, adopted from [331, figure 3]; and **(b)** Collagen density ρ_{col}, adopted from [332, figure 2].

kept constant (figure 7.2a). The three datasets (orientation, density and retardance) are scaled to equal (dimensionless) length and smoothed with a 5-point moving average. The anisotropy parameter (figure 7.2b) is obtained by [329]:

$$\overline{\nu} = \kappa \frac{\Delta}{\rho_{\text{col}}} \tag{7.1}$$

With Δ the retardance (figure 7.2a), ρ_{col} the absolute amount of collagen (figure 7.1b), and κ an arbitrary constant to ensure that $0 \leq \overline{\nu} \leq 1$.

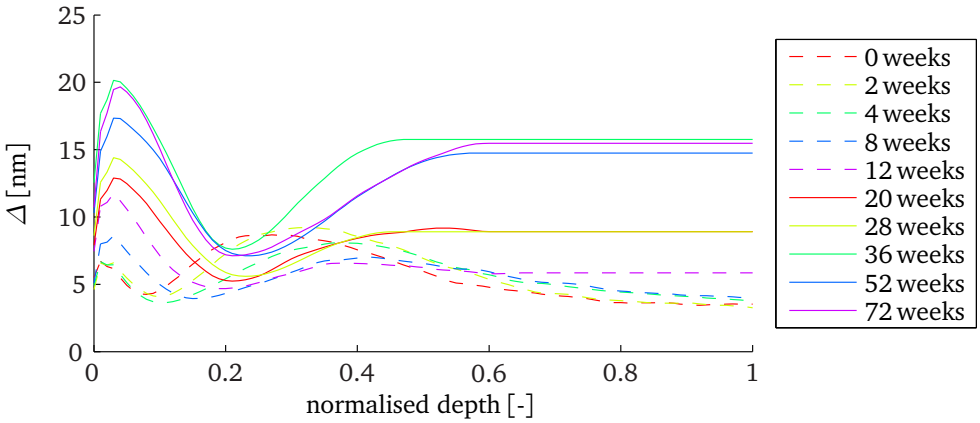

(a)

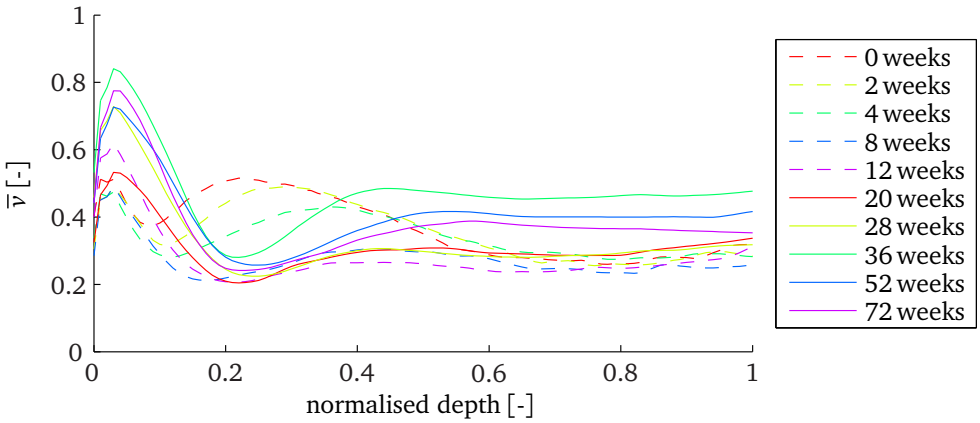

(b)

Figure 7.2: Depth-dependent parameters for the ten different ages that are used for model input in the study as a function of normalised depth: from 0 – the articular surface to 1 – the tide-mark (continued). With **(a)** Retardance patterns from the polarised light microscopy study Δ, adopted from [331, figure 5]; and **(b)** Anisotropy parameter $\overline{\nu}$ (equation 7.1).

Collagen orientation patterns are modelled with two fibrils for the primary network in each integration point [330]. One fibril follows the pattern, its companion follows the pattern mirrored in the vertical axis (or mirrored in 90 ° in figure 7.1a). In this manner, an arcade-like configuration is formed, suitable for 1-D analysis. The secondary network is modelled with seven fibrils [350, 356, 357]. We divide total collagen density over the

two networks according to:

$$\rho_1 = \rho_{\text{col}}\overline{v} \qquad \text{for the primary network} \tag{7.2}$$

$$\rho_2 = \rho_{\text{col}}(1-\overline{v}) \qquad \text{for the secondary network} \tag{7.3}$$

with $\overline{v}$ from equation 7.1 and $\kappa = 1/50$. The constant value of $\overline{v}$ in the first part of the study is selected 0.46 according to previous studies [356, 357].

The finite element geometry and the loading protocol were the same as we used in [330]. The simulations comprised of a 1-dimensional model (figure 7.3) with a single column of 33 equally thick axisymmetric pore pressure elements (CAX4P). Because of the osmosis in the model, the mesh is allowed to equilibrate with its environment before the simulation is started at t_0. The initial mesh height was adapted for each mesh such that

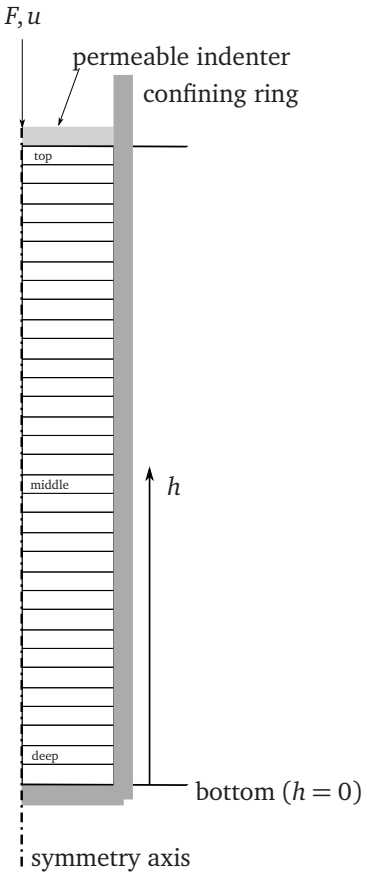

Figure 7.3: Mesh for the confined compression simulations. The mesh is divided into 33 elements and is supported by an impermeable bottom and confined by an impermeable ring. The displacement is applied to the permeable indenter at the articular surface. The layers labelled deep, middle and top are used to present the results.

the height of each mesh after the initial equilibrium step was $h_0 = h_{\max}(t_0) = 1.375$ mm. We prescribed zero pore pressure at the top of the model, i.e. fluid can move freely through this surface. All other surfaces were assumed to be impermeable. Displacements in the radial direction were suppressed. The model was axially compressed in a stepwise manner with 10^{-3} % strain/second in 1 % intervals up to 20 % global strain, and allowed to reach equilibrium after each compressive step (relaxation).

We use the applied normal stress σ and mesh height $h_{\max}$ at equilibrium for computation of global strain ε_g and global effective aggregate modulus H_{Ag}:

$$\varepsilon_g = \frac{h_0 - h_{\max}}{h_0}, \qquad H_{Ag} = \frac{\partial \sigma}{\partial \varepsilon_g} \tag{7.4}$$

with h_0 the mesh height at the start of the simulation. We use the element thickness d at equilibrium for computation of local strain ε_l and local effective aggregate modulus $H_A(h)$ for each element:

$$\varepsilon_l = \frac{d(t_0) - d}{d(t_0)}, \qquad H_A(h) = \frac{\partial \sigma}{\partial \varepsilon_l} \tag{7.5}$$

with $d(t_0)$ the element thickness at the start of the simulation.

7.3 Results

We first compare the depth-dependent mechanical state of the AC at zero global strain (t_0) for four combinations of collagen orientation patterns and collagen density patterns (figure 7.4). These simulations use the constant anisotropy ($\overline{\nu} = 0.46$) and comprise of the four combinations of the collagen orientation patterns at 0 weeks and 72 weeks with the collagen density patterns at 0 weeks and 72 weeks. Both changes in collagen fibril orientations, and changes in collagen densities affect the mechanical state in the cartilage at t_0.

Initial swelling strains (equation 7.4) are larger with collagen orientations of 0 weeks than with the collagen orientations at 72 weeks, except for the superficial layer where collagen orientation does not change during development. Swelling strains are also larger with collagen densities of 0 weeks than with the collagen densities at 72 weeks (figure 7.4a). Collagen densities also increase in the superficial layer between these ages, and the decrease in swelling strain due to collagen densities is present over the entire cartilage depth. The decrease in swelling strain is larger for the changes in collagen orientation than for changes in collagen density.

Fibril strains at t_0 (figure 7.4b) are smaller with collagen orientations of 0 weeks than with the collagen orientations at 72 weeks, where changes in orientation occur. The effect of increased collagen density on fibril strains is opposite: fibril strains are larger with collagen densities of 0 weeks than with the collagen densities at 72 weeks. There is further an interaction of collagen orientation changes and collagen density changes: the increase in fibril strain with increasing collagen density is much smaller for the collagen orientation at 0 weeks than at 72 weeks.

Osmotic pressures at t_0 (figure 7.4c) are higher for both collagen orientations and collagen densities of 72 weeks compared with those of 0 weeks. The increase in osmotic pressures is larger for the changes in collagen density than for changes in collagen orientation. There is also a small interaction: the collagen density related increase in osmotic pressures is a little smaller for the collagen orientation at 0 weeks than at 72 weeks.

The local effective aggregate modulus $H_A(h)$ at t_0 (figure 7.4d) is affected by these changes in the mechanical state at t_0 (figures 7.4a-7.4c). $H_A(h)$ is higher for both collagen orientations and collagen densities of 72 weeks compared with those of 0 weeks, and the increase in $H_A(h)$ is larger towards the bottom of the mesh for both effects. The increase in $H_A(h)$ is larger for the changes in collagen density than for changes in

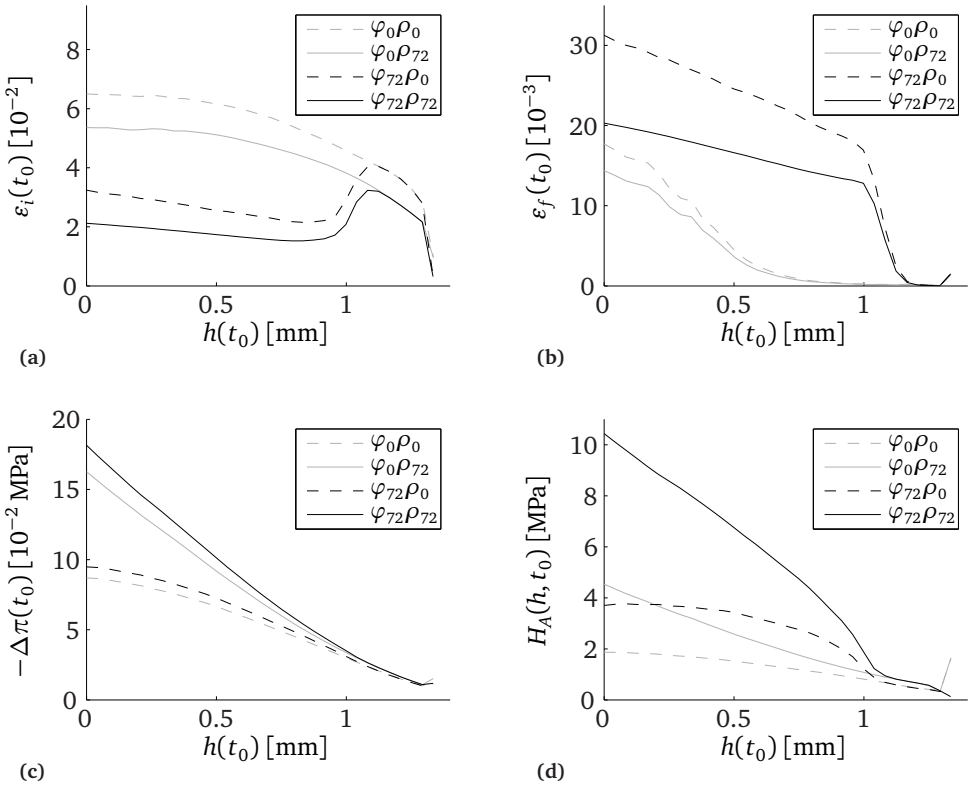

Figure 7.4: Mechanical state at zero global strain (t_0) as a function of mesh height h for four simulations with constant anisotropy. We show the four combinations of the collagen orientation patterns at 0 weeks (φ_0, gray) and 72 weeks (φ_{72}, black) with the collagen density patterns at 0 weeks (ρ_0, dashed) and 72 weeks (ρ_{72}, solid). With: **(a)** initial swelling strain ε_i; **(b)** fibril strain ε_f; **(c)** osmotic pressures $-\Delta\pi$; and **(d)** local effective aggregate modulus $H_A(h)$.

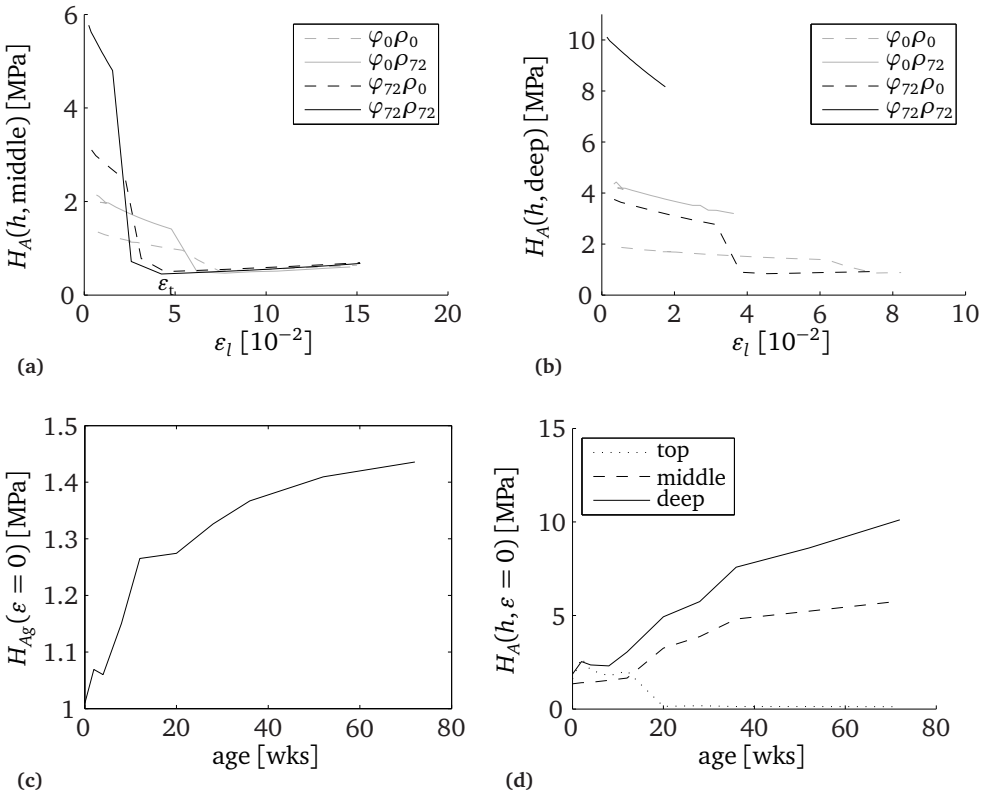

Figure 7.5: Development of the mechanical properties cartilage at t_0 simulated with constant anisotropy. With strain-stiffness relationship for the middle layer **(a)** and deep layer **(b)** for simulations with predominant collagen orientation φ and collagen densities ρ at 0 weeks (subscript 0) and 72 weeks (subscript 72) in the top panels. Panel **(a)** shows the tip over strain $\varepsilon_t \approx 0.05$ for the tension-compression non-linearity for the simulations with φ_{72}; **(c)** Global effective aggregate modulus H_{Ag} as a function of age; and **(d)** Local effective aggregate modulus $H_A(h)$ for the layers top (dotted), middle (dashed) and deep (solid).

collagen orientation close to the bottom of the mesh, and again there is an interaction: the depth-dependent increase in $H_A(h)$ due to collagen densities is much smaller for the collagen orientation at 0 weeks than at 72 weeks. At the top of the mesh $H_A(h)$ is equal for simulations with the same collagen orientation profiles.

Next, we compare the local strain-stiffness relationships for the same four combinations, and we show the development of the (depth-dependent) mechanical properties cartilage with the corresponding orientation patterns and density patterns for each age (figure 7.5), with constant anisotropy. The top layer is already past the tip over strain ε_t

for the (local) tension-compression non-linearity (see figure 7.5a) for very small global strains, and $H_A(h)$ increases slightly with increasing strain (not shown). For this layer, there are only minor differences between ages. Deeper into the cartilage, postnatal collagen reorientation affects both the tip over strain ε_t, and $H_A(h)$ for strains smaller than ε_t (figures 7.5a-7.5b). Postnatal increases in collagen density also increases $H_A(h)$ for strains smaller than ε_t, but do not convincingly affect ε_t itself (figures 7.5a-7.5b). These effects are larger in the deep layer (figure 7.5b) than in the middle layer (figure 7.5a).

The global effective aggregate modulus H_{Ag} increases with age when we model the

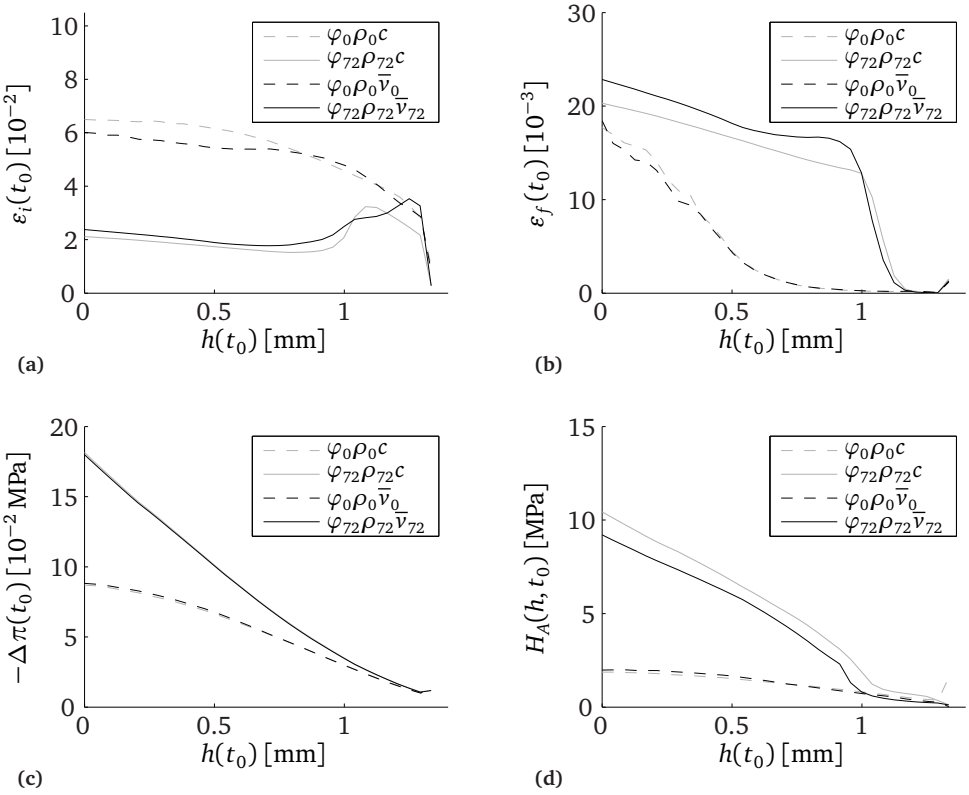

Figure 7.6: Mechanical state at zero global strain (t_0) as a function of mesh height h for the two extreme ages, and with and without depth-dependent anisotropy parameter. We show results of simulations with collagen orientation patterns and collagen density patterns at 0 weeks ($\varphi_0\rho_0$, dashed) and 72 weeks ($\varphi_{72}\rho_{72}$, solid), with constant anisotropy ($\overline{\nu} = 0.46$, labelled C, gray) or with corresponding anisotropy pattern (black) at 0 weeks ($\overline{\nu}_0$) and 72 weeks ($\overline{\nu}_{72}$). With: **(a)** initial swelling strain ε_i; **(b)** fibril strain ε_f; **(c)** osmotic pressures $-\Delta\pi$; and **(d)** local effective aggregate modulus $H_A(h)$.

mechanical properties of cartilage with the corresponding orientation patterns and density patterns for each age. We find the largest rate of increase in early life (i.e. before 12 weeks, figure 7.5c). The local effective aggregate modulus $H_A(h)$ develops differently for the three layers top, middle and deep (figure 7.5d). $H_A(h)$ of the top layer decreases from approximately 2 MPa to 3 MPa in the perinatal animals to approximately 0.13 MPa at 20 weeks, and changes very little for the later ages. For the middle layer and deep layer, $H_A(h)$ increases with age and the increase is larger for the deep layer (1.9 MPa to 10 MPa) than for the middle layer (1.3 MPa to 5.8 MPa).

Implementation of the depth-dependent anisotropy $\overline{\nu}$ (equations 7.1-7.3, figure 7.2b) has only small effects on the mechanical state at zero global strain (figure 7.6), and in compression (not shown). The parameter $\overline{\nu}$ appears to have a smoothing effect on initial swelling strains (figure 7.6a) and fibril strains (figure 7.6b) in the top of the model ($h \geq .8$ mm), especially for 72 weeks. The osmotic pressures appear unaffected (figure 7.6c) and $H_A(h)$ is only affected at 72 weeks (figure 7.6d). The value of $\overline{\nu} < 0.46$ in the deep tissue at 72 weeks decreases $H_A(h)$ compared with the simulations with constant anisotropy ($\overline{\nu} = 0.46$)

7.4 Discussion

In the current paper we performed sequences of simulations with the composition-based FRPVS model for the ten measurements points on the collagen network of developing sheep between birth (0 weeks) and maturity (72 weeks) presented by Van Turnhout et al. [331, 332]. The meshes differed only in predominant collagen fibril orientation, collagen densities and collagen network anisotropy. We aimed to separate the effects of the development of the collagen network from other developmental changes.

This work extends an earlier publication [330] on the effects of postnatal collagen reorientation (i.e. not accounting for collagen densities and network anisotropy). The changes in fibril orientation in the deep zone limit swelling of the tissue under zero global strain (figure 7.4a), and as a result osmotic pressures increase (figure 7.4c). Osmotic pressures are an important factor for the equilibrium stiffness of AC, e.g. [30, 79, 204, 225, 248], and we see that the increase in osmotic pressures correlates with an increase in local $H_A(h)$ (figure 7.4d).

An increase in collagen density is expected to affect the mechanical behaviour in two ways: first, when more collagen is present in the collagen network, the effects of this network will be reinforced; and second, with more collagen present the fraction of extra-fibrillar fluid will decrease, which in turn increases local osmotic pressures [230, 234, 330, 357]. The reinforcement of given collagen networks with increasing collagen densities is e.g. apparent from the decrease in initial swelling strains for an increase in collagen density (figure 7.4a). The increase in osmotic pressures due to the decrease in extra-fibrillar fluid fraction is not immediately visible in figure 7.4, because the increase in osmotic pressures (figure 7.4c) is also an effect of decreased initial swelling strains [330]. Similar to our previous study [330], we find that postnatal collagen reorientation does not affect the superficial layer $H_A(h)$, because collagen orientations do not change at this location during development. The results for the depth-dependent

$H_A(h)$ however, show that the superficial layer $H_A(h)$ increases slightly with increases in collagen density. This illustrates the additional effect of collagen densities on cartilage stiffness: stiffness increases through intra/extra-fibrillar fluid modulation.

Postnatal collagen reorientation and increases in collagen density interact to produce a gradient in cartilage stiffness (figures 7.4d and 7.5d). Collagen reorientation enhances the gradient in $H_A(h)$ for given collagen densities, and the changes in collagen density enhance the gradient for given collagen orientation (figure 7.4d). Our current results show the increase in $H_A(h)$ for the combination of the two effects (reorientation and density increase) to be larger than the sum of the two separate effects. Or alternatively, (1) the effects of postnatal collagen reorientation are relatively small if collagen density is kept at the value of 0 weeks, and (2) the effects of the postnatal increase in collagen density are relatively small if collagen orientation is kept at the value of 0 weeks. Apart from this interaction that results in a depth-dependent $H_A(h)$, it appears that the crucial effect of collagen reorientation is the adaptation of the tension-compression non-linearity, and that the crucial effect of postnatal collagen density development is the adaptation of depth-dependent $H_A(h)$ (figures 7.5a-7.5b). We finally note that the depth-dependent increase in collagen densities decreases the gradient in collagen fibril strains at t_0 in the deep zone (figure 7.4b): maximum fibril strains (near the bone) increase with $> 50\,\%$ when collagen densities do not develop with collagen reorientation. Thus, the depth-dependent development of collagen densities counteracts the increase in fibril strain due to collagen reorientation, such that maximum fibril strain is similar between 0 weeks and 72 weeks in our simulations (figure 7.4b). This observation supports a hypothesis in our earlier publication on the effects of postnatal collagen reorientation [330]: that collagen density increases more in the deep cartilage to counterbalance the increased fibril strains due to collagen reorientation.

We only find small differences when we implement depth-dependent anisotropy $\overline{\nu}$ for the different ages (figure 7.6), particularly for the younger ages. The FRPVS model uses a constant anisotropy parameter of $\overline{\nu} = 0.46$ [351, 356, 357]. The depth-dependent anisotropy parameter $\overline{\nu}$ is also relatively constant in the deep cartilage, with a value close to 0.46 (figure 7.2b). Variations in the anisotropy parameter $\overline{\nu}$ occur mainly at locations with the lowest stiffness and the smallest contribution to the global confined compression modulus (the top of the tissue). This could explain the small influence of $\overline{\nu}$ in our simulations. This apparent agreement of $\overline{\nu}$ with 0.46 in the deep cartilage is accidental. The constant value for $\overline{\nu}$ was quantitatively assessed by Wilson et al. [351] with parameter estimation. We had to use an arbitrary constant κ to ensure that $0 \leq \overline{\nu} \leq 1$ (equations 7.1-7.3), and the value $\kappa = 1/50$ is a rough estimate to find a maximum $\overline{\nu}$ in the series of approximately 0.8 to 0.9. The current results indicate that the value of $\overline{\nu}$ in the current study is close to previous work [351, 356, 357]. As a consequence, we find that the assumption of constant anisotropy is valid for the deep cartilage, and that the error in this assumption for the upper half of the tissue does not result in large differences for the global mechanical behaviour in confined compression.

Although implementation of $\overline{\nu}$ has only small effects in the current study, the parameter is not unimportant. Wilson et al. [351] already found that implementation of the primary 'predominant orientation' network and secondary 'isotropic' network is necessary to correctly model AC mechanics with the FRPVS model. The expected effect of an

increase in $\overline{\nu}$ is a reinforcement of the effects of the primary network. For the simulations for 72 weeks there is a decrease in $H_A(h)$ in the deep cartilage for the simulations with $\overline{\nu} \approx 0.37$ compared with simulations with $\overline{\nu} = 0.46$ (figure 7.6d). However, contrary to first expectations there is a slight increase in $H_A(h)$ for the simulations for 0 weeks with $\overline{\nu} \approx 0.35$ in the deep cartilage compared with simulations with $\overline{\nu} = 0.46$ (figure 7.6d). The predominant collagen fibrils have an orientation close to 180 ° in these animals and these primary fibrils therefore hardly contribute to the mechanical behaviour in the simulations. The secondary 'isotropic' network however, does contribute: this network also limits swelling strains, although to a much lesser degree than the adult primary network. Therefore, cartilage stiffness in confined compression can increase when there is more collagen in the secondary network (smaller $\overline{\nu}$) for the perinatal animals.

The main effect of postnatal collagen network remodelling, the other parameters being equal, is the depth-dependent increase in $H_A(h)$. As a result, global H_{Ag} increases (figure 7.5c) and a large gradient in $H_A(h)$ develops (i.e. $H_A(h)$ increases with distance from the articular surface, figures 7.4d, 7.5d and 7.6d). The gradient in $H_A(h)$ is thought to be important for the adult functions of AC [15, 110, 193, 203, 293] and appears to be the most important effect of postnatal collagen structure remodelling: the changes in local $H_A(h)$ are much larger than the changes in global H_{Ag}. The increase in global H_{Ag} that we find in this study ($\approx$ 45 %) is small compared with measured increases of 180 % and more in literature [57, 167, 349]. In our simulations, collagen network remodelling alone does not suffice to increase H_{Ag} by 180 %, and other developmental changes, such as changes in fixed charge density or fluid fraction, may contribute more to the global stiffness than collagen network remodelling does.

The current study is unable to show a mechanical role for the variable anisotropy pattern in the top of the tissue for 0 weeks (figure 7.6). We note that anisotropy and its depth-dependent variation increase between birth and maturity (figure 7.2b). In addition, the variable anisotropy pattern for 72 weeks appears to smooth gradients in the mechanical state of the top of the tissue at zero global strain, particularly swelling strains (figure 7.6a).

Acknowledgements

The authors kindly thank Dr. Wouter Wilson and Dr. René van Donkelaar at the Materials Technology group of the Faculty of Biomedical Engineering of Eindhoven University of Technology for the use of, and support with, the FRPVS model.

What is reported is different to what is remembered which is different to what was seen which is different to what was present.

Charles G.M. Paxton [267]

8 General discussion

8.1 Overview of postnatal collagen network development

We presented experimental results on articular cartilage (AC) in horses (stillborn, foal and adult, 13 animals, chapter 3) and sheep (stillborn to adult, 10 ages, 48 animals, chapters 4 and 6). The polarised light microscopy results are similar between the two species: stillborn animals have a transversely isotropic collagen network with fibrils parallel to the articular surface throughout the tissue depth and adults animals have the arcade-like collagen fibril structure as seen in other species (figures 3.4, 3.6 and 4.5). The transitional pattern that is present in the horse of 4.5 months (figure 3.5), was also found in the data for the sheep (figure 4.5). We examined a nearly congruent joint in both species (figures 3.1, 4.1 and 6.1) and found only small differences in the temporal and spatial patterns of collagen network development between different anatomical sites (e.g. figures 4.A.3 and 4.A.4), and no differences at maturity. In chapters 5 and 7 we therefore pooled the sheep data for different anatomical sites, and we follow a similar approach to present an overview of postnatal development of the collagen fibril network in figure 8.1.

We assessed three parameters of the collagen network as a function of depth: predominant collagen fibril orientation (figure 8.1a, chapter 4), collagen densities (figure 8.1b, chapter 6) and collagen network anisotropy (figure 8.1c, chapters 2 and 7). In figure 8.1, the data from figures 7.1a, 7.1b and 7.2b are used to show an overview of age- and depth-dependent collagen network development in three separate panels. Figure 8.2 collects the three parameters in a single overview. We measured AC thickness in chapter 4 and we use the fit for cartilage thickness as a function of age (equation 4.5) for the

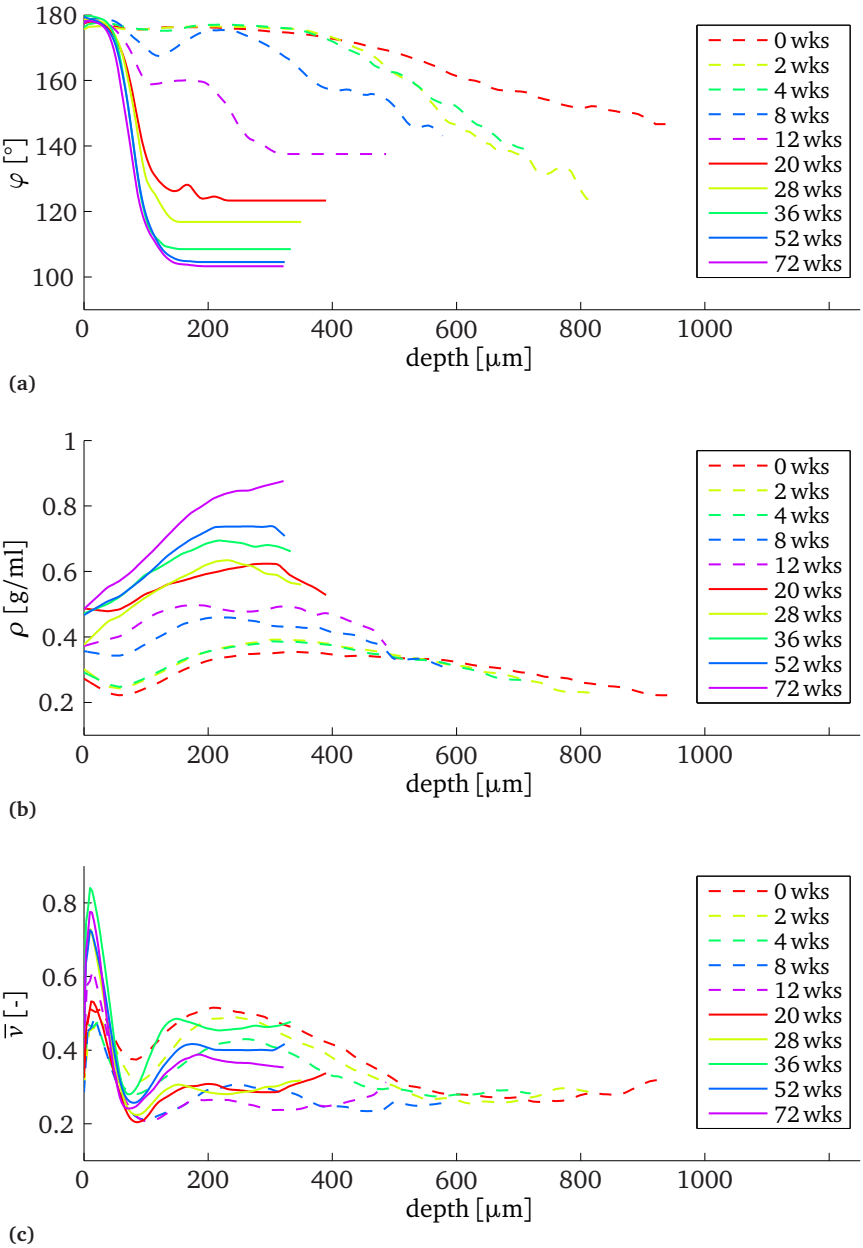

Figure 8.1: Overview of age- and depth-dependent collagen network development for the sheep in this thesis. With **(a)** predominant collagen fibril orientation, adopted from figure 7.1a; **(b)** collagen densities, adopted from figure 7.1b; and **(c)** anisotropy parameter $\overline{\nu}$, adopted from figure 7.2b.

overviews of the results, similar to e.g. figure 4.5.

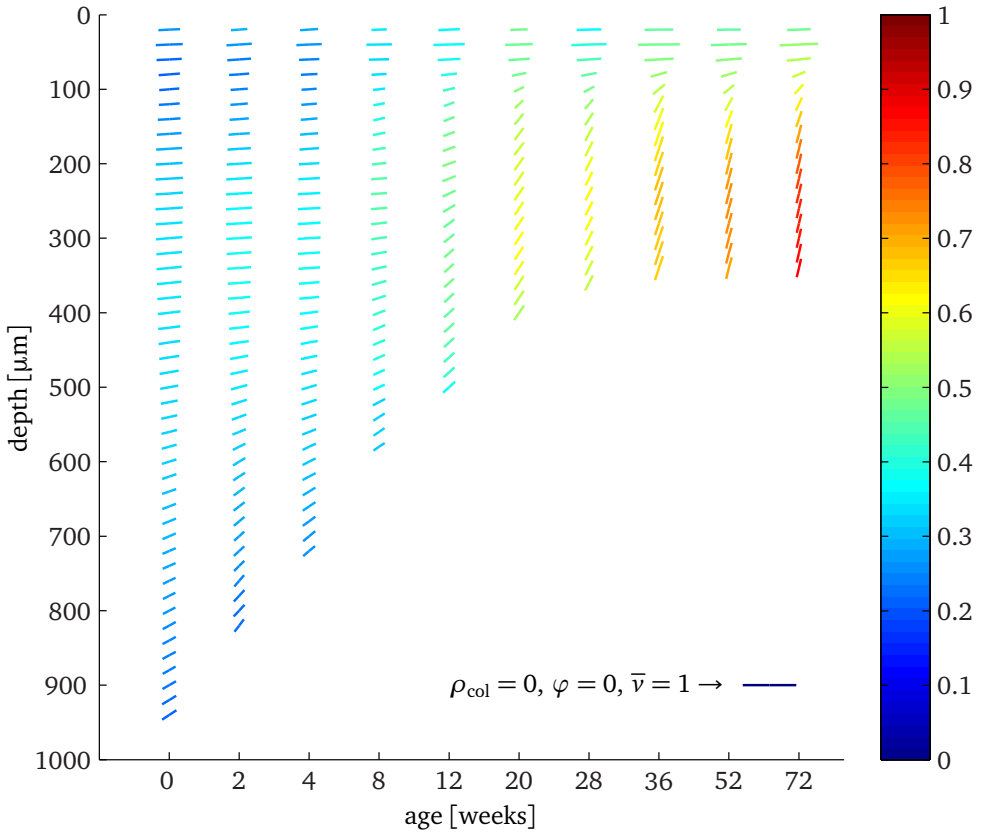

Figure 8.2: Single overview of age- and depth-dependent collagen network development for the sheep in this thesis. The orientation of the dashes represents the predominant collagen fibril orientation, the length of the dashes scales with the fraction of collagen in the predominant network, i.e. with anisotropy $\overline{\nu}$, and the colour of the dashes represents the collagen densities in g/ml. A reference dash for $\overline{\nu} = 1$ is presented in the bottom part of the figure. Note the non-linear scale on the x-axis.

Our results are in line with existing literature, where available. During postnatal AC development, tissue layer thickness decreases [57, 112, 154, 168, 282], collagen densities increase [50, 84, 167, 282, 348] and they increase most in the deep tissue [282], and predominant collagen fibril orientation develops from a structure with fibrils parallel to the articular surface throughout the tissue depth to an arcade-like structure at maturity [6, 168, 282]. Our temporal resolution in the sheep experiments is better than in existing literature on postnatal collagen fibril orientation [168, 282]. Hence we cannot yet compare our intermediate patterns between birth and maturity with previous research.

The small site-dependent differences in the pre-mature collagen network parameters that we observed over a single joint surface, are also hard to compare to existing literature. We explained the lack of differences in collagen structure in mature animals by the near congruency of the joint that we investigated. Investigations into the AC from the proximal phalangeal bone of the equine metacarpophalangeal joint (the cartilage surface that opposes the surface that we investigated in chapter 3) [54, 158], also show site-dependent differences in collagen structure in juvenile horses. Whether or not these differences persist in this similar joint in adult life is not evident from these publications [54, 158, 345].

Several papers on collagen network anisotropy [54, 158, 168, 282, 283, 290] use a parallelism index (PI) introduced by Rieppo et al. [283]. We cannot reproduce PI because it is calculated with microscope-specific parameters that cannot be obtained for our system [283, chapter 2]. We introduced our own microscope-independent measure of anisotropy $\overline{\nu}$ in chapter 2. Both parameters scale between 0 (isotropy) to 1 (maximum anisotropy), and we can qualitatively compare the $\overline{\nu}$-patterns in our study with the PI-patterns in other literature.

Our patterns for $\overline{\nu}$ show a sinusoidal-like variation in the upper half of the tissue, and an almost constant value in the bottom half of the tissue for the older ages (figure 8.1c). This is similar to results for PI for juvenile equine AC by Brama et al. [54]. The patterns for PI by Rieppo et al. [282] for juvenile and adult porcine AC, the patterns by Hyttinen et al. [158] for newborn to adult equine AC, and the patterns by Julkunen et al. [168] for juvenile to adult rabbit AC do not show the sinusoidal-like variation. These patterns for PI [158, 168, 282] generally show a valley near the articular surface instead, and a relatively constant value in the deep cartilage. The spatial resolution of these studies [158, 168, 282] was presumably too low for detection of the sinusoidal-like variation near the articular surface. All studies on the postnatal development of collagen network anisotropy [158, 168, 282, chapter 7] share that anisotropy in the deep tissue is variable in postnatal life, without a clear pattern.

8.2 A contribution to depth-dependent mechanical behaviour

The postnatal development of the collagen network contributes to the gradient in mechanical properties (increasing local effective aggregate modulus $H_A(h)$ with increasing distance from the articular surface) in AC (chapters 5 and 7). We present an overview of the contribution of postnatal collagen network remodelling to $H_A(h)$ at zero global strain ($\varepsilon = 0$) in figure 8.3. We used the simulations in chapter 7 (i.e. with age- and depth-dependent predominant collagen orientation, collagen densities and collagen network anisotropy) to obtain the results for figure 8.3.

In chapters 5 and 7 we kept all compositional parameters constant between the simulations, except for the collagen network parameters. We did this for two reasons: (1) we aimed to separate the contribution of postnatal collagen network remodelling from other developmental changes, and (2) the data that is needed for a complete simulation

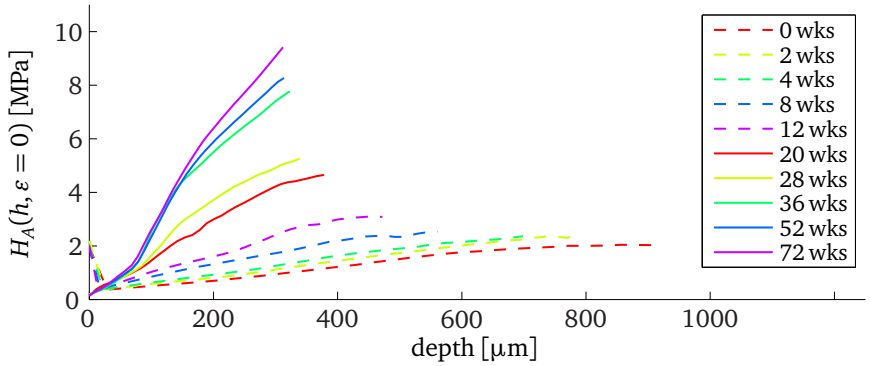

Figure 8.3: Overview of age- and depth-dependent effective aggregate modulus $H_A(h)$ at zero global strain $\varepsilon = 0$, t_0 in our simulations. These results are calculated with ten meshes that were equal except for the collagen network. The collagen network for each age was modelled with the input from figure 8.1, see also chapter 7.

of postnatal AC development is missing. Ideally, we would also measure the changes in (depth-dependent) fluid content, proteoglycan (PG) content and fixed charge densities (FCD) and use these in our simulations. However, these additional measurements were not feasible for the current thesis and this constraint should be kept in mind when interpreting the results.

Other developmental changes in AC may e.g. include an increase in total extracellular matrix (ECM) density (or decrease in fluid volume/total volume fraction) [50] and changes in relative PG content. Note that contrary to the general increase in collagen content that is observed across species and joints, changes in PG are harder to predict: e.g. Brama et al. [50] report a decrease in PG content for the equine metacarpus during postnatal development, but Williamson et al. [349] were unable to show changes in PG content in bovine knee AC. PG content might vary considerably (and would be therefore hard to predict) because PG synthesis by chondrocytes *in situ* responds much more than the collagen network to mechanical joint loads [50, 104, 146, 191, 345], although also on this point, results may vary [159]. The FCD is commonly expressed as the amount of fixed charges per volume of free interstitial fluid, i.e. Meq/ml [357]. The postnatal development of the amount of fixed charges per total volume of ECM is hard to predict due the uncertainties for the development of PG content. However, for small changes of the amount of fixed charges per total volume we may expect an increase in FCD [Meq/ml] due to the decrease in total free interstitial fluid, and because an increase in collagen content further decreases the effective free fluid fraction in AC.

Collagen network remodelling is therefore not the only option for an animal to obtain a gradient in mechanical properties in AC. The profiles for fluid density and FCD also contribute to the depth-dependent mechanical properties, and postnatal changes in these parameters will therefore affect the development of the gradient in mechanical properties in AC. Simulations similar to those in chapter 7 illustrate this (figure 8.4). Compared to a simulation with constant composition over the depth (at the mean of

	n_f [v/v]	c_F [Meq/ml]	φ [°]	n_{coll} [m_s/m_s]	$\overline{\nu}$ [-]
cst	0.8	0.12	0	0.72	0.46
nf	$0.9-0.2z$	0.12	0	0.72	0.46
c_F	0.8	$-0.1z^2+0.24z+0.035$	0	0.72	0.46
φ	0.8	0.12	ch. 7, 72 wk	0.72	0.46
ρ	0.8	0.12	0	ch. 7, 72 wk	0.46
$\overline{\nu}$	0.8	0.12	0	0.72	$0.3(1+z)$

(a)

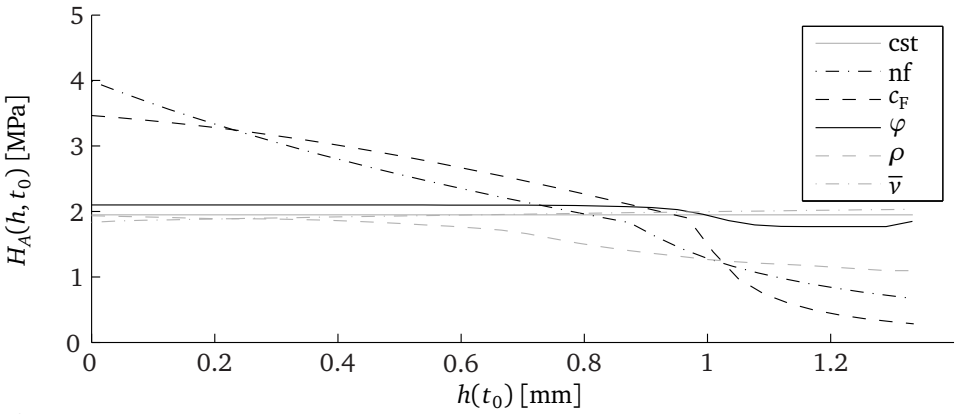

(b)

Figure 8.4: Six simulations to illustrate the effects of a depth-dependent composition and structure on the depth-dependent effective aggregate modulus $H_A(h,t_0)$ at zero global strain $(t_0, \varepsilon = 0)$. With **(a)** model input with z the dimensionless depth. Columns show the input for the simulations for n_f – initial fluid volume fraction, c_F – initial fixed charge density, φ – predominant fibril orientation, n_{coll} – collagen solid mass fraction, and $\overline{\nu}$ – anisotropy parameter. Rows show the six simulations: cst – all input constant, nf – depth-dependent fluid volume fraction, FCD – depth-dependent fixed charge density, φ – depth-dependent predominant fibril orientation, ρ – depth-dependent collagen solid mass fraction, and $\overline{\nu}$ – depth-dependent anisotropy; and **(b)** model results for $H_A(h)$ for these six simulations with different depth-dependent composition and structure.

the depth-dependent profiles) and a horizontal collagen fibril arrangement, implementation of the depth-dependent fluid density profile or FCD profile produces the largest gradients in $H_A(h)$. The changes in predominant fibril orientation, collagen density and network anisotropy also affect the gradient in mechanical properties, but to a lesser degree in this theoretical example. These simulations stress that it is essential to assess more than just collagen network development to provide a more substantial description of the development of the mechanical properties in AC.

We finally note that there may be another way than thus far described in this thesis in which collagen network remodelling affects AC mechanics. When the mechanical properties of the collagen fibril network change, the contribution of this network to the mechanical properties of AC will change. Collagen fibril diameter is reported to increase during postnatal development [84, 107, figure 3.3], and a change in mechanical properties is therefore not unlikely. A numerical-experimental approach that uses a combination of experimental results from mechanical testing with parameter estimation with dedicated finite element models may provide insight into the mechanical properties of the collagen network during development. Again, such an approach can only succeed when the other compositional parameters have also been measurement and incorporated into the simulations.

8.3 Mechanical interactions in collagen network development

8.3.1 Collagen orientation and osmotic pressures

In chapter 5 we observed that the effect of postnatal collagen reorientation on the depth-dependent mechanical properties is affected by local osmotic pressures. This observation is confirmed in the theoretical example in the previous section (figure 8.4): equal collagen fibril orientations with equal osmotic pressures in the deep cartilage, result in equal values for $H_A(h)$ (black solid curve in figure 8.4). This theoretical example further showed that without a gradient in osmotic pressures (fluid volume fraction and fixed charge density constant), only small effects of collagen network remodelling can be expected. Or alternatively, a gradient in osmotic pressures is necessary for our interpretation of the effects of variations in the collagen network at birth.

Experiments have shown that depth-dependent mechanical properties are present in perinatal animals [193, 343, 349], albeit to a much lesser degree than in adult animals. The current work showed that the perinatal collagen network is not responsible for the perinatal depth-dependent mechanical properties in AC. Figure 8.4 illustrates how depth-dependent variations in fluid volume fraction and fixed charge density may affect the gradient in mechanical properties. The increase in $H_A(h)$ is correlated to an increase in osmotic pressures for both compositional changes (not shown). Sweet et al. [314] showed that a depth-dependent fluid volume fraction (fluid fraction highest in the superficial zone, similar to our simulations) exists in immature bovine AC, and Klein et al. [193] showed that PG content increases with depth for foetal and newborn bovine cartilage.

The depth-dependent mechanical properties in perinatal AC [193, 343, 349], and the depth-dependent fluid volume fraction [314] and PG content [193] in immature AC strongly suggest that the gradient in osmotic pressures that is necessary for our interpretation of the effects of variations in the collagen network at birth, is indeed present in perinatal animals.

8.3.2 Collagen orientation and density

The gradient in mechanical properties increases due to postnatal collagen fibril reorientation (chapter 5), and increases due to collagen density increase (chapter 7). We also find that these two effects interact and together result in a gradient that is larger than the sum of the gradients of the two separate effects (figure 7.4d). The effects of the two mechanisms (collagen fibril reorientation and collagen density increase), and the interaction, depend on the local composition and structure of the tissue (chapter 7, figure 8.4).

The effect of postnatal collagen reorientation appears unambiguous in the presence of osmotic pressures: vertical fibrils limit swelling strain and increase osmotic pressures and effective stiffness (chapter 5, figure 8.4). The effects of an increase in collagen densities however, are less straightforward. As explained in chapter 5, there is a balance between osmotic pressures and swelling strains in AC. Limiting swelling strains tends to increase osmotic pressures, and increased osmotic pressures tend to increase swelling strain, until a balance is achieved. Adding collagen to this (vertical) structure will shift the balance between swelling strains and osmotic pressures for two reasons: a vertical structure with more collagen will have a larger tendency to limit swelling, and an increase in collagen density has a tendency to increase osmotic pressures. Chapter 7 showed that the balance shifts to smaller swelling strains and larger osmotic pressures, and therefore higher effective stiffness, during postnatal development.

In our theoretical example in the previous section, increase in collagen content in the deep tissue has no appreciable effect on effective tissue stiffness (figure 8.4, 'cst' and 'ρ'). In fact, the balance between swelling strains and osmotic pressures shifts to slightly larger swelling strains ($4.51 \cdot 10^{-2}$ against $4.43 \cdot 10^{-2}$ at the bottom of the mesh) and slightly smaller osmotic pressures (75 kPa against 84 kPa) when we add collagen to the deep zone cartilage with horizontal predominant fibril orientation. The partitioning of the intra- and extra-fibrillar fluid is not only affected by collagen densities, but also by the local osmotic pressure [234]. This theoretical example illustrates that the complex interaction between the fixed charges in the ECM, local deformations and the partitioning of intra- and extra-fibrillar fluid are hard to predict for a collagen network with predominantly horizontal collagen fibrils.

Thus, collagen reorientation contributes more than increase in collagen density to the establishment of functional depth-dependent mechanical properties through collagen network remodelling (in the presence of an osmotic pressure gradient over the depth of the tissue, see previous section). The theoretical example suggests that the increase in collagen densities needs vertical collagen fibrils to contribute to the depth-dependent mechanical properties. Although the depth-dependent increase in collagen densities reinforce the functional depth-dependent adaptation in our simulations, the increase in collagen density may also serve a different functional role.

8.3.3 Spatial and temporal patterns

In chapter 5 we suggested a relationship between the increase in collagen fibril strains due to collagen reorientation and the increase in collagen density. The rationale behind

this suggestion is that of a maximisation of the efficiacy of the production and maintenance of biological tissue components. In biology, resources are scarce and best spent well. It would be wasteful to recruit collagen fibrils at a locations where fibrils are not yet used to their full potential, certainly when elsewhere fibrils are used beyond their potential. This is served well, if equal strains occur in the tissue.

The paper by Rieppo et al. [282] and chapters 6 and 7 provided evidence for the idea that collagen densities increase most where collagen fibril strains are highest. With $\overline{\nu}$, we can calculate both fibril strains and collagen densities separately for the two networks (predominant and isotropic) and look at the development of these parameters with age (figure 8.5). Simulations with collagen network developmental changes and a fixed collagen density at the age of 0 weeks show a small decrease for fibril strains in the isotropic network, and a small increase in fibril strains in the predominant network (figures 8.5a, 8.5c and 8.5e). When we also implement the age-dependent collagen densities, we see that fibril strains in the isotropic network decrease more, and the increase in fibril strains for the predominant network is limited: i.e. the difference between fibril strains in the two networks in the adult animals is much smaller when we implement the age-dependent collagen densities.

The temporal patterns for collagen densities for the two networks (figures 8.5b, 8.5d and 8.5f) correlate negatively with fibril strains in the two networks for the sequence with constant collagen density. At birth, fibril strain in the isotropic network is much larger than in the predominant network, and in early postnatal life more collagen is added to the isotropic network than to the predominant network. For the top layer we observe that the velocity of collagen density change in the predominant network (figure 8.5b) increases around 36 weeks of age, approximately when the fibril strains in this network start to increase to the maximum value thus far (figure 8.5a). In the middle layer, fibril strains are initially small in the predominant network, and they start to increase between 8 weeks and 20 weeks (figure 8.5c). This correlates with the collagen density increase in the predominant network: it is relatively constant in early life, and starts to increase between 12 weeks and 20 weeks (figure 8.5d). In the deep layer, fibril strains are transferred most from the isotropic network to the predominant network due to collagen fibril reorientation. This layer has the largest fibril strains in the predominant network (figure 8.5e) and the largest increase in collagen density for this network (figure 8.5f). The fibril strains are already relatively high for 0 weeks ($\approx 5\,\%$,), and this corresponds to highest rate of collagen density increase in early life between these three layers. Thus, in our simulations, a maximum fibril strain of $\approx 5\,\%$ in both networks (figures 8.5a, 8.5c and 8.5e) appears to be the result of selective increase in collagen densities for these networks. In these observations, we find further support for a relationship between the increase in collagen fibrils strains due to collagen reorientation and the increase in collagen density.

8.3.4 Anisotropy

Polarised light microscopy on adult AC generally shows a retardance valley near the articular surface. This valley is traditionally associated with the transitional layer, a layer with a weak anisotropic collagen arrangement, in adult animals [37, 150]. The weak

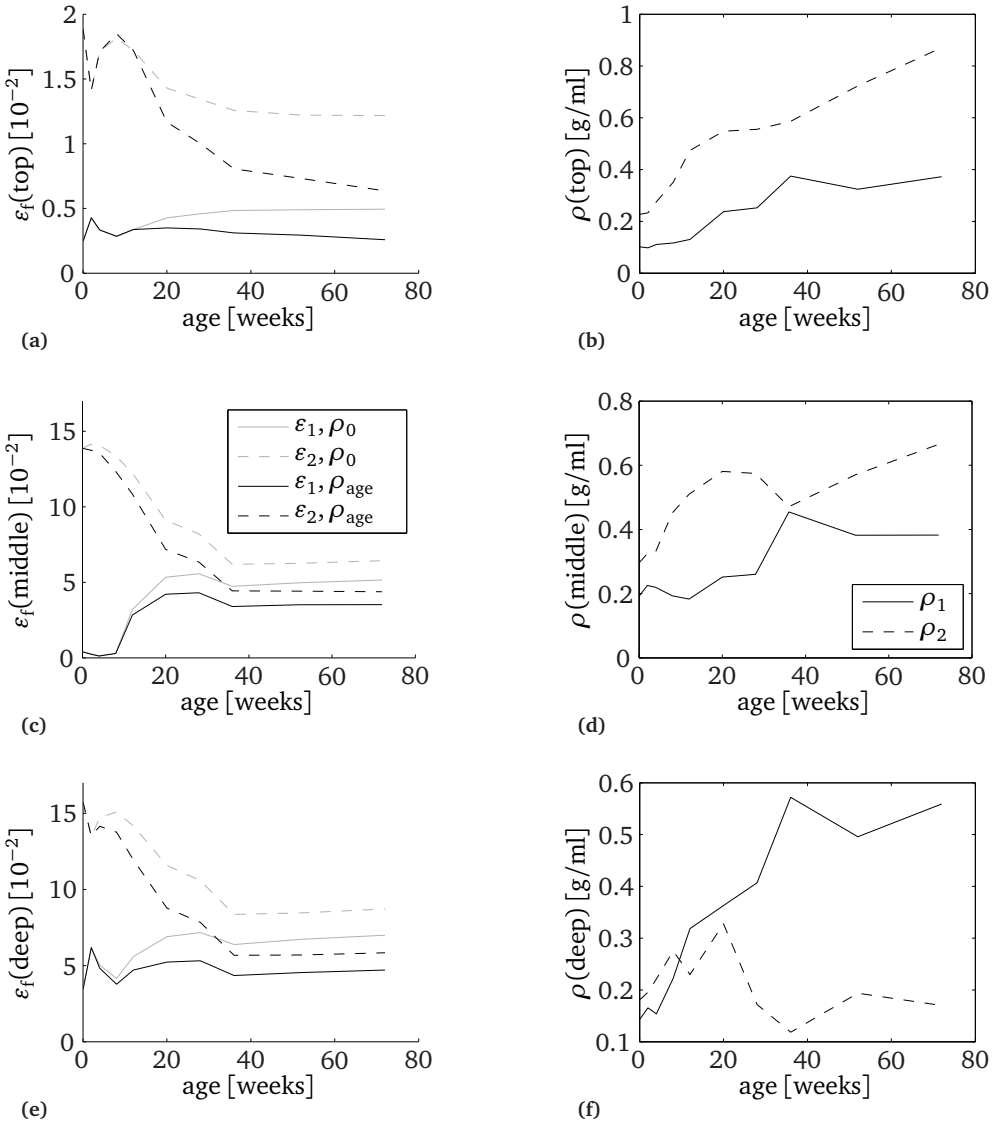

Figure 8.5: Total network fibril strains at zero global strain (ε_f, left panels) and network collagen density (ρ, right panels) for the predominant network (ε_1, ρ_1, solid) and secondary network (ε_2, ρ_2, dashed) as function of age for the three layers top – **(a)** and **(b)**, middle – **(c)** and **(d)**, and deep - **(e)** and **(f)**. Panels **(a)**, **(c)** and **(e)** show total fibril strains for a sequence of simulations with collagen fibril orientation and predicted collagen network anisotropy from measurements as a function of age, and with the collagen density profile of 0 weeks for each simulation (ρ_0, grey) and for a sequence of simulations with all collagen network parameters per age (ρ_{age}, black). Relative collagen densities for panels **(b)**, **(d)** and **(f)** are calculated with $\overline{\nu}$: $\rho_1 = \overline{\nu}\rho_{col}$, and $\rho_2 = (1-\overline{\nu})\rho_{col}$. Curves are labelled in the middle panels.

anisotropic collagen arrangement in this layer is supposedly caused by changes in collagen fibril orientation, i.e. the bending of the arcs in the adult Benninghoff structure (chapter 2). In chapters 3 and 4, we showed that perinatal animals also exhibit a retardance valley near the articular surface, but this valley cannot be correlated to changes in predominant collagen fibril orientation in these perinatal animals. The distance between this valley and the articular surface is relatively constant throughout postnatal life (e.g. figure 4.8c).

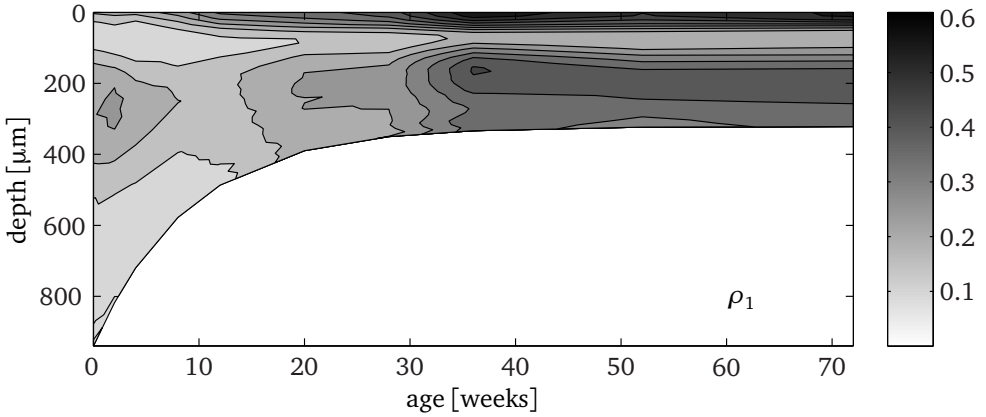

(a)

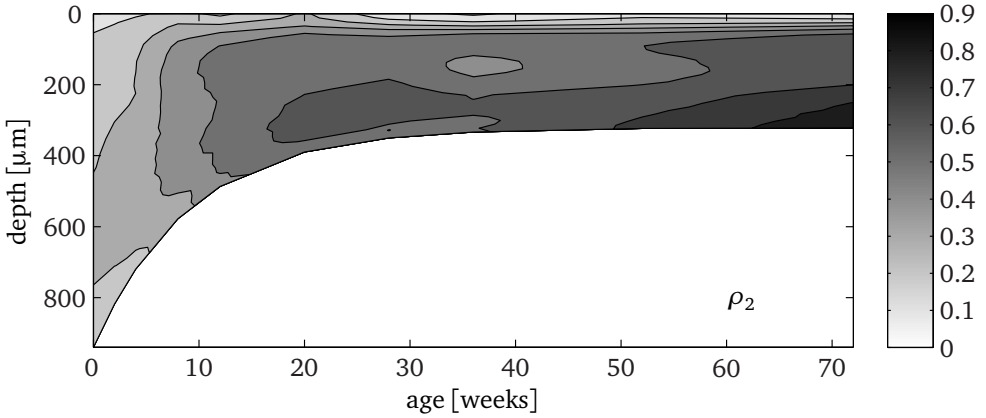

(b)

Figure 8.6: Contour plots of predicted collagen densities [g/ml] as function of age and depth for **(a)** – the predominant collagen network: $\rho_1 = \overline{v}\rho_{\text{col}}$, and **(b)** – the isotropic collagen network: $\rho_2 = (1 - \overline{v})\rho_{\text{col}}$. Note that $\overline{v}$ is scaled with an arbitrary constant and that this figure therefore illustrates spatial and temporal patterns. It does not show an exact quantitative description of the amounts of collagen in the two (theoretical) networks.

Our results for $\overline{\nu}$ (figure 8.1c) indicate that despite the constant predominant collagen fibril orientation in the top of the tissue (figure 8.1a), the transitional layer in perinatal animals has a relatively weak anisotropic collagen arrangement. Figure 8.1c shows that the level of anisotropy in this layer is highest at birth. Collagen densities also showed a valley near the articular surface for the youngest animals (figure 8.1b). This valley disappears in postnatal life, i.e. the increase in collagen densities exhibits a peak at the position of the transitional layer. The anisotropy of the transitional layer decreases between birth and maturity (figure 8.1c). This means that the collagen that is added in this layer, is mostly used to reinforce the isotropic network, and less to reinforce the predominant network. Figure 8.6 illustrates this: there is a distinct transitional layer near the articular surface where collagen densities increase in the isotropic collagen network (figure 8.6b), but not in the predominant network (figure 8.6a).

The simulations in chapter 7 suggested that the relatively weak anisotropy in the transitional layer in adult animals: it aids in decreasing gradients in the mechanical state of the upper half of the tissue. Krishnan et al. [203] noted that the depth-dependent composition and structure of AC do not result in a homogeneous mechanical state in the tissue. Similar to our results (chapters 5 and 7), Krishnan et al. [203] instead find that the main function of the depth-dependent composition and structure is to provide depth-dependent mechanical behaviour. Of course, this primary function (depth-dependent mechanical behaviour) of the depth-dependent composition and structure does not exclude functional adaptations that avoid sharp gradients to occur in the mechanical state of the tissue.

8.4 Modelling parameters and the superficial and transitional layers

Our observations on the role of the weak anisotropy in the transitional layers concerns 1-D swelling only: we did not investigate transient or 2-D behaviour. The work in this thesis is also unable to show a functional mechanical role for this transitional layer in perinatal animals. Nor is it clear why the depth of this transitional layer appears relatively constant in postnatal life. Our model choices for the geometry and loading protocol, and the focus on the equilibrium response, are the most likely reasons for not finding a obvious mechanical role for the transitional layer and its occurrence at a particular depth.

We choose the confined compression geometry and equilibrium response for three reasons: (1) it is the geometry and response for which it has been shown that the model that we use can capture the depth-dependent material properties [357]; (2) it is the preferred geometry and response for experiments that are explicitly meant to assess the depth-dependent mechanical properties in cartilage [79, 193, 293, 349]. Experiments with the unconfined compression geometry are generally used to investigate (*in situ*) chondrocyte deformation, e.g. [69, 75, 80, 103, 359]; and (3) the unconfined compression geometry poses challenges: there will be edge effects, see e.g. [80, figure 1], that should be dealt with in the analysis and interpretation, and the deformations will become

a function of both vertical and horizontal position. Since we wished specifically to investigate the (1-D) depth-dependent material properties, this also hinders a straight forward analysis of the results. We performed simulations with a 2-D unconfined compression geometry for chapter 5 and used the symmetry axis for the analysis. Similar to Julkunen et al. [170] who investigated the influence of composition and structure on the mechanical response of articular cartilage under different loading geometries, we observe only small differences between confined and unconfined compression (not shown). The phenomena and mechanisms that we describe remain valid: e.g. the depth-dependent increase of fibril strains, increase in osmotic pressures, increase in $H_A(h)$, decrease in swelling strains, etc. This 2-D analysis would not alter our conclusions and we feel that the confined compression geometry is the most suitable geometry for the investigations in this thesis.

The 1-D confined compression geometry and equilibrium response however, are not very suitable for investigations into the mechanical role of the local collagen network itself in the transitional and superficial layer. For instance, we hypothesised that orientation of deep fibrils changes due to swelling strains (chapter 5), but we did not provide an explanation for the absence of collagen fibril reorientation in the superficial layer. The collagen fibrils in the superficial zone are predominantly oriented parallel to the articular surface and therefore contribute little to the mechanical outcome in our 1-D simulations (chapters 5 and 7). To investigate the mechanical function of these fibrils and the functional significance of their predominant orientation, transverse strains must be allowed. Likewise, AC has a function in the temporal distribution of (instantaneous) mechanical loads, and the transient mechanical state (and its frequency and duration) should be considered for investigations into the local role of the collagen fibril network.

Our simulations indicated that the deep tissue swells for a large range of physiological strains (chapters 5 and 7). That swelling state remains in the transients between the equilibria in our simulations, and remains also in our 2-D simulations (both not shown). Therefore our hypothesis on the reason for collagen reorientation appears unaffected by the 1-D and equilibrium limitations in this thesis, and these choices mostly affected interpretation of the local role of the collagen network in the upper half tissue. Principle tensile strains are a good predictor for collagen fibril orientation in a range of tissues [14, 96, 97], including articular cartilage [17, 355]. The tensile strains for the superficial layer will be in the lateral direction when AC is subjected to compression, and this may suffice to explain the predominant collagen fibril orientation in this layer. We further note that, depending on the curvature and height of the tissue layer, swelling of AC in 2-D may actually result in transverse strains at the articular surface. We estimated that collagen densities increase in the predominant collagen network in the superficial zone (figure 8.6), and this suggests that the predominant collagen fibrils have a functional role that becomes more important in postnatal life. Finally, inclusion of transient behaviour may elucidate a role for fluid pressurisation and transport for the depth-dependent mechanical state in the tissue, and thus for the mechanical function of the local collagen network in the upper half of the tissue.

8.5 Postnatal development of articular cartilage

8.5.1 A role for chondrocytes

The depth-dependent composition and structure of the ECM are developed and maintained by the chondrocytes. Our knowledge on what signals the chondrocytes to produce a depth-dependent ECM composition and structure is still limited. What we do know, is that the mechanical environment of the chondrocyte has an important role in this cell's functioning, e.g. [113, 126, 143, 182, 220, 222, 306, 315, 343, 359]. The mechanical environment of adult chondrocytes e.g. correlates with local chondrocyte biosynthesis, particularly with proteoglycan synthesis [23, 63, 222, 359], and experiments with cartilage explants and tissue-engineered cartilage have shown correlations between chondrocyte biosynthesis and the external mechanical loading regime [2, 45, 81, 129, 129, 278].

Transients in the mechanical state of the tissue comprise most of the physiological loading regime of AC, and are important for AC maintenance [62, 64, 75, 143]. Two mechanical parameters that are associated with transient behaviour and that affect chondrocyte biosynthesis are intermittent fluid pressures and fluid-induced shear stresses [64, 164, 229, 306–308]. These two parameters (intermittent hydrostatic pressure and shear stress) also have a role in regulating processes near the cartilage-bone junction [33, 70, 71, 141, 275], i.e. they affect the advancement of the secondary ossification front, and thus cartilage thickness.

With advances in our knowledge on the postnatal composition and structure of AC, we will be better able to estimate the local mechanical state of chondrocytes during development. We may then investigate correlations between the changes in composition and structure that occur in postnatal development of AC and the postnatal changes in mechanical environment of the chondrocytes. Multilevel finite element models are used to investigate the mechanical state of (adult) chondrocytes themselves in the tissue, e.g. [132, 172, 197, 198]. Observed changes in postnatal depth-dependent mechanical behaviour can be implemented into such multilevel models to further elucidate the postnatal *in situ* mechanical state of the chondrocytes themselves.

8.5.2 Age matters

As Hyttinen et al. [159] remarked in relation to articular cartilage: age matters. Mature AC has lost most of its neonatal remodelling capacity [94, 182, 220, 243]. The remodelling capacity of the collagen network is particularly limited in adult life [25, 31, 49, 106, 159, 159, 252, 289, 326, 340]. Deviations from the optimal collagen structure that are present in early adulthood, will persist during the remaining life time. The postnatal remodelling of AC is therefore an important process, of which especially postnatal collagen network remodelling needs to succeed succeed before adulthood. Therefore, investigations into mechanisms that drive postnatal collagen network remodelling are certainly warranted.

Experiments have already shown that age also matters for the mechanical behaviour in AC [57, 193, 343, 349]. The work in the current thesis stresses that age also matters for investigations of composition-structure-function relationships in young AC [167, 193,

349]. We showed e.g. that the developing predominant collagen fibril orientations may have profound effects on the global mechanical behaviour of AC, and that knowledge on the depth-dependent predominant collagen fibril orientation of the samples of interest is thus necessary to investigate structure-function relationships. Correct interpretation of structure-function relationships in young AC will be hindered when such knowledge is absent [193, 349] or spatially not well resolved [167].

We finally call for caution when general (adult) mechanical mechanisms for AC are validated with immature cartilage, e.g. [67]. The postnatal changes in composition and structure of AC are substantial, and mechanical mechanisms and processes in young AC may not be representative for adult life.

8.5.3 A role for animal models and healthy articular cartilage

The original motive to undertake the study presented in this thesis, is the large prevalence of developmental orthopaedic diseases (such as osteochondrosis) in horses. To deepen our knowledge of pathologies in postnatal AC development, it is useful to know how postnatal AC development proceeds in normal healthy individuals. Well-specified postnatal equine AC proved difficult to obtain, and therefore we chose to work with a (different) animal model. We chose the sheep in a trade-off between availability, growth rate and size.

Animal models have played an important role for the research into postnatal AC development. The effects of joint immobilisation [131, 189, 338, 339] and forced exercise [11, 13, 28, 54, 134, 190, 207, 344, 345] e.g. have been investigated almost exclusively in larger mammals such as dogs and horses. With these larger animals, the amount of AC that can be used is an advantage, for instance for mechanical testing or spatial analysis. Advances in genetics and cell biology over the past decades have made rats and especially mice a very attractive animal model.

Mice with a mutation that disturbs the development of collagen fibrils in articular cartilage [209, 253], for example may further elucidate the role of the collagen fibril network in AC in general, and its role in postnatal AC development in particular. Mice that e.g. lack skeletal muscle activity [122] can be helpful for the assessment of the relevance of *in utero* joint loading for the perinatal AC composition and structure. Composition-structure-function relationships in AC in which osmosis is impaired, would be very interesting in the light of the results in this thesis.

Because of scaling effects, the results found in the small animal models cannot be directly translated to the larger animals, and vice versa. The challenge we face now, is to merge the knowledge and advantages from the larger animal model species, with the knowledge and (molecular) advantages of the smaller model species. With better knowledge on normal healthy AC development and the contributions of the various relevant processes that play a role, it will become easier to investigate and interpret complex AC pathologies.

8.5.4 Concluding remarks

We have a bright and exciting future ahead of us for the research into postnatal development of AC. Further investigations into the spatial and temporal development of AC composition (e.g. PG content, fluid content, FCD) will increase our ability to assess composition-structure-function relationships in developing AC, and to assess the development of functional depth-dependent mechanical properties in AC. Experiments with, and (multilevel) finite elements of, immature AC can increase our knowledge on the local mechanical environment of chondrocytes during development. Knowledge on the postnatal development of the chondrocyte's mechanical environment can be compared with the spatial and temporal development of AC composition and structure in order to elucidate correlations between mechanical parameters and ECM production. Further investigations with animal models may prove very helpful for our knowledge on composition-structure-function relationships in postnatal AC development.

In this thesis, we presented the first solid observation of a transitional layer in perinatal animals. We further noticed that the distance from the articular surface to this transitional layer is one of the few parameters that is similar in perinatal and adult animals. In our opinion, one of the exciting challenges for future research into postnatal AC development is to elucidate the functional role of this transitional layer, and the relevance of its position relative to the articular surface.

References

[1] Wilbert Aarnoudse, Petra van den Berg, Frans van de Vosse, Maartje Geven, Marcel Rutten, Mark van Turnhout, William Fearon, Bernard de Bruyne and Nico Pijls. Myocardial resistance assessed by guidewire-based pressure-temperature measurement: *in vitro* validation. *Catheterization and Cardiovascular Interventions*, **62**(1):56–63, May 2004. doi: 10.1002/ccd.10793.

[2] B. Ackermann and J. Steinmeyer. Collagen biosynthesis of mechanically loaded articular cartilage explants. *Osteoarthritis & Cartilage*, **13**(10):906–914, October 2005. doi: 10.1016/j.joca.2005.06.001.

[3] Dany Spencer Adams, Ray Keller and M.A.R. Koehl. The mechanics of notochord elongation, straightening and stiffening in the embryo of *Xenopus laevis*. *Development*, **110**(1):115–130, September 1990.

[4] H.A. Alhadlaq, Y. Xia, J.B. Moody and J.R. Matyas. Detecting structural changes in early experimental osteoarthritis of tibial cartilage by microscopic magnetic resonance imaging and polarised light microscopy. *Annals of the Rheumatic Diseases*, **63**(6):709–717, June 2004. doi: 10.1136/ard.2003.011783.

[5] R.C. Appleyard, D. Burkhardt, P. Ghosh, R. Read, M. Cake, M.V. Swain and G.A.C. Murrell. Topographical analysis of the structural, biochemical and dynamic biomechanical properties of cartilage in an ovine model of osteoarthritis. *Osteoarthritis & Cartilage*, **11**(1):65–77, January 2003. doi: 10.1053/joca.2002.0867.

[6] Charles W. Archer, Gary P. Dowthwaite and Philippa Francis-West. Development of synovial joints. *Birth Defects Research Part C: Embryo Today: Reviews*, **69**(2):144–155, May 2003. doi: 10.1002/bdrc.10015.

[7] Charles W. Archer, Jenny McDowell, Michael T. Bayliss, Myra D. Stephens and George Bentley. Phenotypic modulation in sub-populations of human articular chondrocytes *in vitro*. *Journal of Cell Science*, **97 (Pt 2)**:361–371, October 1990.

[8] Charles W. Archer, E. Heather Morrison, Michael T. Bayliss and Mark W.J. Ferguson. The development of articular cartilage: II. The spatial and temporal patterns of glycosaminoglycans and small leucine-rich proteoglycans. *Journal of Anatomy*, **189 (Pt 1)**:23–35, August 1996.

[9] Charles W. Archer, Heather Morrison and Andrew A. Pitsillides. Cellular aspects of the development of diarthrodial joints and articular cartilage. *Journal of Anatomy*, **184 (Pt 3)**:447–456, June 1994.

[10] Sarah J. Armstrong, Richard A. Read and Roger Price. Topographical variation within the articular cartilage and subchondral bone of the normal ovine knee joint: a histological approach. *Osteoarthritis & Cartilage*, **3**(1):25–33, March 1995. doi: 10.1016/S1063-4584(05)80035-4.

[11] J. Arokoski, I. Kiviranta, J. Jurvelin, M. Tammi and H. J. Helminen. Long-distance running causes site-dependent decrease of cartilage glycosaminoglycan content in the knee joints of beagle dogs. *Arthritis and Rheumatism*, **36**(10):1451–1459, Oct 1993.

[12] Jari P.A. Arokoski, Mika M. Hyttinen, Heiki J. Helminen and Jukka S. Jurvelin. Biomechanical and structural characteristics of canine femoral and tibial cartilage. *Journal of Biomedical Materials Research*, **48**(2):99–107, 1999. doi: 10.1002/(SICI)1097-4636(1999)48:2<99::AID-JBM1>3.0.CO;2-N.

[13] Jari P.A. Arokoski, Mika M. Hyttinen, Tuomo Lapveteläinen, Péter Takács, Béla Kosztáczky, László Módis, Vuokko Kovanen and Heikki J. Helminen. Decreased birefringence of the superficial zone collagen network in the canine knee (stifle) articular cartilage after long distance running training, detected by quantitative polarised light microscopy. *Annals of the Rheumatic Diseases*, **55**(4):253–264, April 1996.

[14] Gerard A. Ateshian. Anisotropy of fibrous tissues in relation to the distribution of tensed and buckled fibers. *Journal of Biomechanical Engineering*, **129**(2):240–249, April 2007. doi: 10.1115/1.2486179.

[15] Gerard A. Ateshian. The role of interstitial fluid pressurization in articular cartilage lubrication. *Journal of Biomechanics*, **42**(7):1163–1176, June 2009. doi: 10.1016/j.jbiomech.2009.04.040.

[16] Gerard A. Ateshian, Nadeen O. Chahine, Ines M. Basalo and Clark T. Hung. The correspondence between equilibrium biphasic and triphasic material properties in mixture models of articular cartilage. *Journal of Biomechanics*, **37**(3):391–400, March 2004. doi: 10.1016/S0021-9290(03)00252-5.

[17] Gerard A. Ateshian, Vikram Rajan, Nadeen O. Chahine, Clare E. Canal and Clark T. Hung. Modeling the matrix of articular cartilage using a continuous fiber angular distribution predicts many observed phenomena. *Journal of Biomechanical Engineering*, **131**(6):061003, June 2009. doi: 10.1115/1.3118773.

[18] Gerard A. Ateshian, Michael A. Soltz, Robert L. Mauck, Ines M. Basalo, Clark T. Hung and W. Michael Lai. The Role of Osmotic Pressure and Tension-Compression Nonlinearity in the Frictional Response of Articular Cartilage. *Transport in Porous Media*, **50**(1-2):5–33, January 2003. doi: 10.1023/A:1020618514874.

[19] K.A. Athanasiou, M.P. Rosenwasser, J.A. Buckwalter, T.I. Malinin and V.C. Mow. Interspecies comparisons of in situ intrinsic mechanical properties of distal femoral cartilage. *Journal of Orthopaedic Research*, **9**(3):330–340, May 1991. doi: 10.1002/jor.1100090304.

[20] Margaret B. Aydelotte, Robert R. Greenhill and Klaus E. Kuettner. Differences between sub-populations of cultured bovine articular chondrocytes. II. Proteoglycan metabolism. *Connective Tissue Research*, **18**(3):223–234, 1988.

[21] Margaret B. Aydelotte and Klaus E. Kuettner. Differences between subpopulations of cultured bovine articular chondrocytes. I. Morphology and cartilage matrix production. *Connective Tissue Research*, **18**(3):205–222, 1988.

[22] Frank Baaijens, Carlijn Bouten, Simon Hoerstrup, Anita Mol, Niels Driessen and Ralf Boerboom. Functional tissue engineering of the aortic heart valve. *Clinical Hemorheology and Microcirculation*, **33**(3):197–199, 2005.

[23] Nathaniel M. Bachrach, Wilmot B. Valhmu, Enrico Stazzone, Anthony Raidiffe, W. Michael Lai and Van C. Mow. Changes in proteoglycan synthesis of chondrocytes in articular cartilage are associated with the time-dependent changes in their mechanical environment. *Journal of Biomechanics*, **28**(12):1561–1569, December 1995. doi: 10.1016/0021-9290(95)00103-4.

[24] Angelique Balguid, Mirjam P. Rubbens, Anita Mol, Ruud A. Bank, Ad J.J.C. Bogers, Jorge P. van Kats, Bas A.J.M. de Mol, Frank P.T. Baaijens and Carlijn V.C. Bouten. The role of collagen cross-links in biomechanical behavior of human aortic heart valve leaflets–relevance for tissue engineering. *Tissue Engineering*, **13**(7):1501–1511, July 2007. doi: 10.1089/ten.2006.0279.

[25] Ruud A. Bank, Michael T. Bayliss, Floris P.J.G. Lafeber, Alice Maroudas and Johan M. Tekoppele. Ageing and zonal variation in post-translational modification of collagen in normal human articular cartilage. The age-related increase in non-enzymatic glycation affects biomechanical properties of cartilage. *Biochemical Journal*, **330 (Pt 1)**:345–351, February 1998.

[26] Ruud A. Bank, Michael Soudry, Alice Maroudas, Joseph Mizrahi and Johan M. TeKoppele. The increased swelling and instantaneous deformation of osteoarthritic cartilage is highly correlated with collagen degradation. *Arthritis and Rheumatism*, **43**(10):2202–2210, October 2000. doi: 10.1002/1529-0131(200010)43:10<2202::AID-ANR7>3.0.CO;2-E.

[27] R. Barer, A.R.H. Cole and H.W. Thompson. Infra-red spectroscopy with the reflecting microscope in physics, chemistry and biology. *Nature*, **163**(4136):198–201, February 1949. doi: 10.1038/163198a0.

[28] A. Barneveld and P.R. van Weeren. Conclusions regarding the influence of exercise on the development of the equine musculoskeletal system with special reference to osteochondrosis. *Equine Veterinary Journal Supplement*, (31):112–119, November 1999.

[29] Ines M. Basalo, Nadeen O. Chahine, Michael Kaplun, Faye H. Chen, Clark T. Hung and Gerard A. Ateshian. Chondroitin sulfate reduces the friction coefficient of articular cartilage. *Journal of Biomechanics*, November 2007. doi: 10.1016/j.jbiomech.2006.07.007.

[30] Peter J. Basser, Rosa Schneiderman, Ruud A. Bank, Ellen Wachtel and Alice Maroudas. Mechanical properties of the collagen network in human articular cartilage as measured by osmotic stress technique. *Archives of Biochemistry and Biophysics*, **351**(2):207–219, March 1998. doi: 10.1006/abbi.1997.0507.

[31] Y.M. Bastiaansen-Jenniskens, W. Koevoet, A.C.W. de Bart, J.C. van der Linden, A.M. Zuurmond, H. Weinans, J.A.N. Verhaar, G.J.V.M. van Osch and J. Degroot. Contribution of collagen network features to functional properties of engineered cartilage. *Osteoarthritis & Cartilage*, **16**(3):359–366, March 2008. doi: 10.1016/j.joca.2007.07.003.

[32] Michael T. Bayliss, Mary Venn, Alice Maroudas and S. Yousuf Ali. Structure of proteoglycans from different layers of human articular cartilage. *Biochemical Journal*, **209**(2):387–400, February 1983.

[33] Gary S. Beaupré, Sheila S. Stevens and Dennis R. Carter. Mechanobiology in the development, maintenance, and degeneration of articular cartilage. *Journal of Rehabilitation Research and Development*, **37**(2):145–151, March/April 2000.

[34] August Beer. Bestimmung der Absorption des rothen Lichts in farbigen Flüssigkeiten. *Annalen der Physik*, **162**(5):78–88, 1852. doi: 10.1002/andp.18521620505.

[35] Steven Below, Steven P. Arnoczky, Julie Dodds, Cynthia Kooima and Norman Walter. The split-line pattern of the distal femur: A consideration in the orientation of autologous cartilage grafts. *Arthroscopy*, **18**(6):613–617, 2002. doi: 10.1053/jars.2002.29877.

[36] Stanley H. Bennett. Methods applicable to the study of both fresh and fixed materials - the microscopical investigation of biological materials with polarized light. In: Ruth McClung Jones, editor, *McClung's handbook of microscopical technique*, chapter IX, pp. 591–677. Cassel and company limited, 3rd edition, 1950.

[37] A. Benninghoff. Form und Bau der Gelenkknorpel in ihren Beziehungen zur Funktion. Zweiter Teil: Der Aufbau des Gelenkknorpels in seinen Beziehungen zur Funktion. *Zeitschrift für Zellforschung und Mikroskopische Anatomie*, **2**:783–862, 1925. doi: 10.1007/BF00583443.

[38] Jatta E. Berberat, Mikko J. Nissi, Jukka S. Jurvelin and Miika T. Nieminen. Assessment of interstitial water content of articular cartilage with T1 relaxation. *Magnetic Resonance Imaging*, **27**(5):727–732, June 2009. doi: 10.1016/j.mri.2008.09.005.

[39] X. Bi, G. Li, S.B. Doty and N.P. Camacho. A novel method for determination of collagen orientation in cartilage by Fourier transform infrared imaging spectroscopy (FT-IRIS). *Osteoarthritis & Cartilage*, **13**(12):1050–1058, December 2005. doi: 10.1016/j.joca.2005.07.008.

[40] Maurice A. Biot. General Theory of Three-Dimensional Consolidation. *Journal of Applied Physics*, **12**(2):155–164, 1941. doi: 10.1063/1.1712886.

[41] Sven Björnsson. Simultaneous preparation and quantitation of proteoglycans by precipitation with alcian blue. *Analytical Biochemistry*, **210**(2):282–291, May 1993. doi: 10.1006/abio.1993.1197.

[42] Yvette S. Bland and Doreen E. Ashhurst. Changes in the content of the fibrillar collagens and the expression of their mRNAs in the menisci of the rabbit knee joint during development and ageing. *Histochemical Journal*, **28**(4):265–274, April 1996. doi: 10.1007/BF02409014.

[43] Yvette S. Bland and Doreen E. Ashhurst. Development and ageing of the articular cartilage of the rabbit knee joint: distribution of the fibrillar collagens. *Anatomy and Embryology*, **194**(6):607–619, December 1996. doi: 10.1007/BF00187473.

[44] Patricia Bobeck. Henry Darcy in his own words. *Hydrogeology Journal*, **14**(6):998–1004, September 2006. doi: 10.1007/s10040-005-0013-0.

[45] Lawrence J. Bonassar, Alan J. Grodzinsky, Eliot H. Frank, Salomon G. Davila, Nirav R. Bhaktav and Stephen B. Trippel. The effect of dynamic compression on the response of articular cartilage to insulin-like growth factor-I. *Journal of Orthopaedic Research*, **19**(1):11–17, January 2001. doi: 10.1016/S0736-0266(00)00004-8.

[46] Craig Boote, Sally Dennis and Keith Meek. Spatial mapping of collagen fibril organisation in primate cornea-an X-ray diffraction investigation. *Journal of Structural Biology*, **146**(3):359–367, June 2004. doi: 10.1016/j.jsb.2003.12.009.

[47] Adele Boskey and Nancy Pleshko Camacho. FT-IR imaging of native and tissue-engineered bone and cartilage. *Biomaterials*, **28**(15):2465–2478, May 2007. doi: 10.1016/j.biomaterials.2006.11.043.

[48] P.A.J. Brama, D. Karssenberg, A. Barneveld and P.R. van Weeren. Contact areas and pressure distribution on the proximal articular surface of the proximal phalanx under sagittal plane loading. *Equine Veterinary Journal*, **33**(1):26–32, January 2001.

[49] P.A.J. Brama, J.M. Tekoppele, R.A. Bank, A. Barneveld, E.C. Firth and P.R. van Weeren. The influence of strenuous exercise on collagen characteristics of articular cartilage in Thoroughbreds age 2 years. *Equine Veterinary Journal*, **32**(6):551–554, Nov 2000.

[50] P.A.J. Brama, J.M. TeKoppele, R.A. Bank, A. Barneveld and P.R. van Weeren. Functional adaptation of equine articular cartilage: the formation of regional biochemical characteristics up to age one year. *Equine Veterinary Journal*, **32**(3):217–221, May 2000.

[51] P.A.J. Brama, J.M. TeKoppele, R.A. Bank, A. Barneveld and P.R. van Weeren. Development of biochemical heterogeneity of articular cartilage: influences of age and exercise. *Equine Veterinary Journal*, **34**(3):265–269, May 2002.

[52] P.A.J. Brama, J.M. Tekoppele, R.A. Bank, D. Karssenberg, A. Barneveld and P.R. van Weeren. Topographical mapping of biochemical properties of articular cartilage in the equine fetlock joint. *Equine Veterinary Journal*, **32**(1):19–26, January 2000.

[53] P.A.J. Brama, J.M. TeKoppele, R.A. Bank, P.R. van Weeren and A. Barneveld. Influence of different exercise levels and age on the biochemical characteristics of immature equine articular cartilage. *Equine Veterinary Journal Supplement*, (31):55–61, November 1999.

[54] Pieter A.J. Brama, Jaakko Holopainen, P. René van Weeren, Elwyn C. Firth, Heikki J. Helminen and Mika M. Hyttinen. Effect of loading on the organization of the collagen fibril network in juvenile equine articular cartilage. *Journal of Orthopaedic Research*, **27**(9):1226–1234, September 2009. doi: 10.1002/jor.20866.

[55] W. Braune and O. Fischer. Bewegungen des Kniegelenks nach einer neuen Methode am lebenden Menschen gemessen. In: S. Hirzel, editor, *Abhandlungen der Mathematisch-Physischen Klasse der Königlich-Sächsischen Gesellschaft der Wissenschaften*, volume 17, pp. 75–150. Leipzig, 1891.

[56] N.E. Breslow and D.G. Clayton. Approximate inference in generalized linear mixed models. *Journal of the American Statistical Association*, **88**(421):9–25, March 1993. doi: 10.2307/2290687.

[57] H. Brommer, P.A.J. Brama, M.S. Laasanen, H.J. Helminen, P.R. van Weeren and J.S. Jurvelin. Functional adaptation of articular cartilage from birth to maturity under the influence of loading: a biomechanical analysis. *Equine Veterinary Journal*, **37**(2):148–154, March 2005.

[58] Dennis Brown. Here I come (extended mix). In: *Some like it hot*. Heartbeat, 1992. Catalogue number CDHB 107, track 1.

[59] Mark R. Buckley, Attila J. Bergou, Jonathan Fouchard, Lawrence J. Bonassar and Itai Cohen. High-resolution spatial mapping of shear properties in cartilage. *Journal of Biomechanics*, **43**(4):796–800, March 2009. doi: 10.1016/j.jbiomech.2009.10.012.

[60] Mark R. Buckley, Jason P. Gleghorn, Lawrence J. Bonassar and Itai Cohen. Mapping the depth dependence of shear properties in articular cartilage. *Journal of Biomechanics*, **41**(11):2430–2437, August 2008. doi: 10.1016/j.jbiomech.2008.05.021.

[61] Juan M. Bueno and Jaroslow Jaronski. Spatially resolved polarization properties for *in vitro* corneas. *Ophthalmic and Physiological Optics*, **21**(5):384–392, September 2001. doi: 10.1046/j.1475-1313.2001.00601.x.

[62] P. Bursać, S. Arnoczky and A. York. Dynamic compressive behavior of human meniscus correlates with its extra-cellular matrix composition. *Biorheology*, **46**(3):227–237, 2009. doi: 10.3233/BIR-2009-0537.

[63] Michael D. Buschmann, Ernst B. Hunziker, Young-Jo Kim and Alan J. Grodzinsky. Altered aggrecan synthesis correlates with cell and nucleus structure in statically compressed cartilage. *Journal of Cell Science*, **109 (Pt 2)**:499–508, February 1996.

[64] Michael D. Buschmann, Yuong-Jo Kim, Marcy Wong, Elliot Frank, Ernst B. Hunziker and Alan J. Grodzinsky. Stimulation of aggrecan synthesis in cartilage explants by cyclic loading is localized to regions of high interstitial fluid flow. *Archives of Biochemistry and Biophysics*, **366**(1):1–7, June 1999. doi: 10.1006/abbi.1999.1197.

[65] R.K. De Veulpoepers B.V. *Houdoe, bedankt en blijf wakker!* Polypoepka, Tilburg, The Netherlands, 1982. Catalogue number POEP 8.

[66] M.A. Cake, M.D. Boyce, G.E. Gardner, D.L. Hopkins and D.W. Pethick. Genotype and gender effects on sheep limb bone growth and maturation: selection for loin depth causes bone hypotrophy. *Australian Journal of Experimental Agriculture*, **47**(10):1128–1136, 2007. doi: 10.1071/EA07058.

[67] M. Caligaris and G.A. Ateshian. Effects of sustained interstitial fluid pressurization under migrating contact area, and boundary lubrication by synovial fluid, on cartilage friction. *Osteoarthritis & Cartilage*, **16**(10):1220–1227, October 2008. doi: 10.1016/j.joca.2008.02.020.

[68] Nancy P. Camacho, Paul West, Peter A. Torzilli and Richard Mendelsohn. FTIR microscopic imaging of collagen and proteoglycan in bovine cartilage. *Biopolymers*, **62**(1):1–8, 2001. doi: 10.1002/1097-0282(2001)62:1<1::AID-BIP10>3.0.CO;2-O.

[69] Clare E. Canal, Clark T. Hung and Gerard A. Ateshian. Two-dimensional strain fields on the cross-section of the bovine humeral head under contact loading. *Journal of Biomechanics*, **41**(15):3145–3151, November 2008. doi: 10.1016/j.jbiomech.2008.08.031.

[70] Dennis R. Carter, Gary S. Beaupré, Marcy Wong, R. Lane Smith, Tom P. Andriacchi and David J. Schurman. The mechanobiology of articular cartilage development and degeneration. *Clinical Orthopaedics and Related Research*, (427 Suppl):S69–S77, October 2004. doi: 10.1097/01.blo.0000144970.05107.7e.

[71] Dennis R. Carter, Tracy E. Orr, David P. Fyhrie and David J. Schurman. Influences of mechanical stress on prenatal and postnatal skeletal development. *Clinical Orthopaedics and Related Research*, (219):237–250, June 1987.

[72] Dennis R. Carter and Marcy Wong. Modelling cartilage mechanobiology. *Philosophical Transactions of the Royal Society of London. Series B: Biological Sciences*, **358**(1437):1461–1471, September 2003. doi: 10.1098/rstb.2003.1346.

[73] Bruce Caterson and John R. Baker. The link proteins as specific components of cartilage proteoglycan aggregates *in vivo*. Associative extraction of proteoglycan aggregate from swarm rat chondrosarcoma. *The Journal of Biological Chemistry*, **254**(7):2394–2399, April 1979.

[74] Nadeen O. Chahine, Christopher C.-B. Wang, Clark T. Hung and Gerard A. Ateshian. Anisotropic strain-dependent material properties of bovine articular cartilage in the transitional range from tension to compression. *Journal of Biomechanics*, **37**(8):1251–1261, August 2004. doi: 10.1016/j.jbiomech.2003.12.008.

[75] N.O. Chahine, G.A. Ateshian and C.T. Hung. The effect of finite compressive strain on chondrocyte viability in statically loaded bovine articular cartilage. *Biomechanics and Modeling in Mechanobiology*, **6**(1-2):103–111, January 2007. doi: 10.1007/s10237-006-0041-2.

[76] Mathieu Charlebois, Marc D. McKee and Michael D. Buschmann. Nonlinear tensile properties of bovine articular cartilage and their variation with age and depth. *Journal of Biomechanical Engineering*, **126**(2):129–137, April 2004.

[77] Salman Chegini and Stephen J. Ferguson. Time and depth dependent poisson's ratio of cartilage explained by an inhomogeneous orthotropic fiber embedded biphasic model. *Journal of Biomechanics*, **43**(9):1660–1666, June 2010. doi: 10.1016/j.jbiomech.2010.03.006.

[78] A.C. Chen, W.C. Bae, R.M. Schinagl and R.L. Sah. Depth- and strain-dependent mechanical and electromechanical properties of full-thickness bovine articular cartilage in confined compression. *Journal of Biomechanics*, **34**(1):1–12, January 2001. doi: 10.1016/S0021-9290(00)00170-6.

[79] S.S. Chen, Y.H. Falcovitz, R. Schneiderman, A. Maroudas and R.L. Sah. Depth-dependent compressive properties of normal aged human femoral head articular cartilage: relationship to fixed charge density. *Osteoarthritis & Cartilage*, **9**(6):561–569, August 2001. doi: 10.1053/joca.2001.0424.

[80] Jae Bong Choi, Inchan Youn, Li Cao, Holly A. Leddy, Christopher L. Gilchrist, Lori A. Setton and Farshid Guilak. Zonal changes in the three-dimensional morphology of the chondron under compression: the relationship among cellular, pericellular, and extracellular deformation in articular cartilage. *Journal of Biomechanics*, **40**(12):2596–2603, 2007. doi: 10.1016/j.jbiomech.2007.01.009.

[81] Tina T. Chowdhury, Ronny M. Schulz, Sonpreet S. Rai, Christian Thuemmler, Nico Wuestneck, Augustinus Bader and Gene A. Homandberg. Biomechanical modulation of collagen fragment-induced anabolic and catabolic activities in chondrocyte/agarose constructs. *Arthritis Research & Therapy*, **12**(3):R82, May 2010. doi: 10.1186/ar3009.

[82] John M. Clark. The organization of collagen in cryofractured rabbit articular cartilage: a scanning electron microscopic study. *Journal of Orthopaedic Research*, **3**(1):17–29, 1985. doi: 10.1002/jor.1100030102.

[83] John M. Clark. Variation of collagen fiber alignment in a joint surface: a scanning electron microscope study of the tibial plateau in dog, rabbit, and man. *Journal of Orthopaedic Research*, **9**(2):246–257, March 1991. doi: 10.1002/jor.1100090213.

[84] John M. Clark, Anthony Norman and Hubert Nötzli. Postnatal development of the collagen matrix in rabbit tibial plateau articular cartilage. *Journal of Anatomy*, **191 (Pt 2)**:215–221, August 1997. doi: 10.1046/j.1469-7580.1997.19120215.x.

[85] R.B. Clark and J.B Cowey. Factors Controlling the Change of Shape of Certain Nemertean and Turbellarian Worms. *Journal of Experimental Biology*, **35**(4):731–750, December 1958.

[86] Edward Collett. *Field guide to polarisation*. Spie press, Washington, U.S.A., 2005.

[87] Michael A. Cremer, Edward F. Rosloniec and Andrew H. Kang. The cartilage collagens: a review of their structure, organization, and role in the pathogenesis of experimental arthritis in animals and in human rheumatic disease. *Journal of Molecular Medicine*, **76**(3-4):275–288, March 1998. doi: 10.1007/s001090050217.

[88] F. Dantas, P. Fisher, H. Walach, F. Wieland, D.P. Rastogi, H. Teixeira, D. Koster, J.P. Jansen, J. Eizayaga, M.E.P. Alvarez, M. Marim, P. Belon and L.L.M. Weckx. A systematic review of the quality of homeopathic pathogenetic trials published from 1945 to 1995. *Homeopathy*, **96**(1):4–16, January 2007. doi: 10.1016/j.homp.2006.11.005.

[89] E.M. Darling, S. Zauscher and F. Guilak. Viscoelastic properties of zonal articular chondrocytes measured by atomic force microscopy. *Osteoarthritis & Cartilage*, **14**(6):571–579, June 2006. doi: 10.1016/j.joca.2005.12.003.

[90] Eric M. Darling, Jerry C.Y. Hu and Kyriacos A. Athanasiou. Zonal and topographical differences in articular cartilage gene expression. *Journal of Orthopaedic Research*, **22**(6):1182–1187, November 2004. doi: 10.1016/j.orthres.2004.03.001.

[91] Charles Darwin. *The Expression of the Emotions in Man and Animals*. Filiquarian Publishing, LLC, 2007 (1872).

[92] E. David-Vaudey, A. Burghardt, K. Keshari, A. Brouchet, M. Ries and S. Majumdar. Fourier Transform Infrared Imaging of focal lesions in human osteoarthritic cartilage. *European Cells & Materials Journal*, **10**:51–60, 2005.

[93] Richard Dawkins. *The greatest show on earth – the evidence for evolution*. Bantam publishers, p. 230, 1st edition, 2009.

[94] Marc R. Desjardins and Mark B. Hurtig. Cartilage healing: A review with emphasis on the equine model. *Canadian Veterinary Journal*, **31**(8):565–572, August 1990.

[95] F.G. Donnan. The Theory of Membrane Equilibria. *Chemical Reviews*, **1**(1):73–90, April 1924. doi: 10.1021/cr60001a003.

[96] Niels J.B. Driessen, Carlijn V.C. Bouten and Frank P.T. Baaijens. Improved prediction of the collagen fiber architecture in the aortic heart valve. *Journal of Biomechanical Engineering*, **127**(2):329–336, April 2005. doi: 10.1115/1.1865187.

[97] N.J.B. Driessen, W. Wilson, C.V.C. Bouten and F.P.T. Baaijens. A computational model for collagen fibre remodelling in the arterial wall. *Journal of Theoretical Biology*, **226**(1):53–64, January 2004. doi: 10.1016/j.jtbi.2003.08.004.

[98] J. Dudhia. Aggrecan, aging and assembly in articular cartilage. *Cellular and Molecular Life Sciences*, **62**(19-20):2241–2256, October 2005. doi: 10.1007/s00018-005-5217-x.

[99] Gunter F. Egger, Kirsti Witter, Gerald Weissengruber and Gerhard Forstenpointner. Articular cartilage in the knee joint of the African elephant, *Loxodonta africana*, Blumenbach 1797. *Journal of Morphology*, **269**(1):118–127, January 2008. doi: 10.1002/jmor.10600.

[100] S.R. Eisenberg and A.J. Grodzinsky. The kinetics of chemically induced nonequilibrium swelling of articular cartilage and corneal stroma. *Journal of Biomechanical Engineering*, **109**(1):79–89, February 1987.

[101] Alton Ellis. You make me so happy. In: *Mr. soul of Jamaica*. Treasure Isle, 1967. Catalogue number TI LP 007, side A, track 5.

[102] B. Engel and A. Keen. A simple approach for the analysis of generalized linear mixed models. *Statistica Neerlandica*, **48**(1):1–22, 1994. doi: 10.1111/j.1467-9574.1994.tb01428.x.

[103] Oliver K. Erne, John B. Reid, Larry W. Ehmke, Mark B. Sommers, Steven M. Madey and Michael Bottlang. Depth-dependent strain of patellofemoral articular cartilage in unconfined compression. *Journal of Biomechanics*, **38**(4):667–672, April 2005. doi: 10.1016/j.jbiomech.2004.04.005.

[104] Marcelo Augusto Marretto Esquisatto, Edson Rosa Pimentel and Laurecir Gomes. Extracellular matrix composition of different regions of the knee joint cartilage in cattle. *Annals of Anatomy*, **179**(5):433–437, October 1997.

[105] David Eyre. Collagen of articular cartilage. *Arthritis Research*, **4**(1):30–35, 2002.

[106] David R. Eyre, Mary Ann Weis and Jiann-Jiu Wu. Articular cartilage collagen: an irreplaceable framework? *European Cells & Materials Journal*, **12**:57–63, 2006.

[107] D.R. Eyre. The collagens of articular cartilage. *Seminars in Arthritis and Rheumatism*, **21**(3 Suppl 2):2–11, Dec 1991.

[108] D.R. Eyre and H. Muir. The distribution of different molecular species of collagen in fibrous, elastic and hyaline cartilages of the pig. *Biochemical Journal*, **151**(3):595–602, December 1975.

[109] K. Fackler, L. Klein and A. Hiltner. Polarizing light microscopy of intestine and its relationship to mechanical behaviour. *Journal of Microscopy*, **124**(Pt 3):305–311, December 1981.

[110] Salvatore Federico and Walter Herzog. On the anisotropy and inhomogeneity of permeability in articular cartilage. *Biomechanics and Modeling in Mechanobiology*, **7**(5):367–378, October 2008. doi: 10.1007/s10237-007-0091-0.

[111] Salvatore Federico and Walter Herzog. On the permeability of fibre-reinforced porous materials. *International Journal of Solids and Structures*, **45**(7-8):2160–2172, April 2008. doi: 10.1016/j.ijsolstr.2007.11.014.

[112] E.C. Firth and Y. Greydanus. Cartilage thickness measurement in foals. *Research in Veterinary Science*, **42**(1):35–46, January 1987.

[113] Jonathan B. Fitzgerald, Moonsoo Jin, Delphine Dean, David J. Wood, Ming H. Zheng and Alan J. Grodzinsky. Mechanical compression of cartilage explants induces multiple time-dependent gene expression patterns and involves intracellular calcium and cyclic AMP. *The Journal of Biological Chemistry*, **279**(19):19502–19511, May 2004. doi: 10.1074/jbc.M400437200.

[114] Douglas L. Foster and Leslie M. Jackson. Puberty in the Sheep. In: Jimmy D. Neill, editor, *Knobil and Neill's Physiology of Reproduction*, volume 2, chapter 39, pp. 2127–2176. Elsevier Inc., 3rd edition, 2006.

[115] Ahnders Franzén, Sven Inerot, Sven-Olof Hejderup and Dick Heinegård. Variations in the composition of bovine hip articular cartilage with distance from the articular surface. *Biochemical Journal*, **195**(3):535–543, June 1981.

[116] P. Fratzl, editor. *Collagen: Structure and Mechanics*. Springer US, 2008. doi: 10.1007/978-0-387-73906-9.

[117] A.J.H. Frijns, J.M. Huyghe and J.D. Janssen. A validation of the quadriphasic mixture theory for intervertebral disc tissue. *International Journal of Engineering Science*, **35**(15):1419–1429, 1997. doi: 10.1016/S0020-7225(97)00047-5.

[118] Galileo Galilei. *Dialogues concerning two new sciences*. Prometheus Books, New York, 1991. Translation of Discorsi e dimonstrazioni matematiche (1638) by Henry Crew and Alfonso de Salvio.

[119] Martin Gardner. *Sphere Packing, Lewis Carroll, and Reversi*. Cambridge University Press, 32 Avenue of the Americas, New York, U.S.A., 2009.

[120] Ruth St.C. Gilmore and A.J. Palfrey. Chondrocyte distribution in the articular cartilage of human femoral condyles. *Journal of Anatomy*, **157**:23–31, April 1988.

[121] Mary B. Goldring. Update on the biology of the chondrocyte and new approaches to treating cartilage diseases. *Best Practice & Research Clinical Rheumatology*, **20**(5):1003–1025, October 2006. doi: 10.1016/j.berh.2006.06.003.

[122] Cédric Gomez, Valentin David, Nicola M. Peet, Laurence Vico, Chantal Chenu, Luc Malaval and Timothy M. Skerry. Absence of mechanical loading in utero influences bone mass and architecture but not innervation in MyoD-Myf5-deficient mice. *Journal of Anatomy*, **210**(3):259–271, 2007. doi: 10.1111/j.1469-7580.2007.00698.x.

[123] Santiago Gomez, Renato Toffanin, Sigrid Bernstorff, Milena Romanello, Heinz Amenitsch, Michael Rappolt, Roberto Rizzo and Franco Vittur. Collagen fibrils are differently organized in weight-bearing and not-weight-bearing regions of pig articular cartilage. *Journal of Experimental Zoology*, **287**(5):346–352, October 2000. doi: 10.1002/1097-010X(20001001)287:5<346::AID-JEZ3>3.0.CO;2-P.

[124] John M. Gosline and Robert E. Shadwick. The mechanical properties of fin whale arteries are explained by novel connective tissue designs. *Journal of Experimental Biology*, **199**(Pt 4):985–997, April 1996.

[125] George W. Greene, Bruno Zappone, Olle Söderman, Daniel Topgaard, Gabriel Rata, Hongbo Zeng and Jacob N. Israelachvili. Anisotropic dynamic changes in the pore network structure, fluid diffusion and fluid flow in articular cartilage under compression. *Biomaterials*, **31**(12):3117–3128, Apr 2010. doi: 10.1016/j.biomaterials.2010.01.102.

[126] Alan J. Grodzinsky, Marc E. Levenston, Moonsoo Jin and Eliot H. Frank. Cartilage tissue remodeling in response to mechanical forces. *Annual Review of Biomedical Engineering*, **2**:691–713, 2000. doi: 10.1146/annurev.bioeng.2.1.691.

[127] Jurriaan H. de Groot and Johan L. van Leeuwen. Evidence for an elastic projection mechanism in the chameleon tongue. *Proceedings of the Royal Society B: Biological Sciences*, **271**(1540):761–770, April 2004. doi: 10.1098/rspb.2003.2637.

[128] Wilfried Gründer. MRI assessment of cartilage ultrastructure. *NMR in Biomedicine*, **19**(7):855–876, November 2006. doi: 10.1002/nbm.1092.

[129] Farshid Guilak, B. Christoph Meyer, Anthony Ratcliffe and Van C. Mow. The effects of matrix compression on proteoglycan metabolism in articular cartilage explants. *Osteoarthritis & Cartilage*, **2**(2):91–101, June 1994. doi: 10.1016/S1063-4584(05)80059-7.

[130] Farshid Guilak, Anthony Ratcliffe and Van C. Mow. Chondrocyte deformation and local tissue strain in articular cartilage: a confocal microscopy study. *Journal of Orthopaedic Research*, **13**(3):410–421, May 1995. doi: 10.1002/jor.1100130315.

[131] J. Haapala, J.P. Arokoski, S. Rönkkö, U. Ågren, V.M. Kosma, L.S. Lohmander, M. Tammi, H.J. Helminen and I. Kiviranta. Decline after immobilisation and

recovery after remobilisation of synovial fluid IL1, TIMP, and chondroitin sulphate levels in young beagle dogs. *Annals of the Rheumatic Diseases*, **60**(1):55–60, January 2001. doi: 10.1136/ard.60.1.55.

[132] Mansoor A. Haider, Richard C. Schugart, Lori A. Setton and Farshid Guilak. A mechano-chemical model for the passive swelling response of an isolated chondron under osmotic loading. *Biomechanics and Modeling in Mechanobiology*, **5**(2-3):160–171, June 2006. doi: 10.1007/s10237-006-0026-1.

[133] R. Wheeler Haines. The development of joints. *Journal of Anatomy*, **81**(Pt 1):33–55, January 1947.

[134] Ashley S. Hammond, Jie Ning, Carol V. Ward and Matthew J. Ravosa. Mammalian limb loading and chondral modeling during ontogeny. *The Anatomical Record: Advances in Integrative Anatomy and Evolutionary Biology*, **293**(4):658–670, April 2010. doi: 10.1002/ar.21136.

[135] Mark W. Hamrick. A chondral modeling theory revisited. *Journal of Theoretical Biology*, **201**(3):201–208, December 1999. doi: 10.1006/jtbi.1999.1025.

[136] B. Han, A.A. Cole, Y. Shen, T. Brodie and J.M. Williams. Early alterations in the collagen meshwork and lesions in the ankles are associated with spontaneous osteoarthritis in guinea-pigs. *Osteoarthritis & Cartilage*, **10**(10):778–784, October 2002.

[137] T.E. Hardingham and Helen Muir. The specific interaction of hyaluronic acid with cartilage proteoglycans. *Biochimica et Biophysica Acta*, **279**(2):401–405, September 1972. doi: 10.1016/0304-4165(72)90160-2.

[138] Isao Hasegawa, Shinya Kuriki, Shigeo Matsuno and Goro Matsumoto. Dependence of electrical conductivity on fixed charge density in articular cartilage. *Clinical Orthopaedics and Related Research*, (177):283–288, August 1983.

[139] A.J. Hayes, S. MacPherson, H. Morrison, G. Dowthwaite and C.W. Archer. The development of articular cartilage: evidence for an appositional growth mechanism. *Anatomy and Embryology*, **203**(6):469–479, June 2001. doi: 10.1007/s004290100178.

[140] Eugene Hecht. *Optics*. Addison-Wesley Publishing Company, Inc., 2nd edition, 1987.

[141] J.H. Heegaard, G.S. Beaupré and D.R. Carter. Mechanically modulated cartilage growth may regulate joint surface morphogenesis. *Journal of Orthopaedic Research*, **17**(4):509–517, July 1999. doi: 10.1002/jor.1100170408.

[142] Dick Heinegård. Proteoglycans and more–from molecules to biology. *International Journal of Experimental Pathology*, **90**(6):575–586, December 2009. doi: 10.1111/j.1365-2613.2009.00695.x.

[143] Heikki J. Helminen, Mika M. Hyttinen, Mikko J. Lammi, Jari P.A. Arokoski, Tuomo Lapveteläinen, Jukka Jurvelin, Ilkka Kiviranta and Markku I. Tammi. Regular joint loading in youth assists in the establishment and strengthening of the collagen network of articular cartilage and contributes to the prevention of osteoarthrosis later in life: a hypothesis. *Journal of Bone and Mineral Metabolism*, **18**(5):245–257, August 2000. doi: 10.1007/PL00010638.

[144] Hannah K. Heywood, Martin M. Knight and David A. Lee. Both superficial and deep zone articular chondrocyte subpopulations exhibit the Crabtree effect but have different basal oxygen consumption rates. *Journal of Cellular Physiology*, **223**(3):630–639, June 2010. doi: 10.1002/jcp.22061.

[145] W.A. Hodge, R.S. Fijan, K.L. Carlson, R.G. Burgess, W.H. Harris and R.W. Mann. Contact pressures in the human hip joint measured *in vivo*. *Proceedings of the National Academy of Sciences of the United States of America*, **83**(9):2879–2883, May 1986. doi: 10.1073/pnas.83.9.2879.

[146] Bianca M. van den Hoogen, C.H.A. van de Lest, P.R. van Weeren, L.M.G. van Golde and A. Barneveld. Effect of exercise on the proteoglycan metabolism of articular cartilage in growing foals. *Equine Veterinary Journal Supplement*, (31):62–66, November 1999.

[147] D.L. Hopkins, D.F. Stanley, L.C. Martin and A.R. Gilmour. Genotype and age effects on sheep meat production 1. Production and growth. *Australian Journal of Experimental Agriculture*, **47**(10):1119–1127, 2007.

[148] Clifford C. Hoyt and Rudolf Oldenbourg. Structural analysis with quantitative birefringence imaging. *American Laboratory*, **31**(14):34–42, July 1999.

[149] Xiang-Run Huang and Robert W. Knighton. Microtubules contribute to the birefringence of the retinal nerve fiber layer. *Investigative Ophthalmology and Visual Science*, **46**(12):4588–4593, December 2005. doi: 10.1167/iovs.05-0532.

[150] L.C. Hughes, C.W. Archer and I. ap Gwynn. The ultrastructure of mouse articular cartilage: collagen orientation and implications for tissue functionality. A polarised light and scanning electron microscope study and review. *European Cells & Materials Journal*, **9**:68–84, 2005.

[151] Clark T. Hung, Robert L. Mauck, Christopher C.-B. Wang, Eric G. Lima and Gerard A. Ateshian. A paradigm for functional tissue engineering of articular cartilage via applied physiologic deformational loading. *Annals of Biomedical Engineering*, **32**(1):35–49, January 2004. doi: 10.1023/B:ABME.0000007789.99565.42.

[152] William Hunter. Of the Structure and Diseases of Articulating Cartilages. *Philosophical Transactions*, **42**:514–521, 1743.

[153] E.B. Hunziker, E. Kapfinger and J. Geiss. Corrigendum to "The structural architecture of adult mammalian articular cartilage evolves by a synchronized process of tissue resorption and neoformation during postnatal development" [Osteoarthritis Cartilage 15 (2007) 403–413]. *Osteoarthritis & Cartilage*, 2007. doi: 10.1016/j.joca.2007.06.001.

[154] E.B. Hunziker, E. Kapfinger and J. Geiss. The structural architecture of adult mammalian articular cartilage evolves by a synchronized process of tissue resorption and neoformation during postnatal development. *Osteoarthritis & Cartilage*, **15**(4):403–413, April 2007. doi: 10.1016/j.joca.2006.09.010. Corrigendum in [153].

[155] William C. Hutton, S. Tim Yoon, William A. Elmer, Jun Li, Hideki Murakami, Akihito Minamide and Tomoyuki Akamaru. Effect of tail suspension (or simulated weightlessness) on the lumbar intervertebral disc: study of proteoglycans and collagen. *Spine*, **27**(12):1286–1290, June 2002.

[156] J.M. Huyghe, G.B. Houben, M.R. Drost and C.C. van Donkelaar. An ionised/non-ionised dual porosity model of intervertebral disc tissue. *Biomechanics and Modeling in Mechanobiology*, **2**(1):3–19, Aug 2003. doi: 10.1007/s10237-002-0023-y.

[157] J.M. Huyghe, W. Wilson and K. Malakpoor. On the thermodynamical admissibility of the triphasic theory of charged hydrated tissues. *Journal of Biomechanical Engineering*, **131**(4):044504, April 2009. doi: 10.1115/1.3049531.

[158] Mika M. Hyttinen, Jaakko Holopainen, P. René van Weeren, Elwyn C. Firth, Heikki J. Helminen and Pieter A.J. Brama. Changes in collagen fibril network organization and proteoglycan distribution in equine articular cartilage during maturation and growth. *Journal of Anatomy*, **215**(5):584–591, November 2009. doi: 10.1111/j.1469-7580.2009.01140.x.

[159] M.M. Hyttinen, J.P. Arokoski, J.J. Parkkinen, M.J. Lammi, T. Lapveteläinen, K. Mauranen, K. Király, M.I. Tammi and H.J. Helminen. Age matters: collagen birefringence of superficial articular cartilage is increased in young guinea-pigs but decreased in older animals after identical physiological type of joint loading. *Osteoarthritis & Cartilage*, **9**(8):694–701, November 2001. doi: 10.1053/joca.2001.0466.

[160] Prince Far I. Ask Ask. In: *Umkhonto we sizwe (Spear of the Nation) – a showcase album*. Tamoki-Wambesi, 1984. Catalogue number TWLP 1013, side A, track 3 (mislabelled as track 2).

[161] Natalia Yu Ignatieva, Olga L. Zakharkina, Irina V. Andreeva, Emil N. Sobol, Vladislav A. Kamensky, Alexey V. Myakov, Sergey V. Averkiev and Valery V. Lunin. IR laser and heat-induced changes in annulus fibrosus collagen structure. *Photochemistry and Photobiology*, **83**(3):675–685, May/June 2007. doi: 10.1111/j.1751-1097.2007.072.x.

[162] Kyle D. Jadin, Benjamin L. Wong, Won C. Bae, Kelvin W. Li, Amanda K. Williamson, Barbara L. Schumacher, Jeffrey H. Price and Robert L. Sah. Depth-varying density and organization of chondrocytes in immature and mature bovine articular cartilage assessed by 3D imaging and analysis. *Journal of Histochemistry and Cytochemistry*, **53**(9):1109–1119, September 2005. doi: 10.1369/jhc.4A6511.2005.

[163] Jaroslaw W. Jaronski and Henryk T. Kasprzak. Linear birefringence measurements of the *in vitro* human cornea. *Ophthalmic and Physiological Optics*, **23**(4):361–369, July 2003. doi: 10.1046/j.1475-1313.2003.00128.x.

[164] Monsoo Jin, Eliot H. Frank, Thomas M. Quinn, Ernst B. Hunziker and Alan J. Grodzinsky. Tissue shear deformation stimulates proteoglycan and protein biosynthesis in bovine cartilage explants. *Archives of Biochemistry and Biophysics*, **395**(1):41–48, November 2001. doi: 10.1006/abbi.2001.2543.

[165] R. Clarke Jones. A new calculus for the treatment of optical systems. I. Description and discussion of the calculus. *Journal of the Optical Society of America*, **31**:488–493, July 1941.

[166] Pierre-Simon Jouk, Ayman Mourad, Vuk Milisic, Gabrielle Michalowicz, Annie Raoult, Denis Caillerie and Yves Usson. Analysis of the fiber architecture of the heart by quantitative polarized light microscopy. Accuracy, limitations and contribution to the study of the fiber architecture of the ventricles during fetal and neonatal life. *European Journal of Cardio-Thoracic Surgery*, **31**(5):915–921, May 2007. doi: 10.1016/j.ejcts.2006.12.040.

[167] P. Julkunen, T. Harjula, J. Iivarinen, J. Marjanen, K. Seppänen, T. Närhi, J. Arokoski, M. J. Lammi, P.A. Brama, J.S. Jurvelin and H.J. Helminen. Biomechanical, biochemical and structural correlations in immature and mature rabbit articular cartilage. *Osteoarthritis & Cartilage*, **17**(12):1628–1638, December 2009. doi: 10.1016/j.joca.2009.07.002.

[168] P. Julkunen, J. Iivarinen, P.A. Brama, J. Arokoski, J.S. Jurvelin and H.J. Helminen. Maturation of collagen fibril network structure in tibial and femoral cartilage of rabbits. *Osteoarthritis & Cartilage*, **18**(3):406–415, March 2010. doi: 10.1016/j.joca.2009.11.007.

[169] P. Julkunen, R.K. Korhonen, M.J. Nissi and J.S. Jurvelin. Mechanical characterization of articular cartilage by combining magnetic resonance imaging and finite-element analysis: a potential functional imaging technique. *Physics in Medicine and Biology*, **53**(9):2425–2438, May 2008. doi: 10.1088/0031-9155/53/9/014.

[170] Petro Julkunen, Jukka S. Jurvelin and Hanna Isaksson. Contribution of tissue composition and structure to mechanical response of articular cartilage under different loading geometries and strain rates. *Biomechanics and Modeling in Mechanobiology*, **9**(2):237–245, April 2010. doi: 10.1007/s10237-009-0169-y.

[171] Petro Julkunen, Panu Kiviranta, Wouter Wilson, Jukka S. Jurvelin and Rami K. Korhonen. Characterization of articular cartilage by combining microscopic analysis with a fibril-reinforced finite-element model. *Journal of Biomechanics*, **40**(8):1862–1870, 2007. doi: 10.1016/j.jbiomech.2006.07.026.

[172] Petro Julkunen, Wouter Wilson, Jukka S. Jurvelin and Rami K. Korhonen. Composition of the pericellular matrix modulates the deformation behaviour of chondrocytes in articular cartilage under static loading. *Medical and Biological Engineering and Computing*, **47**(12):1281–1290, December 2009. doi: 10.1007/s11517-009-0547-8.

[173] Petro Julkunen, Wouter Wilson, Jukka S. Jurvelin, Jarno Rieppo, Cheng-Juan Qu, Mikko J. Lammi and Rami K. Korhonen. Stress-relaxation of human patellar articular cartilage in unconfined compression: prediction of mechanical response by tissue composition and structure. *Journal of Biomechanics*, **41**(9):1978–1986, 2008. doi: 10.1016/j.jbiomech.2008.03.026.

[174] P.E. Jupp and K.V. Mardia. A Unified View of the Theory of Directional Statistics, 1975-1988. *International Statistical Review*, **57**(3):261–294, December 1989.

[175] M.J. Kääb, I. ap Gwynn and H.P. Nötzli. Collagen fibre arrangement in the tibial plateau articular cartilage of man and other mammalian species. *Journal of Anatomy*, **193 (Pt 1)**:23–34, July 1998. doi: 10.1046/j.1469-7580.1998.19310023.x.

[176] David Katz and Steve Barrow. *Sleeve notes to 3 CD set 'Arkology' by 'Lee Scratch Perry'*. Island Records Ltd., 1997. Catalogue number: LC 0407 524 3792 CRNCD 6.

[177] Emma Kavanagh, Anne C. Osborne, Doreen E. Ashhurst and Andrew A. Pitsillides. Keratan sulfate epitopes exhibit a conserved distribution during joint development that remains undisclosed on the basis of glycosaminoglycan charge density. *The Journal of Histochemistry & Cytochemistry*, **50**(8):1039–1047, August 2002.

[178] D.A. Kelly. Axial orthogonal fiber reinforcement in the penis of the nine-banded armadillo (*Dasypus novemcinctus*). *Journal of Morphology*, **233**(3):249–255, September 1997. doi: 10.1002/(SICI)1097-4687(199709)233:3<249::AID-JMOR4>3.0.CO;2-Z.

[179] D.A. Kelly. Turtle and mammal penis designs are anatomically convergent. *Proceedings of the Royal Society B: Biological Sciences*, **271**(Suppl. 5):S293–295, August 2004. doi: 10.1098/rsbl.2004.0161.

[180] G.E. Kempson, M.A. Freeman and S.A. Swanson. Tensile properties of articular cartilage. *Nature*, **220**(5172):1127–1128, December 1968.

[181] Michael G. Kenward and James H. Roger. Small sample inference for fixed effects from restricted maximum likelihood. *Biometrics*, **53**(3):983–997, September 1997.

[182] Michael W. Kessler and Daniel A. Grande. Tissue engineering and cartilage. *Organogenesis*, **4**(1):28–32, January 2008.

[183] Partap S. Khalsa and Solomon R. Eisenberg. Compressive behavior of articular cartilage is not completely explained by proteoglycan osmotic pressure. *Journal of Biomechanics*, **30**(6):589–594, June 1997. doi: 10.1016/S0021-9290(97)84508-3.

[184] I.M. Khan, S.N. Redman, R. Williams, G.P. Dowthwaite, S.F. Oldfield and C.W. Archer. The development of synovial joints. *Current Topics in Developmental Biology*, **79**:1–36, 2007. doi: 10.1016/S0070-2153(06)79001-9.

[185] Ehab Kheir and David Shaw. Hyaline articular cartilage. *Orthopaedics and Trauma*, **23**(6):450–455, 2009. doi: 10.1016/j.mporth.2009.01.003.

[186] Areum Kim, Neema Lakshman and W. Matthew Petroll. Quantitative assessment of local collagen matrix remodeling in 3-D culture: the role of Rho kinase. *Experimental Cell Research*, **312**(18):3683–3692, November 2006. doi: 10.1016/j.yexcr.2006.08.009.

[187] K. Király, M.M. Hyttinen, T. Lapveteläinen, M. Elo, I. Kiviranta, J. Dobai, L. Módis, H.J. Helminen and J.P. Arokoski. Specimen preparation and quantification of collagen birefringence in unstained sections of articular cartilage using image analysis and polarizing light microscopy. *Histochemical Journal*, **29**(4):317–327, April 1997. doi: 10.1023/A:1020802631968.

[188] K. Király, M.M. Hyttinen, J.J. Parkkinen, J.A. Arokoski, T. Lapveteläinen, I. Törrönen, K. Kiviranta and H.J. Helminen. Articular cartilage collagen birefringence is altered concurrent with changes in proteoglycan synthesis during dynamic *in vitro* loading. *Anatomical Record*, **251**(1):28–36, May 1998. doi: 10.1002/(SICI)1097-0185(199805)251:1<28::AID-AR6>3.0.CO;2-A.

[189] I. Kiviranta, M. Tammi, J. Jurvelin, J. Arokoski, A.M. Säämänen and H.J. Helminen. Articular cartilage thickness and glycosaminoglycan distribution in the young canine knee joint after remobilization of the immobilized limb. *Journal of Orthopaedic Research*, **12**(2):161–167, March 1994. doi: 10.1002/jor.1100120203.

[190] Ilkka Kiviranta, Markku Tammi, Jukka Jurvelin, Jari Arokoski, Anna-Marja Säämänen and Heikki J. Helminen. Articular cartilage thickness and glycosaminoglycan distribution in the canine knee joint after strenuous running exercise. *Clinical Orthopaedics and Related Research*, (283):302–308, October 1992.

[191] Ilkka Kiviranta, Markku Tammi, Jukka Jurvelin and Heikki J. Helminen. Topographical variation of glycosaminoglycan content and cartilage thickness in canine knee (stifle) joint cartilage. Application of the microspectrophotometric method. *Journal of Anatomy*, **150**:265–276, February 1987.

[192] Panu Kiviranta, Jarno Rieppo, Rami K. Korhonen, Petro Julkunen, Juha Töyräs and Jukka S. Jurvelin. Collagen network primarily controls Poisson's ratio of bovine articular cartilage in compression. *Journal of Orthopaedic Research*, **24**(4):690–699, April 2006. doi: 10.1002/jor.20107.

[193] Travis J. Klein, Manu Chaudhry, Won C. Bae and Robert L. Sah. Depth-dependent biomechanical and biochemical properties of fetal, newborn, and tissue-engineered articular cartilage. *Journal of Biomechanics*, **40**(1):182–190, 2007. doi: 10.1016/j.jbiomech.2005.11.002.

[194] Robert W. Knighton and Xiang-Run Huang. Linear birefringence of the central human cornea. *Investigative Ophthalmology and Visual Science*, **43**(1):82–86, January 2002.

[195] M.A.R. Koehl, Danny S. Adams and Ray E. Keller. Mechanical development of the notochord in *Xenopus* early tail-bud embryos. In: Nuri Akkaş, editor, *Biomechanics of Active Movement and Deformation of Cells*, volume 42 of *NATO ASI Series H, Cell Biology*, pp. 471–485. Springer-Verlag, Berlin, Germany, 1990. Proceedings of Institute Held in Istanbul, Turkey, September 1989.

[196] Satoshi Kogure, Hiroyuki Kohwa and Shigeo Tsukahara. Effect of uncompensated corneal polarization on the detection of localized retinal nerve fiber layer defects. *Ophthalmic Research*, **40**(2):61–68, 2008. doi: 10.1159/000114653.

[197] Rami K. Korhonen and Walter Herzog. Depth-dependent analysis of the role of collagen fibrils, fixed charges and fluid in the pericellular matrix of articular cartilage on chondrocyte mechanics. *Journal of Biomechanics*, **41**(2):480–485, 2008. doi: 10.1016/j.jbiomech.2007.09.002.

[198] Rami K. Korhonen, Petro Julkunen, Wouter Wilson and Walter Herzog. Importance of collagen orientation and depth-dependent fixed charge densities of cartilage on mechanical behavior of chondrocytes. *Journal of Biomedical Engineering*, **130**(2):21003–1–21003–11, April 2008. doi: 10.1115/1.2898725.

[199] Rami K. Korhonen, Mikko S. Laasanen, Juha Töyräs, Reijo Lappalainen, Heikki J. Helminen and Jukka S. Jurvelin. Fibril reinforced poroelastic model predicts specifically mechanical behavior of normal, proteoglycan depleted and collagen degraded articular cartilage. *Journal of Biomechanics*, **36**(9):1373–1379, September 2003. doi: S0021-9290(03)00069-1.

[200] R.K. Korhonen, M.S. Laasanen, J. Töyräs, J. Rieppo, J. Hirvonen, H.J. Helminen and J.S. Jurvelin. Comparison of the equilibrium response of articular cartilage in unconfined compression, confined compression and indentation. *Journal of Biomechanics*, **35**(7):903–909, July 2002. doi: 10.1016/S0021-9290(02)00052-0.

[201] R.K. Korhonen, M. Wong, J. Arokoski, R. Lindgren, H.J. Helminen, E.B. Hunziker and J.S. Jurvelin. Importance of the superficial tissue layer for the indentation stiffness of articular cartilage. *Medical Engineering and Physics*, **24**(2):99–108, March 2002. doi: 10.1016/S1350-4533(01)00123-0.

[202] Renee M. Korol, Helen M. Finlay, Melanie J. Josseau, Alexandra R. Lucas and Peter B. Canham. Fluorescence spectroscopy and birefringence of molecular changes in maturing rat tail tendon. *Journal of Biomedical Optics*, **12**(2):024011, March/April 2007. doi: 10.1117/1.2714055.

[203] Ramaswamy Krishnan, Seonghun Park, Felix Eckstein and Gerard A. Ateshian. Inhomogeneous cartilage properties enhance superficial interstitial fluid support and frictional properties, but do not provide a homogeneous state of stress. *Journal of Biomechanical Engineering*, **125**(5):569–577, October 2003. doi: 10.1115/1.1610018.

[204] M.S. Laasanen, J. Töyräs, R.K. Korhonen, J. Rieppo, S. Saarakkala, M.T. Nieminen, J. Hirvonen and J.S. Jurvelin. Biomechanical properties of knee articular cartilage. *Biorheology*, **40**(1-3):133–140, 2003.

[205] Jérôme E. Lafont. Lack of oxygen in articular cartilage: consequences for chondrocyte biology. *International Journal of Experimental Pathology*, **91**(2):99–106, April 2010. doi: 10.1111/j.1365-2613.2010.00707.x.

[206] W.M. Lai, J.S. Hou and V.C. Mow. A triphasic theory for the swelling and deformation behaviors of articular cartilage. *Journal of Biomechanical Engineering*, **113**(3):245–258, August 1991. doi: 10.1115/1.2894880.

[207] Mikko J. Lammi, Tomi P. Häkkinen, Jyrki J. Parkkinen, Mika M. Hyttinen, Matti Jortikka, Heikki J. Helminen and Markku I. Tammi. Adaptation of canine femoral head articular cartilage to long distance running exercise in young beagles. *Annals of the Rheumatic Diseases*, **52**(5):369–377, May 1993.

[208] Eve Langelier, Rosmarie Suetterlin, Caroline D. Hoemann, Ueli Aebi and Michael D. Buschmann. The chondrocyte cytoskeleton in mature articular cartilage: structure and distribution of actin, tubulin, and vimentin filaments. *The Journal of Histochemistry & Cytochemistry*, **48**(10):1307–1320, October 2000.

[209] Teemu K. Långsjö, Machiko Arita and Heikki J. Helminen. Cartilage collagen fibril network in newborn transgenic mice analyzed by electron microscopic stereology. *Cells Tissues Organs*, **190**(4):209–218, 2009. doi: 10.1159/000209232.

[210] Teemu K. Långsjö, Mika Hyttinen, Alpo Pelttari, Kari Kiraly, Jari Arokoski and Heikki J. Helminen. Electron microscopic stereological study of collagen fibrils in bovine articular cartilage: volume and surface densities are best obtained indirectly (from length densities and diameters) using isotropic uniform random sampling. *Journal of Anatomy*, **195 (Pt 2)**:281–293, August 1999. doi: 10.1046/j.1469-7580.1999.19520281.x.

[211] Teemu K. Långsjö, Jarno Rieppo, Alpo Pelttari, Niku Oksala, Vuokko Kovanen and Heikki J. Helminen. Collagenase-induced changes in articular cartilage as detected by electron-microscopic stereology, quantitative polarized light microscopy and biochemical assays. *Cells Tissues Organs*, **172**(4):265–275, 2002. doi: 10.1159/000067196.

[212] Johan L. van Leeuwen. Why the chameleon has spiral-shaped muscle fibres in its tongue. *Philosophical transactions of the Royal Society of London. Series B, Biological Sciences*, **352**(1353):573–589, May 1997.

[213] Cheng Li, Lisa A. Pruitt and Karen B. King. Nanoindentation differentiates tissue-scale functional properties of native articular cartilage. *Journal of Biomedical Materials Research Part A*, **78**(4):729–738, September 2006. doi: 10.1002/jbm.a.30751.

[214] LePing Li, M.D. Buschmann and A. Shirazi-Adl. The role of fibril reinforcement in the mechanical behavior of cartilage. *Biorheology*, **39**(1-2):89–96, 2002.

[215] L.P. Li, J.T.M. Cheung and W. Herzog. Three-dimensional fibril-reinforced finite element model of articular cartilage. *Medical and Biological Engineering and Computing*, **47**(6):607–615, June 2009. doi: 10.1007/s11517-009-0469-5.

[216] L.P. Li, R.K. Korhonen, J. Iivarinen, J.S. Jurvelin and W. Herzog. Fluid pressure driven fibril reinforcement in creep and relaxation tests of articular cartilage. *Medical Engineering and Physics*, **30**(2):182–189, March 2008. doi: 10.1016/j.medengphy.2007.03.001.

[217] L.P. Li, A. Shirazi-Adl and M.D. Buschmann. Alterations in mechanical behaviour of articular cartilage due to changes in depth varying material properties–a nonhomogeneous poroelastic model study. *Computer Methods in Biomechanics and Biomedical Engineering*, **5**(1):45–52, February 2002. doi: 10.1080/10255840290008088.

[218] L.P. Li, J. Soulhat, M.D. Buschmann and A. Shirazi-Adl. Nonlinear analysis of cartilage in unconfined ramp compression using a fibril reinforced poroelastic model. *Clinical Biomechanics*, **14**(9):673–682, November 1999. doi: 10.1016/S0268-0033(99)00013-3.

[219] Z. Li, S. Yao, M. Alini and S. Grad. Different response of articular chondrocyte subpopulations to surface motion. *Osteoarthritis & Cartilage*, **15**(9):1034–1041, September 2007. doi: 10.1016/j.joca.2007.03.001.

[220] Eric G. Lima, Robert L. Mauck, Shelley H. Han, Seonghun Park, Kenneth W. Ng, Gerard A. Ateshian and Clark T. Hung. Functional tissue engineering of chondral and osteochondral constructs. *Biorheology*, **41**(3-4):577–590, 2004.

[221] Harold Lipshitz, Robert Etheredge III and Melvin J. Glimcher. *In vitro* wear of articular cartilage. *Journal of Bone and Joint Surgery. American Volume*, **57**(4):527–534, June 1975.

[222] Chris B. Little and Peter Ghosh. Variation in proteoglycan metabolism by articular chondrocytes in different joint regions is determined by post-natal mechanical loading. *Osteoarthritis & Cartilage*, **5**(1):49–62, January 1997. doi: 10.1016/S1063-4584(97)80031-3.

[223] Lin Liu, James R. Trimarchi, Rudolf Oldenbourg and David L. Keefe. Increased birefringence in the meiotic spindle provides a new marker for the onset of activation in living oocytes. *Biology of Reproduction*, **63**(1):251–258, July 2000.

[224] Pauno Lötjönen, Petro Julkunen, Juha Töyräs, Mikko J. Lammi, Jukka S. Jurvelin and Heikki J. Nieminen. Strain-dependent modulation of ultrasound speed in articular cartilage under dynamic compression. *Ultrasound in Medicine and Biology*, May 2009. doi: 10.1016/j.ultrasmedbio.2009.03.002.

[225] Xin L. Lu and Van C. Mow. Biomechanics of articular cartilage and determination of material properties. *Medicine and Science in Sports and Exercise*, **40**(2):193–199, February 2008. doi: 10.1249/mss.0b013e31815cb1fc.

[226] T.J. Lyons, R.W. Stoddart, S.F. McClure and J. McClure. The tidemark of the chondro-osseous junction of the normal human knee joint. *Journal of Molecular Histology*, **36**(3):207–215, March 2005. doi: 10.1007/s10735-005-3283-x.

[227] Henning Madry, C. Niek van Dijk and Magdalena Mueller-Gerbl. The basic science of the subchondral bone. *Knee Surgery, Sports Traumatology, Arthroscopy*, **18**(4):419–433, April 2010. doi: 10.1007/s00167-010-1054-z.

[228] Duncan J. Maitland and Joseph T. Walsh, Jr. Quantitative measurements of linear birefringence during heating of native collagen. *Lasers in Surgery and Medicine*, **20**(3):310–318, 1997. doi: 10.1002/(SICI)1096-9101(1997)20:3<310::AID-LSM10>3.0.CO;2-H.

[229] Prasanna Malaviya and Robert M. Nerem. Fluid-induced shear stress stimulates chondrocyte proliferation partially mediated via TGF-β1. *Tissue Engineering*, **8**(4):581–590, August 2002. doi: 10.1089/107632702760240508.

[230] A. Maroudas and C. Bannon. Measurement of swelling pressure in cartilage and comparison with the osmotic pressure of constituent proteoglycans. *Biorheology*, **18**(3-6):619–632, 1981.

[231] A. Maroudas, M.T. Bayliss and M.F. Venn. Further studies on the composition of human femoral head cartilage. *Annals of the Rheumatic Diseases*, **39**(5):514–523, Oct 1980.

[232] A. Maroudas, P. Bullough, S.A.V. Swanson and M.A.R. Freeman. The permeability of articular cartilage. *Journal of Bone and Joint Surgery (British volume)*, **50**(1):166–177, February 1968.

[233] A. Maroudas and M. Venn. Chemical composition and swelling of normal and osteoarthrotic femoral head cartilage. II. Swelling. *Annals of the Rheumatic Diseases*, **36**(5):399–406, Oct 1977.

[234] A. Maroudas, E. Wachtel, G. Grushko, E.P. Katz and P. Weinberg. The effect of osmotic and mechanical pressures on water partitioning in articular cartilage. *Biochimica et Biophysica Acta*, **1073**(2):285–294, March 1991. doi: 10.1016/0304-4165(91)90133-2.

[235] A.I. Maroudas. Balance between swelling pressure and collagen tension in normal and degenerate cartilage. *Nature*, **260**(5554):808–809, April 1976. doi: 10.1038/260808a0.

[236] Alice Maroudas, Helen Muir and Joan Wingham. The correlation of fixed negative charge with glycosaminoglycan content of human articular cartilage. *Biochimica et Biophysica Acta*, **177**(3):492–500, May 1969. doi: 10.1016/0304-4165(69)90311-0.

[237] F. Massoumian, R. Juškaitis, M.A.A. Neil and T. Wilson. Quantitative polarized light microscopy. *Journal of Microscopy*, **209**(Pt 1):13–22, January 2003. doi: 10.1046/j.1365-2818.2003.01095.x.

[238] Ashley N. Mastrangelo, Elise M. Magarian, Matthew P. Palmer, Patrick Vavken and Martha M. Murray. The effect of skeletal maturity on the regenerative function of intrinsic ACL cells. *Journal of Orthopaedic Research*, **28**(5):644–651, May 2010. doi: 10.1002/jor.21018.

[239] G.W. McCutchen. Comment on the fundamental fluid transport mechanisms through normal and pathological articular cartilage during function. I. The formulation and II. The analysis, solution and conclusions. *Journal of Biomechanics*, **10**(4):279–280, 1977. doi: 10.1016/0021-9290(77)90051-3.

[240] C.A. McDevitt. Biochemistry of articular cartilage. Nature of proteoglycans and collagen of articular cartilage and their role in ageing and in osteoarthrosis. *Annals of the Rheumatic Diseases*, **32**(4):364–378, July 1973.

[241] K.M. Meek. The Cornea and Sclera. In: P. Fratzl, editor, *Collagen: Structure and Mechanics*, chapter 13, pp. 359–396. Springer US, 2008. doi: 10.1007/978-0-387-73906-9_13.

[242] Rupert Meller, Frederike Schiborra, Gudrun Brandes, Karsten Knobloch, Thomas Tschernig, Stefan Hankemeier, Carl Haasper, Andreas Schmiedl, Michael Jagodzinski, Christian Krettek and Elmar Willbold. Postnatal maturation of tendon, cruciate ligament, meniscus and articular cartilage: a histological study in sheep. *Annals of Anatomy - Anatomischer Anzeiger*, **191**(6):575–585, December 2009. doi: 10.1016/j.aanat.2009.08.005.

[243] Michael J. Mienaltowski, Liping Huang, Arnold J. Stromberg and James N. MacLeod. Differential gene expression associated with postnatal equine articular cartilage maturation. *BMC Musculoskeletal Disorders*, **9**:149, 2008. doi: 10.1186/1471-2474-9-149.

[244] Edward J. Miller and Victor J. Matukas. Chick cartilage collagen: a new type of α1 chain not present in bone or skin of the species. *Proceedings of the National Academy of Sciences of the United States of America*, **64**(4):1264–1268, December 1969.

[245] R.J. Minns and F.S. Steven. The collagen fibril organization in human articular cartilage. *Journal of Anatomy*, **123**(Pt 2):437–457, April 1977.

[246] L. Módis, Á. Botos, I. Kiviranta, L. Lukácskó and H.J. Helminen. Differences in submicroscopic structure of the extracellular matrix of canine femoral and tibial condylar articular cartilages as revealed by polarization microscopical analysis. *Acta Biologica Hungaria*, **47**(1-4):341–353, 1996.

[247] E.H. Morrison, M.W.J. Ferguson, M.T. Bayliss and C.W. Archer. The development of articular cartilage: I. The spatial and temporal patterns of collagen types. *Journal of Anatomy*, **189 (Pt 1)**:9–22, August 1996.

[248] Van C. Mow and X. Edward Guo. Mechano-electrochemical properties of articular cartilage: their inhomogeneities and anisotropies. *Annual Review of Biomedical Engineering*, **4**:175–209, 2002. doi: 10.1146/annurev.bioeng.4.110701.120309.

[249] Van C. Mow, Mark H. Holmes and W. Michael Lai. Fluid transport and mechanical properties of articular cartilage: a review. *Journal of Biomechanics*, **17**(5):377–394, 1984. doi: 10.1016/0021-9290(84)90031-9.

[250] Van C. Mow, Anthony Ratcliffe and A. Robin Poole. Cartilage and diarthrodial joints as paradigms for hierarchical materials and structures. *Biomaterials*, **13**(2):67–97, 1992. doi: 10.1016/0142-9612(92)90001-5.

[251] V.C. Mow, S.C. Kuei, W.M. Lai and C.G. Armstrong. Biphasic creep and stress relaxation of articular cartilage in compression? Theory and experiments. *Journal of Biomechanical Engineering*, **102**(1):73–84, February 1980.

[252] R.C. Murray, H.L. Birch, K. Lakhani and A.E. Goodship. Biochemical composition of equine carpal articular cartilage is influenced by short-term exercise in a site-specific manner. *Osteoarthritis & Cartilage*, **9**(7):625–632, October 2001. doi: 10.1053/joca.2001.0462.

[253] Jyrki Nieminen, Janne Sahlman, Teemu Hirvonen, Tuomo Lapveteläinen, Markku Miettinen, Ilkka Arnala, Hartmut H. Malluche and Heikki J. Helminen. Disturbed synthesis of type II collagen interferes with rate of bone formation and growth and increases bone resorption in transgenic mice. *Calcified Tissue International*, **82**(3):229–237, March 2008. doi: 10.1007/s00223-008-9110-0.

[254] Miika T. Nieminen, Jarno Rieppo, Juha Töyräs, Juhana M. Hakumäki, Johanna Silvennoinen, Mika M. Hyttinen, Heikki J. Helminen and Jukka S. Jurvelin. T_2 relaxation reveals spatial collagen architecture in articular cartilage: a comparative quantitative MRI and polarized light microscopic study. *Magnetic Resonance in Medicine*, **46**(3):487–493, Sep 2001. doi: 10.1002/mrm.1218.

[255] Juliano Yasuo Oda, Edson Aparecido Liberti, Laura Beatriz Mesiano Maifrino and Romeu Rodrigues de Souza. Variation in articular cartilage in rats between 3 and 32 months old. A histomorphometric and scanning electron microscopy study. *Biogerontology*, **8**(3):345–352, June 2007. doi: 10.1007/s10522-006-9076-0.

[256] Ralf Oettmeier, Jari Arokoski, Andreas J. Roth, Heikki J. Helminen, Markky Tammi and Klaus Abendroth. Quantitative study of articular cartilage and subchondral bone remodeling in the knee joint of dogs after strenuous running training. *Journal of Bone and Mineral Research*, **7 Suppl 2**:S419–S424, December 1992.

[257] Alex Ogston. On Articular Cartilage. *Journal of Anatomy & Physiology*, **10**(Pt 1):49–74, October 1875.

[258] Kaoru Ohtani, Tuoya Yao, Mari Kobayashi, Rie Kusakabe, Shigeru Kuratani and Hiroshi Wada. Expression of Sox and fibrillar collagen genes in lamprey larval chondrogenesis with implications for the evolution of vertebrate cartilage. *Journal of Experimental Zoology Part B: Molecular and Developmental Evolution*, **310**(7):596–607, November 2008. doi: 10.1002/jez.b.21231.

[259] R. Oldenbourg and G. Mei. New polarized light microscope with precision universal compensator. *Journal of Microscopy*, **180**(Pt 2):140–147, November 1995.

[260] R. Oldenbourg, E.D. Salmon and P.T. Tran. Birefringence of single and bundled microtubules. *Biophysical Journal*, **74**(1):645–654, January 1998.

[261] Rudolf Oldenbourg. Polarization microscopy with the LC-microscope. In: Robert D. Goldman and David L. Spector, editors, *Live Cell Imaging: A Laboratory Manual*, chapter 13, pp. 205–238. Cold Spring Harbor Laboratory Press, 2004.

[262] Rudolf Oldenbourg. Analysis of microtubule dynamics by polarized light. In: Jun Zhou, editor, *Microtubule Protocols*, volume 137 of *Methods in Molecular Medicine*, chapter 8, pp. 111–123. Humana Press, 2007. doi: 10.1007/978-1-59745-442-1_8.

[263] Ikemefuna Onyekwelu, Mary B. Goldring and Chisa Hidaka. Chondrogenesis, joint formation, and articular cartilage regeneration. *Journal of Cellular Biochemistry*, **107**(3):383–392, June 2009. doi: 10.1002/jcb.22149.

[264] Jan L. Palmer, Alicia L. Bertone and A.S. Litsky. Contact area and pressure distribution changes of the equine third carpal bone during loading. *Equine Veterinary Journal*, **26**(3):197–202, May 1994.

[265] Harri E. Panula, Mika M. Hyttinen, Jari P.A. Arokoski, Teemu K. Långsjö, Alpo Pelttari, Ilkka Kiviranta and Heikki J. Helminen. Articular cartilage superficial zone collagen birefringence reduced and cartilage thickness increased before surface fibrillation in experimental osteoarthritis. *Annals of the Rheumatic Diseases*, **57**(4):237–245, April 1998.

[266] Seonghun Park, Steven B. Nicoll, Robert L. Mauck and Gerard A. Ateshian. Cartilage mechanical response under dynamic compression at physiological stress levels following collagenase digestion. *Annals of Biomedical Engineering*, **36**(3):425–434, March 2008. doi: 10.1007/s10439-007-9431-6.

[267] Charles G.M. Paxton. The plural of 'anecdote' can be 'data': statistical analysis of viewing distances in reports of unidentified large marine animals 1758-2000. *Journal of Zoology*, **279**(4):381–387, 2009. doi: 10.1111/j.1469-7998.2009.00630.x.

[268] R.W. Payne, S.A. Harding, D.A. Murray, D.M. Soutar, D.B. Baird, A.I. Glaser, I.C. Channing, S.J. Welham, A.R. Gilmour, R. Thompson and R. Webster. *The Guide to GenStat Release 12*. VSN International, Hemel Hempstead, 2009.

[269] Cory Pelletier, David L. Keefe and James R. Trimarchi. Noninvasive polarized light microscopy quantitatively distinguishes the multilaminar structure of the zona pellucida of living human eggs and embryos. *Fertility and Sterility*, **81 Suppl 1**:850–856, March 2004. doi: 10.1016/j.fertnstert.2003.09.033.

[270] Fred H. Perrin. Whose Absorption Law? *Journal of the Optical Society of America*, **38**(1):72–74, 1948. doi: 10.1364/JOSA.38.000072.

[271] W. Matthew Petroll, H. Dwight Cavanagh, Patricia Barry, Peter Andrews and James V. Jester. Quantitative analysis of stress fiber orientation during corneal wound contraction. *Journal of Cell Science*, **104**(2):353–363, 1993.

[272] L.E.R. Picken, M.G.M. Pryor and M.M. Swann. Orientation of fibrils in natural membranes. *Nature*, **159**:434, March 1947. doi: 10.1038/159434a0.

[273] Martin Pirzer and Jürgen Sawatzki. Method of processing and correcting spectral data in two-dimensional representation. US patent 7359815, April 15th, 2008.

[274] Anna H.K. Plaas, Shirley Wong-Palms, Peter J. Roughley, Ronald J. Midura and Vincent C. Hascall. Chemical and immunological assay of the nonreducing terminal residues of chondroitin sulfate from human aggrecan. *Journal of Biological Chemistry*, **272**(33):20603–20610, August 1997.

[275] Jeffrey H. Plochocki, Carol V. Ward and Douglas E. Smith. Evaluation of the chondral modeling theory using FE-simulation and numeric shape optimization. *Journal of Anatomy*, **214**(5):768–777, May 2009. doi: 10.1111/j.1469-7580.2009.01070.x.

[276] Kimberlee Potter, Linda H. Kidder, Ira W. Levin, E. Neil Lewis and Richard G.S. Spencer. Imaging of collagen and proteoglycan in cartilage sections using Fourier transform infrared spectral imaging. *Arthritis and Rheumatism*, **44**(4):846–855, April 2001. doi: 10.1002/1529-0131(200104)44:4<846::AID-ANR141>3.0.CO;2-E.

[277] Robert R. Provine. Yawning. In: Atul Gawande, editor, *The Best American Science Writing 2006*, pp. 291–305. Harper Perennial, 2006.

[278] Thomas M. Quinn, Alan J. Grodzinsky, Michael D. Buschmann, Young-Jo Kim and Ernst B. Hunziker. Mechanical compression alters proteoglycan deposition and matrix deformation around individual cells in cartilage explants. *Journal of Cell Science*, **111 (Pt 5)**:573–583, March 1998.

[279] Thomas M. Quinn, Adrian A. Maung, Alan J. Grodzinsky, Ernst B. Hunziker and John D. Sandy. Physical and biological regulation of proteoglycan turnover around chondrocytes in cartilage explants. Implications for tissue degradation and repair. *Annals of the New York Academy of Sciences*, **878**:420–441, June 1999.

[280] Igal Raizman, J.N. Amritha De Croos, Jean-Philippe St-Pierre, Robert M. Pilliar and Rita A. Kandel. Articular cartilage subpopulations respond differently to cyclic compression *in vitro*. *Tissue Engineering – Part A*, **15**(12):3789–3798, December 2009. doi: 10.1089/ten.TEA.2008.0530.

[281] Donald J. Responte, Roman M. Natoli and Kyriacos A. Athanasiou. Collagens of articular cartilage: structure, function, and importance in tissue engineering. *Critical Reviews in Biomedical Engineering*, **35**(5):363–411, 2007.

[282] J. Rieppo, M.M. Hyttinen, E. Halmesmaki, H. Ruotsalainen, A. Vasara, I. Kiviranta, J.S. Jurvelin and H.J. Helminen. Changes in spatial collagen content and collagen network architecture in porcine articular cartilage during growth and maturation. *Osteoarthritis & Cartilage*, **17**(4):448–455, April 2009. doi: 10.1016/j.joca.2008.09.004.

[283] Jarno Rieppo, Jarmo Hallikainen, Jukka S. Jurvelin, Ilkka Kiviranta, Heikki J. Helminen and Mika M. Hyttinen. Practical considerations in the use of polarized light microscopy in the analysis of the collagen network in articular cartilage. *Microscopy Research and Technique*, **71**(4):279–287, April 2007. doi: 10.1002/jemt.20551.

[284] Jarno Rieppo, Mika M. Hyttinen, Jukka S. Jurvelin and Heikki J. Helminen. Reference sample method reduces the error caused by variable cryosection thickness in Fourier transform infrared imaging. *Applied Spectroscopy*, **58**(1):137–140, January 2004. doi: 10.1366/000370204322729577.

[285] Jarno Rieppo, Juha Töyräs, Miika T. Nieminen, Vuokko Kovanen, Mika M. Hyttinen, Rami K. Korhonen, Jukka S. Jurvelin and Heikki J. Helminen. Structure-function relationships in enzymatically modified articular cartilage. *Cells Tissues Organs*, **175**(3):121–132, 2003. doi: 10.1159/000074628.

[286] J.M. Rieppo, J. Hallikainen, J.S. Jurvelin, H.J. Helminen and M.M. Hyttinen. Novel quantitative polarization microscopic assessment of cartilage and bone collagen birefringence, orientation and anisotropy. *Transactions of the ORS*, **28**, 2003. Paper nr. 0570 at the 49th Annual Meeting of the Orthopaedic Research Soceity, New Orleans, Louisiana.

[287] L. Rieppo, S. Saarakkala, T. Närhi, J. Holopainen, M. Lammi, H.J. Helminen, J.S. Jurvelin and J. Rieppo. Quantitative analysis of spatial proteoglycan content in articular cartilage with Fourier transform infrared imaging spectroscopy: Critical evaluation of analysis methods and specificity of the parameters. *Microscopy Research and Technique*, **73**(5):503–512, May 2010. doi: 10.1002/jemt.20789.

[288] S. Ross, R. Newton, Y.-M. Zhou, J. Haffegee, M.-W. Ho, J.P. Bolton and D. Knight. Quantitative image analysis of birefringent biological material. *Journal of Microscopy*, **187**(Pt 1):62–67, July 1997. doi: 10.1046/j.1365-2818.1997.2160776.x.

[289] Ehsan Saadat, Howard Lan, Sharmila Majumdar, David M. Rempel and Karen B. King. Long-term cyclical *in vivo* loading increases cartilage proteoglycan content in a spatially specific manner: an infrared microspectroscopic imaging and polarized light microscopy study. *Arthritis Research & Therapy*, **8**(5):R147, 2006. doi: 10.1186/ar2040.

[290] S. Saarakkala, P. Julkunen, P. Kiviranta, J. Mäkitalo, J.S. Jurvelin and R. Korhonen. Depth-wise progression of osteoarthritis in human articular cartilage: investigation of composition, structure and biomechanics. *Osteoarthritis & Cartilage*, **18**(1):73–81, January 2010. doi: 10.1016/j.joca.2009.08.003.

[291] Robert Schall. Estimation in generalized linear models with random effects. *Biometrika*, **78**(4):719–727, 1991. doi: 10.1093/biomet/78.4.719.

[292] Luc Scheres, Jurjen ter Maat, Marcel Giesbers and Han Zuilhof. Microcontact printing onto oxide-free silicon via highly reactive acid fluoride-functionalized monolayers. *Small*, **6**(5):642–650, March 2010. doi: 10.1002/smll.200901650.

[293] Robert M. Schinagl, Donnell Gurskis, Albert C. Chen and Robert L. Sah. Depth-dependent confined compression modulus of full-thickness bovine articular cartilage. *Journal of Orthopaedic Research*, **15**(4):499–506, July 1997. doi: 10.1002/jor.1100150404.

[294] E.M. Shapiro, A. Borthakur, J.H. Kaufman, J.S. Leigh and R. Reddy. Water distribution patterns inside bovine articular cartilage as visualized by ^{1}H magnetic resonance imaging. *Osteoarthritis & Cartilage*, **9**(6):533–538, August 2001. doi: 10.1053/joca.2001.0428.

[295] Y. Shen, T. Stalf, C. Mehnert, U. Eichenlaub-Ritter and H.-R. Tinneberg. High magnitude of light retardation by the zona pellucida is associated with conception cycles. *Human Reproduction*, **20**(6):1596–1606, June 2005. doi: 10.1093/humrep/deh811.

[296] Shunichi Shibata, Kenji Fukada, Shoichi Suzuki, Takuya Ogawa and Yasuo Yamashita. Histochemical localisation of versican, aggrecan and hyaluronan in the developing condylar cartilage of the fetal rat mandible. *Journal of Anatomy*, **198**(Pt 2):129–135, February 2001. doi: 10.1046/j.1469-7580.2001.19820129.x.

[297] Adrian C. Shieh and Kyriacos A. Athanasiou. Biomechanics of single zonal chondrocytes. *Journal of Biomechanics*, **39**(9):1595–1602, 2006. doi: 10.1016/j.jbiomech.2005.05.002.

[298] R. Shirazi and A. Shirazi-Adl. Deep vertical collagen fibrils play a significant role in mechanics of articular cartilage. *Journal of Orthopaedic Research*, **26**(5):608–615, May 2008. doi: 10.1002/jor.20537.

[299] R. Shirazi, A. Shirazi-Adl and M. Hurtig. Role of cartilage collagen fibrils networks in knee joint biomechanics under compression. *Journal of Biomechanics*, **41**(16):3340–3348, December 2008. doi: 10.1016/j.jbiomech.2008.09.033.

[300] Michael Shribak and Rudolf Oldenbourg. Techniques for fast and sensitive measurements of two-dimensional birefringence distributions. *Applied Optics*, **42**(16):3009–3017, June 2003.

[301] F.H. Silver and W.J. Landis. Viscoelasticity, Energy Storage and Transmission and Dissipation by Extracellular Matrices in Vertebrates. In: P. Fratzl, editor, *Collagen: Structure and Mechanics*, chapter 6, pp. 133–154. Springer US, 2008. doi: 10.1007/978-0-387-73906-9_6.

[302] R. Simon. The connection between Mueller and Jones matrices of polarization optics. *Optics Communications*, **42**(5):293–297, August 1982. doi: 10.1016/0030-4018(82)90234-6.

[303] W.H. Simon. Scale effects in animal joints. I. Articular cartilage thickness and compressive stress. *Arthritis and Rheumatism*, **13**(3):244–256, May-June 1970. doi: 10.1002/art.1780130305.

[304] William H. Simon, Steven Friedenberg and Steven Richardson. Joint congruence. A correlation of joint congruence and thickness of articular cartilage in dogs. *Journal of Bone and Joint Surgery. American Volume*, **55**(8):1614–1620, December 1973.

[305] Elizabeth M. Slayter. *Optical Methods in Biology*. Wiley-Interscience, 1970.

[306] R. Lane Smith, Dennis R. Carter and David J. Schurman. Pressure and shear differentially alter human articular chondrocyte metabolism: a review. *Clinical Orthopaedics and Related Research*, (427 Suppl):S89–S95, October 2004.

[307] R. Lane Smith, B.S. Donlon, M.K. Gupta, M. Mohtai, P. Das, D.R. Carter, J. Cooke, G. Gibbons, N. Hutchinson and D.J. Schurman. Effects of fluid-induced shear on articular chondrocyte morphology and metabolism *in vitro*. *Journal of Orthopaedic Research*, **13**(6):824–831, November 1995. doi: 10.1002/jor.1100130604.

[308] R. Lane Smith, M.C.D. Trindade, T. Ikenoue, M. Mohtai, P. Das, D.R. Carter, S.B. Goodman and D.J. Schurman. Effects of shear stress on articular chondrocyte metabolism. *Biorheology*, **37**(1-2):95–107, 2000.

[309] Donald P. Speer and Laurence Dahners. The collagenous architecture of articular cartilage. Correlation of scanning electron microscopy and polarized light microscopy observations. *Clinical Orthopaedics and Related Research*, (139):267–275, March/April 1979.

[310] R.A. Stockwell. Chondrocytes. *Journal of Clinical Pathology. Supplement (Royal College of Pathologists)*, **12**:7–13, 1978.

[311] R.A. Stockwell. Morphometry of cytoplasmic components of mammalian articular chondrocytes and corneal keratocytes: species and zonal variations of mitochondria in relation to nutrition. *Journal of Anatomy*, **175**:251–261, April 1991.

[312] M. Stolberg. Inventing the randomized double-blind trial: the Nuremberg salt test of 1835. *Journal of the Royal Society of Medicine*, **99**(12):642–643, December 2006. doi: 10.1258/jrsm.99.12.642.

[313] Elsa Strawich and Marcel E. Nimni. Properties of a collagen molecule containing three identical components extracted from bovine articular cartilage. *Biochemistry*, **10**(21):3905–3911, October 1971. doi: 10.1021/bi00797a017.

[314] M.B.E. Sweet, E.J.-M.A. Thonar and A.R. Immelman. Regional distribution of water and glycosaminoglycan in immature articular cartilage. *Biochimica et Biophysica Acta*, **500**(1):173–186, November 1977. doi: 10.1016/0304-4165(77)90057-5.

[315] Jon D. Szafranski, Alan J. Grodzinsky, Elke Burger, Veronique Gaschen, Han-Hwa Hung and Ernst B. Hunziker. Chondrocyte mechanotransduction: effects of compression on deformation of intracellular organelles and relevance to cellular biosynthesis. *Osteoarthritis & Cartilage*, **12**(12):937–946, December 2004. doi: 10.1016/j.joca.2004.08.004.

[316] Malba Tahan. *De man die kon rekenen*. Sijthoff, Amsterdam, 2009. Translated from O Homem que Calculava (1949) by Joost de Wit.

[317] Kotaro Tanimoto, Reiko Kitamura, Yuki Tanne, Takashi Kamiya, Ryo Kunimatsu, Motoko Yoshioka, Nobuaki Tanaka, Eiji Tanaka and Kazuo Tanne. Modulation of hyaluronan catabolism in chondrocytes by mechanical stimuli. *Journal of Biomedical Materials Research Part A*, **93**(1):373–380, April 2010. doi: 10.1002/jbm.a.32540.

[318] R. Teshima, T. Otsuka, N. Takasu, N. Yamagata and K. Yamamoto. Structure of the most superficial layer of articular cartilage. *Journal of Bone and Joint Surgery. British Volume*, **77**(3):460–464, May 1995.

[319] Dimitrios A. Theocharis. Comparisons between extracted and residual proteoglycans on the glycosaminoglycan level and changes with ageing. *International Journal of Biochemistry*, **17**(2):155–160, 1985. doi: 10.1016/0020-711X(85)90109-0.

[320] Masato Tomiya, Kyosuke Fujikawa, Shoichi Ichimura, Toshiyuki Kikuchi, Yasuo Yoshihara and Koichi Nemoto. Skeletal unloading induces a full-thickness patellar cartilage defect with increase of urinary collagen II CTx degradation marker in growing rats. *Bone*, **44**(2):295–305, February 2009. doi: 10.1016/j.bone.2008.10.038.

[321] P.A. Torzilli and V.C. Mow. On the fundamental fluid transport mechanisms through normal and pathological articular cartilage during function - II. The analysis, solution and conclusions. *Journal of Biomechanics*, **9**(9):587–606, 1976. doi: 10.1016/0021-9290(76)90100-7.

[322] P.A. Torzilli and V.C. Mow. On the fundamental fluid transport mechanisms through normal and pathological articular cartilage during function–I. The formulation. *Journal of Biomechanics*, **9**(8):541–552, 1976. doi: 10.1016/0021-9290(76)90071-3.

[323] Theodore T. Tower, Michael R. Neidert and Robert T. Tranquillo. Fiber alignment imaging during mechanical testing of soft tissues. *Annals of Biomedical Engineering*, **30**(10):1221–1233, November 2002. doi: 10.1114/1.1527047.

[324] Phong Tran, E.D. Salmon and Rudolf Oldenbourg. Quantifying single and bundled microtubules with the polarized light microscope. *Biological Bulletin*, **189**(2):206, October/November 1995.

[325] Phong T. Tran, Shinya Inoué, Edward D. Salmon and Rudolf Oldenbourg. Muscle fine structure and microtubule birefringence measured with a new pol-scope. *Biophysical Journal*, **187**:244–245, October 1994.

[326] Nicolas Tran-Khanh, Caroline D. Hoemann, Marc D. McKee, Janet E. Henderson and Michael D. Buschmann. Aged bovine chondrocytes display a diminished capacity to produce a collagen-rich, mechanically functional cartilage extracellular matrix. *Journal of Orthopaedic Research*, **23**(6):1354–1362, November 2005. doi: 10.1016/j.orthres.2005.05.009.1100230617.

[327] Mark van Turnhout, Gerrit Peters, Anke Stekelenburg and Cees Oomens. Passive transverse mechanical properties as a function of temperature of rat skeletal muscle *in vitro*. *Biorheology*, **42**(3):193–207, May 2005.

[328] Mark C. van Turnhout, Monique B. Haazelager, Merel A.L. Gijsen, Henk Schipper, Sander Kranenbarg and Johan L. van Leeuwen. Quantitative description of collagen structure in the articular cartilage of the young and adult equine distal metacarpus. *Animal Biology*, **58**(4):353–370, December 2008. doi: 10.1163/157075608X383674.

[329] Mark C. van Turnhout, Sander Kranenbarg and Johan L. van Leeuwen. Modelling optical behaviour of birefringent biological tissues for evaluation of quantitative polarised light microscopy. *Journal of Biomedical Optics*, **14**(5):054018, September/October 2009. doi: 10.1117/1.3241986.

[330] Mark C. van Turnhout, Sander Kranenbarg and Johan L. van Leeuwen. Contribution of postnatal collagen reorientation to depth-dependent mechanical properties of articular cartilage. *Biomechanics and Modeling in Mechanobiology*, June 2010. doi: 10.1007/s10237-010-0233-7. Online first.

[331] Mark C. van Turnhout, Henk Schipper, Bas Engel, Willem Buist, Sander Kranenbarg and Johan L. van Leeuwen. Postnatal development of collagen structure in ovine articular cartilage. *BMC Developmental Biology*, **10**:62, June 2010. doi: 10.1186/1471-213X-10-62.

[332] Mark C. van Turnhout, Henk Schipper, Barend van Lagen, Han Zuilhof, Sander Kranenbarg and Johan L. van Leeuwen. Postnatal development of depth-dependent collagen density in ovine articular cartilage. *BMC Developmental Biology*, **10**:108, October 2010. doi: 10.1186/1471-213X-10-108.

[333] Nadya Ugryumova, Don P. Attenburrow, C. Peter Winlove and Stephen J. Matcher. The collagen structure of equine articular cartilage, characterized using polarization-sensitive optical coherence tomography. *Journal of Physics D: Applied Physics*, **38**(15):2612–2619, August 2005. doi: 10.1088/0022-3727/38/15/012.

[334] Graham J.G. Upton and Bernhard Fingleton. *Spatial data analysis by example – Volume 2: Categorical and directional data.* Wiley series in probability and mathematical statistics. John Wiley and Sons, 1989.

[335] J.P.G. Urban and A. Maroudas. The measurement of fixed charged density in the intervertebral disc. *Biochimica et Biophysica Acta*, **586**(1):166–178, August 1979. doi: 10.1016/0304-4165(79)90415-X.

[336] E.J. Vanderploeg, C.G. Wilson and M.E. Levenston. Articular chondrocytes derived from distinct tissue zones differentially respond to *in vitro* oscillatory tensile loading. *Osteoarthritis & Cartilage*, **16**(10):1228–1236, October 2008. doi: 10.1016/j.joca.2008.02.016.

[337] Eric J. Vanderploeg, Stacy M. Imler, Kathryn R. Brodkin, Andrés J. García and Marc E. Levenston. Oscillatory tension differentially modulates matrix metabolism and cytoskeletal organization in chondrocytes and fibrochondrocytes. *Journal of Biomechanics*, **37**(12):1941–1952, December 2004. doi: 10.1016/j.jbiomech.2004.02.048.

[338] B. Vanwanseele, E. Lucchinetti and E. Stüssi. The effects of immobilization on the characteristics of articular cartilage: current concepts and future directions. *Osteoarthritis & Cartilage*, **10**(5):408–419, May 2002. doi: 10.1053/joca.2002.0529.

[339] Fernando Augusto Vasilceac, Adriana Frias Renner, Walcy Rosólia Teodoro and Stela Márcia Mattiello-Rosa. The remodeling of collagen fibres in rats ankles submitted to immobilization and muscle stretch. *Rheumatology International*, February 2010. doi: 10.1007/s00296-010-1371-z. Online first.

[340] Anne Vaughan-Thomas, Jayesh Dudhia, Michael T. Bayliss, Karl E. Kadler and Victor C. Duance. Modification of the composition of articular cartilage collagen fibrils with increasing age. *Connective Tissue Research*, **49**(5):374–382, 2008. doi: 10.1080/03008200802325417.

[341] M. Venn and A. Maroudas. Chemical composition and swelling of normal and osteoarthrotic femoral head cartilage. I. Chemical composition. *Annals of the Rheumatic Diseases*, **36**(2):121–129, April 1977.

[342] S.K. de Visser, J.C. Bowden, E. Wentrup-Byrne, L. Rintoul, T. Bostrom, J.M. Pope and K.I. Momot. Anisotropy of collagen fibre alignment in bovine cartilage: comparison of polarised light microscopy and spatially resolved diffusion-tensor measurements. *Osteoarthritis & Cartilage*, **16**(6):689–697, June 2008. doi: 10.1016/j.joca.2007.09.015.

[343] Christopher C.-B. Wang, X. Edward Guo, Dongning Sun, Van C. Mow, Gerard A. Ateshian and Clark T. Hung. The functional environment of chondrocytes within cartilage subjected to compressive loading: a theoretical and experimental approach. *Biorheology*, **39**(1-2):11–25, 2002.

[344] P.R. van Weeren and A. Barneveld. Study design to evaluate the influence of exercise on the development of the muscoskeletal system of foals up to age 11 months. *Equine Veterinary Journal Supplement*, **31**:4–8, November 1999.

[345] P.R. van Weeren, E.C. Firth, H. Brommer, M.M. Hyttinen, A.E. Helminen, C.W. Rogers, J. Degroot and P.A.J. Brama. Early exercise advances the maturation of glycosaminoglycans and collagen in the extracellular matrix of articular cartilage in the horse. *Equine Veterinary Journal*, **40**(2):128–135, March 2008. doi: 10.2746/042516408X253091.

[346] Terri Wells, Catherine Davidson, Matthias Mörgelin, Joseph L.E. Bird, Michael T. Bayliss and Jayesh Dudhia. Age-related changes in the composition, the molecular stoichiometry and the stability of proteoglycan aggregates extracted from human articular cartilage. *Biochemical Journal*, **370**(Pt 1):69–79, February 2003. doi: 10.1042/BJ20020968.

[347] Gregory M. Williams, Stephen M. Klisch and Robert L. Sah. Bioengineering cartilage growth, maturation, and form. *Pediatric Research*, **63**(5):527–534, May 2008. doi: 10.1203/PDR.0b013e31816b4fe5.

[348] Amanda K. Williamson, Albert C. Chen, Koichi Masuda, Eugene J.-M.A. Thonar and Robert L. Sah. Tensile mechanical properties of bovine articular cartilage: variations with growth and relationships to collagen network components. *Journal of Orthopaedic Research*, **21**(5):872–880, September 2003. doi: 10.1016/S0736-0266(03)00030-5.

[349] Amanda K. Williamson, Albert C. Chen and Robert L. Sah. Compressive properties and function-composition relationships of developing bovine articular cartilage. *Journal of Orthopaedic Research*, **19**(6):1113–1121, November 2001. doi: 10.1016/S0736-0266(01)00052-3.

[350] W. Wilson, C.C. van Donkelaar and J.M. Huyghe. A comparison between mechano-electrochemical and biphasic swelling theories for soft hydrated tissues. *Journal of Biomechanical Engineering*, **127**(1):158–165, February 2005.

[351] W. Wilson, C.C. van Donkelaar, B. van Rietbergen and R. Huiskes. A fibril-reinforced poroviscoelastic swelling model for articular cartilage. *Journal of Biomechanics*, **38**(6):1195–1204, June 2005. doi: 10.1016/j.jbiomech.2004.07.003. Erratum in J. Biomech. 38(10):2138–2140, see [353].

[352] W. Wilson, C.C. van Donkelaar, B. van Rietbergen, K. Ito and R. Huiskes. Stresses in the local collagen network of articular cartilage: a poroviscoelastic fibril-reinforced finite element study. *Journal of Biomechanics*, **37**(3):357–366, March 2004. doi: 10.1016/S0021-9290(03)00267-7. Erratum in J. Biomech. 38(10):2138–2140, see [353].

[353] W. Wilson, C.C. van Donkelaar, B. van Rietbergen, K. Ito and R. Huiskes. Erratum to "Stresses in the local collagen network of articular cartilage: a poroviscoelastic fibril-reinforced finite element study" [Journal of Biomechanics 37 (2004) 357–366] and "A fibril-reinforced poroviscoelastic swelling model for articular cartilage" [Journal of Biomechanics 38 (2005) 1195–1204]. *Journal of Biomechanics*, **38**(10):2138–2140, October 2005. doi: 10.1016/j.jbiomech.2005.04.024.

[354] W. Wilson, C.C. van Donkelaar, R. van Rietbergen and R. Huiskes. The role of computational models in the search for the mechanical behavior and damage mechanisms of articular cartilage. *Medical Engineering and Physics*, **27**(10):810–826, December 2005. doi: 10.1016/j.medengphy.2005.03.004.

[355] W. Wilson, N.J.B. Driessen, C.C. van Donkelaar and K. Ito. Prediction of collagen orientation in articular cartilage by a collagen remodeling algorithm. *Osteoarthritis & Cartilage*, **14**(11):1196–1202, November 2006. doi: 10.1016/j.joca.2006.05.006.

[356] W. Wilson, J.M. Huyghe and C.C. van Donkelaar. A composition-based cartilage model for the assessment of compositional changes during cartilage damage and adaptation. *Osteoarthritis & Cartilage*, **14**(6):554–560, June 2006. doi: 10.1016/j.joca.2005.12.006.

[357] W. Wilson, J.M. Huyghe and C.C. van Donkelaar. Depth-dependent compressive equilibrium properties of articular cartilage explained by its composition. *Biomechanics and Modeling in Mechanobiology*, **6**(1-2):43–53, January 2007. doi: 10.1007/s10237-006-0044-z.

[358] M. Wong, M. Ponticiello, V. Kovanen and J.S. Jurvelin. Volumetric changes of articular cartilage during stress relaxation in unconfined compression. *Journal of Biomechanics*, **33**(9):1049–1054, September 2000. doi: 10.1016/S0021-9290(00)00084-1.

[359] M. Wong, P. Wuethrich, M.D. Buschmann, P. Eggli and E. Hunziker. Chondrocyte biosynthesis correlates with local tissue strain in statically compressed adult articular cartilage. *Journal of Orthopaedic Research*, **15**(2):189–196, March 1997. doi: 10.1002/jor.1100150206.

[360] M. Wong, P. Wuethrich, P. Eggli and E. Hunziker. Zone-specific cell biosynthetic activity in mature bovine articular cartilage: a new method using confocal microscopic stereology and quantitative autoradiography. *Journal of Orthopaedic Research*, **14**(3):424–432, May 1996. doi: 10.1002/jor.1100140313.

[361] John Z. Wu and Walter Herzog. Analysis of the mechanical behavior of chondrocytes in unconfined compression tests for cyclic loading. *Journal of Biomechanics*, **39**(4):603–616, 2006. doi: 10.1016/j.jbiomech.2005.01.007.

[362] J.P. Wu and T.B. Kirk. Study of altered mechanical properties of articular cartilage in relation to the collagen network. *Advanced Materials Research*, **41-42**:9–14, 2008. doi: 10.4028/www.scientific.net/AMR.41-42.9.

[363] Y. Xia, N. Ramakrishnan and A. Bidthanapally. The depth-dependent anisotropy of articular cartilage by Fourier-transform infrared imaging (FTIRI). *Osteoarthritis & Cartilage*, **15**(7):780–788, July 2007. doi: 10.1016/j.joca.2007.01.007.

[364] Yang Xia. Averaged and depth-dependent anisotropy of articular cartilage by microscopic imaging. *Seminars in Arthritis and Rheumatism*, **37**(5):317–327, April 2008. doi: 10.1016/j.semarthrit.2007.07.001.

[365] Yang Xia, Jonathan B. Moody and Hisham Alhadlaq. Orientational dependence of T_2 relaxation in articular cartilage: A microscopic MRI (μMRI) study. *Magnetic Resonance in Medicine*, **48**(3):460–469, September 2002. doi: 10.1002/mrm.10216.

[366] Yang Xia, Jonathan B. Moody, Hisham Alhadlaq and Jiani Hu. Imaging the physical and morphological properties of a multi-zone young articular cartilage at microscopic resolution. *Journal of Magnetic Resonance Imaging*, **17**(3):365–374, March 2003. doi: 10.1002/jmri.10269.

[367] I. Youn, J.B. Choi, L. Cao, L.A. Setton and F. Guilak. Zonal variations in the three-dimensional morphology of the chondron measured in situ using confocal microscopy. *Osteoarthritis & Cartilage*, **14**(9):889–897, September 2006. doi: 10.1016/j.joca.2006.02.017.

[368] Jing Yu, Uday Tirlapur, Jeremy Fairbank, Penny Handford, Sally Roberts, C. Peter Winlove, Zhanfeng Cui and Jill Urban. Microfibrils, elastin fibres and collagen fibres in the human intervertebral disc and bovine tail disc. *Journal of Anatomy*, **210**(4):460–471, April 2007. doi: 10.1111/j.1469-7580.2007.00707.x.

[369] N.Z. Zambrano, G.S. Montes, K.M. Shigihara, E.M. Sanchez and L.C. Junqueira. Collagen arrangement in cartilages. *Acta Anatomica*, **113**(1):26–38, 1982. doi: 10.1159/000145534.

[370] Margherita Zanetti, Anthony Ratcliffe and Fiona M. Watt. Two subpopulations of differentiated chondrocytes identified with a monoclonal antibody to keratan sulfate. *Journal of Cell Biology*, **101**(1):53–59, July 1985. doi: 10.1083/jcb.101.1.53.

[371] J.M. Zarek and J. Edwards. A note on the stress-structure relationship in articular cartilage. *Medical Electronics & Biological Engineering*, **3**(4):449–450, October 1965. doi: 10.1007/BF02476145.

[372] Y.P. Zheng, H.J. Niu, F.T. Arthur Mak and Y.P. Huang. Ultrasonic measurement of depth-dependent transient behaviors of articular cartilage under compression. *Journal of Biomechanics*, **38**(9):1830–1837, September 2005. doi: 10.1016/j.jbiomech.2004.08.020.

From the fact that a child can hardly tickle itself, or in a much lesser degree than when tickled by another person, it seems that the precise point to be touched must not be known; so with the mind, something unexpected– a novel or incongruous idea which breaks through an habitual train of thought– appears to he [sic] a strong element in the ludicrous.

Charles Darwin [91]

Most human yawners are not rewarded with orgasms.

Robert R. Provine [277]

Summary

Articular cartilage (AC) is the thin layer of tissue that covers the ends of the bones in the synovial joints in mammals. Functional adult AC has depth-dependent mechanical properties that are not yet present at birth. These depth-dependent mechanical properties in adult life are the result of a depth-dependent composition and structure that develops in postnatal life. Our knowledge on how postnatal AC remodelling proceeds, and how the functional depth-dependent mechanical properties develop in postnatal life is still limited.

In this thesis, we investigated the properties of the postnatal collagen network in AC, and the contribution of postnatal collagen network remodelling to the adult depth-dependent mechanical properties of AC. We used horses and (mostly) sheep as experimental animals to obtain measurements on three parameters of the postnatal collagen network (predominant collagen fibril orientation, collagen densities and collagen network anisotropy). We used a composition-based finite element model for computational analysis of the role of this collagen network in the postnatal development of depth-dependent mechanical properties.

We first investigated how collagen structure in AC affects the parameters that are measured by quantitative polarised light microscopy (qPLM), because qPLM is the most popular technique to investigate properties of the collagen network in AC. We quantified the contributions of the three collagen network parameters (orientation, density and anisotropy) to the measured predominant fibril orientation and the measured total tissue birefringence (retardance), and showed that collagen network anisotropy can be quantified when the retardance from polarised light microscopy is corrected for collagen densities.

In the study on horses, we investigated differences in predominant collagen orientation for equine articular cartilage in stillborn and adult animals with scanning electron microscopy and quantitative polarised light microscopy (qPLM). In the study on sheep, we first investigated the predominant collagen orientation in animals divided over ten sample points between birth and maturity (72 weeks) with qPLM. Both studies confirmed the remark by Archer et al. [6] that the collagen fibrils in perinatal animals lie predominantly parallel to the articular surface, and we confirmed and quantified the

adult 'Benninghoff' structure in the mature animals in both studies. We further observed a transitional layer with weak fibril anisotropy in the perinatal animals that is not correlated to changes in predominant collagen fibril orientation as in the adult Benninghoff structure.

To investigate the contribution of collagen reorientation to the development of depth-dependent mechanical properties, we implemented the results on postnatal predominant collagen fibril orientation in the sheep in a composition-based finite element model. We described the interactions between collagen orientation, free swelling strains, osmotic pressures and effective AC stiffness in confined compression. Based on the results, we hypothesised that collagen densities increase most in the deep tissue due to increased collagen fibril strains that result from postnatal collagen fibril reorientation.

In sheep, we measured collagen densities with Fourier transform infrared micro-spectroscopy. Collagen density increased in postnatal life, and they increased most in the deep tissue (near the bone), which supported our earlier hypothesis. Perinatal animals showed a valley in collagen densities near the articular surface, i.e. at the position of the transitional layer. We showed that this valley disappears in early postnatal life. We corrected the qPLM retardance from our sheep data with the collagen densities from the sheep data to assess collagen network anisotropy. The results showed that anisotropy is relatively constant in the deep tissue, and that anisotropy is stronger in the transitional layer of perinatal animals compared with the transitional layer of adult animals.

To investigate interactions in postnatal collagen network remodelling, we implemented the three collagen network parameters (orientation, density and anisotropy) that we obtained from the sheep in the finite element model. Based on the results, we suggested different functional roles for the three collagen network parameters: collagen fibril reorientation contributes most to the development of depth-dependent mechanical properties, collagen density increases appear to equalise collagen fibril strains, and the weak anisotropy in the transitional layer appears to smooth gradients in the mechanical state of the tissue in adult animals.

Om alleen wetenschap te bedrijven voor het praktische nut is het ontzielen van de wetenschap.

Malba Tahan [316]

Samenvatting

Articulair kraakbeen (AK) is de dunne laag weefsel die het einde van de botten bekleedt in de synoviale gewrichten in zoogdieren. Functioneel volwassen AK heeft diepteafhankelijke mechanische eigenschappen die nog niet aanwezig zijn bij de geboorte. Deze diepteafhankelijke mechanische eigenschappen in volwassen dieren zijn het resultaat van een diepteafhankelijke compositie en structuur die zich ontwikkelt in de postnatale periode. Onze kennis over hoe de postnatale remodellering in AK verloopt, en over hoe de diepteafhankelijke mechanische eigenschappen ontwikkelen, is beperkt.

In dit proefschrift hebben we de eigenschappen onderzocht van het postnatale collageennetwerk, evenals de contributie van postnatale collageennetwerk remodellering aan de ontwikkeling van diepteafhankelijke mechanische eigenschappen in volwassen AK. We hebben paarden en (voornamelijk) schapen gebruikt in dierexperimenten om drie parameters van het postnatale collageennetwerk te meten (voorkeursrichting van de collageenvezels, collageendichtheden en collageennetwerkanisotropie). We hebben een eindige elementen model gebruikt dat rekening houdt met de compositie en structuur van AK voor numerieke analyses van de rol van het postnatale collageennetwerk voor de ontwikkeling van diepteafhankelijke mechanische eigenschappen.

We hebben eerst onderzocht hoe de collageenstructuur in AK de parameters beïnvloedt die gemeten worden met kwantitatieve gepolariseerd licht microscopie (kPLM), omdat kPLM de meest populaire techniek is voor onderzoek naar de eigenschappen van het collageennetwerk in AK. We hebben de bijdragen gekwantificeerd van de drie collageennetwerkparameters (orientatie, dichtheid en anisotropie) aan de gemeten voorkeursrichting en totale weefsel dubbelbrekendheid (retardatie). We laten zien dat collageennetwerkanisotropie gekwantificeerd kan worden wanneer the retardatie uit kPLM gecorrigeerd wordt voor collageendichtheden.

In de studie met paarden hebben we verschillen onderzocht in voorkeursrichting van de collageenvezels in doodgeboren en volwassen dieren met scanning elektronenmicroscopie en kPLM. In de studie met schapen hebben we eerst de voorkeursrichting van de collageenvezels onderzocht in dieren die waren verdeeld over 10 samplepunten tussen geboorte en volwassenheid (72 weken) met kPLM. Beide studies bevestigde de opmerking door Archer et al. [6] dat in perinataal AK de voorkeursrichting van de collageenvezels parallel is aan het kraakbeenoppervlak, en we bevestigde en kwantificeerde de 'Benninghoff'-structuur in de volwassen dieren in beide studies. Daarnaast zagen we een transitionele laag met zwakke collageenvezel anisotropie in de perinatale dieren die niet is gecorreleerd met veranderingen in voorkeursrichting van de collageenvezels zoals in de volwassen Benninghoffstructuur.

Om de bijdrage te onderzoeken van collageenvezelreoriëntatie aan de ontwikkeling van diepteafhankelijke mechanische eigenschappen, hebben we de resultaten voor de postnatale voorkeursrichting van collageenvezels in de schapen geïmplementeerd in het eindige elementen model. We hebben de interacties onderzocht tussen collageenvezeloriëntatie, zwelrekken, osmotische drukken en effectieve AK stijfheid in 1-D compressie. Op basis van de resultaten formuleerde we de hypothese we dat collageendichtheden het meest zullen toenemen in de buurt van het bot vanwege de toegenomen vezelrekken tengevolge van de postnatale collageenvezelreoriëntatie.

In de schapen hebben we collageendichtheden gemeten met Fourier transformatie infrarood microspectroscopie. Collageendichtheden nemen toe in de postnatale periode en ze nemen het meest toe in de buurt van het bot hetgeen onze eerdere hypothese bevestigd. In perinatale dieren vonden we een vallei in collageendichtheden in de buurt van het kraakbeenoppervlak op de positie van de transitionele laag. We hebben laten zien dat deze vallei verdwijnt in de vroege postnatale periode. We hebben de kPLM-data voor retardaties gecorrigeerd voor collageendichtheden om collageennetwerkanisotropie te bepalen. De resultaten lieten zien dat anisotropie relatief constant is in de diepere lagen van het weefsel, en dat anisotropie sterker is in de transitionele laag in perinataal AK dan in de transitionele laag in volwassen AK.

Om interacties in de postnatale collageenvezelnetwerk remodellering te onderzoeken hebben we de drie parameters voor het collageenvezelnetwerk (oriëntatie, dichtheden en anisotropie) die we gevonden hebben in de schapen geïmplementeerd in het eindige elementen model. Op basis van de resultaten hebben we verschillende functionele rollen voorgesteld voor de drie parameters voor het collageenvezelnetwerk: collageenvezelreoriëntatie levert de grootste bijdrage aan de ontwikkeling van diepteafhankelijke mechanische eigenschappen; de toename in collageendichtheden lijkt collageenvezelrekken te nivelleren; en de zwakke anisotropie in de transitionele laag lijkt gradiënten in de mechanische toestand van het weefsel af te vlakken in de volwassen dieren.

You make me so very happy, I'm so glad you came into my life

Alton Ellis [101]

Dankwoord

Beste Johan. Op weg naar mijn sollicitatie bij EZO (april 2005) las ik weinig lovende dingen over Wageningen Universiteit: er was net een college 'praten met bomen' gestart. Au. Gelukkig werd me tijdens ons gesprek indertijd erg snel duidelijk dat dat bericht niet bepaald representatief was voor de WUR. Integendeel, en tot mijn grote vreugde. Ik heb je leren kennen als iemand met een groot hart voor de wetenschap, die oprecht boos kan worden als er tegen de regels van de kunst wordt gezondigd. Je liefde voor de biologie is gruwelijk aanstekelijk. Ik heb ontzettende bewondering voor je respect voor (goede) argumenten en voor je toewijding aan je AIOs: die is groot en reikt veel, veel, verder dan de (nood)zakelijke promotor-AIO-relatie. Johan, het was een eer en verrijking om bij je te mogen promoveren. Ik zou het zo weer doen!

Kees, bedankt voor je begeleiding aan het begin van mijn aanstelling. Het is jammer dat je afscheid moest nemen voor het echt leuk begon te worden, maar dat laat onverlet dat we samen veel plezier gehad hebben. Je hebt een enorm oog voor detail en daar heb ik zeker van geprofiteerd. Ik wil je bedanken voor je tijd, humor en vertrouwen in die eerste periode van mijn aanstelling. Ze hebben zeker bijgedragen aan het volbrengen van dit project.

Sander, je nam de begeleiding over toen Kees' aanstelling eindigde en ik heb bijzonder veel aan je gehad. Je inbreng in onze wetenschappelijke discussies was (is) van grote waarde. Alsjeblieft, blijf me tergen met vragen als de uitleg van deze technische ingenieur niet afdoende lijkt voor 'een biologenpubliek'; en al helemaal als het lijkt dat de uitleg niet het volledige verhaal dekt of gewoon onjuist is. Ik vind dat belangrijk en heb het zeer gewaardeerd, ondanks mijn misschien soms norse reactie. Ik kan me verder maar met de uiterste inspanning onttrekken aan het idee dat het ook wel tussen ons geboterd had als je me niet had hoeven begeleiden (getuige je hulp bij onze verhuizing, bijvoorbeeld). En ik was niet van plan die inspanning te gaan leveren, wat jij? Dankjewel!

Henk! Rododendron, wat heb je een hoop werk voor me verzet. Je staat rotsvast op een tweede plaats in mijn lijstje 'meest behulpzame mensen die ik ken'. Iedereen kan bij jou onaangekondigd binnenlopen, je storen, en dan toch nog rekenen op je aandacht en tijd. Dat je nog zoveel werk voor me hebt weten te verzetten mag bijna een wonder heten als ik bedenk hoe vaak ik je zelf ben komen storen. Je was natuurlijk ook van onschatbare waarde voor me vanwege je inbreng van je histologische kennis en, bijvoorbeeld, die slordige 3000 coupes van 7 μm. En als ik afleiding nodig had, kon ik ook nog eens (onaangekondigd, storend) binnenlopen voor een praatje. Mijn verwachtingen om nog eens met zo'n analist te mogen werken zijn eerlijk gezegd matig- tot laaggespannen. Ik ben daarom nu al plannen aan het smeden om de komende twee jaar een soort van samenwerking in stand te houden. Ik zie er nu al naar uit!

Een eerbetoon aan Henk –de duizendpoot– Schipper

Waarde collegae bij EZO, en bij 'onze vrienden van het CBI'. Jullie werk is inspirerend, jullie hulp is hartelijk, jullie collegialiteit, humor en gezelligheid worden bijzonder gewaardeerd, en jullie praten raar met een eigenaardige 'g'. Dat laatste is niet erg. Ik hoor dat de laatste tijd ook steeds vaker over mezelf. Carla, het organiseren van De Labuitje2006 (en de nasleep) ontaarde in een hoop plezier, voor ons. Dankjewel! David, het was goed om een Delftse collega te hebben, in het bijzonder binnen WIAS. Arie, je lessen Mens en Dierkunde waren (zijn) uit de kunst! Toen ik nog uit Eindhoven moest komen, stond er steevast bij aankomst op Zodiac verse, echte, koffie klaar. Onovertroffen! Ik wil de mensen die daar voor verantwoordelijk waren (Adri, Trudi en Anja, gok ik) van harte bedanken. Mees en Kier, hartelijke dank voor de tijd en moeite die jullie in

de belastingsopstelling hebben gestoken. Eric, ook bedankt voor het werk aan de belastingsopstelling; en voor de 'kleine' klusjes die je voor ons hebt gedaan (waar je altijd over meedacht). John en Karen, bedankt voor jullie lessen en hulp in het kweeklab. Staat niet bijzonder veel van in dit proefschrift, maar ik vond het leuk. Jos, het was een genoegen om in je laatste drie weken bij EZO nog even voor 100 % van je (legendarische) hulpvaardigheid en ervaring gebruik te kunnen maken, en je hout brandt uitstekend! Mijn kamergenoten over de afgelopen vijf jaar (Igor, Kees, Patricia, Ansa en Maurijn) verdienen niets dan lof: ik mocht van jullie mijn eigen muziek draaien. Van Annemarie mocht ik zelfs meezingen. Irie!

Beste studenten, geachte dames: Anouk, Merel, Noëlle, Monique, Miriam, Lisette, Marit, Anneke en Alex. Bedankt voor jullie bijdragen aan, en enthousiasme voor, ons onderzoek. Dat geldt natuurlijk ook voor Marcel, hoewel hij noch een dame, noch een student 'van mij' is. Ik wens jullie veel succes en plezier met het afronden van jullie studie en het vervolg van jullie carrière. Ansa, Patricia, Maurijn, Sebastian en Wijbrand, veel succes met het afronden van jullie promotie. Jullie zijn bij EZO in uitstekende handen. Sebastian, welkom bij EZO (jouw 'g' is trouwens bij verre de beste van de hele leerstoelgroep)! Ansa, vergeet je niet je visjes te verzorgen voor me? En Annemarie, (verdorie, das twee keer!), pas je een beetje goed op Johan voor me?

Hartelijke dank aan Barend en Han, en de rest van de Organische Chemie groep. Ik heb me zeer welkom gevoeld tijdens mijn metingen bij jullie. Barend en Han natuurlijk ook bedankt voor jullie concrete bijdrage aan hoofdstuk 6. Ik vond het een fijne samenwerking. Bedank ook de 'geheime commissie' die me vereerde met een stukje in het Sinterklaasgedicht. Erg treffend! Harry, bedankt voor je ondersteuning (en de koffie) bij de leerstoelgroep Fysica en Fysische Chemie van Levensmiddelen. Ik vond het leuk bij jullie en bij de reometer, hoewel ook die proeven het proefschrift niet hebben gehaald. Ries, Willem, Wim, Andre, Antoinette en andere collegae bij het proefdierbedrijf, hartelijke dank voor jullie goede zorgen voor onze schaapjes, jullie bijdragen aan een goed verloop van onze dierproeven, en jullie oprechte interesse voor het verloop van het onderzoek.

Verder niets dan goeds voor m'n vrienden buiten de universitaire wereld (jullie weten wel: Suurland, AOR, Boschdijk, Hajraa, Gewis, St. Paulus Lyceum...). Altijd goed om jullie in de buurt te kunnen hebben als ik even niet aan kraakbeen dacht.

Mijn ouders, Jan en Servien, zijn de reden dat Henk zich zal moeten verzoenen met een tweede plaats. Bedankt voor jullie steun en hulp en begrip en etentjes en gastvrij-, gul-, oprecht- en hartelijkheid en die dingen die wij in onze familie zo vanzelfsprekend vinden.

Maar voor alles, dank ik Elles, voor alles. 'Je maakt me zo ontzettend gelukkig, ik ben zo blij dat je in mijn leven bent gekomen.' Samen 80 duurt gelukkig nog heel lang!

Beste mensen,

"Houdoe, bedankt en blijf wakker!" [65]

On your way up be good to those people you met, 'ca ya gonna meet the same people deh on your way going down

Prince Far I [160]

Copyrights, credits and final acknowledgements

Copyright and -left

Figures and photographs

The cover shows a sketch of the Lego Enhanced General Orientation (LEGO) device. This LEGO device was indeed used for experiments for chapter 2 (results not shown). It's appearance on the cover is to convince my parents that their steady supply of Lego during my youth was not in vain.

The 'sketchy' part refers to the pencil and paper that I frequently use for taking notes and of course for doing math; to the idea that postnatal cartilage is 'not yet finished', but still in development; to the creative, back-of-the-envelope, quick-and-dirty, processes in science; and finally to science in general, a discipline that will always be in development, and will never be finished.

The sketch was converted from a photograph by ImageMagick, the cover was made with Inkscape. The font on the cover is Hommage à Escher v2, used under the terms of the Creative Commons Attribution-Noncommercial-No Derivative Works 3.0 Unported License.

Graphs of data were created with a combination of Matlab, LaPrint, psfragx and LaTeX. Line art by the author was performed with Inkscape. Bitmap manipulation by the author was performed with gimp.

Cover		original photograph by Henk Schipper.
Figure 1.1	p. 1	photograph by Jos van den Boogaart.
Figure 1.4	p. 5	drawing by Elles Middeljans.
Figure 2.1	p. 16	drawing by Elles Middeljans.
Figure 2.10	p. 25	PLM images by Henk Schipper.
Figure 3.1	p. 36	photograph on the left by Monique Haazelager.
Figure 3.1	p. 36	drawing on the right by Elles Middeljans.
Figure 3.2a	p. 38	SEM image by Merel Gijsen.
Figures 3.3	p. 41	SEM images by Merel Gijsen.
Figure 4.1	p. 54	drawings by Elles Middeljans.
Figure 4.3	p. 58	PLM images by Henk Schipper.
Figure 4.A.1	p. 71	photographs by Henk Schipper.
Figure 4.A.2	p. 72	PLM images by Henk Schipper.
Figure 4.A.6	p. 75	PLM image by Henk Schipper.
Figure 6.1	p. 97	drawings by Elles Middeljans.
Henks tribute	p. 182	drawing by Elles Middeljans.

Final acknowledgements

This thesis is typeset with LaTeX 2_ε, with the scrbook-class and the following packages (and their dependencies): appendix, fontenc, inputenc, ae, aecompl, mathdesign (with charter fonts), quotchap, scrpage2, crop, textpos, polymers, hcycle, chemist, epic, array, sizeredc, tabularx, colortbl, multirow, natbib, hyperref, hypernat, graphicx, color, psfragx, caption, subfig, textcomp, gensymb, units, empheq, wasysym, etexcmds, lscape, marvosym and babel.

The developers, maintainers and communities of the following Open Source Software packages have further contributed to the work that is presented in this thesis: GNU/Linux (in particular: Ubuntu), Gnome, Inkscape, gimp, ImageMagick, Octave, Maxima, R, LaTeX, BibTeX, TeX Live, JabRef, TeXworks, dvips, Ghostscript, LaPrint, Latexmk, Wine, Foobar2000 (Last 'windows'-program standing. Now retired by Quod Libet), GCC, gfortran, bash (& find & grep & wget, etc.), Thunderbird, Firefox, Lightning, FileZilla, Samba, rsync, OpenSSH, OpenOffice, regexxer, xxdiff, 7-Zip, Pan, Transmission, Nicotine, aMule, and scroogle (among others).

Total cost: zero.
Value: priceless.

Finally, a big thanks to the singers and players of instruments! You were there, and that was irie. As I would say.

Here, here I come again
Have no fear, for it is only I

Dennis Brown [58]

Personalia

Curriculum vitae

Mark was born on the last nation-wide car-less Sunday in the Netherlands (at the moment of writing), and grew up. He then started a study Mechanical Engineering at Eindhoven University of Technology. He soon found out that mechanical engineering was not his craft, and he switched to the study Biomechanical Engineering.

During his first (experimental) internship, Mark worked on thermodilution in a physiologically representative *in vitro* model of the coronary circulation, see [1]. During his second (numerical) internship, he worked on a 3-D finite element mesh for parameter estimation with *in vivo* experiments on human skin. The work for his M.Sc.-thesis consisted of an experimental part: determining the passive mechanical properties in vitro as a function of temperature of rat skeletal muscle [327]; and a numerical part: finite element modeling of an *in vivo* indentation experiment on the same rat muscle.

After his study at Eindhoven University of Technology, Mark started the PhD project 'Postnatal development of articular cartilage' with Prof. Johan van Leeuwen at the Experimental Zoology Group at Wageningen University. During his employment in Wageningen, he also worked several months on a side project to minimise mastitis in dairy cattle and he participated in writing a STW grant proposal to minimise claw disorders, also in dairy cattle.

At the moment, Mark is back with the group where he did his M.Sc. work, the Soft Tissue Biomechanics & Engineering Group of Eindhoven University of Technology, for a two year postdoc in the NIH project 'Multiscale Modeling of the Human Knee'. He will focus on the role of the pericellular matrix for the protection of chondrocytes in articular cartilage (which has become his favourite tissue over the last years).

Mark does not love to write about himself in the third-person singular form. He does love Elles, science, and (Jamaican) music.

Journal publications

Mark C. van Turnhout, Sander Kranenbarg & Johan L. van Leeuwen. Modelling postnatal collagen structure development in articular cartilage: interactions of orientation, density and structure. Submitted.

Mark C. van Turnhout, Henk Schipper, Barend van Lagen, Han Zuilhof, Sander Kranenbarg & Johan L. van Leeuwen. Postnatal development of depth-dependent collagen density in ovine articular cartilage. *BMC Developmental Biology*, **10**:108, October 2010. doi: 10.1186/1471-213X-10-108

Mark C. van Turnhout, Sander Kranenbarg & Johan L. van Leeuwen. Contribution of postnatal collagen reorientation to depth-dependent mechanical properties of articular cartilage. *Biomechanics and Modeling in Mechanobiology*, online first, June 7th, 2010. doi: 10.1007/s10237-010-0233-7

Mark C. van Turnhout, Henk Schipper, Bas Engel, Willem Buist, Sander Kranenbarg & Johan L. van Leeuwen. Postnatal development of collagen structure in ovine articular cartilage. *BMC Developmental Biology*, **10**:62, June 2010. doi: 10.1186/1471-213X-10-62

Mark C. van Turnhout, Sander Kranenbarg & Johan L. van Leeuwen. Modelling optical behaviour of birefringent biological tissues for evaluation of quantitative polarised light microscopy. *Journal of Biomedical Optics*, **14**(5):054018, September/October 2009. doi: 10.1117/1.3241986

Mark C. van Turnhout, Monique B. Haazelager, Merel A.L. Gijsen, Henk Schipper, Sander Kranenbarg & Johan L. van Leeuwen. Quantitative description of collagen structure in the articular cartilage of the young and adult equine distal metacarpus. *Animal Biology*, **58**(4):353–370, December 2008. doi: 10.1163/157075608X383674

Mark van Turnhout, Gerrit Peters, Anke Stekelenburg & Cees Oomens. Passive transverse mechanical properties as a function of temperature of rat skeletal muscle *in vitro*. *Biorheology*, **42**(3):193–207, May 2005.

Wilbert Aarnoudse, Petra van den Berg, Frans van de Vosse, Maartje Geven, Marcel Rutten, Mark van Turnhout, William Fearon, Bernard de Bruyne & Nico Pijls. Myocardial resistance assessed by guidewire-based pressure-temperature measurement: *in vitro* validation. *Catheterization and Cardiovascular Interventions*, **62**(1):56–63, May 2004. doi: 10.1002/ccd.10793

Abstracts

Mark van Turnhout, Henk Schipper, Sander Kranenbarg & Johan L. van Leeuwen. Postnatal development of collagen architecture in articular cartilage. *Comparative Biochemistry and Physiology, Part A, Molecular & Integrative Physiology*, **150**(3/Suppl.):S75, July 2008. Abstracts of the Anual Main Meeting of the Society for Experimental Biology, 6th–10th July 2008, Marseille, France. doi: 10.1016/j.cbpa.2008.04.111

Mark van Turnhout, Kees Spoor & Johan van Leeuwen. Finite element modelling of articular cartilage. *Comparative Biochemistry and Physiology, Part A, Molecular & Integrative Physiology*, **143A**(4/Suppl.):S95, April 2006. Abstracts of the Anual Main Meeting of the Society for Experimental Biology, 2nd–7th April 2006, University of Kent at Canterbury, UK. doi: 10.1016/j.cbpa.2006.01.041

M. Haazelager, H. Schipper, M. van Turnhout & J. van Leeuwen. Quantification of collagen fibril structure in developing cartilage. *Abstracts of the 14th Benelux Congress of Zoology*, p13, November 2007.